

**STUDY OF ADDITIVE EFFECTS ON THE STRUCTURAL,
MAGNETIC AND TRANSPORT PROPERTIES OF
COBALT FERRITES**

By

Saroaut Noor
Roll No: 0555752
Session: July' 2005

A THESIS SUBMITTED TO THE DEPARTMENT OF PHYSICS,
KHULNA UNIVERSITY OF ENGINEERING & TECHNOLOGY, KHULNA-9203
IN PARTIAL FULFILMENT OF THE REQUIRMENT FOR THE DEGREE OF
DOCTOR OF PHILOSOPHY

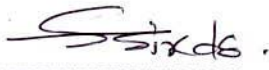


DEPARTMENT OF PHYSICS
KHULNA UNIVERSITY OF ENGINEERING & TECHNOLOGY
KHULNA-9203, BANGLADESH
APRIL-2011

DECLARATION

This is to certify that the thesis work entitled as “**Study of Additive Effects on the Structural, Magnetic and Transport Properties of Cobalt Ferrites**” has been carried out in partial fulfillment of the requirement for Ph. D. degree in the department of physics, Khulna University of Engineering & Technology, Khulna-9203, Bangladesh. The above research work or any part of this work has not been submitted to anywhere for the award of any degree or diploma. No other person’s work has been used without due acknowledgement.

1. Supervisor



Prof. Dr. S. S. Sikder

Candidate



Saraut Noor

2. Joint-Supervisor



Dr. A. K. M. Abdul Hakim

To

My Late Parents

KHULNA UNIVERSITY OF ENGINEERING & TECHNOLOGY
DEPARTMENT OF PHYSICS

CERTIFICATION OF THESIS WORK



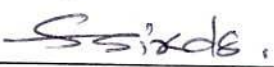



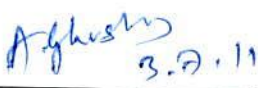

A THESIS ON

**Study of Additive Effects on the Structural, Magnetic and Transport
Properties of Cabalt Ferrites**

By
Saroaut Noor

has been accepted as satisfactory in partial fulfillment for the degree of Doctor of Philosophy in Physics and it is certified that the student demonstrated a satisfactory knowledge in the field covered by her thesis in an oral examination held on July 03, 2011.

Board of Examiners

1. Prof. Dr. Shibendra Shekher Sikder
Department of Physics
Khulna University of Engineering & Technology
Khulna-9203, Bangladesh

Supervisor & Chairman
2. Dr. A. K. M. Abdul Hakim
Chief Engineer (PRL)
Materials Science Division
Atomic Energy Centre, Dhaka- 1000

Joint Supervisor & Member
3. Head
Department of Physics
Khulna University of Engineering & Technology

Member
4. Prof. Dr. Md. Mahbub Alam
Department of Physics
Khulna University of Engineering & Technology

Member
5. Prof. Dr. Md. Rafiqul Islam
Department of Electrical and Electronic Engineering
Khulna University of Engineering & Technology

Member
6. Dr. Dilip Kumar Saha
Chief Scientific Officer
Materials Science Division
Atomic Energy Centre
Ramna, Dhaka-1000, Bangladesh

Member
7. Prof. Dr. Amitabha Ghoshray
Experimental Condensed Matter Physics Division
Saha Institute of Nuclear Physics
1/ AF, Bidhanagar, Kolkata 700 064
West Bengal, India

Member (External)
8. Prof. Dr. Md. Abu Hashan Bhuiyan
Department of Physics
Bangladesh University of Engineering & Technology
Dhaka-1000, Bangladesh

Member (External)

বাংলাদেশ প্রকৌশল বিশ্ববিদ্যালয়



বাংলাদেশ প্রকৌশল বিশ্ববিদ্যালয়
ঢাকা

Report on the Ph. D. Thesis entitled “Study of Additive Effects on the Structural, Magnetic and Transport Properties of Cobalt Ferrites” Submitted to the Khulna University of Engineering and Technology, Khulna, Bangladesh by Ms. Saroaut Noor

Ferrites are well known for their multidimensional scientific and industrial applications. For these reasons, researchers throughout the globe are engaged to explore best ferrites for suitability of application in devices. In this respect this work, definitely, will have contributions to the scientific arena. She considered the cadmium (Cd) and zinc (Zn) doped Cobalt (Co)-based spinel ferrites rare earth substituted diluted systems for the investigation of the structural, magnetic and transport properties. The findings have been reported in different chapters of the thesis.

The thesis consists of eight chapters. In these chapters the scholar discusses the synthesis of the different ferrite materials by conventional double sintering technique. She has doped the Co-based ferrites by Cd and Zn and then diluted by holmium (Ho) and samarium (Sm). Then the scholar used various techniques to evaluate the structural, magnetic and transport behaviour. For these purposes, she has used XRD for structural investigation; permeability, low field hysteresis and magnetization measurements for magnetic study and DC and AC measurements for transport properties. Ferrites with Cd and Zn have single phase structure but when diluted by Ho and Sm, a secondary phase arises. The appearance of the secondary phase has shifted the T_c to higher temperature. Using of Gd and Eu has decreased magnetization. The magnetic behaviour has been described by Yafet-Kittel model and the dielectric behaviour has been discussed in the light of MW interfacial polarization..

The overall findings of this study are of much interest for both researches and engineers. The research work and the presentation of the thesis is well organized. Two contributions on this work have been published in international journals three have published in proceedings. There are handful numbers of presented articles.

Therefore, in the light of the above discussion, I strongly recommend that the Thesis submitted by Ms. Saroaut Noor in the Department of Physics be accepted for the award a Ph. D. degree by KUET, Khulna, Bangladesh.

Dr. Md. Abu Hashan Bhuiyan
23/5/2011

Dr. Md. Abu Hashan Bhuiyan

Professor, Department of Physics
Bangladesh University of Engineering and
Technology (BUET)
Dhaka 1000, BANGLADESH
E-mail: abhuiyan@phy.buet.ac.bd



Report on the thesis entitled “**Study of Additive Effects on the Structural, Magnetic and Transport Properties of Cobalt Ferrite**” submitted by Ms. Saraut Noor, Ph. D student of the Dept. of Physics, Khulna University of Engineering and Technology, Khulna 9203, Bangladesh.

This thesis reports the detailed and systematic investigation on the effect of doping of bivalent Cd and Zn ions in CoFe_2O_4 ferrite. All the samples were prepared by solid state reaction and characterized using XRD studies. Prepared samples were in single phase. Temperature and frequency dependence of the permeability, B-H loop at room temperature, AC and DC (both FC and ZFC) magnetization were used to study the system. Dielectric constant and room temperature resistivity were also measured. Over all phase diagram of the doped ferrite was established. Some of the finding e.g. spin glass behaviour for large doping case was very interesting and deserve further attention.

Small part of the thesis deals with the rare-earth substitution on doped ferrite and some important findings have been reported.

Detail Report:

In chapter I “Introduction”, the candidate has elaborated the aims and objective of the present work emphasizing the need for further study the subject of ferrite, in particular, the dilution effect of CoFe_2O_4 by Cd^{2+} and Zn^{2+} ions. A small part of the thesis also deals with the substitution effect of rare earth ions. Important findings of the present thesis has been summarized, followed by review work on “ferrite”. Also, the outline of the thesis has been indicated.

Chapter II deals with the theoretical aspects of magnetism and the magnetic materials with a special emphasis to ferrite. Starting from the introduction of magnetism, she explained in detail different magnetization processes, types of magnetism etc. It seems that the candidate has acquired necessary theoretical understanding to carry out the research on magnetic materials and capability to explain phenomena observed in the experimental findings. The second part describes details of ferrite including its classification, structural aspects arising out of cation distribution, microscopic view on the different possible magnetic interaction present and the conduction mechanism of ferrite to explain their transport properties.

In chapter III, experimental procedures adopted during the course of the work were explained. The details of the sample preparation was mentioned. Different techniques like XRD, permeability measurement including its frequency characteristics, low field hysteresis, magnetization measurement (DC and AC) and the details of DC and AC resistivity and Dielectric constant were discussed in detail.

Chapter IV deals with the detailed results and discussion on Cd doped CoFe_2O_4 . The motivation was to see the effects of substitution of Cd^{2+} in place of Co^{2+} ions (in the range $x=0 - 1.0$) on the structural, magnetic and transport properties.

The structural analysis was done on sintered samples from XRD studies. All the

samples show well defined diffraction lines characteristic of single-phase cubic spinel structure. The lattice parameter, a increases linearly with Cd content, the Cd having larger ionic radius than that of Co^{2+} ion. The " a " for the end members CoFe_2O_4 and CdFe_2O_4 matches very well with the literature value.

The magnetic property of the samples was determined by measuring the temperature and the frequency dependence of initial permeability for the toroid shaped samples. It was observed that permeability increases with the increase of Cd content and falls sharply at the Curie point. It has been observed that Curie temp. decreases linearly with Cd content till $x=0.7$. The linear decrease in Curie temp. was explained qualitatively by considering the fact that Cd^{2+} ion replaces Fe^{3+} ion in the A site, thereby reducing the strength of the A-B exchange interaction. It was also pointed out that lattice parameter increases as Cd concentration is increased; consequently, the distance between the magnetic ions increases. The reason for the increase of permeability with the increase of non-magnetic Cd content was explained either due to increase of magnetic moment and/or simultaneous reduction in the anisotropy constant K_1 . Though it was shown that magnetization really increases for samples up to $x=0.4$, this explanation need clarification during viva examination.

Frequency dependence of the permeability at room temperature was also measured. μ for $x=0-0.3$ remains fairly constant up to 10 MHz, while for $x=0.4-0.6$, it remains constant up to 3 MHz. Dispersion behaviour related to permeability was explained using different mechanism having different time constant. Variation of permeability with sintering temperature was also analyzed.

Low field B-H loop at room temperature reveals that coercivity decreases linearly with Cd content up to $x=0.6$. In summary, the hysteresis curve and the permeability reveal softer nature of the ferromagnetic behaviour because of addition Cd^{2+} ions.

Magnetization at 5 K for samples $0 < x < 0.7$ increases sharply at very low field corresponding to magnetic domain reorientation and then goes on to saturation. It is also observed that saturation magnetization increases with Cd content up to $x=0.4$ and decreases beyond 0.4 concentration. The explanation for increase of magnetization using the idea of preferential occupation of A sites by Cd^{2+} ion displacing equal number of Fe^{3+} ion from A site to B site seems logical. The decrease of magnetization for samples with $x > 0.5$, is explained due to non-collinear spin structure in the B sites. Y-K angles have also been calculated and the large values indicate a departure from Neel's collinear model.

In chapter V, results in $\text{Co}_{1-x}\text{Zn}_x\text{Fe}_2\text{O}_4$ ($x=0.0-1.00$) have been presented. Single phase spinel structure was confirmed from XRD studies. Linear increase of lattice parameter and decrease of Curie temperature with addition Zn^{2+} ion were observed. Initial permeability also increases up to $x=0.5$. Softer ferromagnetic nature was established from the observation of decreasing trend of the coercivity in the B-H loop as Zn^{2+} content increases. Saturation magnetization and magnetic moment also show increment with Zn content up to $x < 0.5$. All these features are more or less similar to that found in Cd doped system. Thus essentially, Cd and Zn doped samples show softer ferromagnetic properties with high resistivity.

In chapter VI, results of low field magnetisation in FC and ZFC condition, magnetic hysteresis at low temperature, frequency dependent AC susceptibility in $\text{Co}_{1-x}\text{Cd}_x\text{Fe}_2\text{O}_4$ and

$\text{Co}_{1-x}\text{Zn}_x\text{Fe}_2\text{O}_4$ with $x = 0.7, 0.8, 0.9$ and 1.0 have been reported. For $x = 0.7$ and 0.8 , the sequence of PM-FM-RSG phase transition was demonstrated with ample evidence and careful understanding. Whereas, in $x = 0.9$ and 1.0 , evidence of SG behaviour was revealed from frequency dependent AC susceptibility. Manifestation of non equilibrium dynamics of the spin glass such as aging, rejuvenation and memory effects observed in these two samples clearly signifies the PM-SG behaviour. Thus a complete phase diagram was achieved. However, a curve should have been illustrated.

Chapter VII, deals with the results on rare-earth doped system. Though, a single phase compound was not achieved in all cases, some interesting results have been obtained.

The thesis ends up with the chapter on conclusion. Details of the references have also been listed.

Recommendation:

Considering the overall presentation and the volume of work, results and analysis of the data, **I have no hesitation to recommend that the candidate Ms. Saaout Noor would be awarded for Ph. D degree of the university.**

Aghoshray

Prof. Amitabha Ghoshray
ECMP Division
Saha Institute of Nuclear Physics
1/AF, Bidhannagar, Kolkata 700064
India

Prof. A. GhoshRay
E.C.M.P. Division
Saha Institute of Nuclear Physics
1/AF, Bidhannagar, Kolkata-700 064
INDIA

Acknowledgements

It gives me immense pleasure and satisfaction to acknowledge the blessings of the Almighty Allah, the creator of the universe who is the most gracious, compassionate and beneficent to His creature, who blessed me with knowledge and potential to implement my research work.

I express, with due respect, my deep sense of sincere gratitude and indebtedness to my supervisor Professor Dr. Shibendra Shekher Sikder, Department of Physics, Khulna University of Engineering & Technology (KUET) for his indispensable guidance, keen interest, constructive suggestions, fruitful discussion and constant inspiration throughout the research work.

I am very much indebted to my Joint Supervisor Engineer Dr. A. K. M. Abdul Hakim, Director, Planning & Development Division, Bangladesh Atomic Energy Commission, Dhaka for introducing the present research topic and for inspiring guidance and valuable suggestion throughout this research work. It would have not been possible for me to bring out this thesis without his help and constant encouragement.

I would like to express my gratitude to Professor Dr. Mahbub Alam, Department of Physics, Khulna University of Engineering & Technology (KUET) for his co-operation in one way or the other. I wish to record my thanks and gratitude to him for his valuable suggestions and encouragements at various stages of the work.

I am also grateful to Dr. D. K. Saha, Chief Scientific Officer, Materials Science Division, Atomic Energy Centre, Dhaka for his generous help in doing measurements and analysis of XRD results and whose vast knowledge in the field of science has enlightened me of this research work.

I am deeply grateful to Shireen Akhter, Head and Chief Scientific Officer, Materials Science Division, Atomic Energy Centre, Dhaka, for her interest and encouragement for my thesis. I am also thankful to Dr. Sk. Manjura Hoque, Principal Scientific Officer, Materials Science Division, Atomic Energy Centre, Dhaka for her help and co-operation.

I am grateful to Mr. Md. Nazrul Islam Khan, Mr. H. N. Das and Mr. M. A. Mamun, Scientific Officer, Materials Science Division, Atomic Energy Centre, Dhaka, for providing me with technical assistance from time to time during my research work.

I express my sincere gratitude to Professor Per Nordblad for his enormous assistance and kind supervision during the period of research work at Ångström Laboratory. I am also grateful to Professor Peter Svedlindh for his kind help during the experimental work.

I am really indebted to assistant Professor Roland Mathieu for his sincere help and co-operation during my research work. I also gratefully acknowledge of Ph.D. Students Matthias Hudl and Magnus Wikberg the assistance and heartfelt co-operation during my experimental work.

I express my gratefulness to the International Programme in Physical Sciences (IPPS), Uppsala University, Sweden for the financial support through a fellowship to conduct this research work in Sweden. I deeply appreciate Professor Ernst Van Groningen, Director IPPS for his kind co-operation and his positive attitude in every aspect.

I express my deepest sense of gratitude to Szuzanna Kristofi, Elizabeth Johannesson, Pravina Gajjar, Dr. Hossein Aminaey and others of IPPS for their “always ready to help” attitude and their ever smiling face to solve any problem to make my stay comfortable in Uppsala, Sweden.

I would like to express my immense thanks and gratitude to the Condensed Matter Physics Division, Saha Institute of Nuclear Physics, Kolkata, India for providing me the Low temperature magnetization measurement support.

I gratefully acknowledge Mr. Abdullah Elleas Akter, and Dr. Mrs. Jolly Sultana, Associate Professor, Department of Physics, KUET, for their co-operation and inspiration during this work.

I sincerely thank to Professor Dr. M. Manjurul Haque, Department of Applied Physics, Islamic University, Kushtia and Dr. Md. Sultan Mahmud, Associate Professor, Department of Physics, University of the Asia Pacific, Dhaka for their useful suggestions and help to carry out my research work.

I am very much grateful to Dr. Mihir Kanti Majumder, Secretary, Rural Development & Co-operative Division, Ministry of LGRD & Co-operatives, Bangladesh, Advocate S. M. Amzad Hossen, Ex. Education Minister, Ministry of Education, Bangladesh, Professor Mahfuza Begum, Directorate of Secondary and Higher Education, Bangladesh, Dhaka and Professor Minati Rani Mondal, Principal, Govt. Pioneer Mohila College, Khulna for their wise suggestions during this work.

I am really grateful to Mr. Saiduzzaman, Mr. Robiul Islam, Mr. Zakir Hossen Khan, Mr. Siba Pada Mondal, Ms. S. Akther and all other post graduate students of our group and friends for their fruitful co-operation.

I am thankful to Ms. Alhamra Parveen, Ms. Anjuman Ara Begum, Ms. Nazmunahar Begum, Mr. Mohsin, Mr. Mostafizur Rahman, Mr. Ferozur Rahman and Ms. Halima Sadia of Materials Science Division, AECD for their constant help during my research work.

I would like to thank my younger sister Shahi Noor (Nipa) and other family members, brother, Uncle Ashraf Uddin Ahmed, Aunt Hamida Ashraf for their support and love which has been a constant source of strength for everything I do.

My thanks are due to Director, Atomic Energy Centre, Dhaka for his kind permission to use the Laboratory of Magnetic Material Division, Atomic Energy Center, Dhaka.

I also wish to thank the authority of Khulna University of Engineering & Technology (KUET) for providing me with the necessary permission and financial assistance for conducting this thesis work.

Saroout Noor

Abstract

A detailed study was carried out on four different series of spinel Co-based ferrites, with composition $\text{Co}_{1-x}\text{Cd}_x\text{Fe}_2\text{O}_4$ and $\text{Co}_{1-x}\text{Zn}_x\text{Fe}_2\text{O}_4$ (where $x = 0.0 - 1.0$ in steps of 0.1), rare-earth (RE) substituted diluted system $\text{Co}_{0.2}\text{Cd}_{0.8}\text{Fe}_{2-x}\text{RE}_x\text{O}_4$ (RE = Ho and Sm; $x = 0.05, 0.1$) and $\text{Co}_{0.2}\text{Zn}_{0.8}\text{Fe}_{2-x}\text{RE}_x\text{O}_4$ (RE = Gd and Eu; $x = 0.05, 0.1$). The samples were prepared by conventional double sintering ceramic technique and were found to be single-phase cubic spinel structure of Co-Cd and Co-Zn series by X-ray diffraction technique, while all rare-earth (RE) doped samples showed additional peaks other than spinel. The lattice constant of $\text{Co}_{1-x}\text{Cd}_x\text{Fe}_2\text{O}_4$ and $\text{Co}_{1-x}\text{Zn}_x\text{Fe}_2\text{O}_4$ ferrites increase linearly with the increase of Cd and Zn content, followed Vegard's law. Bulk density and X-ray density increases significantly with the increase of Cd and Zn content. Curie temperature, T_c decreases almost linearly with increasing x content up to $x = 0.7$.

Samples with $x > 0.8$ show paramagnetic characteristic at $T = 5\text{K}$ with no spontaneous magnetization that revealed through Arrot-Belov-Kouvel plots. The continuous decrease of T_c with the substitution of non-magnetic Cd and Zn in $\text{Co}_{1-x}\text{Cd}_x\text{Fe}_2\text{O}_4$ and $\text{Co}_{1-x}\text{Zn}_x\text{Fe}_2\text{O}_4$ system is attributed to progressive weakening of the strength of A-B intersublattice exchange interaction, J_{AB} . Small thermal Hysteresis of initial permeability, μ' is observed below T_c . Saturation magnetization, M_s and magnetic moment are observed to increase upto $x = 0.4 - 0.5$ and decrease thereafter due to the spin canting in B-sites. The change of saturation magnetization with the increase of Cd/Zn substitution has been explained on the basis of Neel's collinear two-sublattice magnetization model and Yafet-Kittel's non-collinear magnetization model. The initial permeability is found to increase with the increase of Cd^{2+} and Zn^{2+} ions upto $x = 0.6$.

Temperature dependence of low field DC magnetization in the field-cooled and zero-field cooled conditions are performed for the dilute $\text{Co}_{1-x}\text{Cd}_x\text{Fe}_2\text{O}_4$ and $\text{Co}_{1-x}\text{Zn}_x\text{Fe}_2\text{O}_4$ ($x = 0.7, 0.8, 0.9, 1.0$) spinel ferrites. Samples with $x = 0.7$ and $x = 0.8$ show re-entrant spin-glass behavior while the samples, $x = 0.9$ and $x = 1$ show the spin-glass behavior. Frequency dependent complex AC susceptibility measurement as a function of temperature as the samples CdFe_2O_4 and ZnFe_2O_4 indicates a spin-glass behavior with the manifestation of shift of spin freezing temperature. The samples also show a typical spin-glass behavior with a manifestation of non-equilibrium dynamics, such as aging, rejuvenation, and memory effects.

Large magnetic hysteresis effect has been observed at low temperature for the diluted ferrite compositions. Low field B-H loops, at room temperature, were measured at constant frequency. The hysteresis behavior of $\text{Co}_{1-x}\text{Cd}_x\text{Fe}_2\text{O}_4$ and $\text{Co}_{1-x}\text{Zn}_x\text{Fe}_2\text{O}_4$ reveals the softer ferromagnetic

nature of the studied materials with the increase of Cd and Zn content. DC electrical resistivity increases significantly with the increase of Cd and Zn content. The AC resistivity and dielectric constant, ϵ' , of the samples are found to decrease with increasing frequency, exhibiting normal ferrimagnetic behavior. Dielectric constant, ϵ' , decreases rapidly with the increase in frequency at lower frequencies and slowly at higher frequencies, which may be due to the Maxwell-Wagner interfacial polarization. The variation of electrical and dielectric properties is explained on the basis of $\text{Fe}^{2+}/\text{Fe}^{3+}$ ionic concentration as well as the electronic hopping frequency between Fe^{2+} and Fe^{3+} ions.

Rare-earth (RE) doping of Ho^{3+} and Sm^{3+} in $\text{Co}_{0.2}\text{Cd}_{0.8}\text{Fe}_{2-x}\text{RE}_x\text{O}_4$ ferrite shows some anomalous behavior. A minority second ferromagnetic phase having well defined T_c has been detected Ho^{3+} doped sample, where T_c is found to increase with Ho^{3+} content. This ferromagnetic phase may be assigned as ferromagnetic cluster containing Ho^{3+} . Magnetization is found to increase with Ho^{3+} addition having higher magnetization for higher Ho^{3+} content while Sm^{3+} addition reduces magnetization. The decrease of magnetization with Sm^{3+} substitution for Fe^{3+} may be explained as due to lower free ion magnetic moment of Sm^{3+} . Samples $\text{Co}_{0.2}\text{Zn}_{0.8}\text{Fe}_{2-x}\text{RE}_x\text{O}_4$ (RE = Gd and Eu) show substantial increase of magnetization with Gd^{3+} which attains higher value with higher content of Gd^{3+} while decreasing with Eu^{3+} doped sample. The decrease of magnetization for Eu^{3+} doping is due to nonmagnetic nature of Eu which has no magnetic moment of the free Eu^{3+} ion even at low temperature.

List of the Symbols Used

Absolute value of admittance	$ Y $
Absolute value of impedance	$ Z $
Angular frequency	ω
Antiferromagnetic	AFM
Arrot-Belov-Kouvel	ABK
Anisotropy constant	K_1
Bohr magneton	μ_B
Bragg's angle	θ
Bulk density	ρ_B
Charge of electron	e
Coercivity	H_c
Cross-sectional area of toroid	S
Curie temperature	T_c
DC resistivity	ρ_{dc}
Dielectric constant	ϵ'
Exchange integral	J
Exchange-coupling constant	J_{ij}
Face centered cubic	f c c
Field cooled	FC
Ferromagnetism	FM
Frequency	f
Grain size	D
Imaginary part of initial permeability	μ''
Impedance	Z
Inductance	L
Initial permeability	μ_i
Inter planner spacing	d
Lattice parameter	a
Local spin canting	LSC
Loss factor	$\tan \delta$
Magnetization	M

Magnetic field	H
Magnetic induction	B
Neel temperature	T_N
Nelson-Riley function	$F(\theta)$
Permeability in free space	μ_0
Porosity	P
Real part of initial permeability	μ'
Rear-earth	RE
Re-entrant spin-glass	RSG
Retentivity	Br
Resistance	R
Saturation magnetization	M_s
Saturation induction	B_s
Spin freezing temperature	T_f
Sintering temperature	T_s
Superconducting Quantum Interface Device	SQUID
Susceptibility	χ
X-ray density	ρ_x
X-ray diffraction	XRD
Yafet-Kittel	Y-K
Zero-field-cooled	ZFC
Wavelength	λ

Contents

Page No

Chapter-I : Introduction

1.1	Introduction	1
1.2	The Aim and Objectives of the Present Work	5
1.3	Reason for Choosing this Research Work	7
1.4	Findings of this Work	7
1.5	Review Work	8
1.6	Outline of the Thesis	13

Chapter-II : Theoretical Aspects

2.1	Introduction to Magnetism	14
2.1.1	Magnetic Materials	14
2.1.2	The Basis of Magnetism	14
2.1.3	Electron Spin	17
2.1.4	Magnetic Dipole	17
2.1.5	Magnetic Field	18
2.1.6	Magnetic moment	18
2.2	Magnetization Process	19
2.2.1	Magnetic Flux and Flux Density	19
2.2.2	Origin of Magnetic Moments	20
2.2.3	Magnetic Properties of Solid	21
2.2.4	Magnetic Domain and Domain Wall Motion	22
2.2.5	Magnetostatic or Demagnetization Energy	24
2.2.6	Magnetocrystalline Anisotropy Energy	25
2.2.7	Magnetostriction	25
2.2.8	Hysteresis	27
2.2.9	Magnetization and Temperature	29
2.2.10	Theory of Permeability	30
2.3	Types of Magnetism	31
2.3.1	Diamagnetism	32
2.3.2	Paramagnetism	32
2.3.3	Ferromagnetism	33
2.3.4	Antiferromagnetism	35
2.3.5	Ferrimagnetism	35
2.4	Classification of Ferrites	36
2.4.1	Soft Ferrite	36
2.4.2	Hard Ferrite	37
2.4.3	Cubic Ferrite of Spinel Type	37

2.5 Cation Distribution in Ferrites	39
2.5.1 Normal Spinel Structure	39
2.5.2 Inverse Spinel Structure	39
2.5.3 Intermediate Structure	39
2.6 Magnetic Exchange Interaction	40
2.6.1 Superexchange Interaction	41
2.6.2 Neel's Collinear Model of Ferrimagnetism	42
2.6.3 Non-collinear Model of Ferrimagnetism	43
2.6.4 Re-entrant Spin-Glass Behavior	43
2.6.5 Spin-Glass Behavior	43
2.7 Transport Properties	46
2.7.1 Conduction Mechanism in Ferrites	46
2.7.2 Hopping Model of Electrons	46

Chapter-III : Experimental

3.1 Sample Preparation	48
3.1.1 Composition of Ferrites	48
3.1.2 Sample Preparation Technique	48
3.1.2.1 Preparing a Mixture of Materials	49
3.1.2.2 Pre-firing the Mixture to form Ferrite at Wet Milling	49
3.1.2.3 Pre-sintering	49
3.1.2.4 Sintering	51
3.1.3 Method of Sample Preparation	53
3.1.3.1 Solid State Reaction Method	53
3.2 X-ray Diffraction (XRD) Technique	56
3.2.1 Different Parts of the PHILIPS X' Pert PRO XRD System	59
3.2.2 Interpretation of the XRD data	60
3.2.3 X-ray Density and Bulk Density	61
3.2.4 Porosity	61
3.3 Permeability Measurement	62
3.3.1 Curie Temperature	62
3.3.2 Measurement of Curie Temperature by Observing the Variation of Initial Permeability with Temperature	62
3.3.3 Permeability	64
3.3.4 Mechanisms of Permeability	65
3.3.5 Technique of Measurements of Permeability	66
3.3.6 Frequency Characteristic of Ferrite Samples	66
3.4 Low Field Hysteresisgraph	67
3.4.1 Measurement of an Initial B-H Curve	68
3.4.2 AC B-H Curve Measurement	69
3.4.3 Materials Geometry	69
3.4.4 Windings	71
3.4.5 DC Measurement	72

3.5	Magnetization measurement	75
3.5.1	SQUID Magnetometer	75
3.5.2	The Features of MPMS XL SQUID Magnetometer	80
3.5.2.1	Improvement Sensitivity	80
3.5.2.2	Extended Low Temperature Capability	81
3.5.2.3	Reciprocating Sample Measurement System	81
3.5.2.4	Continuous Low Temperature Control and Enhanced Thermometry	82
3.5.2.5	Configuration	82
3.5.2.6	Measurement Condition	83
3.6	Transport Property	83
3.6.1	DC and AC Resistivity	83
3.6.2	Dielectric Constant	85

Chapter-IV : Results and Discussion of $\text{Co}_{1-x}\text{Cd}_x\text{Fe}_2\text{O}_4$ Ferrites

4.0	Introduction	86
4.1	X-ray Diffraction (XRD)	87
4.1.1	Phase Analysis	87
4.1.2	Lattice Parameter	88
4.1.3	Density	89
4.2	Magnetic Properties	91
4.2.1	Temperature Dependence of Initial Permeability	91
4.2.2	Compositional Dependence of Curie Temperature	94
4.2.3	Frequency Dependence of Initial Permeability	95
4.2.4	Low Field B-H loop at Room Temperature	98
4.2.5	Magnetization Measurement	101
4.3	Electrical Transport Property	106
4.3.1	Compositional Dependence of DC Electrical Resistivity	106
4.3.2	Frequency Dependence of AC Resistivity	107
4.3.3	Frequency Dependence of Dielectric Constant	108
4.4	Summary	110

Chapter-V : Results and Discussion of $\text{Co}_{1-x}\text{Zn}_x\text{Fe}_2\text{O}_4$ Ferrites

5.0	Introduction	111
5.1	X-ray diffraction Analysis	112
5.1.1	Phase Analysis	112
5.1.2	Lattice Parameter	113
5.1.3	Density	114
5.2	Electromagnetic Properties	115
5.2.1	Temperature Dependence of Initial Permeability	115
5.2.2	Frequency Dependence of Initial Permeability	118
5.2.3	Low field B-H loop at Room Temperature	121

5.2.4	Magnetization Measurement	122
5.2.5	DC Electrical Resistivity	126
5.4	Summary	127

Chapter-VI : Results and Discussion of Dilute Ferrites

6.0	Introduction	128
6.1	Field-Cooled (M_{FC}) and Zero-Field-Cooled (M_{ZFC}) Magnetization	129
6.2	High field Hysteresis Behavior	138
6.3	Temperature and Frequency Dependence of Complex AC Susceptibility	142
6.4	Ageing, Rejuvenation and Memory Effects	145
6.5	Summary	147

Chapter-VII : Results and Discussion of Rare-earth Substitution in Diluted $Co_{0.2}M_{0.8}Fe_2O_4$ ($M = Zn, Cd$) Ferrites

7.0	Introduction	148
7.1	X-ray Diffraction (XRD)	149
7.2	Temperature Dependence of Magnetization (M_{ZFC} and M_{FC})	151
7.3	High field Magnetic Hysteresis	162
7.4	Summary	166

Chapter-VIII : Conclusion

References	169
------------	-----

List of publication and Presented paper in International and National Conferences/Seminars:

List of Figures

CHAPTER-II	Page No.
Fig. 2.1 Magnetic lines of a bar magnet.	16
Fig. 2.2 (a) Electron orbit around the nucleus (b) Electron spin.	17
Fig. 2.3 Rotation of orientation and increase in size of magnetic domains due to an externally applied field.	23
Fig. 2.4 The magnetization change from one direction to another one.	24
Fig. 2.5 Magnetic hysteresis loop.	27
Fig. 2.6 Typical M-T curve for magnetic material.	29
Fig. 2.7 Varieties of magnetic orderings (a) paramagnetic, (b) ferromagnetic, (c) ferrimagnetic, (d) antiferromagnetic and (e) superparamagnetic.	33
Fig. 2.8 The inverse susceptibility varies with temperature T for (a) paramagnetic, (b) ferromagnetic, (c) ferrimagnetic, (d) antiferromagnetic materials. T_N and T_c are Neel temperature and Curie temperature, respectively.	34
Fig. 2.9 Schematic of two subcells of a unit cell of the spinel structure, showing octahedral and tetrahedral sites.	38
Fig. 2.10 Three major types of superexchange interactions in spinel ferrites are as follows: J_{AB} , J_{BB} and J_{AA} . The small empty circle is A-site, the small solid circle is B-site, and the large empty circle is oxygen anion.	42
Fig. 2.11 Examples of (a) an unfrustrated and (b) a frustrated spin configuration.	45
 CHAPTER -III	
Fig. 3.1 Rubber-lined mill with stainless-steel balls.	54
Fig. 3.2 Hydraulic press used to make different shaped samples.	55
Fig. 3.3 Toroid and disk shape sample.	55
Fig. 3.4 Flowchart of Ferrite sample preparation.	56
Fig. 3.5 Bragg's diffraction pattern.	57
Fig. 3.6 Block diagram of the PHILIPS PW 3040 X' Pert PRO XRD system.	58
Fig. 3.7 Internal arrangement of a PHILIPS X'- Pert PRO X-ray diffractometer.	59
Fig. 3.8 Impedance analyzer (LCR meter) Model-Hewlett-Packard 4192A.	64
Fig. 3.9 B-H loop tracer.	67
Fig. 3.10 Schematic diagram of commercial hysteresisgraph.	68
Fig. 3.11 Sample geometry.	70
Fig. 3.12 DC measuring cable.	73
Fig. 3.13 The measuring and magnetizing connections are in the plastic tool inside the opening case.	74
Fig. 3.14 Hysteresis cycle.	74
Fig. 3.15 MPMS XL SQUID Magnetometer.	76
Fig. 3.16 Attaching the Sample to the Sample Rod.	78
Fig. 3.17 Illustration of an RSO measurement with very small amplitude. The large bold curve represents the ideal SQUID response to a dipole moving completely through the SQUID pickup coils.	79



CHAPTER -IV

Fig. 4.1	XRD patterns in $\text{Co}_{1-x}\text{Cd}_x\text{Fe}_2\text{O}_4$ ferrites with different Cd content.	87
Fig. 4.2	XRD patterns of CoFe_2O_4 ferrites.	88
Fig. 4.3	Variation of lattice constant 'a' as a function of Cd content (x) of $\text{Co}_{1-x}\text{Cd}_x\text{Fe}_2\text{O}_4$ ferrites.	89
Fig. 4.4	Variation of density with Cd content (x) of $\text{Co}_{1-x}\text{Cd}_x\text{Fe}_2\text{O}_4$ ferrites.	90
Fig. 4.5	Temperature dependence of real permeability, μ' of $\text{Co}_{1-x}\text{Cd}_x\text{Fe}_2\text{O}_4$ ferrites.	92
Fig. 4.6	Determination of Curie temperature from the temperature dependence of (a, b) μ' , μ'' and $d\mu'/dT$ as a function of temperature.	92
Fig. 4.7	Thermal Hysteresis of initial permeability (μ') for (a) $x = 0.0$ and (b) $x = 0.5$ of $\text{Co}_{1-x}\text{Cd}_x\text{Fe}_2\text{O}_4$ ferrites samples sintered at $1050^\circ\text{C}/3\text{hrs}$.	93
Fig. 4.8	Variation of Curie temperature, T_c with Cd content (x) of $\text{Co}_{1-x}\text{Cd}_x\text{Fe}_2\text{O}_4$ ferrites.	94
Fig. 4.9	Frequency dependence of the real part of the permeability, μ' and imaginary component, μ'' of $\text{Co}_{1-x}\text{Cd}_x\text{Fe}_2\text{O}_4$ ferrites sintered at 1050°C , 1075°C and 1100°C for 3hrs	96
Fig. 4.10	Variation of initial permeability, μ' at frequency 100 kHz with Cd content (x) of $\text{Co}_{1-x}\text{Cd}_x\text{Fe}_2\text{O}_4$ ferrites.	98
Fig. 4.11	Magnetic hysteresis graphs of $\text{Co}_{1-x}\text{Cd}_x\text{Fe}_2\text{O}_4$ ferrite sintered at 1050°C , 1075°C and 1100°C for 3 hours at constant frequency $f = 1\text{kHz}$.	99
Fig. 4.12	The coercivity, H_c and permeability, μ' versus composition x of $\text{Co}_{1-x}\text{Cd}_x\text{Fe}_2\text{O}_4$ ferrite with $x = 0-0.6$ rings sintered for $1050^\circ\text{C}/3\text{hr}$ at constant frequency $f = 1\text{kHz}$.	100
Fig. 4.13	Field dependence of magnetization for $x = 0.0 - 1.0$ of $\text{Co}_{1-x}\text{Cd}_x\text{Fe}_2\text{O}_4$ ferrites at temperature $T = 5\text{K}$.	102
Fig. 4.14	Saturation magnetization (M_s) of $\text{Co}_{1-x}\text{Cd}_x\text{Fe}_2\text{O}_4$ as a function of Cd content (x) at temperature, $T = 5\text{K}$.	103
Fig. 4.15	Variation of magnetic moment as a function of Cd content (x) of $\text{Co}_{1-x}\text{Cd}_x\text{Fe}_2\text{O}_4$ ferrites.	105
Fig. 4.16	Room temperature DC resistivity as a function of Cd content of $\text{Co}_{1-x}\text{Cd}_x\text{Fe}_2\text{O}_4$ ferrites.	106
Fig. 4.17	Frequency dependence of AC resistivity of $\text{Co}_{1-x}\text{Cd}_x\text{Fe}_2\text{O}_4$ ferrites sintered at $1050^\circ\text{C}/2\text{hrs}$.	107
Fig. 4.18	Dielectric constant as a function of frequency of the ferrite system $\text{Co}_{1-x}\text{Cd}_x\text{Fe}_2\text{O}_4$ ferrite sintered at $1050^\circ\text{C}/2\text{hrs}$.	108

CHAPTER -V

Fig. 5.1	XRD patterns of $\text{Co}_{1-x}\text{Zn}_x\text{Fe}_2\text{O}_4$ ferrite with different Zn content.	112
Fig. 5.2	Variation of lattice constant 'a' as a function of Zn content (x) of $\text{Co}_{1-x}\text{Zn}_x\text{Fe}_2\text{O}_4$ ferrites.	113
Fig. 5.3	Variation of density with Zn content(x) of $\text{Co}_{1-x}\text{Zn}_x\text{Fe}_2\text{O}_4$ ferrites.	114
Fig. 5.4	Temperature dependence of permeability, μ' of $\text{Co}_{1-x}\text{Zn}_x\text{Fe}_2\text{O}_4$ ferrites.	116
Fig. 5.5	Determination of Curie temperature from the temperature dependence of μ' , μ'' and $d\mu'/dT$ as a function of temperature of $\text{Co}_{1-x}\text{Zn}_x\text{Fe}_2\text{O}_4$ ferrites with $x = 0.4$.	117
Fig. 5.6	Variation of Curie temperature, T_c with Zn content (x) of $\text{Co}_{1-x}\text{Zn}_x\text{Fe}_2\text{O}_4$ ferrites.	117
Fig. 5.7	Frequency dependence of real part of permeability of $\text{Co}_{1-x}\text{Zn}_x\text{Fe}_2\text{O}_4$ ferrites sintered at (a) 1100°C and (b) 1150°C for 2 hours.	119

Fig. 5.8	Variation of initial permeability, μ' at frequency 100 kHz with Zn content (x) of $\text{Co}_{1-x}\text{Zn}_x\text{Fe}_2\text{O}_4$ ferrites sintered at temperature 1100° and 1150° for 2 hours.	120
Fig. 5.9	Magnetic hysteresis graphs of $\text{Co}_{1-x}\text{Zn}_x\text{Fe}_2\text{O}_4$ ferrite with x sintered at (a) 1100°C and (b) 1150°C for 2 hours at constant frequency $f = 1\text{ kHz}$.	121
Fig. 5.10	Field dependence of magnetization for $x = 0.0-1.0$ of $\text{Co}_{1-x}\text{Zn}_x\text{Fe}_2\text{O}_4$ ferrites at temperature $T = 5\text{ K}$.	123
Fig. 5.11	Saturation magnetization, M_s versus Zn content in $\text{Co}_{1-x}\text{Zn}_x\text{Fe}_2\text{O}_4$ ferrites.	124
Fig. 5.12	Variation of magnetic moment, n_B as a function of Zn content (x) of $\text{Co}_{1-x}\text{Zn}_x\text{Fe}_2\text{O}_4$ ferrites.	125
Fig. 5.13	Room temperature DC resistivity as a function of Zn content (x) $\text{Co}_{1-x}\text{Zn}_x\text{Fe}_2\text{O}_4$ ferrites.	126

CHAPTER -VI

Fig. 6.1	M_{ZFC} and M_{FC} curves of the sample (a) $\text{Co}_{0.3}\text{Cd}_{0.7}\text{Fe}_2\text{O}_4$ (b) $\text{Co}_{0.3}\text{Zn}_{0.7}\text{Fe}_2\text{O}_4$ with field $H = 50\text{ Oe}$.	130
Fig. 6.2 (a)	M_{ZFC} and M_{FC} Curves of the sample $\text{Co}_{0.2}\text{Cd}_{0.8}\text{Fe}_2\text{O}_4$ with applied field $H = 50-200\text{ Oe}$.	131
Fig. 6.2 (b)	Derivative of dM/dT as a function of temperature of the sample $\text{Co}_{0.2}\text{Cd}_{0.8}\text{Fe}_2\text{O}_4$ with applied field $H = 50\text{ Oe}$.	131
Fig. 6.2 (c)	ABK from $T = 5 -100\text{ K}$ with field $H = 50\text{ kOe}$ of $\text{Co}_{0.2}\text{Cd}_{0.8}\text{Fe}_2\text{O}_4$ ferrites.	132
Fig. 6.2 (d)	Inverse of susceptibility vs temperature curve of the sample $\text{Co}_{0.2}\text{Cd}_{0.8}\text{Fe}_2\text{O}_4$ with applied field $H = 50\text{ Oe}$.	132
Fig. 6.3 (a)	M_{ZFC} Curves of the sample $\text{Co}_{0.2}\text{Zn}_{0.8}\text{Fe}_2\text{O}_4$ with applied field $H = 50\text{ Oe}$.	133
Fig. 6.3 (b)	ABK plot from $T = 5 -100\text{ K}$ with field $H = 50\text{ kOe}$ of $\text{Co}_{0.2}\text{Zn}_{0.8}\text{Fe}_2\text{O}_4$ ferrites.	134
Fig. 6.3 (c)	Inverse of susceptibility vs temperature curve of the sample $\text{Co}_{0.2}\text{Zn}_{0.8}\text{Fe}_2\text{O}_4$ with applied field $H = 50\text{ Oe}$.	134
Fig. 6.4	M_{ZFC} and M_{FC} curves of the sample (a) $\text{Co}_{0.1}\text{Cd}_{0.9}\text{Fe}_2\text{O}_4$ (b) CdFe_2O_4 with applied field $H = 50\text{ Oe}$.	136
Fig. 6.5	M_{ZFC} and M_{FC} curves of the sample (a) $\text{Co}_{0.1}\text{Zn}_{0.9}\text{Fe}_2\text{O}_4$ (b) ZnFe_2O_4 with applied field $H = 50\text{ Oe}$.	136
Fig. 6.6	ABK plot from $T = 5\text{ K}$ with field $H = 50\text{ kOe}$ of (a) $\text{Co}_{0.1}\text{Cd}_{0.9}\text{Fe}_2\text{O}_4$ (b) CdFe_2O_4 ferrites.	137
Fig. 6.7	ABK plot from $T = 5\text{ K}$ with field $H = 50\text{ kOe}$ of (a) $\text{Co}_{0.1}\text{Zn}_{0.9}\text{Fe}_2\text{O}_4$ (b) ZnFe_2O_4 ferrites.	137
Fig. 6.8	Magnetic Phase diagram	138
Fig. 6.9	Magnetization hysteresis loops at $T = 5\text{ K}$ and 100 K with field $H = 50\text{ kOe}$ of the sample (a) $\text{Co}_{0.3}\text{Cd}_{0.7}\text{Fe}_2\text{O}_4$ (b) $\text{Co}_{0.3}\text{Zn}_{0.7}\text{Fe}_2\text{O}_4$. Inset at $T = 5\text{ K}$.	139
Fig. 6.10	Magnetization hysteresis loops at different temperatures between $T = 5\text{ K}-300\text{ K}$ with field 50 kOe of the sample (a) $\text{Co}_{0.2}\text{Cd}_{0.8}\text{Fe}_2\text{O}_4$. (b) $\text{Co}_{0.2}\text{Zn}_{0.8}\text{Fe}_2\text{O}_4$. Inset at $T = 5\text{ K}$.	140
Fig. 6.11	Magnetization hysteresis loops at different temperatures between $T = 5\text{ K}-50\text{ K}$ with field 50 kOe of the sample (a) $\text{Co}_{0.1}\text{Cd}_{0.9}\text{Fe}_2\text{O}_4$ (b) CdFe_2O_4 . Inset at $T = 5\text{ K}$.	140
Fig. 6.12	Magnetization hysteresis loops at different temperatures between $T = 5\text{ K}-50\text{ K}$ with field 50 kOe of the sample (a) $\text{Co}_{0.1}\text{Zn}_{0.9}\text{Fe}_2\text{O}_4$ (b) ZnFe_2O_4 (Inset: $T = 5\text{ K}$).	141

Fig. 6.13	The temperature dependence of the real part of AC susceptibility χ' measured at $\omega/2\pi = 1.7, 17$ and 170 Hz, respectively for (a) CdFe_2O_4 and (b) ZnFe_2O_4 ferrites.	143
Fig. 6.14	Variation of imaginary part of AC susceptibility with temperature for different frequencies of (a) CdFe_2O_4 and (b) ZnFe_2O_4 .	144
Fig. 6.15	FC and ZFC magnetizations superimposing ZFC curves with isothermal holding time at $T_g/T_f = 0.8$ for 3h of (a) CdFe_2O_4 and (b) ZnFe_2O_4 ferrites.	146

CHAPTER-VII

Fig. 7.1	XRD patterns of sample $\text{Co}_{0.2}\text{Cd}_{0.8}\text{Fe}_{2-x}\text{RE}_x\text{O}_4$ with (a) $\text{RE}=\text{Ho}$, $\text{RE} = \text{Sm}$ and sample $\text{Co}_{0.2}\text{Zn}_{0.8}\text{Fe}_{2-x}\text{RE}_x\text{O}_4$ with (c) $\text{RE} = \text{Gd}$, (d) $\text{RE} = \text{Eu}$ for ($x = 0.0, 0.05, 0.1$).	150
Fig. 7.2	M_{ZFC} Curves of the sample $\text{Co}_{0.2}\text{Cd}_{0.8}\text{Fe}_2\text{O}_4$ with applied field $H = 10 - 5000$ Oe. curves.	151
Fig. 7.3	M_{ZFC} and M_{FC} Curves of the sample $\text{Co}_{0.2}\text{Cd}_{0.8}\text{Fe}_2\text{O}_4$ with applied field $H = 500$ Oe. Inset: dM/dT curve.	152
Fig. 7.4	M_{ZFC} and M_{FC} curves of sample $\text{Co}_{0.2}\text{Cd}_{0.8}\text{Fe}_{2-x}\text{Ho}_x\text{O}_4$ (a) $x = 0.05$ (b) $x = 0.10$ with field $H = 50$ Oe.	154
Fig. 7.5	M_{ZFC} and M_{FC} curves of sample $\text{Co}_{0.2}\text{Cd}_{0.8}\text{Fe}_{2-x}\text{Ho}_x\text{O}_4$ (a) $x = 0.05$ with field ZFC 5000 Oe (b) $x = 0.10$ with field $H = 500$ Oe.	155
Fig. 7.6	The temperature dependence of AC susceptibility measured at $\omega/2\pi = 1.7, 17$ and 170 Hz respectively for (a) the real $\chi'(T)$ part and (b) imaginary $\chi''(T)$ part of $\text{Co}_{0.2}\text{Cd}_{0.8}\text{Fe}_{1.95}\text{Ho}_{0.05}\text{O}_4$ ferrites.	156
Fig. 7.7	The temperature dependence of AC susceptibility measured at $\omega/2\pi = 1.7, 17$ and 170 Hz respectively for (a) the real $\chi'(T)$ part and (b) imaginary $\chi''(T)$ part of $\text{Co}_{0.2}\text{Cd}_{0.8}\text{Fe}_{1.9}\text{Ho}_{0.1}\text{O}_4$ ferrites.	157
Fig. 7.8	M_{ZFC} and M_{FC} curves of sample $\text{Co}_{0.2}\text{Cd}_{0.8}\text{Fe}_{2-x}\text{RE}_x\text{O}_4$; $\text{RE} = \text{Sm}$ (a) $x = 0.05$ (b) $x = 0.10$ with field $H = 50$ Oe.	158
Fig. 7.9	M_{ZFC} and M_{FC} curves of sample $\text{Co}_{0.2}\text{Cd}_{0.8}\text{Fe}_{2-x}\text{Sm}_x\text{O}_4$ (a) $x = 0.05$ with field $H = 5000$ Oe (b) $x = 0.10$ with field $H = 500$ Oe	159
Fig. 7.10	M_{ZFC} and M_{FC} curves of sample $\text{Co}_{0.2}\text{Zn}_{0.8}\text{Fe}_{2-x}\text{Gd}_x\text{O}_4$ $x = 0.05$ (b) $x = 0.10$ with field $H = 50$ Oe.	160
Fig. 7.11	M_{ZFC} and M_{FC} curves of sample $\text{Co}_{0.2}\text{Zn}_{0.8}\text{Fe}_{2-x}\text{Gd}_x\text{O}_4$ (a) $x = 0.05$ (b) $x = 0.10$ with field $H = 500$ Oe.	161
Fig. 7.12	Magnetization hysteresis loops of sample $\text{Co}_{0.2}\text{Cd}_{0.8}\text{Fe}_{2-x}\text{Ho}_x\text{O}_4$ (a) $x = 0.05$ (b) $x = 0.1$ at different temperatures $5\text{K}-300\text{K}$ with field $H = 50$ kOe.	163
Fig. 7.13	Magnetization hysteresis loops of sample $\text{Co}_{0.2}\text{Cd}_{0.8}\text{Fe}_{2-x}\text{Sm}_x\text{O}_4$ (a) $x = 0.05$ and (b) $x = 0.1$ at different temperatures $5\text{K}-300\text{K}$ with field $H = 50$ kOe.	163
Fig. 7.14	Magnetization hysteresis loops of sample $\text{Co}_{0.2}\text{Zn}_{0.8}\text{Fe}_{2-x}\text{Gd}_x\text{O}_4$ (a) $x = 0.05$ and (b) $x = 0.1$ at different temperatures $5\text{K}-300\text{K}$ with field $H = 50$ kOe.	164
Fig. 7.15	Magnetization hysteresis loops of sample $\text{Co}_{0.2}\text{Zn}_{0.8}\text{Fe}_{2-x}\text{Eu}_x\text{O}_4$ (a) $x = 0.05$ (b) $x = 0.1$ at different temperatures $5\text{K}-300\text{K}$ with field $H = 50$ kOe.	164

List of Tables

	Page No.
Table 2.1 Curie temperature of selected materials.	30
Table 4.1 Data of the lattice parameter (a), X-ray density (ρ_x), bulk density (ρ_B), porosity (P%), Curie temperature (T_c), permeability (μ') at frequency 100 kHz and DC resistivity (ρ_{dc}) of $Co_{1-x}Cd_xFe_2O_4$ samples sintered at 1050°C /3hrs.	91
Table 4.2 Data of the coercivity (H_c), retentivity (B_r), saturation induction (B_s), B_r/B_s ratio and losses of $Co_{1-x}Cd_xFe_2O_4$ ferrite with $x = 0 - 0.7$ rings sintered for 1050°C, 1075°C and 1100°C for 3 hours at constant frequency $f = 1k$ Hz.	101
Table 4.3 Data of saturation magnetization (M_s), theoretical and experimental magnetic moment (n_B) and Yafet-Kittel angle (α_{Y-K}).	105
Table 5.1 Lattice parameter (a), X-ray density (ρ_x), bulk density (ρ_B), porosity (P%) of sintered $Co_{1-x}Zn_xFe_2O_4$ ferrite with different Zn content.	115
Table 5.2 Data of the Curie temperature (T_c), permeability (μ') at frequency 100 KHz sintered at 1100°C and 1150°C for 2hrs and dc resistivity (ρ_{dc}) at room temperature, of $Co_{1-x}Zn_xFe_2O_4$ samples.	120
Table 5.3 The calculated values of coercive force (H_c), remanence induction (B_r), saturation induction (B_s), B_r/B_s ratio and losses of $Co_{1-x}Zn_xFe_2O_4$ samples at room temperature with constant frequency ($f = 1kHz$) at different temperature.	122
Table 5.4 Data of saturation magnetization (M_s), theoretical and experimental magnetic moment (n_B) and Yafet-Kittel angle (α_{Y-K}) of $Co_{1-x}Zn_xFe_2O_4$ ferrites at temperature $T = 5K$.	124
Table 6.1 Data of the spin freezing temperature (T_f), coercive force (H_c) at $T = 5K$ of $Co_{1-x}Cd_xFe_2O_4$ and $Co_{1-x}Zn_xFe_2O_4$ ferrites (with $x = 0.7 - 1.0$).	141
Table 7.1 The hysteresis parameters such as magnetization (M) at $H = 50$ kOe, and Coercive field H_c at different temperature $T = 5 - 300$ K.	165

CHAPTER-I
Introduction

Introduction

1.1 Introduction

The history of ferrites began centuries before the birth of Christ with the discovery of stones that attract iron. The most abundant deposits of these stones were found in the district of Magnesia in Asia Minor, and hence the name of the materials becomes magnetite, Fe_3O_4 (or $\text{FeO} \cdot \text{Fe}_2\text{O}_3$). Ferrites fall in to the category of ferrimagnetic materials. The term ferrites mean certain double oxide of iron and another metal, which have two unequal sublattices and are ordered anti parallel to each other. Each sublattice exhibits spontaneous magnetization at room temperature, like the ferrimagnetic. Ferrites are the ferrimagnetic mixed oxides having the general formula MFe_2O_4 where M is a divalent metal ion such as Mg, Mn, Zn, Ni, Co, Fe, Cd and Cu. Owing to their important electrical and magnetic properties, ferrites are extensively used in electronic industry.

Spinel ferrites commanded the attention first when S. Hilpert [1.1] focused on the usefulness of ferrites at high frequency applications. The ferrites were developed into commercially important materials, chiefly during the years 1933 - 1945 by Snoek [1.2] and his associates at the Philips Research Laboratories in Holland. At the same time, Takai [1.3] in Japan was engaged in the research work on the ferrite materials. In a classical paper published in 1948 by Neel [1.4] provided the theoretical key to an understanding of the ferrites. The subject has been covered at length in books by Smit. [1.5] and Standley [1.6] and reviewed by Smart [1.7], Wolf [1.8], and Gorter [1.9]. Snoek had laid the foundation of the physics and technology of practical ferrites by 1945 and now embrace a very wide diversity of compositions, properties and applications [1.10]. Technological advances in a variety of areas have generated a growing demand for the soft magnetic materials in devices. Among the soft magnetic materials, polycrystalline ferrites have received special attention due to their good magnetic properties and high electrical resistivity over a wide range of frequencies; starting from a few hundred Hz to several GHz. Spinel type ferrites are commonly used in many electronic and magnetic devices due to their high magnetic permeability and low magnetic losses [1.11, 1.12]. They are also used in electrode materials for high temperature applications because of their high thermodynamic stability, electrical resistivity, electrolytic activity and resistance to corrosion [1.13, 1.14].

Moreover, these low cost materials are easy to synthesize and offer the advantages of greater shape formability than their metal and amorphous magnetic counterparts. Almost every item of electronic equipment produced today contains some ferrimagnetic spinel ferrite materials. Loudspeakers, motors, deflection yokes, electromagnetic interference suppressors, radar absorbers, antenna rods, proximity sensors, humidity sensors, memory devices, recording heads, broadband transformers, filters, inductors etc. are frequently based on ferrites. Ferromagnetic materials are defined as one which below a transition temperature exhibits a spontaneous magnetization that arises from non parallel arrangement of the strongly coupled magnetic moments.

Ferrites are ferrimagnetic cubic spinels that possess the combined properties of magnetic materials and insulators. They have been extensively investigated and become the subject of great interest because of their importance in many technological applications from both the fundamental and the applied research point of view. The important structural, electrical and magnetic properties of these spinels are responsible for their applications in various fields. The spinel ferrite belongs to an important class of magnetic materials because of their remarkable magnetic properties, particularly in radio frequency region, physical flexibility, high electrical resistivity, mechanical hardness and chemical stability [1.15 - 1.17].

Ferrites exhibit a substantial spontaneous magnetization at room temperature, like the normal ferromagnetic. They have two unequal sub-lattices called tetrahedral (A-site) and octahedral (B-site) and are ordered antiparallel to each other. In ferrites, the cations occupy the tetrahedral A-site and octahedral B-site of the cubic spinel lattice and experience competing nearest neighbor (J_{AB}) and the next nearest neighbor (J_{AA} and J_{BB}) interactions with $|J_{AB}| \gg |J_{BB}| > |J_{AA}|$. The magnetic properties of ferrites are dependent on the type of magnetic ions residing on the A and B sites and the relative strengths of the inter (J_{AB}) and intrasublattice (J_{BB} , J_{AA}) interactions. When the J_{AB} is much stronger than J_{BB} and J_{AA} interactions, the magnetic spins have a collinear structure in which the magnetic moments on the A sublattice are antiparallel to the moments on the B sublattice. But when J_{BB} or J_{AA} becomes comparable with J_{AB} , it may lead to non-collinear spin structure [1.18]. When magnetic dilution of the sublattices is introduced by substituting nonmagnetic ions in the lattice, frustration and/ or disorder occurs leading to collapse of the collinearity of the ferromagnetic phase by local spin canting exhibiting a wide spectrum of magnetic ordering e.g. antiferromagnetic, ferrimagnetic, re-entrant spin-glass, spin-glass, cluster spin-glass properties [1.19, 1.20]. Small amount of site disorder i.e. cations redistribution between

A and B site is sufficient to change the super-exchange interactions which are strongly dependent on thermal history i.e. on sintering temperature, time and atmosphere as well as heating/ cooling rates during materials preparation.

Co-ferrite is considered as a potential magnetic material due to its high electrical resistivity, high Curie temperature, low cost and high mechanical hardness. CoFe_2O_4 is generally an almost inverse ferrite in which Co^{2+} ions mainly occupies B-sites and Fe^{3+} ions are distributed almost equally between A and B sites. It has been demonstrated that the inversion is not complete in CoFe_2O_4 and the degree of inversion sensitively depends on the thermal treatment and method of preparation condition [1.21], Co-ferrite is known to have a large cubic magnetocrystalline anisotropy ($K_1 = +2 \times 10^6 \text{ erg/cm}^3$) [1.22] due to the presence of Co^{2+} ions on B-sites. It is well-known that Co-ferrite is a hard magnetic material due to its high coercivity (5.40 kOe) and moderate saturation magnetization (80 emu/g) as well as its remarkable chemical stability and mechanical hardness [1.23]. It is therefore a good candidate for use in isotropic permanent magnets, magnetic recording media and magnetic fluids. Co-ferrite crystallizes in partially inverse spinel structure are represented as $(\text{Co}_x^{2+} \text{Fe}_{1-x}^{3+})_A [\text{Co}_{1-x}^{2+} \text{Fe}_{1+x}^{3+}]_B \text{O}_4$, where x depends on thermal history and preparation conditions [1.24, 1.25]. It is ferromagnetic with Curie temperature, T_c around 520°C [1.26] which suggests that the magnetic interaction in these ferrites is very strong and show a relative large magnetic hysteresis which distinguishes it from the rest of spinel ferrites. CdFe_2O_4 and ZnFe_2O_4 are generally assumed to be normal spinel with all Fe^{3+} ions on B-sites and all Cd^{2+} and Zn^{2+} ions on A-sites [1.27, 1.28].

The magnetic properties of ferrites such as permeability, magnetization, coercive field, Curie temperature are affected by composition as well as by the type of substitution, cation distribution and method of preparation [1.29]. Globus *et.al.* [1.30] studied the size effect of nonmagnetic ions Cd and Zn on the magnetic properties of Ni-ferrites. It was concluded that the variation of magnetic properties results from the ion concentration as well as difference in ionic radius. The variation of magnetization for Cu-Cd ferrite system with Cd concentration indicated the existence of Y-K type of magnetic ordering in the mixed ferrite [1.30, 1.31]. Such a result has been confirmed for different ferrites [1.32]. Zn substituted spinel ferrites showed good magnetic properties which are characterized by a maximum in saturation magnetization in certain composition [1.33 - 1.35]. The partial replacement of nonmagnetic Cd ions in cobalt ferrite is expected to weaken the magnetic coupling resulting in decrease of Curie temperature. A little works were found on mixed Co-Cd ferrites [1.36, 1.37].

Co-Zn ferrites are quite important in the field of microwave industry which is a mixture of CoFe_2O_4 with long range ferromagnetic ordering with $T_c \approx 520^\circ\text{C}$ and ZnFe_2O_4 with antiferromagnetic ordering having Neel temperature $T_N \approx 9\text{K}$. Zinc is known to play a decisive role in determining the ferrite properties [1.38]. Zn-ferrite is normal ferrite while Co-ferrite is an inverse ferrite; therefore, Co-Zn ferrite is a mixed type with interesting properties. When Co^{2+} is replaced by Zn^{2+} in $\text{Co}_{1-x}\text{Zn}_x\text{Fe}_2\text{O}_4$, Zn^{2+} ions preferentially occupies the tetrahedral site and the Fe^{3+} ions are displaced to the octahedral sites. Thus, with increasing x , the $\text{Fe}_A\text{-O-Fe}_B$ interaction becomes weak and T_c is expected to decrease.

A selective magnetic dilution is very important in ferrites. The nonmagnetic ions such as Zn^{2+} and Cd^{2+} ions that can be used in such dilution should have ionic radius comparable with that of the magnetic ions. It is well known that diamagnetic substitution can result in spin canting, i.e. non-collinear spin arrangements [1.39 - 1.42]. Yafet and Kittel [1.43] formulated a simple model, which could explain the canting in these materials. The possibility of continuously changing the concentration of nonmagnetic zinc ions in the MgFe_2O_4 ferrite causes dilute Mg-Zn ferrite system. When ferrites are sufficiently diluted with nonmagnetic ions (such as Zn or Cd) they can exhibit a wide spectrum of magnetic orderings: ferromagnetism (FM), local spin canting (LSC), antiferromagnetism (AFM), re-entrant spin glass (RSG), and spin-glass (SG) [1.39, 1.40, 1.44]. This is because the spinel ferrites intra-sublattice interactions are weaker than the inter-sublattice interaction; as a result there are unsatisfied bonds in the ferromagnetic phase. Due to these unsatisfied bonds, increasing the magnetic dilution accentuates the competition between the various exchange interactions resulting in a variety of magnetic structures [1.36, 1.40, 1.41].

A phase diagram has been proposed by J. L. Dormann *et. al.* [1.39] to classify the different substituted ferrite compounds. Frustration [1.45] and randomness are necessary to obtain such types of magnetic phases and are evidently present in substituted ferrites. A spin-glass is a magnetically disordered material exhibiting high magnetic frustration in which each electron spin freezes in a random direction below the spin freezing temperature, T_f [1.46]. The most important features characterizing the spin-glass include the existence of irreversibility between field-cooled (FC) and zero-field-cooled (ZFC) magnetizations. Some works have been performed on Co-Zn [1.47], Co-Ti-Zn [1.48], Co-Cd [1.49, 1.50] Co-Cr [1.51], Co-In [1.52] ferrites. The effects of substitution of Zn^{2+} and Cd^{2+} ions in place of Co^{2+} ions covering a wide range of concentration on the structural, magnetic and electrical properties of Co-Zn (Cd) ferrites.

The rare-earth oxides are found recently to exhibit important modifications for the improvement of the properties of ferrites. Rare-earth (RE) element having large magnetic moments, large magnetocrystalline anisotropy and magnetostriction at low temperature due to their 4f orbital totally screened by 5s and 5p orbital plays an important role in deciding the electrical and magnetic properties of the ferrites since it interacts with 3d electrons of transition metals [1.53]. RE³⁺ ions possess a variety of magnetic properties [1.54]:

- (i) their magnetic momentum vary from 0 (La³⁺) to 10.5 (Dy³⁺) and
- (ii) they can be isotopic in relation to the variation in the f-electron orbital contribution to magnetic interactions.

This is for instance minimal in Ho³⁺ (4f¹⁰), Gd³⁺ (4f⁷) and maximal in Sm³⁺ (4f⁶), Eu³⁺ (4f⁶) cations. A lot of serious works reported phase segregation and diffusion of the RE species to the grain boundaries even for very low RE content, causing the precipitation of extra amorphous or crystalline phases like orthoferrites (REFeO₃) [1.55, 1.56]. In this work another attempt was taken to substitute trivalent Fe³⁺ ions by trivalent RE cations in the composition Co_{0.2}M_{0.8}RE_xFe_{2-x}O₄ (where M= Cd/Zn, RE = Ho³⁺, Sm³⁺, Gd³⁺, Eu³⁺ and x = 0.0, 0.05 and 0.1) to study their magnetic and transport properties. Substitution of RE³⁺ in place of Fe³⁺ ion in the octahedral site is expected to show interesting electromagnetic properties.

1.2 The Aim and Objectives of the Present Work

CoFe₂O₄ is an important technical material because of its specific hard magnetic properties which other spinel ferrites do not have. Again CoFe₂O₄ is a good magnetostrictive material suitable for use in transducer which has been observed recently. Also it is a good inductor material for ultra high frequency application when suitable additives/dopants are incorporated.

The objective of the present work is to study the effect of nonmagnetic additives such as Zn and Cd to the basic CoFe₂O₄ with extended concentration of Zn/Cd up to pure ZnFe₂O₄ and CdFe₂O₄ on the detail structural, magnetic and electrical properties of the whole series and particularly with extreme magnetically diluted system when Zn/Cd content exceeds x = 0.6 and above i.e in Co_{1-x}M_xFe₂O₄, M = Zn/Cd, x = 0.6 - 1.0.

From fundamental and scientific points of view these diluted systems are expected to show interesting and novel magnetic properties such as spin-glass type of behavior. Spin-glass is a kind of magnetic material having peculiar magnetic behavior at low temperature with the manifestation of a sharp cusp in a χ (T) curve. Other feature of a spin-glass transition is that

- (i) It shows high coercive value of hysteresis,
- (ii) Spin freezing temperature, T_f where a sharp cusp in $\chi(T)$ takes place which shifts with frequency,
- (iii) It has a ageing effect i.e when a spin-glass material is subjected to an external applied field and then the field removed, magnetization changes slowly up to infinitely long time which can be fitted with a log scale linearly and
- (iv) It has a memory effect i.e it memorizes its space and position with respect to a temperature cycling.

Addition of small amount of RE ions to ferrites produces a change in their magnetic and electrical as well as structural properties depending upon the type and the amount of RE elements used. RE addition has also been undertaken with a diluted system of $\text{Co}_{1-x}\text{M}_x\text{Fe}_2\text{O}_4$ ($\text{M} = \text{Zn}/\text{Cd}$, $x = 0.8$) with RE such as Eu, Gd, Sm, Ho to look into the possible interesting magnetic properties since RE is expected to show some interesting structural and co-related magnetic properties. It is to be noted that some RE have large magnetic moment at low temperature and have complicated spin structure such as Ho^{3+} , Gd^{3+} etc.

The main objectives of the present research work are:

- To synthesize a series of $\text{Co}_{1-x}\text{Cd}_x\text{Fe}_2\text{O}_4$ ($x = 0.0 - 1.0$) and $\text{Co}_{1-x}\text{Zn}_x\text{Fe}_2\text{O}_4$ ($x = 0.0 - 1.0$ in steps of 0.1) ferrites by conventional ceramic method and to investigate the effect of Cd/Zn substitution on the structural and electromagnetic properties.
- Determination of physical properties such as density and porosity as affected by Cd/Zn substitution which ultimately determines the overall properties of the studied ferrites
- Determination of intrinsic/extrinsic magnetic properties i.e Curie temperature, saturation magnetization, remanance, coercivity and frequency dependence of permeability for different concentrations of Zn and Cd in Co-ferrites from temperature $M(T)$ and field $M(H)$ dependence of magnetization, permeability, B-H and M-H loops.
- Determination of the degree of spin canting in diluted system by calculating Y-K angle.
- Determination of electrical properties namely: DC electrical resistivity at room temperature, AC electrical resistivity and dielectric constant as a function of frequency.
- Substitution of trivalent Fe^{3+} ions by trivalent RE cations in the composition $\text{Co}_{0.2}\text{M}_{0.8}\text{RE}_x\text{Fe}_{2-x}\text{O}_4$ (where $\text{M} = \text{Cd}/\text{Zn}$, $\text{RE} = \text{Ho}^{3+}$, Sm^{3+} , Gd^{3+} , Eu^{3+} and $x = 0.0, 0.05$ and 0.1) to study their structural, magnetic and transport properties.

1.3 Reason for Choosing this Research Work

- $\text{Co}_{1-x}\text{Zn}_x\text{O}_4$ ferrites have been studied by many investigators upto $x = 0.6$ and Co-Cd ferrites have not been investigated in much detail until now.
- Dilute ferrites with $x > 0.6$ up to pure (Cd/Zn) Fe_2O_4 are interesting from the fundamental point of view because they are expected to show various magnetic behaviors including spin-glass behavior, a new type of magnetic ordering with the manifestation of memory and aging effects which has not been studied before in much detail. In this present thesis, a thorough study of complete magnetic behavior of $\text{Co}_{1-x}\text{M}_x\text{Fe}_2\text{O}_4$, where $\text{M} = \text{Cd/Zn}$ and $x = 0.0 - 1.0$ would be carried out for a complete understanding on these two scientifically interesting systems.
- Detail permeability study as a function of frequency on $\text{Co}_{1-x}\text{M}_x\text{Fe}_2\text{O}_4$, where $\text{M} = \text{Cd/Zn}$ system has not been carried out before.
- To the study most exhaustively the permeability and magnetization of the whole series as a function of frequency, field and temperature.
- RE is an interesting additive for its high anisotropy which manifests peculiar / complicated spin structure and few RE's has high magnetic moment at low temperature. So, dilute ferrite with small amount of RE at low temperature is expected to display some novel properties. There has not been much study with RE additive effects on the cobalt and its substituted ferrites.

1.4 Findings of this Work

- An enhancement of permeability with Zn/Cd contents is observed which means that Co-ferrites which is well known for its hard magnetic nature has been converted to softer magnetic materials with increasing addition of Zn and Cd resulting in an enhancement of permeability and subsequent reduction of coercivity. In other words Cd/Zn substitution has facilitate the magnetic domain wall to move easily by reducing the domain wall energy and spin rotation probably by reducing the global anisotropy energy of the prepared samples.
- Decrease of coercivity, H_c and increase of magnetization/induction, M_s/B_r with Zn/Cd content has been clearly manifested in low field B-H loop measurement.

- Some new findings that dilute composition of Co-Cd and Co-Zn ferrite with $x = 0.7 - 1.0$ display re-entrant and spin-glass behavior which has hitherto not been carried out before. It has been shown through memory experiment that the Zn ferrite and Cd-ferrite are spin-glass that displays memory effect i.e. it has a memory with respect to change of temperature. This novel experiment could have been possible due to the use of highly sophisticated and sensitive equipment like SQUID magnetometer at very low temperature down to 5 K.
- Enhancement of magnetization at low temperature with RE doping such as Ho^{3+} and Gd^{3+} has been observed due to large magnetic moment of these added species.
- Nonsoluble nature of RE has been detected as a second phase in XRD.

1.5 Review Work

The use of ferrites for certain application depends on their structural, magnetic and transport properties, which in turn are sensitive to the preparation condition as well as the type and amount of substitution. A large number of scientists and technologists are engaged in this area of research to bring about improvement on the properties of ferrites.

A. M. M. Farea *et. al.* [1.57] has studied dielectric properties, loss tangent, ac conductivity as a function of frequency, temperature and composition of $\text{Co}_{0.5}\text{Cd}_x\text{Fe}_{2.5-x}\text{O}_4$. The dielectric constant, loss tangent and ac conductivity decreases as the frequency of applied ac electric field increase but these parameters increase as the temperature increases due to the increase in thermal activation of hopping frequency and drift mobility of charge carriers. These are explained on the basis of space charge polarization according to Maxwell and Wagner's two layer models and the hopping between adjacent Fe^{2+} and Fe^{3+} as well as the hole hopping between Co^{3+} and Co^{2+} ions on B-sites.

A. A Ghani *et.al.* [1.58] reported the composition dependence of magnetization in $\text{Co}_{1-x}\text{Cd}_x\text{Fe}_2\text{O}_4$ ferrites. The saturation magnetization is maximum at $x = 0.35$ at high magnetic field up to 150 kOe and in the temperature range 4.2 to 300K. The non-collinear spin structure (canted) was found from the behavior of magnetization in the high field region 75 - 150 kOe. The dielectric constants and dielectric loss tangents of Li-Ti ferrites of different compositions have been investigated M. Bhagavantha Reddy *et.al.* [1.59]. The dielectric constant is found to decrease continuously with increasing frequency for all the specimens under investigation. This behavior

may be explained qualitatively as due to the fact that electronic exchange between ferrous and ferric ions can not follow the frequency of externally applied alternating field beyond a critical frequency value. The compositional variation of resistivity and dielectric constant indicated the inverse trend with each other, giving an impression that both the dielectric constant ϵ' and electrical conductivity $1/\rho$ behave more or less in a similar way. They assumed that the same mechanism is responsible for both phenomena. In addition, they assumed that the electron exchange interaction $\text{Fe}^{2+} \leftrightarrow \text{Fe}^{3+}$ results in local displacement of electrons in the direction of the field, which determines the polarization of the ferrite.

Magnetic properties of the mixed spinel $\text{CoFe}_{2-x}\text{Cr}_x\text{O}_4$ have been investigated H. Mohan *et.al.* [1.60]. They measured variation of magnetic moment per formula unit at 80K with Cr-content obtained from magnetization and Mössbauer data for $x = 0 - 0.6$ display a discrepancy between them, thus exhibiting a significant canting on the B-site. The ac susceptibility indicates a paramagnetic \rightarrow unstable ferromagnetic \rightarrow cluster spin-glass type transition as the temperature is lowered for $x = 0.0 - 1.2$. The further increase in x from $x > 1.2$ increases frustration and disorder in the system suppressing the ferromagnetic ordering and the system approaches a cluster spin glass-type ordering at $x = 1.4 - 1.6$. A. R. Shitre *et.al.* [1.61] studied the X-ray diffraction and dielectric study of $\text{Co}_{1-x}\text{Cd}_x\text{Fe}_{2-x}\text{Cr}_x\text{O}_4$ ferrite system with ($x = 0, 0.1, 0.2, 0.3, 0.4$ and 0.5). They observed that the lattice parameter increases with the increase of compositional parameter x . The dielectric constant and dielectric loss tangent decreases with increasing frequency. The dielectric loss decreases with increasing frequency at a faster rate than that of the dielectric constant.

Electrical properties of Co-Zn ferrites have been studied by M. A. Ahmed [1.62]. It was found that the lattice parameter increases linearly with the increase of zinc content. The X-ray densities for all compositions of Co-Zn ferrites increase with the increase of zinc content. The X-ray densities are higher than the bulk values. The addition of Zn, reduce the porosity thus increasing the density of the sample. The conductivity increases due to the increase in mobility of charge carriers. P. B. Panday *et.al.* [1.63] has synthesized Co-Zn ferrite by the co-precipitation method and studied the structural and bulk magnetic properties. All the samples are single phase spinel showed the X-ray diffraction pattern. The lattice constant gradually decreases on increasing Zn content, shows a minimum at $x \sim 0.5$ and then increases on further dilution. The magneton number, i.e., saturation magnetization per formula unit in Bohr magneton (n_B) at 298K initially increases and then decreases as x is increased up to $x \leq 0.3$. The decrease in magnetization of

these materials after $x = 0.3$ is primarily associated with canting of the magnetic moments. Curie temperature decreases with small addition of Zn.

M. Manjurul Haque *et.al.* [1.64] reported the effect of Zn^{2+} substitution on the magnetic properties of $Mg_{1-x}Zn_xFe_2O_4$ ferrites prepared by solid-state reaction method. They observed that the lattice parameter increases linearly with the increase in Zn content. The Curie temperature decreases with the increase in Zn content. The saturation magnetization (M_s) and magnetic moment are observed to increase up to $x = 0.4$ and thereafter decreases due to the spin canting in B-sites. The initial permeability increases with the addition of Zn^{2+} ions but the resonance frequency shifts towards the lower frequency. O. M. Hemeda [1.65] reported that Mn substituted Co-Zn ferrites have shown the varying the Mn content the saturation magnetization decreases continuously with increase of Mn content up to $x = 0.8$. Above $x = 0.8$, the reduction of the B-B interaction which increase the magnetic moment due to the canting effect. The particle size was increased by increasing Mn content. Akther Hossain *et. al.* [1.66] has studied $Ni_{1-x}Zn_xFe_2O_4$ ($x = 0.2, 0.4$) samples sintered at different temperatures. They observed that the DC electrical resistivity decreases as the temperature increases indicating that the samples have semiconductor like behavior. As the Zn content increases, the Curie temperature (T_c), resistivity and activation energy decrease while the magnetization, initial permeability and the relative quality factor increases. A Hopkinson peak is obtained near T_c in the real part of the initial permeability vs. temperature curves. The ferrite with higher permeability has relatively lower frequency. The initial permeability and magnetization of the samples have been found to correlate with density and average grain sizes.

R. N. Bhowmik *et.al.* [1.67] studies the cluster glass behavior in $Co_{0.2}Zn_{0.8}Fe_{2-x}Rh_xO_4$ ($x = 0 - 1.0$). The X-ray diffraction spectrum shows that the system is single phase cubic spinel structure. The lattice parameter is gradually increasing with substitution in Rh. This is due to the substitution of larger radius Rh^{3+} ions in place of smaller radius Fe^{3+} ions. On diluting the B site moments, the system shows a typical cluster freezing phenomena at $T \leq T_f$ due to frustration effects. The field cooled DC magnetization measurement suggests that the clusters more stable in presence of DC field.

Jingjing sun *et.al.* [1.68] measured the effects of La_2O_3 and Gd_2O_3 on some properties of Ni-Zn ferrite. The R_2O_3 ($R = La$ or Gd) substitutions decrease samples density and increases lattice parameter. A higher sintering temperature is necessary for densification with R_2O_3 . R_2O_3 substitutions cause poor value of permeability with higher cut-off frequency and higher electrical

resistivity. R_2O_3 substitution tends to flatten dielectric constant versus frequency curves, increases the values of dielectric constant and lowers the value of loss factor. Electrical resistivity and thermoelectric power of Cu-Cd ferrites with different rare earth substitutions have been investigated by A. A. Sattar [1.69]. He found that electrical resistivity increases due to the presence of rare earth ions at B-site which will increase the separation between Fe^{2+} and Fe^{3+} in proportion to its ionic radius. Thus it impedes the electron transfer between Fe^{2+} and Fe^{3+} i.e., it increases the activation energy and hence the resistivity according to its ionic radius. The presence of La ion at grain boundaries seems to facilitate the electron transfer between Fe^{2+} and Fe^{3+} in the B-site. He suggested that as E_p is higher than 0.2 eV (which is the transition energy between Fe^{2+} and Fe^{3+}), the conduction mechanism is predominantly due to small polaron than the electron hopping mechanism.

Some microstructure related properties of $Li_{0.5-x/2}Cd_xFe_{2.5-x/2}O_4$ ferrites have been reported S. S. Belled *et. al.* [1.70]. The variation of initial permeability and ac susceptibility with temperature shows normal ferrimagnetic behavior. The value of Curie temperature decreases continuously with increasing x is due to the dilution of strength of the A-B interaction. The decrease of magnetization above $x = 0.3$ is due to the canting of spin magnetic moments on an octahedral B-site. The increase of initial permeability above $x = 0.3$ is due to the decrease in non-magnetic grain boundary thickness. M. Manjurul Haque *et.al.* [1.71] studies the thermal hysteresis of permeability of Mn substituted Mg-Cu-Zn ferrites. They observed that the initial permeability of the sample exhibits thermal hysteresis when the temperature is cycled from above the Curie temperature T_c to below. The Curie temperature is found to increase with increasing Mn content.

Zn and Cd substituted mixed ferrites show canted spin arrangement on the B-site. The canting of the spins gives rise to Yafet-Kittel (Y-K) angles, which suggests that A-B and B-B superexchange interactions are comparable in strength. R. V. Upadhyay *et. al.* [1.72] has investigated $Cd_xMg_{1-x}Fe_2O_4$ ferrite system for $x \leq 0.8$ to study the variation of the saturation magnetization with Cd concentration and to gain information about the Y-K angles in the system. They employed the molecular approximation by Satyamurthy *et.al.* [1.73] using a non-collinear three sublattice model. From the results, it is clear that Y-K angles do not exist up to $x \leq 0.3$ but for $x \geq 0.4$, Y-K angles are present. Thus, the observed variation of the saturation magnetization with Cd concentration has been explained on the basis of the existence of Y-K angles on the B-site spins.

Some physical and magnetic properties of $Mg_{1-x}Zn_xFe_2O_4$ ferrites have been studied by Mazen *et.al.* [1.74]. It was found that the lattice parameter increases with increasing the Zn concentration. The basic composition $MgFe_2O_4$ shows lowest magnetization while the composition with $x = 0.4$ shows the highest one. The behavior of magnetization versus Zn content was discussed on the basis of cation distribution. From the B-H loops, the remanence induction, B_r , saturation induction B and coercive force H_c were determined as a function of Zn content. It was found that the Curie temperature decreases with increasing Zn-content. The behavior of μ' with temperature indicates that the samples with $x = 0 - 0.3$ show multi-domain nature, while the samples with $x = 0.4$ and 0.5 are single-domain. The effects of compositional variation on magnetic susceptibility, saturation magnetization, Curie temperature and magnetic moments of $Cu_{1-x}Zn_xFe_2O_4$ ferrites have been reported by Rana *et. al.* [1.75]. The Curie temperature and saturation magnetization increases from zinc content 0.0 to 0.75. The Y-K angles increases gradually with increasing Zn content and extrapolates to 90° for $ZnFe_2O_4$. From the Y-K angles for Zn substituted ferrites, it was concluded that the mixed zinc ferrites exhibit a non-collinearity of the Y-K type while $CuFe_2O_4$ shows a Neel type of ordering. Ravinder *et.al.* [1.76] observed the abnormal behavior of dielectric properties in $Mn_{1-x}Zn_xFe_2O_4$ ferrites, giving a peak at a certain frequency. They found that the peak shifts to lower frequency due to increasing zinc concentration. The decrease of f_{max} with increasing zinc content indicates that the hopping or jumping probability per unit time is decreased continuously.

A. K. M. Zakaria *et.al.* [1.77] studies the magnetic phase transition and initial permeability in addition of Al in Co-Zn ferrites. The effect of adding Al the permeability in respect of frequency is a desired for soft magnetic materials. Decrease of T_c with increasing Al content in the system. Substitution of Zn^{2+} and Cd^{2+} in spinel ferrites is interesting consequences. Karche *et.al.* [1.78] has studied magnetic properties such as saturation magnetization, AC susceptibility, initial permeability of $Cd_xMg_{1-x}Fe_2O_4$ ($x = 0.0, 0.2, 0.4, 0.6, 0.8$ and 1.0) system. They reported that Neel's two sublattice model is applicable upto $x \leq 0.4$ while Yafet-Kittel (Y-K) three sublattice model is predominant for $x > 0.4$. They also found that the addition of Cd^{2+} alters the domain structure from multi-domain to single-domain superparamagnetic transition, while $x = 0.8$ and $CdFe_2O_4$ are paramagnetic at room temperature. Low frequency dispersion in initial permeability depicts that μ_i is mainly contributed by domain wall motion. Increase of μ_i with temperature can be explained as the rate of decreasing of K_1 with temperature is much greater than that of M_s . L. Zhao *et al.* [1.79] reported influence of Gd on magnetic properties of

(Ni_{0.7}Mn_{0.3})Gd_xFe_{2-x}O₄ ferrites. It was found the crystallite sizes decreased when Gd ions were doped into NiMn ferrites. With Gd-substitution, when $x > 0.06$ all Gd ions could not enter into the ferrite lattice but resided at the grain boundary. The maximum content of Gd³⁺ ions in ferrite lattices was substituted when $x = 0.06$. The values of H_c and M_s were zero for all the samples calcined at 600°C. In addition, the H_c and M_s Values of the samples calcined at 800°C were larger than those sintered at 850°C, with Gd contents less than 0.08. Whereas, when the Gd contents at $x = 0.08$ and $x = 0.10$, the H_c and M_s Values of the samples increase with the calcinations temperature.

1.6 Outline of the Thesis

The thesis has been divided into eight chapters: **Chapter-I** presents a brief introduction of Co-ferrite and organization of thesis. This chapter incorporates background information to assist in understanding the aims and objectives of this investigation, and also reviews recent reports by other investigators with which these results can be compared.

Chapter-II briefly describes the theories necessary to understand the present work.

Chapter-III enunciates with the detail experimental process related to this research work. Describes the results and discussion about **Chapter-IV**, the structural, magnetic and transport properties of Co_{1-x}Cd_xFe₂O₄ ferrites. **Chapter-V** describes about the structural, magnetic and transport properties of Co_{1-x}Zn_xFe₂O₄ ferrites. **Chapter-VI** describes about the magnetization behavior of dilute ferrites. **Chapter-VII** describes about the rare-earth substitution in diluted sample. **Chapter-VIII** contains the concluding remarks.

CHAPTER-II
Theoretical Aspects



Theoretical Aspects

2.1 Introduction to Magnetism

2.1.1 Magnetic Materials

The term magnetism is derived from Magnesia, the name of a region in Asia Minor where lodestone, a naturally magnetic iron ore, was found in ancient times. Iron is not the only material that is easily magnetized when placed in a magnetic field; others include nickel and cobalt. Carbon steel was long the material commonly used for permanent magnets but more recently other materials have been developed that are much more efficient as permanent magnets, including certain ferroceramics, iron, aluminum, nickel, cobalt, copper, some rare earth metals and some of their alloys (e.g., Alnico). A permanent magnet is an object made from a material that is magnetized and creates its own persistent magnetic field. An everyday example is a refrigerator magnet used to hold notes on a refrigerator door. Materials that respond strongly to a magnetic field are called ferromagnetic. The ability of a material to be magnetized or to strengthen the magnetic field in its vicinity is expressed by its magnetic permeability. Ferromagnetic materials have permeabilities of as much as 1,000 or more times that of free space (a vacuum). A number of materials are very weakly attracted by a magnetic field, having permeabilities slightly greater than that of free space; these materials are called paramagnetic. A few materials, such as bismuth and antimony, are repelled by a magnetic field, having permeabilities less than that of free space; these materials are called diamagnetic. Some ferromagnetic materials can be magnetized by a magnetic field but do not tend to remain magnetized when the field is removed; these are termed soft. Permanent magnets are made from magnetically hard ferromagnetic materials that stay magnetized.

2.1.2 The Basis of Magnetism

The electrical basis for the magnetic properties of matter has been verified down to the atomic level. Because the electron has both an electric charge and a spin, it can be called a charge in motion. This charge in motion gives rise to a tiny magnetic field. In the case of many atoms, all the electrons are paired within energy levels, according to the exclusion principle, so that the electrons in each pair have opposite (antiparallel) spins and their magnetic fields cancel. In some atoms, however, there are more electrons with spins in one direction than in the other, resulting in

a net magnetic field for the atom as a whole; this situation exists in a paramagnetic substance. If such a material is placed in an external field, e.g., the field created by an electromagnet, the individual atoms will tend to align their fields with the external one. The alignment will not be complete, due to the disruptive effect of thermal vibrations. Because of this, a paramagnetic substance is only weakly attracted by a magnet. In a ferromagnetic substance, there are also more electrons with spins in one direction than in the other. The individual magnetic fields of the atoms in a given region tend to line up in the same direction, so that they reinforce one another. Such a region is called a domain. In an unmagnetized sample, the domains are of different sizes and have different orientations. When an external magnetic field is applied, domains whose orientations are in the same general direction as the external field will grow at the expense of domains with other orientations. When the domains in all other directions have vanished, the remaining domains are rotated so that their direction is exactly the same as that of the external field. After this rotation is complete, no further magnetization can take place. If the external field is then reduced to zero, it is found that the sample still retains some of its magnetism; this is known as hysteresis.

The effects on interactions between charges due to their motion and spin may appear in various forms, including electric currents and permanent magnets. They are described in terms of the magnetic field, although the field hypothesis cannot be tested independently of the electrokinetic effects by which it is defined. The magnetic field complements the concept of the electrostatic field used to describe the potential energy between charges due to their relative positions. Special relativity theory relates the two, showing that magnetism is a relativistic modification of the electrostatic forces. The two together form the electromagnetic interactions which are propagated as electromagnetic waves, including light. They control the structure of materials at distances between the long-range gravitational actions and the short-range "strong" and "weak" forces most evident within the atomic nucleus.

The magnetic field can be visualized as a set of lines shown in Fig. 2.1 illustrated by iron filings scattered on a suitable surface. The intensity of the field is indicated by the line spacing and the direction by arrows pointing along the lines. The sign convention is chosen so that the Earth's magnetic field is directed from the north magnetic pole toward the south magnetic pole. The field can be defined and measured in various ways, including the forces on the equivalent magnetic poles, and on currents or moving charges. Bringing a coil of wire into the field, or removing it, induces an electromotive force (emf) which depends on the rate at which the number

of field lines, referred to as lines of magnetic flux, linking the coil changes in time. This provides a definition of flux, in terms of the emf, e , given by Eqⁿ. (2.1)

$$e = -N \frac{d\phi}{dt} \quad (2.1)$$

For a coil of N turns wound sufficiently closely to make the number of lines linking each the same. The SI unit of the weber (Wb) is defined accordingly as the volt-second. The symbol B is used to denote the flux, or line, density, as in Eqⁿ. (2.2),

$$B = \frac{\phi}{\text{area}} \quad (2.2)$$

when the area of the coil is sufficiently small to sample conditions at a point, and the coil is oriented so that the induced emf is a maximum. The SI unit of B , the tesla (T), is the Wb/m². The sign of the emf, e , is measured positively in the direction of a right-hand screw pointing in the direction of the flux lines. It is often convenient, particularly when calculating induced emfs, to describe the field in terms of a magnetic vector potential function instead of flux.

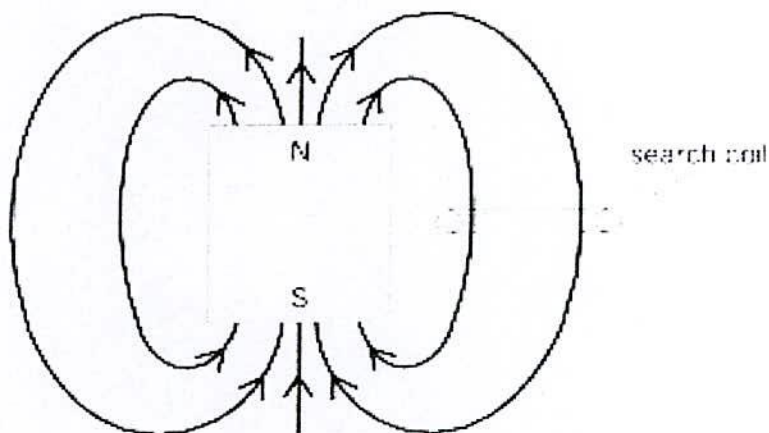


Fig. 2.1 Magnetic lines of a bar magnet.

2.1.3 Electron Spin

With the concept of electron spin introduced by Goudsmit in 1925 and Uhlenbeck in 1926, the origin of magnetism was explained. Spin corresponds to movement of electric charge in the electron, hence an electric current which produces a magnetic moment in the atom. The net magnetic moment is the vector sum of the individual spin and orbital moments of the electrons in the outer shells [2.1]. Next figure illustrate these two phenomena:

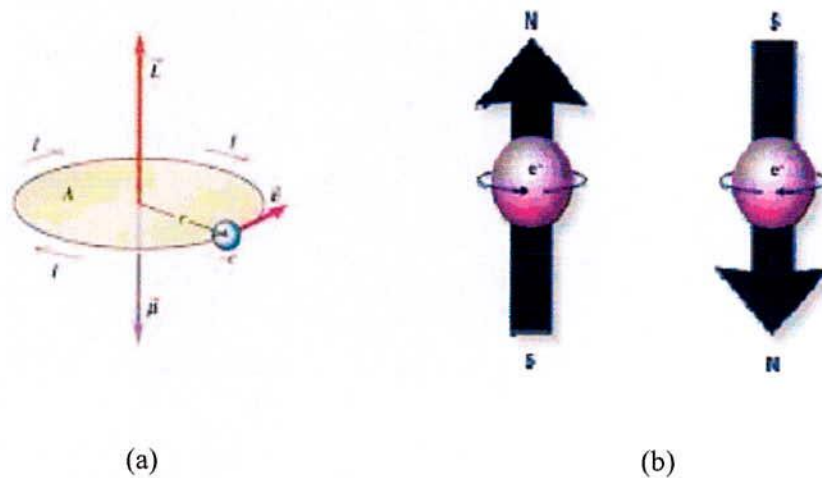


Fig. 2.2 (a) Electron orbit around the nucleus (b) Electron spin.

The electron spin can be represented in two modes pointed up or down. In an atom, with opposed paired spins cancel and do not result in magnetic moment, while the unpaired spins will give rise to a net magnetic moment.

2.1.4 Magnetic Dipole

The Earth's magnetic field, which is approximately a magnetic dipole. However, the N- pole and S-pole are labeled here geographically, which is the opposite of the convention for labeling the poles of a magnetic dipole moment

In physics, there are two kinds of dipoles:

(i) An electric dipole is a separation of positive and negative charges. The simplest example of this is a pair of electric charges of equal magnitude but opposite sign, separated by some (usually small) distance. A permanent electric dipole is called an electret.

(ii) A magnetic dipole is a closed circulation of electric current. A simple example of this is a single loop of wire with some constant current flowing through it [2.2, 2.3].

2.1.5 Magnetic Field

The magnetic field (B) is a vector field. The magnetic field vector at a given point in space is specified by two properties:

- (i) Its direction, which is along the orientation of a compass needle.
- (ii) Its magnitude (also called strength), which is proportional to how strongly the compass needle orients along that direction.

The units for magnetic field strength H are ampere/meter. A magnetic field strength of 1 ampere/meter is produced at the center of a single circular conductor with a one meter diameter carrying a steady current of 1 ampere.

2.1.6 Magnetic Moment

A magnet's magnetic moment (also called magnetic dipole moment, and usually denoted μ) is a vector that characterizes the magnet's overall magnetic properties. For a bar magnet, the direction of the magnetic moment points from the magnet's south pole to its north pole, and the magnitude relates to how strong and how far apart these poles are. In SI units, the magnetic moment is specified in terms of $A\cdot m^2$. A magnet both produces its own magnetic field and it responds to magnetic fields. The strength of the magnetic field it produces is at any given point proportional to the magnitude of its magnetic moment. In addition, when the magnet is put into an external magnetic field, produced by a different source, it is subject to a torque tending to orient the magnetic moment parallel to the field. The amount of this torque is proportional both to the magnetic moment and the external field. A magnet may also be subject to a force driving it in one direction or another, according to the positions and orientations of the magnet and source. If the field is uniform in space, the magnet is subject to no net force, although it is subject to a torque.

2.2 Magnetization Process

2.2.1 Magnetic Flux and Flux Density

Magnetic flux is defined in terms of the forces exerted by the magnetic field on electric charge. The forces can be described in terms of changes in flux with time Eqⁿ. (2.1), caused either by motion relative to the source or by changes in the source current, describing the effect of charge acceleration. Since the magnetic, or electrokinetic, energy of current flowing in parallel wires depends on their spacing, the wires are subject to forces tending to change the configuration. The force, dF , on an element of wire carrying a current, i , is given by Eqⁿ. (2.3)

$$dF = B i dl \quad (2.3)$$

and this provides a definition of the flux density, B , due to the wires which exert the force. The SI unit of B , called the tesla or Wb/m^2 , is the $\text{N/A}\cdot\text{m}$. The flux density, B , equals $\mu_0 H$ in empty space, or in any material which is not magnetically from Eqⁿ. (2.4)

$$B = \mu H \quad (2.4)$$

An example is the force, F , per meter (length) which is exerted by a long straight wire on another which is parallel to it, at distance r . From Eqⁿ. (2.5)

$$H = \frac{I}{2\pi r} \quad (2.5)$$

this force is given by Eqⁿ. (2.6)

$$F = \frac{\mu_0 I i}{2\pi r} = 2 \times 10^{-7} \frac{I i}{r} \quad (2.6)$$

when the wires carry currents I and i . The force, F , is accounted for by the electrokinetic interactions between the conduction charges, and describes the relativistic modification of the electric forces between them due to their relative motion.

In general, any charge, q , moving at velocity u is subject to a force given by Eqⁿ.(2.7)

$$f = q u \times B \quad (2.7)$$

denotes the cross-product between vector quantities. That is, the magnitude of f depends on the sine of the angle θ where $\mathbf{u} \times \mathbf{B}$ between the vectors \mathbf{u} and \mathbf{B} , of magnitudes u and B , according to Eqⁿ. (8)

$$f = quB \sin \theta \quad (2.8)$$

The force on a positive charge is at right angles to the plane containing \mathbf{u} and \mathbf{B} and points in the direction of a right-hand screw turned from \mathbf{u} to \mathbf{B} .

The same force also acts in the axial direction on the conduction electrons in a wire moving in a magnetic field, and this force generates an emf in the wire. The emf in an element of wire of length dl is greatest when the wire is at right angles to the \mathbf{B} vector, and the motion is at right angles to both. The emf is then given by Eqⁿ. (2.9)

$$emf = u B dl \quad (2.9)$$

More generally, u is the component of velocity normal to \mathbf{B} , and the emf depends on the sine of the angle between $d\mathbf{l}$ and the plane containing the velocity and the \mathbf{B} vectors. The sign is given by the right-hand screw rule, as applied to Eqⁿ. (2.8)

2.2.2 Origin of Magnetic Moments

The magnetic moment or magnetic dipole moment is a measure of the strength of a magnetic source. In the simplest case of a current loop, the magnetic moment is defined as:

$$m = I \int da \quad (2.10)$$

where 'a' is the vector area of the current loop, and the current, I is a constant. By convention, the direction of the vector area is given by the right hand rule.

In the more complicated case of a spinning charged solid, the magnetic moment can be found by the following equation:

$$m = \int_2^1 \mathbf{r} \times \mathbf{J} d\tau, \quad (2.11)$$

where $d\tau = r^2 \sin \theta dr d\theta d\phi$ and J is the current density.

The magnetic moment in a magnetic field is a measure of the magnetic flux set up by the gyration of an electric charge in a magnetic field. The moment is negative, indicating it is diamagnetic, and equal to the energy of rotation divided by the magnetic field. In atomic and nuclear physics, the symbol m represents moment, measured in Bohr magnetons, associated with the intrinsic spin of the particle and with the orbital motion of the particle in a system, also called

magnetic dipole moment. For a system of charges, the magnetic moment is determined by summing the individual contributions of each charge-mass-radius component.

2.2.3 Magnetic Properties of Solid

Materials may be classified by their response to externally applied magnetic fields as diamagnetic, paramagnetic and ferromagnetic. These magnetic responses differ greatly in strength. Diamagnetism is property of all materials and opposes applied magnetic fields, but is very weak paramagnetism, when present, is stronger than diamagnetism and produces magnetization in the direction of the applied field and proportional to the applied field. Ferromagnetic effects are very large, producing magnetizations sometimes orders of magnitude greater than the applied field and as such are much larger than either diamagnetic or paramagnetic effects. The magnetization of a material is expressed in terms of density of net magnetic dipole moments μ in the material. We define a vector quantity called the magnetization M by

$$M = \frac{\mu_{total}}{V} , \quad (2.12)$$

when the total magnetic field B in the material is given by

$$B = B_0 + \mu_0 M , \quad (2.13)$$

where μ_0 is the magnetic permeability of space and B_0 is the externally applied magnetic field. When magnetic fields inside of materials are calculated using Ampere's law or the Biot- Savart law, then the μ_0 in those equations is typically replaced by just μ with the definition

$$\mu = \mu_r \mu_0 , \quad (2.14)$$

where μ_r is called the relative permeability. If the material does not respond to the external magnetic field by producing any magnetization then $\mu_r = 1$. Another commonly used magnetic quantity is the magnetic susceptibility

$$\chi = \mu_r - 1 \quad (2.15)$$

For paramagnetic and diamagnetic materials the relative permeability is very close to 1 and the magnetic susceptibility very close to zero. For ferromagnetic materials, these quantities may be very large. Another way to deal with the magnetic fields which arise from magnetization of

materials is to introduce a quantity called magnetic field strength H . It can be defined by the relationship

$$H = \frac{B_0}{\mu_0} = \frac{B}{\mu_0} - M \quad (2.16)$$

and has the value of unambiguously designating the driving magnetic influence from external currents in a material independent of the materials magnetic response. The relationship for B above can be written in the equivalent form

$$B = \mu_0(H + M) , \quad (2.17)$$

H and M will have the same units, amperes/meter

The magnetic susceptibility (χ) is defined as the ratio of magnetization to magnetic field

$$\chi = \frac{M}{H} \quad (2.18)$$

The permeability and susceptibility of a material is correlated with respect to each other by

$$\mu = \mu_0(1 + \chi) \quad (2.19)$$

2.2.4 Magnetic Domain and Domain Wall Motion

- In addition to susceptibility differences, the different types of magnetism can be distinguished by the structure of the magnetic dipoles in regions called domains.
- Each domain consists of magnetic moments that are aligned, giving rise to a permanent net magnetic moment per domain.
- Each of these domains is separated from the rest by domain boundaries/domain walls. Boundaries, also called Bloch walls, are narrow zones in which the direction of the magnetic moment gradually and continuously changes from that of one domain to that of the next.
- The domains are typically very small about 50 μm or less, while the Bloch walls are about 100 nm thick. For a polycrystalline specimen, each grain may have more than one microscopic sized domain.
- Domains exist even in absence of external field.
- In a material that has never been exposed to a magnetic field, the individual domains have a random orientation. This type of arrangement represents the lowest free energy.

- When the bulk material is un-magnetized, the net magnetization of these domains is zero, because adjacent domains may be orientated randomly in any number of directions, effectively canceling each other out.
- The average magnetic induction of a ferro-magnetic material is intimately related to the domain structure.
- When a magnetic field is imposed on the material, domains that are nearly lined up with the field grow at the expense of unaligned domains. This process continues until only the most favorably oriented domains remain.
- In order for the domains to grow, the Bloch walls must move, the external field provides the force required for this moment.
- When the domain growth is completed, a further increase in the magnetic field causes the domains to rotate and align parallel to the applied field. At this instant material reaches saturation magnetization and no further increase will take place on increasing the strength of the external field.
- Under these conditions the permeability of these materials becomes quite small.

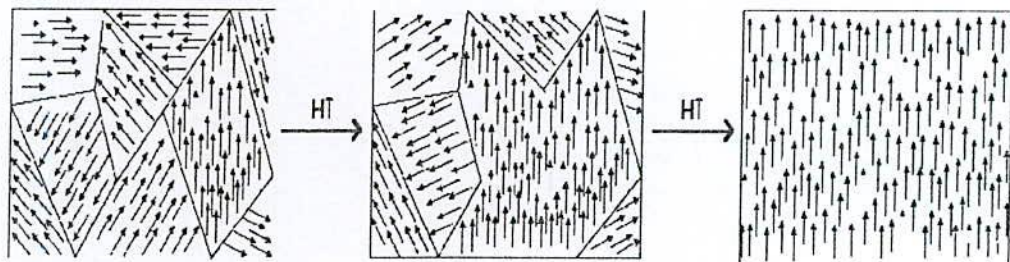


Fig. 2.3 Rotation of orientation and increase in size of magnetic domains due to an externally applied field.

In magnetism, a domain wall is an interface separating magnetic domains. It is a transition between different magnetic moments and usually undergoes an angular displacement of 90° or 180° . Although they actually look like a very sharp change in magnetic moment orientation, when looked at in more detail there is actually a very gradual reorientation of individual moments across a finite distance [2.4]. The energy of a domain wall is simply the difference between the magnetic moments before and after the domain wall was created. This value is more often than not expressed as energy per unit wall area. The width of the domain wall varies due to the two

opposing energies that create it: the magnetocrystalline anisotropy energy and the exchange energy, both of which want to be as low as possible so as to be in a more favorable energetic state. The anisotropy energy is lowest when the individual magnetic moments are aligned with the crystal lattice axes thus reducing the width of the domain wall, whereas the exchange energy is reduced when the magnetic moments are aligned parallel to each other and thus makes the wall thicker, due to the repulsion between them (where anti-parallel alignment would bring them closer working to reduce the wall thickness).

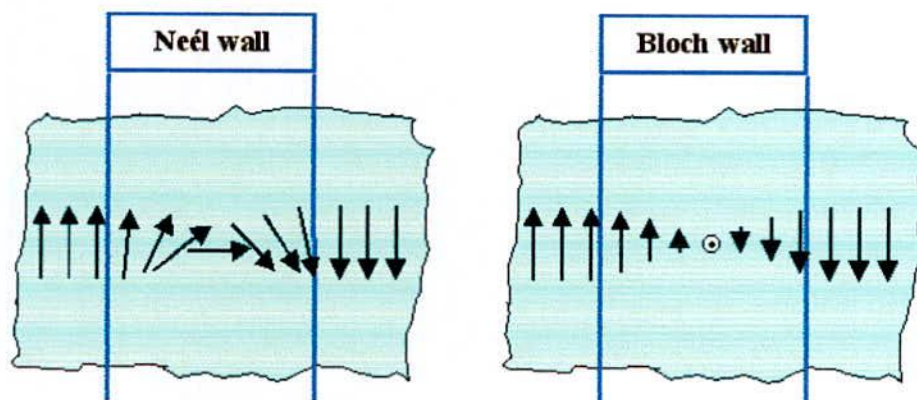


Fig. 2.4 The magnetization changes from one direction to another one.

In the end equilibrium is reached between the two and the domain wall's width is set as such. An ideal domain wall would be fully independent of position; however, they are not ideal and so get stuck on inclusion sites within the medium, also known as crystallographic defects. These include missing or different (foreign) atoms, oxides, and insulators and even stresses within the crystal. In most bulk materials, we find the Bloch wall: the magnetization vector turns bit by bit like a screw out of the plane containing the magnetization to one side of the Bloch wall. In thin layers (oft the same material), however, Neél walls will dominate. The reason is that Bloch walls would produce stray fields, while Neél walls can contain the magnetic flux in the material [2.5]

2.2.5 Magneto Static or Demagnetization Energy

The materials consist of a single domain than it behaves as a block magnet. The external demagnetizing field has a magneto static energy that depends on the shape of the sample and is the field that slows work to be done by the magnetized sample in order to minimize static energy must be minimized .This can be achieved by decreasing the external demagnetizing field by

dividing the material into domains. Adding extra domains increases the exchange energy as the domains cannot align parallel, however the total energy has been decreased as the magnetostatic energy is the dominant effect. The magnetostatic energy can be reduced to zero by a domain structure that leaves no external demagnetizing field is the main driving force for the formation of domains.

2.2.6 Magnetocrystalline Anisotropy Energy

In some materials the domain magnetization tends to align in a particular crystal direction (the so-called easy axis). The material is easiest to magnetize to saturation or demagnetize from saturation if the field is applied along an easy axis. The energy difference between aligning the domain in the easy and another direction (hard direction) is called magnetocrystalline anisotropy energy. Anisotropy energy is the energy needed to rotate the moment from the easy direction to a hard direction. For materials with cubic crystalline structure (such as ferrites), the energy is expressed in terms of anisotropy constants and the direction to which the magnetization rotates.

$$E_k = k_1 \sin^2 \theta + k_2 \sin^4 \theta \dots \dots \dots \text{(Hexagonal structure)} \quad (2.20)$$

$$E_k = k_1(\alpha_1^2 \alpha_2^2 + \alpha_2^2 \alpha_3^2 + \alpha_3^2 \alpha_1^2) + k_2(\alpha_1^2 \alpha_2^2 \alpha_3^2 + \dots \dots) \text{(Cubic structure)}, \quad (2.21)$$

where, k is the anisotropy constant, θ is the angle between the easy axis and the direction of magnetization, and α 's are the direction cosines, which are the ratios of the individual components of the magnetization projected on each axis divided by the magnitude of the magnetization. A crystal is higher in anisotropy energy when the magnetization points in the hard direction rather than along the easy direction. The formation of domains permits the magnetization to point along the easy axis, resulting in a decrease in the net anisotropy energy.

2.2.7 Magnetostriction

Magnetostriction is a property of ferromagnetic materials that causes them to change their shape or dimensions during the process of magnetization. The variation of material's magnetization due to the applied magnetic field changes the magnetostrictive strain until reaching its saturation value. The phenomenon was discovered in 1842 by J. Joule. In ferromagnets and ferrimagnets (such as iron, nickel, cobalt, gadolinium and terbium, as well as a number of alloys and ferrites) magnetostriction reaches a significant magnitude (relative

extension, $\frac{\Delta l}{l} \sim 10^{-6}-10^{-2}$). Magnetostriction is very small in antiferromagnets, paramagnets, and diamagnets. The change of length of a ferromagnetic substance when it is magnetized, more generally, magnetostriction is the phenomenon that the state of strain of a ferromagnetic sample depends on the direction and extent of magnetization. The phenomenon has an important application in devices known as magnetostriction transducers. The magnetostrictive effect is exploited in transducers used for the reception and transmission of high-frequency sound vibrations. Nickel is often used for this application. The phenomenon that is the inverse of magnetostriction a change in the magnetization of a ferromagnetic specimen upon deformation is called the magnetoelastic effect, or sometimes the Villari effect.

In the modern theory of magnetism, magnetostriction is considered to be a result of the manifestation of the fundamental types of interactions in ferromagnetic bodies (electrical exchange interaction and magnetic interaction). Accordingly, two types of essentially different magnetostriction deformations of a crystal lattice are possible: those resulting from a change in magnetic forces (dipole-dipole and spin-orbital deformations) and those resulting from a change in exchange forces.

Magnetostriction caused by exchange forces is observed in ferromagnets in the region of magnetization above technical saturation, where the magnetic moments of the domains are fully oriented in the direction of the field and only an increase in the absolute magnitude of J_s (the paraprocess, or true magnetization) takes place. Magnetostriction caused by exchange forces in cubic crystals is isotropic that is, it is manifested in a change in the volume of the body. In hexagonal crystals (such as gadolinium), such magnetostriction is anisotropic. In most ferromagnetic substances at room temperature, magnetostriction resulting from the paraprocess is small; it is also small close to the Curie point, where the paraprocess almost entirely determines the ferromagnetic properties of a substance. Significant magnetostriction of the paraprocess is also found in ferrites upon annihilation or creation of noncollinear magnetic structures by a magnetic field. Magnetostriction is widely used in technology. It is the basis for the operation of magnetostriction transformers (sensors) and relays, ultrasonic radiators and receivers, filters and frequency stabilizers in electronic devices, and magnetostriction delay lines.

2.2.8 Hysteresis

Magnetic hysteresis is an important phenomenon and refers to the irreversibility of the magnetization and demagnetization process, when a material shows a degree of irreversibility it is known as hysteretic. When a demagnetized ferromagnetic material is placed in an applied magnetic field, the magnetic field grows at the expense of the other domain wall. Such growth occurs by motion of the domain walls. Initially domain wall motion is reversible, and if the applied field is removed, the magnetization will return to the initial demagnetized state. In this region the magnetization curve is reversible and therefore does not show hysteresis. The crystal will contain imperfections which the domain boundaries encounter during their movement. These imperfections have an associated magneto static energy when a domain wall intersects the crystal imperfection this magneto static energy can be eliminated as closure domains from this pins the domain wall to the imperfection as if it is a local energy minima.

A great deal of information can be learned about the magnetic properties of a material by studying its hysteresis loop. A hysteresis loop shows the relationship between the induced magnetic flux density (**B**) and the magnetizing force (**H**). It is often referred to as the B-H loop. An example hysteresis loop is shown below.

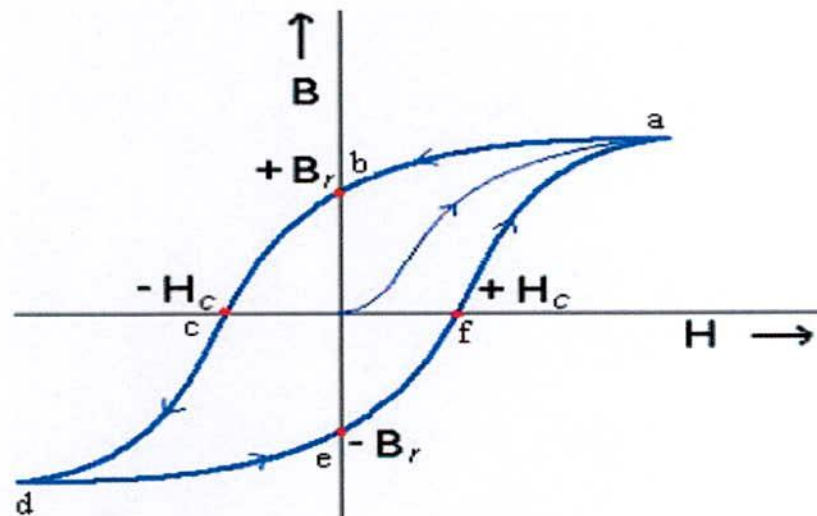


Fig. 2.5 Magnetic hysteresis loop.

The loop is generated by measuring the magnetic flux of a ferromagnetic material while the magnetizing force is changed. A ferromagnetic material that has never been previously

magnetized or has been thoroughly demagnetized will follow the dashed line as H is increased. As the line demonstrates, the greater the amount of current applied ($+H$), the stronger the magnetic field in the component ($+B$). At point "a" almost all of the magnetic domains are aligned and an additional increase in the magnetizing force will produce very little increase in magnetic flux. The material has reached the point of magnetic saturation. When H is reduced to zero, the curve will move from point "a" to point "b". At this point, it can be seen that some magnetic flux remains in the material even though the magnetizing force is zero. This is referred to as the point of retentivity on the graph and indicates the remanence (B_r) or level of residual magnetism in the material. (Some of the magnetic domains remain aligned but some have lost their alignment.) As the magnetizing force is reversed, the curve moves to point "c", where the flux has been reduced to zero. This is called the point of coercivity on the curve. (The reversed magnetizing force has flipped enough of the domains so that the net flux within the material is zero.) The force required to remove the residual magnetism from the material is called the coercive force (H_c) or coercivity of the material. As the magnetizing force is increased in the negative direction, the material will become magnetically saturated but in the opposite direction (point "d"). Reducing H to zero brings the curve to point "e". It will have a level of residual magnetism equal to that achieved in the other direction. Increasing H back in the positive direction will return B to zero. Notice that the curve did not return to the origin of the graph because some force is required to remove the residual magnetism. The curve will take a different path from point "f" back to the saturation point where it will complete the loop.

From the hysteresis loop, a number of primary magnetic properties of a material can be determined:

- (i) **Retentivity**, a measure of the residual flux density corresponding to the saturation induction of a magnetic material. In other words, it is a material's ability to retain a certain amount of residual magnetic field when the magnetizing force is removed after achieving saturation. The value of B is at point "b" on the hysteresis curve.
- (ii) **Residual Magnetism** or **Residual Flux**, the magnetic flux density that remains in a material when the magnetizing force is zero. Residual magnetism and retentivity are the same when the material has been magnetized to the saturation point. However, the level of residual magnetism may be lower than the retentivity value when the magnetizing force did not reach the saturation level.

- (iii) **Coercive Force**, the amount of reverse magnetic field which must be applied to a magnetic material to make the magnetic flux return to zero. The value of H is at point "c" on the hysteresis curve.

2.2.9 Magnetization and Temperature

The influence of temperature on magnetic material can be determined in the magnetic properties of these materials. Raising the temperature of a solid, results in the increase of the thermal vibrations of atoms, with this the atomic magnetic moments are free to rotate. This phenomenon the atoms tend to randomize the directions of any moments that may be aligned [2.6]. With increasing temperature, the saturation magnetization diminishes gradually and abruptly drops to zero at what is called the Curie temperature (T_c). The Curie point of a ferromagnetic material is the temperature above which it loses its characteristic ferromagnetic ability. At temperatures below the Curie point the magnetic moments are partially aligned within magnetic domains in ferromagnetic materials. As the temperature is increased from below the Curie point, thermal fluctuations increasingly destroy this alignment, until the net magnetization becomes zero at and above the Curie point.

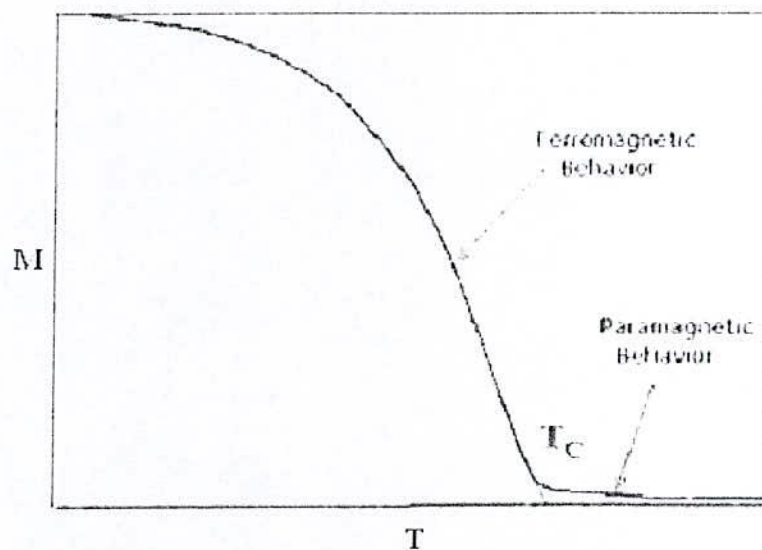


Fig. 2.6 Typical M-T curve for magnetic material.

Above the Curie point, the material is purely paramagnetic. At temperatures below the Curie point, an applied magnetic field has a paramagnetic effect on the magnetization, but the

combination of paramagnetism with ferromagnetism leads to the magnetization following a hysteresis curve with the applied field strength. Table-2.1 shows some examples of Curie temperature for various materials.

Table- 2.1 Curie Temperature of selected Mterials

Material	Curie temperature (K)
Gadolinium	292
Nickel	631
Magnetite	858
Iron	1043
Cobalt	1393

2.2.10 Theory of Permeability

Permeability is namely defines as the proportional constant between the magnetic field induction B and applied intensity H:

$$B = \mu H \quad (2.22)$$

If a magnetic material is subjected to an AC magnetic field as given below:

$$H = H_0 e^{i\omega t} \quad (2.23)$$

Then it is observed that the magnetic flux density B experiences a delay. The delay is caused due to presence of various losses and is thus expressed as

$$B = B_0 e^{i(\omega t - \delta)} \quad (2.24)$$

where δ is the phase angle and marks the delay of B with respect to H. The permeability is then given by

$$\mu = \frac{B}{H} = \frac{B_0 e^{i(\omega t - \delta)}}{H_0 e^{i\omega t}} \quad (2.25)$$

$$= \frac{B_0 e^{-i\delta}}{H_0} = \mu' - i\mu'' \quad (2.26)$$

$$\text{Where } \mu' = \frac{B_0}{H_0} \cos \delta \quad (2.27)$$

$$\mu'' = \frac{B_0}{H_0} \sin \delta \quad (2.28)$$

The real Part μ' of complex permeability μ as expressed in Eqⁿ. (2.26) represent the component of B which is in phase with H, so it corresponds to the normal permeability. If there is no losses , we should have $\mu = \mu'$, The imaging part μ'' corresponds to the part of B which is delayed by phase angle arranging up to 90° from H . The presence of such a component requires a supply of energy to maintain the alternating magnetization regardless of the origin of delay. The ratio of μ'' to μ' gives

$$\frac{\mu'}{\mu''} = \frac{\frac{B_0}{H_0} \sin \delta}{\frac{B_0}{H_0} \cos \delta} = \tan \delta \quad (2.29)$$

This $\tan \delta$ is called the loss Factor or loss tangent. The Q-Factor or quality factor is defined as the reciprocal of this loss factor, i.e

$$Q = \frac{1}{\tan \delta} \quad (2.30)$$

2.3 Types of Magnetism

The origin of magnetism lies in the orbital and spin motion motions of electrons and how the electrons interact with one another. The best way to introduce the different types of magnetism is to describe how materials respond to magnetic fields. This may be surprising to some, but all matter is magnetic. It's just that some materials are much more magnetic than others. The main distinction is that in some materials there is no collective interaction of atomic magnetic moments, whereas in other materials there is a very strong interaction between atomic moments.

The magnetic behavior of materials can be classified into the following major groups:

- Diamagnetism
- Paramagnetism
- Ferromagnetism, Antiferromagnetism and ferrimagnetisms are considered as subclasses of ferromagnetism.

2.3.1 Diamagnetism

Diamagnetism is a weak repulsion from a magnetic field. The orbital motion of electrons creates tiny atomic current loops, which produce magnetic fields. When an external field is applied to a material, these current loops will tend to align in such a way as to oppose the applied field. This may be viewed as an atomic version of Lenz's law: induced magnetic fields tend to oppose the change which created them. Materials in which this effect is the only magnetic response are called diamagnetic. The other characteristic behavior of diamagnetic materials is that the susceptibility is temperature independent. The typical values of susceptibility are in the order of 10^{-5} to 10^{-6} . Any conductor will show a strong diamagnetic effect in the presence of changing magnetic fields because circulating currents will be generated in the conductor to oppose the magnetic field changes [2.6]. A superconductor will be a perfect diamagnet since there is no resistance to the forming of the current loops. Most of the materials are diamagnetic, including Cu, B, S, Ag, Si, N₂ and most organic compounds.

2.3.2 Paramagnetism

In a paramagnet, the magnetic moments tend to be randomly oriented due to thermal fluctuations when there is no magnetic field. In an applied magnetic field these moments start to align parallel to the field. Materials that are paramagnetic become magnetized in the same direction as that of an applied magnetic field and the amount of magnetization is proportional to that of the applied magnetic field [2.7 - 2.11]. Paramagnetic materials are attracted to magnetic fields; hence have a relative magnetic permeability greater than one or equivalently, a positive magnetic susceptibility and the values of susceptibility are very small with the order of 10^{-5} to 10^{-3} . Paramagnets do not retain any magnetization in the absence of an externally applied magnetic field. Superparamagnetism is a phenomenon by which magnetic materials may exhibit a behavior similar to paramagnetism even when at temperatures below the Curie temperature. This is a small length scale phenomenon, where the energy required to change the direction of the magnetic moment of a particle is comparable to the thermal energy at room temperature. At this point, the rate at which the particles will randomly reverse direction becomes significant. O₂, NO, Mn and Cr are just a few examples of the paramagnetic materials. The susceptibility of a paramagnetic material is inversely dependent on temperature, which is known as Curie law

$$\chi = \frac{C}{T}, \quad (2.31)$$

where C is the Curie constant.

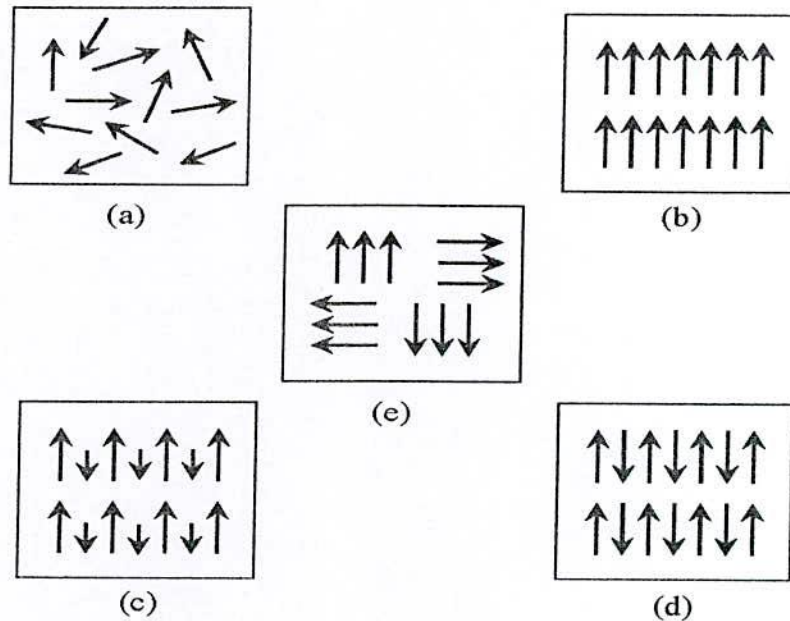


Fig. 2.7 Varieties of magnetic orderings (a) paramagnetic, (b) ferromagnetic, (c) ferrimagnetic, (d) antiferromagnetic and (e) superparamagnetic

2.3.3 Ferromagnetism

A ferromagnet, like a paramagnetic substance, has unpaired electrons. However, in addition to the electrons intrinsic magnetic moments wanting to be parallel to an applied field, there is also in these materials a tendency for these magnetic moments to want to be parallel to each other. Thus even when the applied field is removed, the electrons in the material can keep each other continually pointed in the same direction. Every ferromagnetic substance has its own individual temperature, called the Curie temperature, above which it loses its ferromagnetic properties [2.9]. This is because the thermal tendency to disorder overwhelms the energy lowering due to ferromagnetic order. The susceptibility of a ferromagnetic material does not follow the Curie law, but displayed a modified behavior defined by Curie-Weiss law Fig. 2.8 (b)

$$\chi = \frac{C}{T - \theta}, \quad (2.32)$$

where C is a constant and θ is called Weiss constant. For ferromagnetic materials, the Weiss constant is almost identical to the Curie temperature (T_c). The elements Fe, Ni and Co and many of their alloys are typical ferromagnetic materials.

Two distinct characteristics of ferromagnetic materials are:

- Spontaneous magnetization and
- The existence of magnetic ordering temperature (Curie temperature)

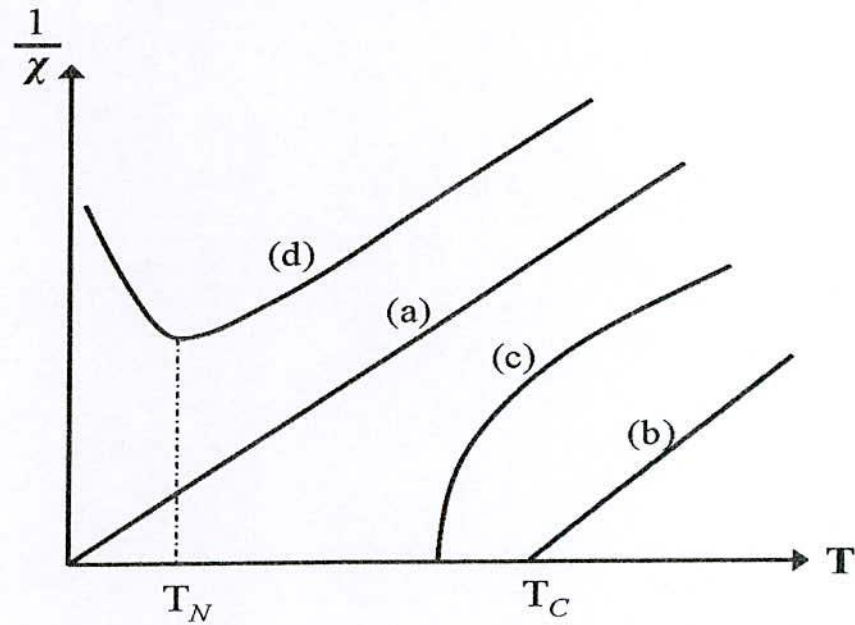


Fig. 2.8. The inverse susceptibility varies with temperature T for (a) paramagnetic, (b) ferromagnetic, (c) ferrimagnetic, (d) antiferromagnetic materials. T_N and T_c are Neel temperature and Curie temperature, respectively.

The spontaneous magnetization is the net magnetization that exists inside a uniformly magnetized microscopic volume in the absence of a field. The magnitude of this magnetization, at 0K is dependent on the spin magnetic moments of electrons. Spontaneous magnetization is the term used to describe the appearance of an ordered spin state (magnetization) at zero applied magnetic field in a ferromagnetic or ferrimagnetic material below a critical point called the Curie temperature or T_c . This fact led Weiss to make the bold brilliant assumption that a molecular field acted in a ferromagnetic substance below its Curie temperature as well as above and that this field was so strong that it could magnetize the substance to saturation even in the absence of an applied field. The substance is then self-saturating or spontaneously magnetized. Saturation magnetization is an intrinsic property independent of particle size by dependent on

temperature. Even though electronic exchange forces in ferromagnets are very large thermal energy eventually overcomes the exchange energy and produces a randomizing effect. This occurs at a particular temperature called the Curie temperature (T_c). Below the Curie temperature the ferromagnetic is ordered and above it, disordered. The saturation magnetization goes to zero at the Curie temperature.

2.3.4 Antiferromagnetism

Antiferromagnetic material adjacent magnetic moments parallel to each other without an applied field. In the simplest case adjacent magnetic moments are equal in magnitude and opposite therefore there is no overall magnetization. The natural state makes it difficult for the material to become magnetized in the direction of the applied field but still demonstrates a relative permeability slightly greater than above a critical temperature known as the Neel temperature the material becomes paramagnetic [2.11]. The antiferromagnetic susceptibility is followed by the Curie-Weiss law with a negative θ as in the inverse susceptibility as a function of temperature is shown in Fig. 2.8 (d). Common examples of materials with antiferromagnetic ordering include MnO, FeO, CoO and NiO.

2.3.5 Ferrimagnetism

Ferrimagnetic material has the aligned magnetic moments are not of the same size; that is to say there is more than one type of magnetic ion. An overall magnetization is produced but not all the magnetic moment may give a positive contribution to the overall magnetization. The magnitude of magnetic moment in one direction differs from that of the opposite directions. As a result a net magnetic moment remains in the absence of external magnetic field, the behavior of susceptibility of a ferrimagnetic material also obeys Curie-Weiss law and has a negative Q as well as in Fig. 2.8(c). While these materials may also demonstrate a relative permeability >1 , their temperature dependence are not as consistent as with ferromagnetic materials and can result in some very unusual results. Ferrimagnetism is therefore similar to ferromagnetism. It exhibits all the hallmarks to ferromagnetic behavior like spontaneous magnetization, Curie temperature hysteresis, and remanence. However ferro and ferrimagnets have very different magnetic ordering. In ionic compounds, such as oxides, more complex forms of magnetic ordering can occur as a result of the crystal structure. The magnetic structure is composed of two magnetic

sublattices (called A and B) separated by oxygens. The exchange interactions are mediated by the oxygen anions. When this happens, the interactions are called indirect or superexchange interactions.

2.4 Classification of Ferrites

Ferrites are essentially ceramic materials, compound of iron, boron, barium strontium, lead, zinc, magnesium or manganese. The ingredients are mixed, prefired, milled/crushed, dried, shaped and finally pressed and fired into their final hard brittle state. Ferrites are a class of chemical compounds with the formula AB_2O_4 , where A and B represent various metal cations usually including iron. These ceramic materials are used in applications ranging from magnetic components in micro electronics.

At high frequencies ferrites are considered superior to other magnetic materials because they have low eddy current losses and high DC electrical resistivity. The DC electrical resistivity of ferrites at room temperature can vary depending upon the chemical composition between about $10^{-2} \Omega\text{-cm}$ and higher than $10^{11} \Omega\text{-cm}$ [2.12].

Ferrites are classified into two categories based on their coercive field strength. They are:

- (i) Soft ferrite with coercive field strength $< 10 \text{ Oe}$
- (ii) Hard ferrite with coercive field strength $> 1250 \text{ Oe}$

2.4.1 Soft Ferrite

Soft ferrites are characterized by low coercive forces and high magnetic permeabilities; and are easily magnetized and de-magnetized. They generally exhibit small hysteresis losses. One of the most common types of soft ferrite is made up of oxides of manganese (Mn) and zinc (Zn). Most common ferrite contains 50% iron oxide. At high frequency metallic soft magnetic materials simply cannot be used due to the eddy current losses. Therefore soft ferrite, which is ceramic insulators, becomes the most desirable material. These materials are ferromagnetic with a cubic crystal structure and the general composition $MO.Fe_2O_3$, where M is a transition metal such as nickel, manganese, magnesium or zinc. The magnetically soft ferrites first came into commercial production in 1948. Additionally, part of the family of soft ferrite are the microwave ferrites e.g. Yttrium iron garnet. These ferrite are used in the frequency range from 100 MHz to 500 GHz. For waveguides for electromagnetic radiation and in microwave device such as phase shifters.

Application of soft ferrite include: cores for electro-magnets, electric motors, transformers, generators, and other electrical equipment.

2.4.2 Hard Ferrite

Hard magnets are characterized by high remanent inductions and high coercivities. They generally exhibit large hysteresis losses. Hard ferrite referred to as permanent magnets retain their magnetism after being magnetized. Hard ferrite likes Ba-ferrite, Sr-ferrite, Pb-ferrite are used in communication device operating with high frequency currents because of their high resistivity, negligible eddy currents and lower loss of energy due to Joule heating and hysteresis. These are found useful in many applications including fractional horse-power motors, automobiles, audio- and video- recorders, earphones, computer peripherals, and clocks.

According to the crystallographic structures ferrite fall into three categories.

- (i) Cubic ferrites of spinel type,
- (ii) Cubic ferrites of garnet type and
- (iii) Hexagonal Ferrites.

2.4.3 Cubic Ferrite of Spinel Type

This ferrite is also called ferros spinels because they crystallize in the same crystal structure as the mineral spinel and they derive their general formula $MeFe_2O_4$ and that $(MgAl_2O_4)$ of spinal. In this formula Me represents a divalent ion of metal. Beside the divalency another condition to qualify a metal in ferros spinel is its ionic radius which should fall between 0.6 and 1.0 Å. Mg, Fe, Co, Ni, Cu, Zn and Cd all satisfy these two conditions and thus from various single cubic ferrites magnetic which contains one ferrous ion and two ferric ions in each formula unit is a typical ferrite. The crystal structure of ferrite is based on a face-centered cubic lattice of the oxygen ions. Each unit cell contains eight formula units. Therefore there are $32O^-$ anions $16Fe^{3+}$ cations and 8 Me^{2+} cations in the cell and the lattice constant is rather large of the order of 8.50 in each unit cell there are 64 tetrahedral or A- sites and 32 octahedral or B- site .These site are so named because they are surrounded by four and six oxygen ions at equal distances respectively.

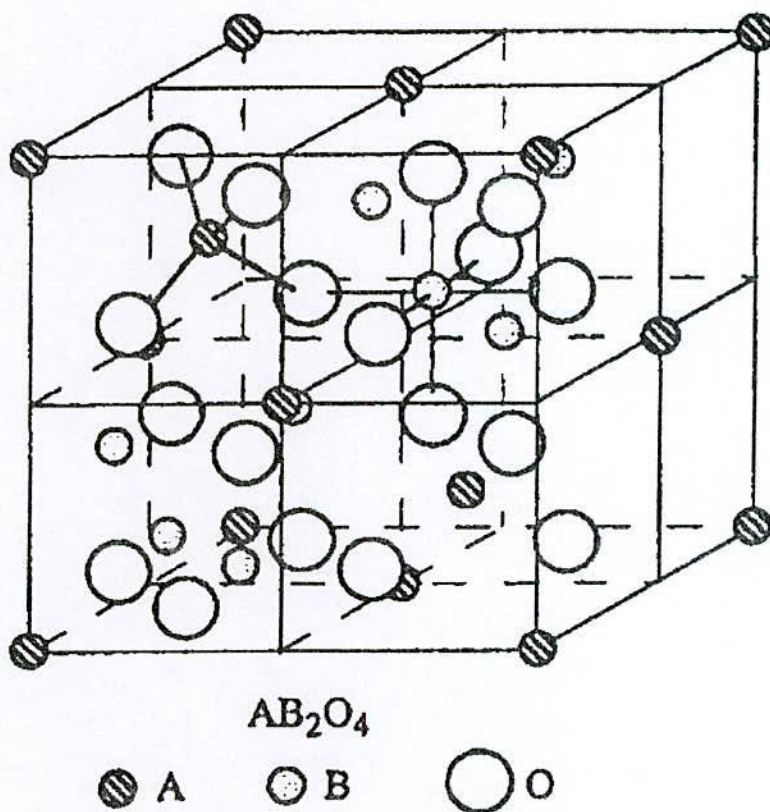


Fig. 2.9 Schematic of two sub cells of a unit cell of the spinel structure, showing octahedral and tetrahedral sites.

The lattice characteristics of a spinel include a face centre cubic (FCC) site for the oxygen atoms and two cationic sites occupying A and B-sites [2.13, 2.14, 2.15]. In a spinel, there are 64 A-sites, 32 B-sites, and 32 oxygen sites in a unit cell. Due to their exchange coupling, spinel ferrites are ferrimagnetically aligned where all of the moments of A-sites are aligned parallel with respect to one another while moments of A and B-sites are antiparallel to each other. The charge neutrality requires the presence of the cations within the structure to counter balance the charge of these oxygen anions. These cations rest on two types of interstitial sites to preserve the charge neutrality namely A and B-sites. The magnetic properties of spinel ferrites are generally influenced by composition and cation distribution. Variation of cation distribution between the cationic sites leads to different electrical and magnetic properties even if the composition of the spinel is the same. The distribution of cations over A and B-sites is determined by their ionic radius, electronic configuration and electrostatic energy in the spinel lattice [2.12]. The octahedral sites are larger than the tetrahedral sites, thus, the divalent ions are localized in the octahedral sites

whereas trivalent ions are in the tetrahedral sites [2.16]. Each type of lattice site will accept other metal ions with a suitable, 0.65 - 0.80Å at B-sites and 0.40 - 0.64Å at A-sites.

2.5 Cation Distribution in Ferrites

The cation distribution in the spinel $Me^{2+}Me_2^{3+}O_4$ can be as follows [2.16]

2.5.1 Normal Spinel Structure

The divalent cation (Me^{2+}) are in tetrahedral A-sites and two trivalent (Fe^{3+}) cations are in octahedral B- site which is represented as $(Me^{2+})_A[Fe^{3+}Fe^{3+}]_BO_4$. Both zinc and cadmium ferrite have this structure and they are both magnetic i.e. paramagnetic

2.5.2 Inverse Spinel Structure

In this case divalent (Me^{2+}) cations are in octahedral B-sites and the trivalent (Fe^{3+}) cations are equally divided between A and B sites (the divalent and trivalent ions normally occupy the B sites in a random fashion i.e. they are disordered) arrangement is as $(Fe^{3+})_A[Me^{2+}Fe^{3+}]_BO_4$. Iron, cobalt and Nickel ferrites have the inverse structure, and they are all ferromagnetic.

2.5.3 Intermediate Structure

X-ray and neutron diffraction experiments and magnetization measurements show that there is a whole range of cation distribution between the normal and inverse structures. The arrangement of the from $(Fe^{3+}_{1-x}Me^{2+}_x)_A[Fe^{3+}_{1+x}Me^{2+}_{1-x}]_BO_4$ is often referred as mixed spinel, where cations in the parentheses are at (A) sites and those in the brackets are at [B] sites and x is called the inversion parameter. The extreme case $x = 1$ corresponds to the normal spinel structure, and $x = 0$ corresponds to the inverse structure $0 < x < 1$ for intermediate used commercially are mixed ferrite [2.17].

The factor affecting the cation distribution over A and B sites are as follows [2.16, 2.18]

- The size of the cations
- The electronic configuration of cations
- The electronic energy
- The saturation magnetization of the lattice

Smaller cations (trivalent ions) prefer to occupy the A-sites. The cations have special preference for A and B sites and the preference depends on the following factors:

- Ionic radius
- Size of interstices
- Temperature
- Orbital preference for the specific coordination.

The preference of cations is according to Verwey- Heilmann scheme [2.19, 2.20]

- Ions with strong preference for A-sites Zn^{2+} , Cd^{2+} , Ga^{2+} , In^{3+} , Ge^{4+} .
- Ions with strong preference for B-sites Ni^{2+} , Cr^{3+} , Ti^{4+} , Sn^{4+} .
- Indifferent ions are Mg^{2+} , Al^{3+} , Fe^{2+} , Co^{2+} , Mn^{2+} , Fe^{3+} , Cu^{2+} .

Moreover the electrostatic energy also affects the cation distribution in the spinel lattice.

The cations of the smallest positive charge reside on the B-sites having six anions in surrounding i.e. the most favorable electrostatic conduction. It has been observed that X-ray powder diffraction, in conjunction with appropriate computational method, has enough sensitivity to determine the degree of inversion δ , and oxygen positional parameter U. A difference of one electron between two different cations can be enough to render them distinguishable.

2.6 Magnetic Exchange Interaction

The electron spin of the two atoms S_i and S_j , which is proportional to their product. The exchange energy can be written as universally in terms of Heisenberg Hamiltonian [2.21]

$$H = -\sum J_{ij} S_i \cdot S_j = -\sum J_{ij} S_i S_j \cos\phi, \quad (2.33)$$

where J_{ij} is the exchange integral represents the strength of the coupling between the spin angular momentum i and j and ϕ is the angle between the spins. It is well known that the favored situation is the one with the lowest energy and it turns out that there are two ways in which the wave functions can combine there are two possibilities for lowering the energy by H . These are:

- (i) If J_{ij} is positive and the parallel spin configuration ($\cos\phi = 1$) the energy is minimum,
- (ii) If J_{ij} is negative and the spins are antiparallel ($\cos\phi = -1$) energy is maximum. This situation leads to antiferromagnetism.

2.6.1 Superexchange Interaction

The magnetic interaction in magnetic oxide cannot be explained on the basis of direct interaction because of the following facts:

- The magnetic ions are located too far apart from each other shielded by the non magnetic anion i.e., oxygen. This is because these are not band type semiconductor [2.22]. The non magnetic anion such as oxygen is situated in the line joining magnetic cations
- Superexchange interaction appears, i.e. indirect exchange via anion p-orbital that may be strong enough to order the magnetic moments. The P orbital of an anion (center) interact with the d orbital of the transitional metal cations.

Three major types of superexchange interactions in spinel ferrites are: J_{AB} , J_{BB} , and J_{AA} . Ferromagnetic oxides are one kind of magnetic system in which there exist at least two inequivalent sublattices for the magnetic ions. The antiparallel alignment between these sublattices (ferrimagnetic ordering) may occur provided the intersublattice (J_{AB}) exchange interaction are antiferromagnetic (AF) and some requirements concerning the signs and strength of the intra-sublattice (J_{AA} , J_{BB}) exchange interactions are fulfilled. Since usually in ferromagnetic oxides the magnetic cations are surrounded by bigger oxygen anions (almost excluding the direct overlap between cation orbitals) magnetic interactions occur via indirect superexchange interactions depends both on the electronic structure of the cations and their geometrical arrangement [2.23]. In most of ferromagnetic oxides the crystallographic and electronic structure give rise to antiferromagnetic inter and intra-sublattice competing interactions.

The magnitude of negative exchange energies between two magnetic ions M and M' depends upon the distance from these ions to the oxygen ion O^{2-} , via which the superexchange takes place, and on the angle $M-O-M'$ (φ). According to the superexchange theory the angle $\varphi = 180^\circ$ gives rise to the greatest exchange energy, and this energy decreases very rapidly as the distance between the ions increases. The magnetic properties of the spinel ferrites are governed by the type of magnetic ions residing on the A and B-sites and the relative strengths of the inter-sublattice (J_{AB}) and intra-sublattice (J_{AA} , J_{BB}) exchange interactions.

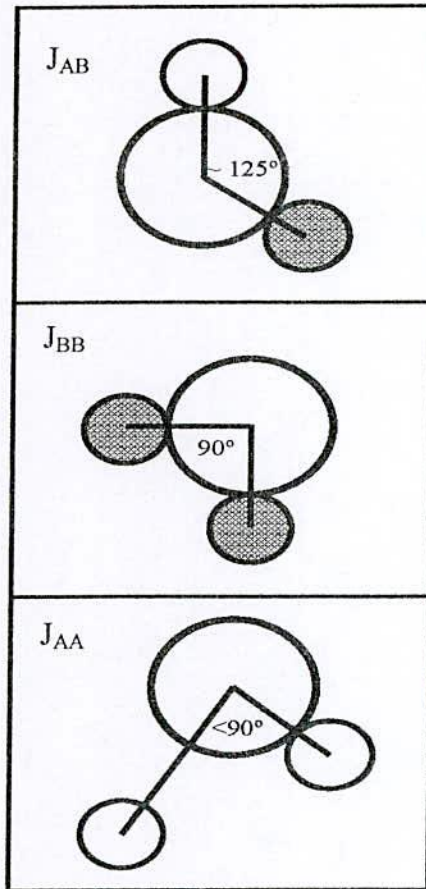


Fig. 2.10 Three major types of superexchange interactions in spinel ferrites are as follows: J_{AB} , J_{BB} and J_{AA} . The small empty circle is A-site, the small solid circle is B-site, and the large empty circle is oxygen anion.

2.6.2 Neel's Collinear Model of Ferrimagnetism

Soft ferrites belong to the cubic spinel structure. According to Neel's theory, the magnetic ions are assumed to be distributed among the tetrahedral A and octahedral B-sites of the spinel structure. The magnetic structure of such crystals essentially depends upon the type of magnetic ions residing on the A and B sites and the relative strengths of the inter (J_{AB}) and intra-sublattice exchange interactions (J_{AA} , J_{BB}). Negative exchange interactions exist between A-A, A-B and B-B ions. When A-B antiferromagnetic interaction is the dominant one, A and B-sublattices will be magnetized in opposite direction below a transition temperature. When the A-A (or B-B) interaction is dominant, Neel found that the above transition will not take place and he concluded that the substance remains paramagnetic down to the lower temperature. But this conclusion was

not correct, as in the presence of strong interactions, some kind of ordering may be expected to occur at low temperature as claimed by Yafet and Kittel [2.24].

2.6.3 Non-Collinear Model of Ferrimagnetism

The discrepancy in the Neel's theory was resolved by Yafet and Kittel [2.24] and they formulated the non-collinear model of ferrimagnetism. They concluded that the ground state at 0K might have one of the following configurations:

- have an antiparallel arrangement of the spins on two sites,
- consists of triangular arrangements of the spins on the sublattices and
- an antiferromagnetic in each of the sites separately.

2.6.4 Re-entrant Spin-Glass Behavior

When a piece of material is cooled down its constituent atoms or molecules become more and more ordered. Some systems, however, seem to become disordered again when the temperature continues to decrease. Such a behavior is commonly referred to as reentrant transition, because the system reenters a disordered phase when lowering the temperature. When such a system is cooled from a high temperature, it first exhibits a transition from paramagnetic to a ferromagnetic phase. Upon further lowering the temperature, the spins are progressively frozen below a freezing temperature T_f . The low temperature spin frozen state is called a reentrant spin glass (RSG) or mixed state, in which ferromagnetic order is argued to coexist with spin-glass order [2.25, 2.26]. If the cooling proceeds, a transition to a RSG phase occurs. For comparison, in a diluted spin glass, spins freeze directly from a paramagnetic state.

2.6.5 Spin-Glass Behavior

A spin glass is a magnet with frustrated interactions, augmented by stochastic disorder, where usually ferromagnetic and antiferromagnetic bonds are randomly distributed. Its magnetic ordering resembles the positional ordering of a conventional, chemical glass. There exchange interaction, J_{ij} , between atomic spins, S_i , is a random variable. A positive sign favors an antiparallel alignment of a spin pair, while a negative sign favors an antiparallel alignment. A consequence of such random exchange interactions between the moments is a

frustrated system, i.e., for a representative spin there is no obvious direction relative to its neighbours to align,

$$H = -\sum_{(i,j)} J_{ij} S_i S_j \quad (2.34)$$

If $J_{ij} = J > 0$, parallel orientation of the spins is favoured and at low temperatures all spins will be aligned ferromagnetically. Such a system has two phases. At temperature high compared to J , the entropy dominates the energy and the spins fluctuate almost independently. In this paramagnetic phase, the expectation value of a spin is $\langle S_i \rangle$ ($\langle \rangle$ denotes the time average over long times). At temperature low compared to J , the energy dominates the entropy and the spins of the system are predominantly aligned in the same direction, i.e. $\langle S_i \rangle \neq 0$. This phase is called ferromagnetic. A transition between the two phases occurs at a finite critical temperature, T_c . An order parameter is associated to the transition, with the property that it is zero above and non-zero below the phase transition. For $J_{ij} = J < 0$, the low temperature phase is antiferromagnetic with the spins aligned anti-parallel. If $J_{ij} = 0$, the Hamiltonian describes a system being paramagnetic at all temperatures.

If positive and negative interactions are mixed the situation becomes more complicated. Then there is a possibility that not all of the exchange interactions can be satisfied simultaneously. This property is called frustration [2.27]. An example of frustration is given in Fig. 2.11. Here the frustration arises due to bond disorder, but it may also arise from randomness in spin positions (site disorder). If only a small fraction of the interactions are of opposite sign the ground state will still be ferromagnetic or antiferromagnetic, with only a small fraction of the spins misaligned. If the densities of positive and negative interactions are comparable, the system will be strongly frustrated. Such systems are called spin glasses (SG).

It is the time dependence which distinguishes spin glasses from other magnetic systems. The spin glass transition temperature, T_c , so-called "freezing temperature" T_f where the spin glass exhibits more typical magnetic behavior if an external magnetic field is applied and the magnetization is plotted versus temperature, it follows the typical Curie law (in which magnetization is inversely proportional to temperature) until T_c is reached, at which point the magnetization becomes virtually constant (this value is called the field-cooled magnetization). This is the onset of the spin glass phase. When the external field is removed, the spin glass has a rapid decrease of magnetization to a value called the remanent magnetization, and then a slow

decay as the magnetization approaches zero (or some small fraction of the original value this remains unknown).

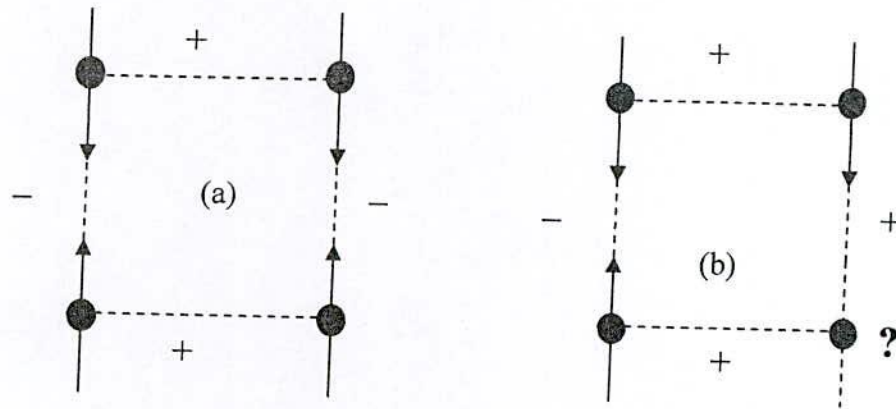


Fig. 2.11 Examples of (a) an unfrustrated and (b) a frustrated spin configuration.

This decay is non-exponential and no simple function can fit the curve of magnetization versus time adequately. This slow decay is particular to spin glasses. If instead, the spin glass is cooled below T_c in the absence of an external field and then a field is applied, there is a rapid initial increase to a value called the zero-field-cooled magnetization followed by a slow upward drift toward the field cooled magnetization. The combination of randomness with these ferromagnetic and antiferromagnetic competing interactions causes "spin frustration". Below a SG freezing temperature T_g , a highly irreversible metastable frozen state occurs without any usual long-range spatial spin order [2.28, 2.29]. Spin glass was first observed by Canella and Mydosh [2.29] in 1972 by observing a peak in the ac susceptibility, and predicted the existence of a phase transition to a low temperature spin glass phase.

In recent years, aging dynamics, of SG systems has been extensively studied theoretically [2.30, 2.31] and experimentally [2.32-2.36]. The low temperature SG phase below a SG freezing temperature T_g exhibits intriguing non-equilibrium dynamics which is characterized by the chaotic nature and ageing behavior. The zero-field SG never reaches equilibrium. The non-equilibrium character can be experimentally observed from an age-dependence of the magnetic response. When the SG system is quenched from a high temperature above the SG transition temperature T_g to a low temperature T below T_g (this process is called the zero-field cooled (ZFC) aging protocol), the initial state is not thermodynamically stable and relaxes to more stable state. The

aging behaviors depend strongly on their thermal history within the SG phase. The rejuvenation (chaos) and memory effects are also significant features of the aging dynamics. These effects are typically measured from the low frequency AC magnetic susceptibility. The SG phase is also susceptible to any perturbation in the form of temperature or field changes, which consequently, if large enough, effectively reinitializes the ageing process (temperature chaos). Both aging behavior and chaotic nature of the low temperature SG phase have been viewed first as additional difficulty in the understanding of SG's. However, it proved to be a key feature of the SG behavior, offering the unique opportunity to explore the nature of the SG phase.

2.7 Transport Properties

2.7.1 Conduction Mechanism in Ferrites

The conduction mechanism in ferrites is quite different from that in semiconductors. Ferrites are ferromagnetic semiconductors that could be used in electronic devices. The increasing demand for low loss ferrites resulted in detailed investigations on conductivity and on the influence of various substitutions on the electrical conductivity, thermoelectric power, etc. In ferrites, the temperature dependence of mobility affects the conductivity and the carrier concentration is almost unaffected by temperature variation. In semiconductors, the band type conduction occurs, where in ferrites, the cations are surrounded by closed pack oxygen anions and as a first approximation can well be treated as isolated from each other. There will be a little direct overlap of the anion charge clouds or orbital. In other words, the electrons associated with particular ion will largely remain isolated and hence a localized electron model is more appropriate than a collective electron (band) model. This accounts for the insulating nature of ferrites. These factors led to the hopping electron model [2.37]. An appreciable conductivity in these ferrites is found to be due to the presence of Fe-ions with different valence states at crystallographically different equivalent lattice points [2.38]. Conduction is due to exchange of 3d electrons, localized at the metal ions, from Fe^{3+} to Fe^{2+} [2.22].

2.7.2 Hopping Model of Electrons

The materials like ferrites, there is a possibility in exchanging valency of a considerable fraction of metal ions and especially that of iron ions. In the presence of lattice vibrations the ions

occasionally come close enough together for transfer to occur with high degree of probability. Thus only the lattice vibrations induce the conduction and in consequence the carrier mobility shows temperature dependence characterized by activation energy. The temperature dependence of conductivity arises only due to mobility and not due to the number of charge carriers in the sample. It is noted that for hopping conduction mechanism;

- The mobility has a minimum value much lower than the limiting value ($0.1 \text{ cm}^2/\text{Vs}$) taken as minimum for band conduction [2.39].
- The independence of Seebeck coefficient on temperature is due to the fact that in hopping model the number of charge carriers is fixed.
- Thermally activated process with activation energy E_a called hopping activation energy.
- Occurrence of n-p transitions with charge carriers in the Fe^{2+} or oxygen concentration in the system.

CHAPTER-III
Experimental

Experimental

3.1 Sample Preparation

3.1.1 Composition of Ferrites

In the present research work conventional ceramic method has been employed for a series of various compositions of Co-ferrite were studied. The powder preparation process are sintering facility available at Materials Science Division, Atomic Energy Centre, Dhaka has been utilized in the preparation of samples. The following compositions were fabricated characterized and investigated thoroughly.

- (i) CoFe_2O_4
- (ii) $\text{Co}_{1-x}\text{Cd}_x\text{Fe}_2\text{O}_4$ (where $x = 0.1 - 1.0$ in the steps of 0.1)
- (iii) $\text{Co}_{1-x}\text{Zn}_x\text{Fe}_2\text{O}_4$ (where $x = 0.1 - 1.0$ in the steps of 0.1)
- (iv) $\text{Co}_{0.2}\text{Cd}_{0.8}\text{Fe}_{2-x}\text{RE}_x\text{O}_4$ (where RE = Ho and Sm; $x = 0.05$ and 0.1)
- (v) $\text{Co}_{0.2}\text{Zn}_{0.8}\text{Fe}_{2-x}\text{RE}_x\text{O}_4$ (where RE = Eu and Gd; $x = 0.05$ and 0.1)

3.1.2 Sample Preparation Technique

The preparation of Polycrystalline ferrites with optimized properties has always demanded delicate handling and cautious approach in materials synthesis and appropriate knowledge of thermodynamics control of the chemical composition and homogeneity. The ferrite is not completely defined by its chemistry and crystal structure but also requires knowledge and control of parameters of its microstructure such as density, lattice parameter, porosity and their intra- and intergranular distribution. It is well known that almost all ferrites decompose at the elevated temperature if we want to sinter them under normal conditions. This happens because the oxygen splits off at higher temperature reducing Fe^{3+} to Fe^{2+} . There are several techniques to prepare ferrites, such as solid state reaction method [3.1]; high energy ball milling [3.2]; Sol gel method [3.3]; chemical co-precipitation method [3.4]; microwave sintering method [3.5]; auto combustion method [3.6] etc for preparation of polycrystalline ferrite materials. The normal methods of preparation of ferrites comprise of the conventional ceramic method i.e., solid state reaction

method involving milling of reactions following by sintering at elevated temperature range and nonconventional method, also called wet method. Chemical co-precipitation method and sol-gel method etc. are examples of wet method. In the present investigation solid state reaction has been employed for the preparation of Co-ferrite samples for its relative simplicity and availability.

The overall preparation process generally comprised of the following four major steps:

- (i) Preparing a mixture of materials,
- (ii) Pre-firing the mixture to form ferrite at wet milling,
- (iii) Pre-sintering and
- (iv) Sintering.

3.1.2.1 Preparing a Mixture of Materials

Ferric oxide Fe_2O_3 and whatever oxides MO are required are taken in powder form with the cations in the ratio corresponding to that in the final product. Metal carbonates may also be used; during the later firing, CO_2 will be given off and they will be converted to oxides.

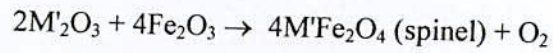
3.1.2.2 Pre-firing the Mixture to form Ferrite at Wet Milling

The extend of this work in this step varies greatly depending on the starting materials, when component oxides are used, the corresponding step involves a mere mixing of the oxides by wet milling. Prolonged wet grinding of the powder mixture in steel ball mills produces good mixing and a smaller particle size, which in turn decreases the porosity of the final product. To avoid iron contamination, mixing is done in a rubber-lined mill with stainless-steel balls and a fluid such as distilled water or acetone/ ethanol is used to prepare the mixture in to slurry.

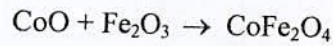
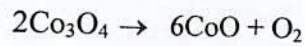
3.1.2.3 Pre-sintering

The pre-sintering is very crucial because in this step of sample preparation a ferrite is formed from its component oxides. The slurry prepared in step (1) is dried, palletized and then transferred to a porcelain crucible for pre-firing at temperature between $900^{\circ}C$ and $1200^{\circ}C$. This was performed in a furnace named Gallen Kamp at Materials Science Division, Atomic Energy Centre, Dhaka. This is done in air, and the temperature goes up to about $1200^{\circ}C$ down to $200^{\circ}C$ in about 20hours of time. Solid-state reactions take place between the component oxides in this stage, leading to the formation of ferrites actually achieved by counter diffusion. This means that

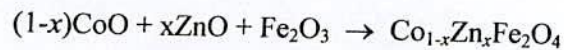
the diffusion involves two or more species of ions which move in opposite direction initially across the interface of two contacting particles of different component oxides. During the pre-sintering stage, the reaction of Fe_2O_3 with metal oxide (MO or $\text{M}'_2\text{O}_3$, where M is divalent and M' is the trivalent metal atom) takes place in the solid state to form spinel according to the reactions [3.7]:



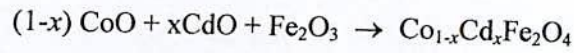
For Co-ferrite,



For Co-Zn ferrite,

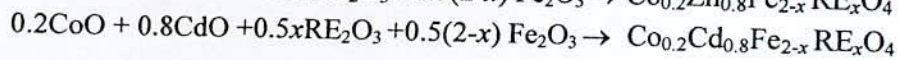
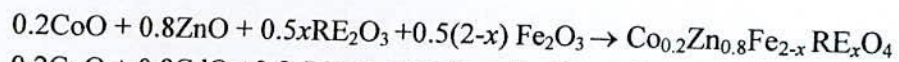


For Co-Cd ferrite,



(Where $x = 0.0 - 1.0$ in steps of 0.1)

The reaction of the Rare-earth doped ferrite system,



As far as the final composition of the ferrite is concerned step (2) is most crucial because subsequent steps would not change the composition substantially. However, the 'raw' ferrite thus formed has two defects its composition is not homogeneous and it contains pores. In order to produce chemically homogeneous, dense and magnetically better material of desired shape and size, sintering at an elevated temperature is needed.

These undesirable features of the raw ferrites are eliminated in the following two steps:

(i) **Grinding:** The ferrite produced via presintering is usually in the lump form. In this step, it is first ground into powder in a steel ball mill. Grinding eliminates intraparticle pores,

homogenizes the ferrite, reduces the particle size to $\ll 1\mu\text{m}$ and promote mixing of any unreacted oxides.

(ii) **Pressing or Extrusion:** The dry powder is mixed with an organic binder and pressed in to compacts of desired shapes either by the conventional method in a die-punch assembly or by hydrostatic or isostatic compaction. Most shapes, such as toroidal cores, are pressed (at 1 - 10 ton / cm^2 , 14 - 140 MPa), but rods and tubes are extruded.

2.1.2.4 Sintering

Sintering is the final and a very critical step of preparing a ferrite with optimized properties. The sintering time, temperature and the furnace atmosphere play very important role on the magnetic property of final materials. Sintering commonly refers to processes involved in the heat treatment by which a mass of compacted powder is transformed into a highly densified object by heating it in a furnace below its melting point. Ceramic processing is based on the sintering of powder compacts rather than melting/ solidifications/cold working (characteristic for metal), because:

- (i) Ceramics melt at high temperatures
- (ii) As solidified microstructures cannot be modified through additional plastic deformation and re-crystallization due to brittleness of ceramics
- (iii) The resulting coarse grains would act as fracture initiation sites
- (iv) Low thermal conductivities of ceramics ($< 30 - 50 \text{ W / mK}$) in contract to high thermal conductivity of metals (in the range $50 - 300 \text{ W / mK}$) cause large temperature gradients, and thus thermal stress and shock in melting-solidification of ceramics.

Sintering is the bonding together of a porous aggregate of particles at high temperature. The thermodynamic driving force is the reduction in the specific surface area of the particles. The sintering mechanism usually involves atomic transport over particle surfaces, along grain boundaries and through the particle interiors. Any unreacted oxides form ferrite, inter diffusion occurs between adjacent particles so that they adhere (sinter) together, and porosity is reduced by the diffusion of vacancies to the surface of the part. Strict control of the furnace temperature and atmosphere is very important because these variables have marked effects on the magnetic properties of the product. Sintering may result in densification, depending on the predominant diffusion pathway. It is used in the fabrication of metal and ceramic components, the

agglomeration of ore fines for further metallurgical processing and occurs during the formation of sandstones and glaciers. Sintering must fulfill three requirements:

- (a) to bond the particles together so as to impart sufficient strength to the product
- (b) to densify the grain compacts by eliminating the pores and
- (c) to complete the reactions left unfinished in the pre-sintering step [3.8]

The theory of heat treatment is based on the principle that when a material has been heated above a certain temperature, it undergoes a structural adjustment or stabilization when cooled at room temperature. The cooling rate plays an important role on which the structural modification is mainly based.

Why do need Sintering?

The principle goal of sintering is the reduction of compact porosity. Sometimes the initial spaces between compacted grains of ceramics are called “voids”, to differentiate term from the isolated spaces = pores, which occur in the final stages of sintering. The sintering process is usually accompanied by other changes within the materials, some desirable and some undesirable. The largest- changes occur in;

- (i) To bind the particles together so as to impart sufficient strength to the products,
- (ii) To densify the green compacts by eliminating the pores,
- (iii) To homogenizer the materials by completing the relation left unpreshed in the pre-sintering step,
- (iv) To make strength of elastic modulus,
- (v) To make hardness and fracture toughness,
- (vi) To make homogeneous distribution of grain number, grain size and shape,
- (vii) To improve the average pore size and shape and
- (viii) To get a stable chemical composition and crystal structure.

Sintering is a widely used but very complex phenomenon. The fundamental quantification of change in pore fraction and geometry during sintering can be attempted by several techniques, such as: dilatometry, buoyancy, gas absorption, porosimetry indirect methods (e.g. hardness) and quantitative microscopy etc. The description of the sintering process has been derived from model

experiments (e.g. sintering of a few spheres) and by observing powdered compact behavior at elevated temperatures.

The following phenomena were observed:

- (i) Increase of inter- particle contact area with time,
- (ii) Rounding- off of sharp angles and points of contacts,
- (iii) In most cases the approach of particle centers and overall densification,
- (iv) Decreases in volume of inter connected pores,
- (v) Continuing isolation of pores and
- (vi) Grain growth and decreases in volume of isolated pores.

3.1.3 Method of Sample Preparation

3.1.3.1 Solid State Reaction Method

Polycrystalline ferrites are prepared normally by power metallurgy or ceramic technology. This means that ferrites attain their homogeneous compositions by reactions in the solid state and the shapes of the ferrite products are produced by pressing and subsequent sintering. A series of polycrystalline samples of mixed ferrites were prepared by the standard double sintering ceramic methods at the Materials Science Division, Atomic Energy Centre, Dhaka. In this method high purity oxides (99.99%) such as Fe_2O_3 , Co_3O_4 , CdO , ZnO and Rare earth oxide of E-Mark of Germany were weighted precisely according to their molecular weight. The weight percentage of the oxide to be mixed for various samples was calculated by using formula:

$$\text{Weight \% of oxide} = \frac{M.\text{wt. of oxide} \times \text{required weight of the sample}}{\text{Sum of Mol.wt. of each oxide in a sample}}$$

The constituent in required stoichiometric proportions of materials were trough mixed using ceramic mortar and pestle for 4 hrs and then ball milled in a planetary ball mill in ethyl alcohol media for 2hrs with stainless steel balls of different sizes in diameter Fig. 3.1. The slurry was dried and the powder was pressed into disc shape. The disc shaped sample was pre-sintered at 950°C for 5hrs. The sample was then cooled down to room temperature at the same rate as that of heating. After that samples were crushed again and subsequently wet ball milled for 6hrs hours in

distilled water to reduce it to small crystallites of uniform size. In order to produce chemically homogeneous and magnetically better material this prefired lump material was crushed.

These oxide mixtures were milled thoroughly for 4-6 hours to obtain homogeneous mixture. The mixture was dried and a small amount of saturated solution of polyvinyl alcohol (PVA) were added as a binder and pressed into pellet and toroid shape respectively under pressure 1.75 ton-cm^{-2} and 1.2 ton-cm^{-2} using hydraulic press Fig. 3.2. The prepared samples shown in Fig 3.3 were sintered at 1050°C - 1200°C for 2-3 hrs with a microprocessor controlled muffle furnace. The samples were polished in order to remove any oxide layer formed during the process of sintering.

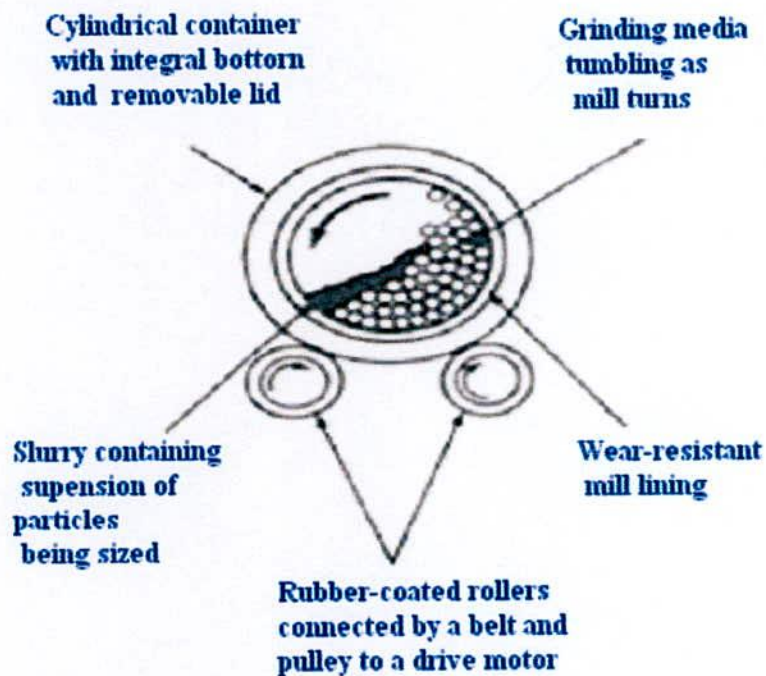


Fig. 3.1 Rubber-lined mill with stainless-steel balls



Fig. 3.2 Hydraulic press used to make different shaped samples.



Fig. 3.3 Toroid and disk shape sample.

The following block diagram in Fig. 3.4 represents the method employed for the Co-ferrites:

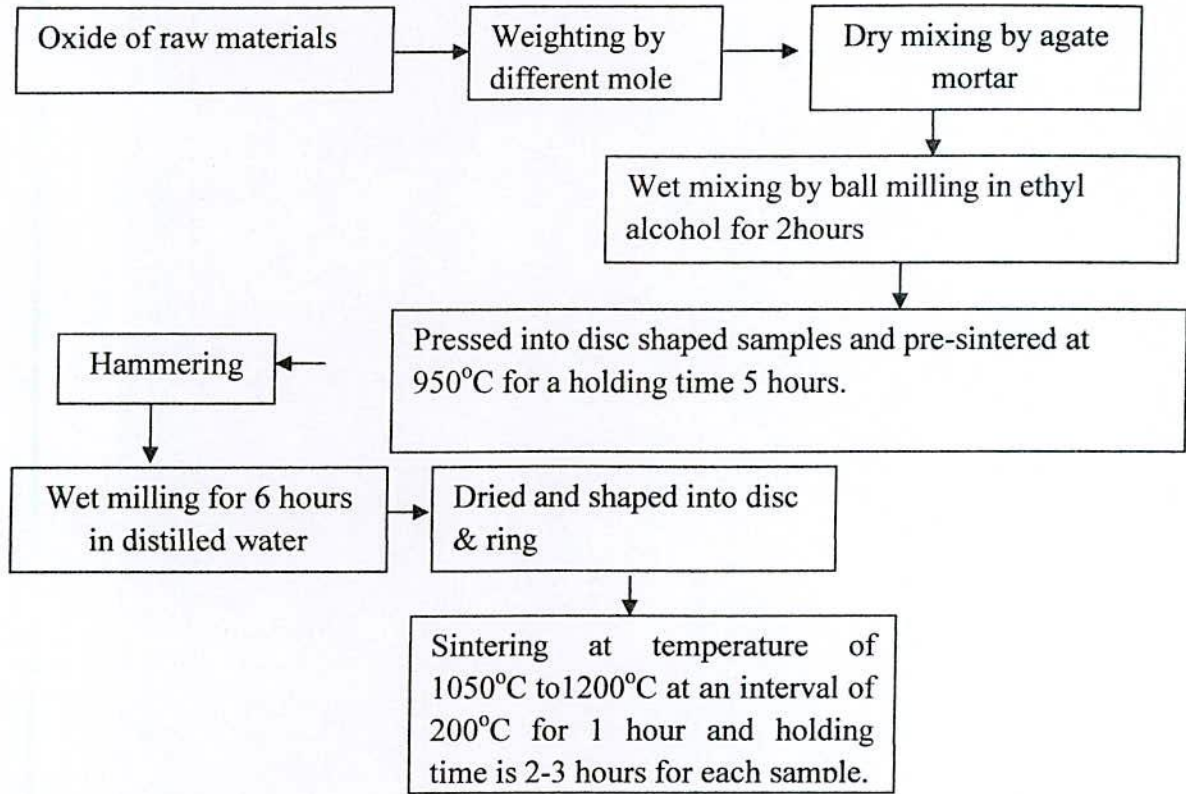


Fig. 3.4 Flowchart of Ferrite sample preparation.

3.2 X-ray Diffraction (XRD) Technique

X-rays are the electromagnetic waves whose wavelength is in the neighborhood of 1\AA . The wavelength of an X-ray is that the same order of magnitude as the lattice constant of crystals and it is this which makes X-ray so useful in structural analysis of crystals. X-ray diffraction (XRD) provides precise knowledge of the lattice parameter as well as the substantial information on the crystal structure of the material under study. X-ray diffraction is a versatile nondestructive analytical technique for identification and quantitative determination of various crystalline phases of powder or solid sample of any compound. When X-ray beam is incident on a material, the photons primarily interact with the electrons in atoms and get scattered. Diffracted waves from different atoms can interfere with each other and the resultant intensity distribution is strongly modulated by this interaction. If the atoms are arranged in a periodic fashion, as in

crystals, the diffracted waves will consist of sharp interference maxima (peaks) with the same symmetry as in the distribution of atoms. Measuring the diffraction pattern therefore allows us to deduce the distribution of atoms in a material. It is to be noted here that, in diffraction experiments, only X-rays diffracted via elastic scattering are measured.

The peaks in an X-ray diffraction pattern are directly related to the atomic distance. Let us consider an incident X-ray beam interacting with the atoms arranged in a periodic manner as shown in two dimensions in Fig. 3.5. The atoms, represented as spheres in the illustration, can be viewed as forming different sets of planes in the crystal. For a given set of lattice planes with an inter-plane distance of d , the condition for a diffraction (peak) to occur can be simple written as

$$2d \sin n\theta = n\lambda, \quad (3.1)$$

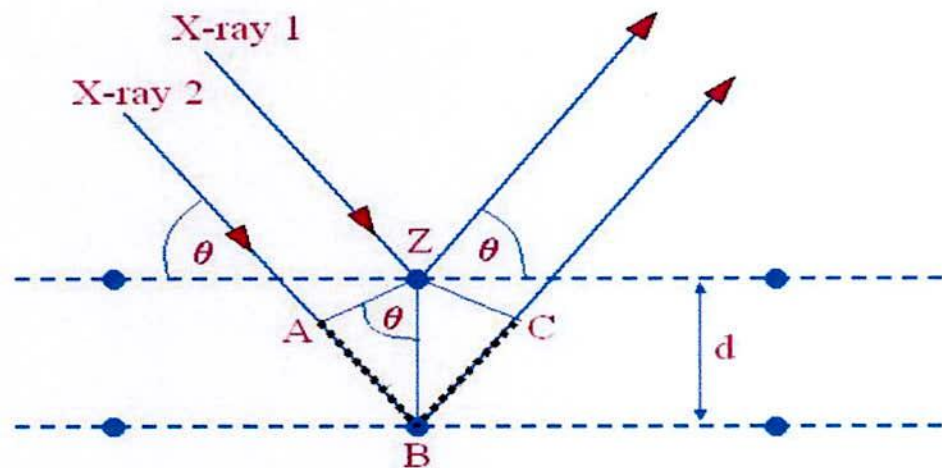


Fig. 3.5 Bragg's diffraction pattern.

which is known as Bragg's law. In the equation, λ is the wavelength of the X-ray, θ is the scattering angle, and n is an integer representing the order of the diffraction peak. The Bragg's Law is one of the most important laws used for interpreting X - ray diffraction data. From the law, we find that the diffraction is only possible when $\lambda < 2d$ [3.9].

In the present work, A PHILIPS PW 3040 X'pert PRO X-ray diffractometer was used for the lattice parameter to study the crystalline phases of the prepared samples in the Materials Science division, Atomic Energy Centre, Dhaka. Fig. 3.6 shows the block diagram of X'pert XRD system.

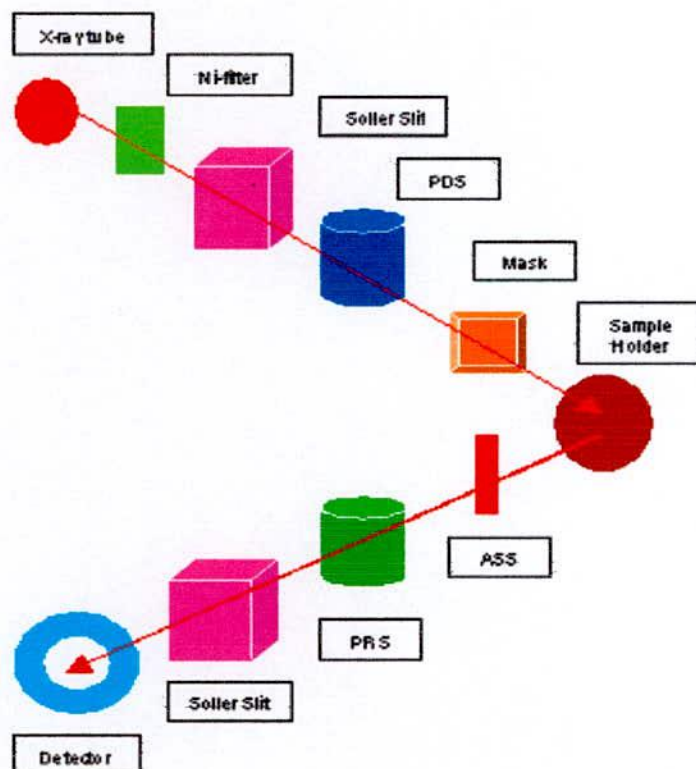


Fig. 3.6 Block diagram of the PHILIPS PW 3040 X' Pert PRO XRD system.

The powder diffraction technique was used with a primary beam powder of 40 kV and 30mA for Cu-K_α radiation. A nickel filter was used to reduce Cu-K_β radiation and finally Cu-K_α radiation was only used as the primary beam. The experimental has been performed at room temperature. A 2θ scan was taken from 15° to 75° to get possible fundamental peaks of the samples with the sampling pitch of 0.02° and time for each step data collection was 1.0 sec. Both the programmable divergence and receiving slits were used to control the irradiated beam area and output intensity from the powder sample, respectively. An antiscatter slit was used just after the tube and in front of the detector to get parallel beam only. All the data of the samples were stored in the computer memory and later on analyzed them using computer "software, X' PERT HJGHS CORE". For XRD experiment each sample was set on a glass slide and fixed the sample by putting adhesive typed the two ends of the sample.

For each composition, the cylindrical samples of weight more than 2 gm are converted into powder. For XRD experiment each sample was set on a glass slide and fixed the sample by putting adhesive tape at the two ends of the sample X-ray diffraction patterns were carried out to confirm the crystal structure. Instrumental broadening of the system was determined from $\theta-2\theta$ scan of standard Si. At (311) reflection's position of the peak, the value of instrumental broadening was found to be 0.07° . This value of instrumental broadening was subtracted from the pattern. After that, using the X-ray data, the lattice constant (a) and hence the X-ray densities were calculated.

3.2.1 Different Parts of the PHILIPS X'Pert PRO XRD System

Fig. 3.7 shows the inside view of the X'pert PRO XRD system. A complex of instruments of X-ray diffraction analysis has been established for both materials research and specimen characterization.

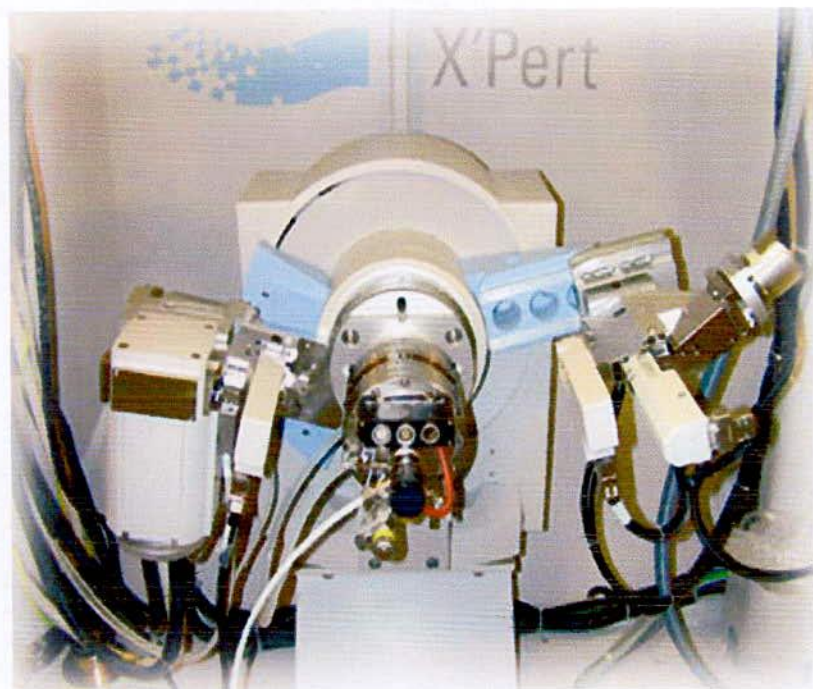


Fig. 3.7 Internal arrangement of a PHILIPS X'Pert PRO X-ray diffractometer.

These include facilities for studying single crystal defects, and a variety of other materials problems.

The PHILIPS X' Pert PRO XRD system comprised of the following parts;

- (i) "Cu-Tube" with maximum input power of 60 kV and 55 mA,
- (ii) "Ni- Filter" to remove Cu-K_α component,
- (iii) "Solar slit" to pass parallel beam only,
- (iv) "Programmable Divergent slits" (PDS) to reduce divergence of beam and control irradiated beam area,
- (v) "Mask" to get desired beam area,
- (vi) "Sample holder" for powder sample,
- (vii) "Anti Scatter slit" (ASS) to reduce air scattering back ground,
- (viii) "Programmable Receiving slit" (PRS) to control the diffracted beam intensity and
- (ix) "Solar slit" to stop scattered beam and pass parallel diffracted beam only.

3.2.2 Interpretation of the XRD data

The XRD data consisting of θ_{hkl} and d_{hkl} values corresponding to the different crystallographic planes are used to determine the structural information of the samples like lattice parameter and constituent phase. Lattice parameters of Co-ferrites samples were determined. Normally, lattice parameter of an alloy composition is determined by the Debye-Scherrer method after extrapolation of the curve. We determine the lattice spacing (interplaner distance), d using these reflections from the equation which is known as Bragg's Law.

$$2d_{hkl} \sin\theta = \lambda$$

$$\text{i.e. } d_{hkl} = \frac{\lambda}{2 \sin \theta} \quad , \quad (3.2)$$

where λ is the wavelength of the X-ray, θ is the diffraction angle and n is an integer representing the order of the diffraction.

The lattice parameter for each peak of each sample was calculated by using the formula:

$$a = d_{hkl} \times \sqrt{h^2 + k^2 + l^2} \quad , \quad (3.3)$$

where h, k, l are the indices of the crystal planes. We get d_{hkl} values from the computer using software "X' Pert HJGHS CORE". So we got ten 'a' values for ten reflection planes such as a_1 ,

a_2 a_3 etc. Determine the exact lattice parameter for each sample, through the Nelson-Riley extrapolation method. The values of the lattice parameter obtained from each reflected plane are plotted against Nelson-Riley function [3.10]. The Nelson-Riley function $F(\theta)$, can be written as

$$F(\theta) = \frac{1}{2} \left[\frac{\cos^2 \theta}{\sin \theta} + \frac{\cos^2 \theta}{\theta} \right], \quad (3.4)$$

where θ is the Bragg's angle. Now drawing the graph of 'a' vs $F(\theta)$ and using linear fitting of those points will give us the lattice parameter ' a_0 '. This value of ' a_0 ' at $F(\theta) = 0$ or $\theta = 90^\circ$. These ' a_0 's are calculated with an error estimated to be $\pm 0.0001 \text{ \AA}$.

3.2.3 X-ray Density and Bulk Density

X-ray density, ρ_x was also calculated usual from the lattice constant. The relation between ρ_x and 'a' is as follows,

$$\rho_x = \frac{ZM}{Na^3}, \quad (3.5)$$

where M is the molecular weight of the corresponding composition, N is the Avogadro's number ($6.023 \times 10^{23} \text{ mole}^{-1}$), 'a' is the lattice parameter and Z is the number of molecules per unit cell, ($Z = 8$ for the spinel cubic structure). The bulk density was calculated considering a cylindrical pellet of mass (m) and volume (V) of the pellets using the relation

$$\rho_B = \frac{m}{V} = \frac{m}{\pi r^2 h}, \quad (3.6)$$

where m is the mass of the pellet sample, r is the radius and h is the thickness of the pellet.

3.2.4 Porosity

Porosity is a parameter which is inevitable during the process of sintering of oxide materials. It is noteworthy that the physical and electromagnetic properties are strongly dependent on the porosity of the studied samples. Therefore an accurate idea of percentage of pores in a prepared sample is prerequisite for better understanding of the various properties of the studied samples to correlate the microstructure property relationship of the samples under study. The porosity of a material depends on the shape, size of grains and on the degree of their storing and packing. The

difference between the bulk density ρ_B and X-ray density ρ_x gave us the measure of porosity. Percentage of porosity has been calculated using the following relation [3.11]

$$P = \left(1 - \frac{\rho_B}{\rho_x}\right) \times 100\% \quad (3.7)$$

3.3 Permeability Measurement

3.3.1 Curie temperature

Curie temperature measurement is one of the most important measurements because it provides substantial information on magnetic status of the substance in respect to the strength of exchange interaction. Above Curie temperature spontaneous magnetization vanishes and ferromagnetic materials behave like paramagnetic materials. So the determination of Curie temperature accurately is of great importance. The temperature dependence properties of ferrite materials depend upon its sublattice distribution and spin orientations of the metal ions and we can predict about the sublattice magnetization by measuring the Curie temperature.

There are several processes of measuring the Curie temperature; these are

- (i) by measuring magnetization against temperature,
- (ii) by measuring variation of initial permeability against temperature,
- (iii) by measuring susceptibility against temperature and
- (iv) by measuring the variation of resistivity of the sample against temperature.

In our present research work, we measured the Curie temperature of the samples by observing the variation of initial permeability of the ferrite samples with temperature and magnetization against temperature.

3.3.2 Measurement of Curie Temperature by Observing the Variation of Initial Permeability with Temperature

For ferrimagnetic materials in particular, for ferrite it is customary to determine the Curie temperature by measuring the permeability as a function of temperature. According to Hopkinson effect [3.12] which arises mainly from the intrinsic anisotropy of the material has been utilized to determine the Curie temperature of the samples. According to this phenomenon, the permeability

increases gradually with temperature and reaching to a maximum value just before the Curie temperature.

Curie temperature measurements were done by using Hewlett Packard 4192A LF Impedance Analyzer shown in Fig. 3.8. Impedance parameters absolute value of impedance ($|Z|$), absolute value of admittance ($|Y|$), phase angle (θ), resistance (R), reactance (X), conductance (G), susceptance (B), inductance (L), capacitance (C), dissipation (D) and quality factor (Q). Measurement range of $|Z|/R/X$ is 0.1m Ω to 1.2999 M Ω , $|Y|/G/B$ is 1 ns to 12.999 s; θ is -180° to +180°; L is 0.1mH to 1.000 kH; C is 0.1PF to 100.0 mF, D is 0.0001 to 19.999; Q is 0.1 to 1999.9. All have a basic accuracy of 0.1% and resolution of $4\frac{1}{2}$ digits. Number of display digits dependence on measuring frequency and OSC level setting. We made use of the excellent experimental facilities available at the Materials Science Division, Atomic Energy Centre, Dhaka.

The temperature dependent permeability was measured by using induction method. The specimen formed the core of the coil. The number of turns in each coil was 5. We used a constant frequency (100 kHz) of a sinusoidal wave, AC signal of 100mV. HP 4192A impedance analyzer with continuous heating rate of ≈ 5 K / min with very low applied ac field of $\approx 10^{-3}$ Oe. By varying temperature, inductance of the coil as a function of temperature was measured. Dividing this value of L_0 (inductance of the coil without core material), we got the permeability of the core i.e. the sample. When the magnetic state inside the ferrite sample changes from ferromagnetic to paramagnetic, the permeability falls sharply. From this sharp fall at specific temperature the Curie temperature was determined. For the measurement of Curie temperature, the sample was kept inside a cylindrical oven with a thermocouple placed at the middle of the sample. The thermocouple measures the temperature inside the oven and also of the sample.

The sample was kept just in the middle part of the cylindrical oven in order to minimize the temperature gradient. The temperature of the oven was then raised slowly. If the heating rate is very fast then the temperature of the sample may not follow the temperature inside the oven and there can be misleading information on the temperature of the samples. The thermocouple showing the temperature in that case will be erroneous. Due to the closed winding of wires the sample may not receive the heat at once. So, a slow heating rate can eliminate this problem. The

cooling and heating rates are maintained as approximately $0.5^{\circ}\text{C min}^{-1}$ in order to ensure a homogeneous sample temperature. Also a slow heating ensures accuracy in the determination of Curie temperature.

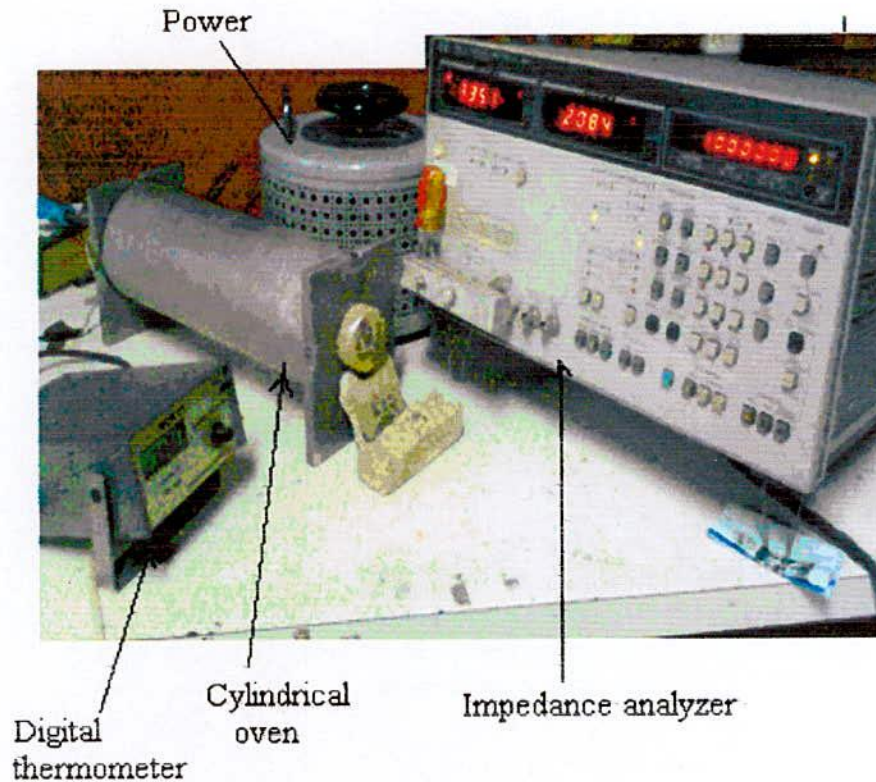


Fig. 3.8 Impedance Analyzer Model-Hewlett-Packard 4192A.

The oven was kept thermally insulated from the surroundings. The temperature was measured with a digital thermometer attached close to the sample and put inside the furnace where the temperature fluctuation is almost negligible. Then the permeability versus temperature curve was plotted from which the Curie temperature was calculated.

3.3.3 Permeability

From the frequency dependence of complex permeability, evolution of permeability and magnetic loss component at different stages of ferrite sample as affected by thermal treatment at different temperature was determined using toroids shape sample prepared with insulating Cu wire. The 4192 LF Impedance analyzer directly measure the value of inductance, L and loss factor.

$$D = \tan \delta \quad (3.8)$$

From inductance the value of real part of complex permeability, μ' can be obtained by using the relation

$$\mu' = \frac{L}{L_0}, \quad (3.9)$$

where L is the inductance of the toroid and L_0 is the inductance of the coil of same geometric shape in vacuum, L_0 is determined by using the relation,

$$L_0 = \frac{\mu_0 N^2 S}{\pi \bar{d}} \quad (3.10)$$

Here μ_0 is the permeability of the vacuum, N is the number of turns (here $N = 5$), S is the cross-sectional area of the toroid shaped sample, $S = dh$, where, $d = \frac{d_1 + d_2}{2}$ and \bar{d} is the average diameter of the toroid sample given as

$$\bar{d} = \frac{d_1 + d_2}{2}, \quad (3.11)$$

where, d_1 and d_2 are the inner and outer diameter of the toroid samples.

3.3.4 Mechanisms of Permeability

Mechanisms of permeability can be explained as the following way: a demagnetized magnetic material is divided into number of Weiss domains separated by block walls. In each domain all the magnetic moments are oriented in parallel and the magnetization has its saturation value M_s . In the walls the magnetization direction changes gradually from the direction of magnetization in one domain to that in the next. The equilibrium positions of the walls results from the interactions with the magnetization in neighboring domains and from the influence of pores; crystal boundaries and chemical in homogeneities which tend to favor certain wall positions.

3.3.5 Technique of Measurements of Permeability

Measurements of permeability normally involve the measurements of the change in self inductance of a coil presence of the magnetic core. The behavior of a self inductance can now be described as follows. Suppose we have an ideal lossless air coil of inductance L_0 . On insertion of magnetic core with permeability μ , the inductance will be μL_0 . The complex impedance Z of this coil can be expressed as,

$$Z = R + jX = j\omega L_0(\mu' - j\mu''), \quad (3.12)$$

where the resistive part is

$$R = \omega L_0 \mu'', \quad (3.13)$$

and the reactive part is

$$X = \omega L_0 \mu' \quad (3.14)$$

The radio frequency (RF) permeability can be derived from the complex impedance of a coil Z (Eqn. 3.12). The core is usually toroidal to avoid demagnetization effects. The quantity L_0 is derived geometrically.

3.3.6 Frequency Characteristic of Ferrite Samples

The frequency characteristics of the cubic ferrite sample i.e. the permeability spectra were investigated using a Hewlett Packard Impedance Analyzer of Model No.4192A provide the value of inductance, L and loss factor, $D = \tan\delta$. The measurements of inductances were taken in the frequency range of 1 kHz to 13 MHz. The values of measured parameters obtained as a function of frequency and the real (μ') and imaginary part (μ'') of permeability and the loss factor are calculated. μ' is calculated by using the Eqⁿ.3.9 and Eqⁿ.3.10 and μ'' is calculated by using the following equation

$$\mu'' = \mu' \tan\delta \quad (3.15)$$

3.4 Low Field Hysteresisgraph

Hysteresis is well known in ferromagnetic materials. When an external magnetic field is applied to a ferromagnet, the atomic dipoles align themselves with the external field. Even when the external field is removed, part of the alignment will be retained: the material has become magnetized.



Fig. 3.9 B-H loop tracer.

A general view of the B-H loop tracer with its system components is shown in Fig. 3.9. A hysteresisgraph or BH- Meter allows for the magnetic properties of soft magnetic materials to be measured. A schematic diagram of commercial hysteresisgraph has been presented Fig. 3.10. A hysteresisgraph has two major functions. It produces current to produce a magnetic field, and measures voltage over time to measure magnetic induction. By determining the induction response of the test sample to the applied current, the magnetic properties of the material is

determined. Most soft magnetic materials are measured using ring geometry. Two coils of wire are wound around the sample.

A current from a bi-polar power supply is passed through the primary coil to generate a magnetic field in the ring. The applied magnetic field is proportional to the current. As the sample magnetic induction changes in response to the applied magnetic field, a voltage is induced in the secondary windings. This induced voltage is integrated over time with a circuit often called a fluxmeter, as it is used in many applications to measure magnetic flux. The integrated voltage is proportional to the magnetic induction of the test samples. The current in the primary coil is determined by measuring the voltage across a resistor. All the data of the samples were analyzed using computer software to control the applied field and measure both B and H simultaneously.

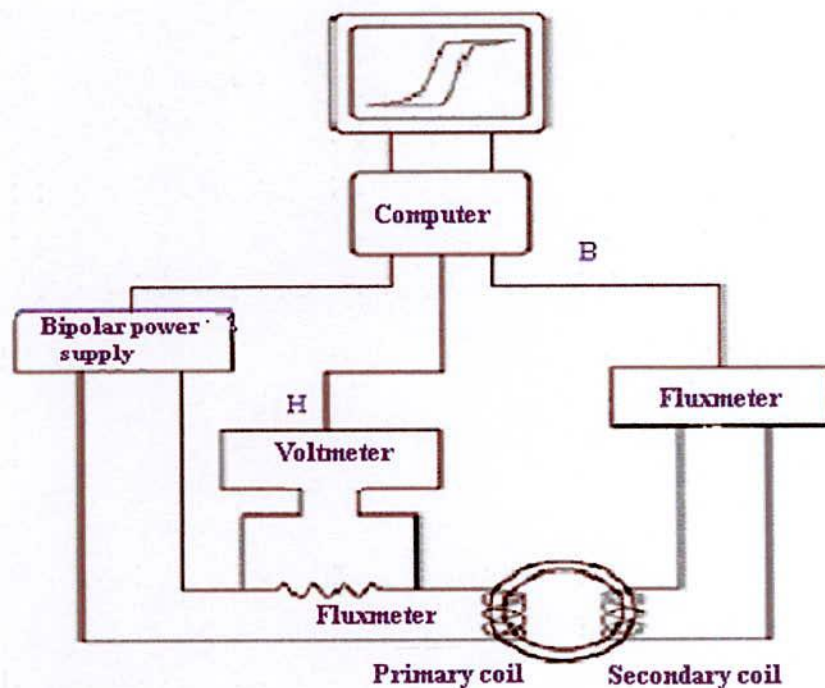


Fig. 3.10 Schematic diagram of commercial hysteresis graph.

3.4.1 Measurement of an Initial B-H Curve

As these are important curves for magnetic design, these curves are measured using a hysteresis graph. For accurate initial curves, the sample must be demagnetized prior to the

measurement. This demagnetization can be performed either externally, or in many cases, the sample can be demagnetized by the hysteresis graph. Residual magnetization can greatly distort the response of a soft magnetic material near zero field.

3.4.2 AC B-H Curve Measurement

In many applications, soft magnetic materials are subjected to cyclical magnetic field. The response of a soft magnetic material can be very complicated in this case, and is determined by both material parameters, such as sample permeability and material geometry. It can be exceedingly difficult to make accurate predictions of material performance through computer models. Therefore, the best way to determine the performance of these materials is to measure the BH-curve under cyclical applied magnetic fields. This can be performed using a hysteresis graph. The bi-polar power is driven at the test frequency, and the fluxmeter can measure the varying magnetic induction of the material. The resulting BH-curves are called AC BH-curves, and yield important information in regards to the material such as AC permeability and core loss. For these types of measurements, it is important that the hysteresis graph components have the appropriate frequency response to measure the AC BH-curve properly.

3.4.3 Materials Geometry

The AMH-series permeameter measures characteristics of soft magnetic materials, according to the IEC 60404-4 and IEC 60404-6 standards. The ideal sample geometry of soft magnetic material is a ring. This shape is preferable because ring shape eliminates factors that can distort the magnetic test results. The main source of distortion of test data on soft magnetic materials is usually from air-gaps present in the magnetic test circuit. These air gaps lower the apparent permeability of the material, and can be difficult to control. As ring geometry is continuous path, the magnetic circuit is closed, without any air gaps that cause distortion. In addition, the magnetic path length, which is required to convert the applied current in the sense windings into applied magnetic field, is easy to calculate and unambiguous for ring samples. In ring shaped samples, primary windings are wound on the ring to generate a magnetic field in the sample via applied current to the primary windings. A secondary coil is also wound onto the ring to inductively measure the magnetic induction of the sample. If this machining process is on a sample must be form of ring can be made in different methods:

- (i) made as an unique dense piece of material, obtained by mechanical works or by casting, sintering, etc.
- (ii) made by stacking several disks with the same internal and external diameter, that can be obtained by punching, laser cutting, etc.
- (iii) made by a unique thin strip wound as a clock-spring.

The external diameter D_e should be higher than 1.4 times the internal diameter D_i . The cross section A of the sample is calculated by the geometrical relation

$$A = \frac{(D_e - D_i)h}{2}, \quad (3.15)$$

where h is the thickness of the sample. The thickness can be measured normally with a gauge if the sample is a solid ring. If it is made by stacked rings, sometimes it is preferred to use the mass and the density, calculating the thickness h with the formula:

$$h = \frac{4m}{\rho\pi(D_e^2 - D_i^2)}, \quad (3.16)$$

where ρ is the density of the material.

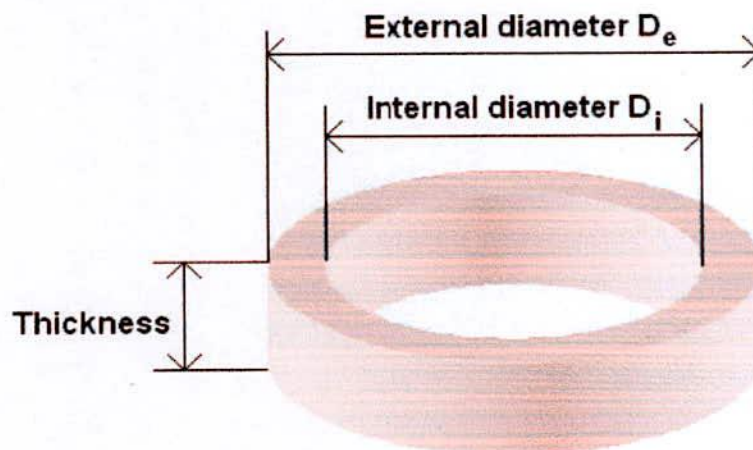


Fig. 3.11 Sample geometry.

3.4.4 Windings

In these instances accurate magnetic measurements can still be performed, since the sample geometry creates a closed magnetic circuit. For these measurements, primary and secondary coils are wound onto the sample, as with ring measurement. The magnetic path length of the test circuit must be either determined or known in order to convert the applied primary current into applied magnetic field.

Two types of windings are necessary for the measure:

- (i) Magnetization winding (N_H number of turns) and
- (ii) Measuring winding (N_B number of turns)

The magnetization winding consists of a suitable number of turns N_H in which flows the magnetization current, i . The current produces the magnetic field H following the relationship:

$$H = \frac{N_H i}{l_m}, \quad (3.18)$$

where l_m is the mean magnetic path length. If D_e does not exceed D_i more than 10 %, we can approximate l_m with the mean circumference:

$$l_m = \pi \frac{D_e + D_i}{2} \quad (3.19)$$

If $D_e \gg D_i$, then it is preferable to use the

$$l_m = \pi \frac{D_e - D_i}{\ln\left(\frac{D_e}{D_i}\right)} \quad (3.20)$$

The value of l_m is automatically calculated by the software.

The magnetic flux induced in the sample under test is measured using a computer-controlled integrating fluxmeter attached to the secondary winding. The secondary winding produces the induced voltage V_2 from which the magnetic flux Φ is obtained:

$$\Phi = - \int V_2 dt , \quad (3.21)$$

The integrating fluxmeter is the preferred method of measuring induced magnetic flux when the H field is being varied at frequencies from DC (typically 0.01Hz) to 10 kHz and numerically by the computer controlled software for AC measurements. The common method for implementing an electronic integrator consists of a DC amplifier with resistive–capacitive feedback and the magnetic induction, B is then obtained by the flux by the relationship:

$$B = \frac{\Phi}{N_B A} , \quad (3.22)$$

3.4.5 DC Measurement

DC measurements are made using a field that change very slowly, and that can be considered quasi-static. Since the variation of H, and in general the variation of B, is very slow, the inducted voltage is very small, and a numerical integration will give inaccurate results. The integration of the inducted voltage is performed by the fluxmeter, which is more precise and can follow very well the variation of B at such slow rate. After winding, the ring must be connected to the fluxmeter through the special cable for DC measure shown in Fig.3.12. This cable is simply an extension that takes signal from measuring connections to fluxmeter's inputs. For devices with two fluxmeters, use the B/J fluxmeter. This fluxmeter is then connected by the analog output (in the back panel) to the PC board. A 4-poles connector permits the connection to auxiliary optional devices. Connect the H turns to magnetization connectors and the B turns in the connections in the DC cable. Then connect the other terminals to the fluxmeter shown in Fig 3.13. The sample put on the fan grid.

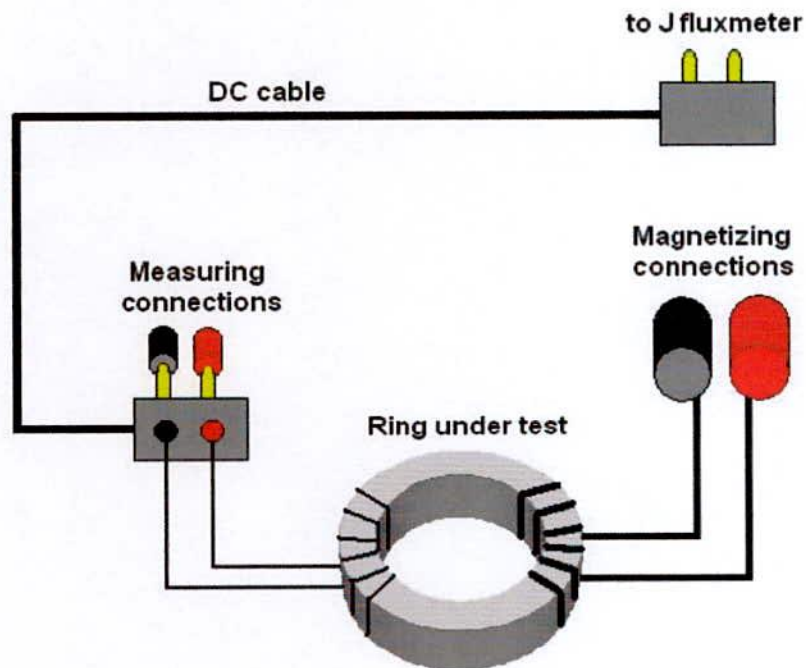


Fig. 3.12 DC measuring cable.

AC/DC hysteresis graph for hard and soft magnetic materials of the prepared samples measured AMH-1K-1800-HS B-H loop tracer in the Materials Science division, Atomic Energy Centre, Dhaka. In DC conditions, H and B are always in phase, and the max value of H corresponds to the max value of B. The Hysteresis cycle always has some sharp vertex. The DC normal magnetization curve is the set of all the vertex of different amplitude. The ratio between B and $\mu_0 H$ is a ratio between two simultaneous values, and it is called relative permeability. In Ac conditions, this is not always true, because the max H and max B can be 'shifted' by a phase angle. In this case, the hysteresis cycle has rounded vertex shown in Fig. 3.14. The ratio between B and $\mu_0 H$ is a ratio between two non-simultaneous values, and it is called amplitude permeability.

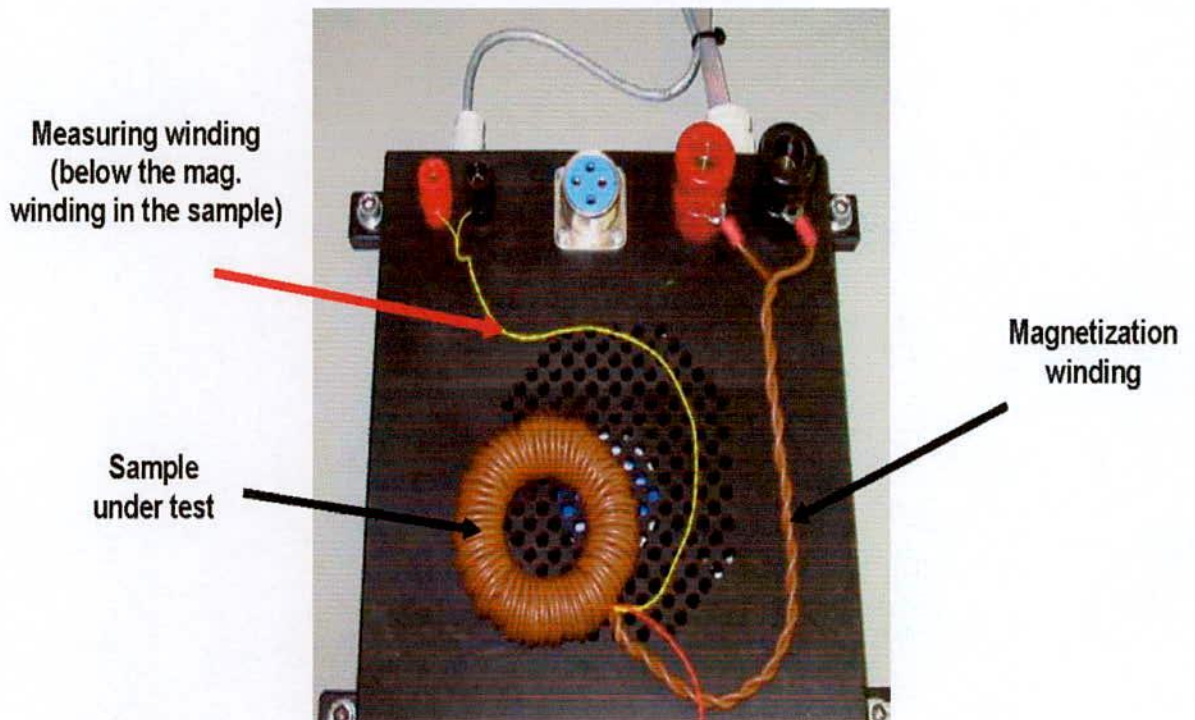


Fig. 3.13 The measuring and magnetizing connections are in the plastic tool inside the opening case.

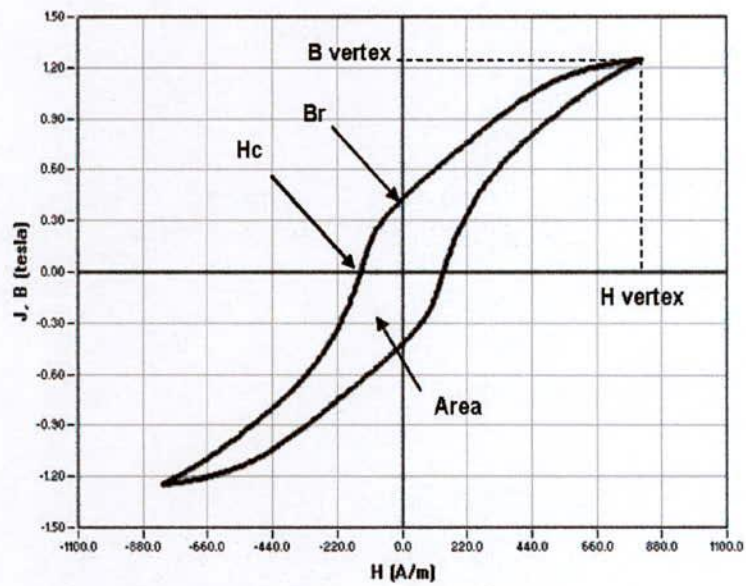


Fig.3.14 Hysteresis cycle.

3.5 Magnetization Measurement

Field cooled (M_{FC}) and zero field cooled (M_{ZFC}) magnetization, and temperature dependence of AC susceptibility measurements were done by using a Superconducting Quantum Interference Device (SQUID) MPMS XL magnetometer at Solid State Physics, Uppsala University, Sweden.

Field-cooled magnetization (M_{FC}): the sample is cooled in a field and the magnetization is recorded either on cooling or heating.

Zero-field-cooled magnetization (M_{ZFC}): the sample is cooled in zero magnetic field, a field is applied at the lowest measurement temperature, and then the magnetization is recorded on reheating.

3.5.1 SQUID Magnetometer

Superconducting Quantum Interface Device (SQUID) magnetometer MPMS XL, USA is the most sensitive available device for measuring magnetization at the Department of Engineering Sciences, Ångstrom laboratory, Uppsala University, Sweden. The magnetic properties measurement system MPMS XL is a sophisticated analytical instrument configured specially for the study of the magnetic properties of small samples over a broad range of temperature from 4.2 K to 400 K and magnetic fields from -50 KOe to +50 KOe. This standard system can measure the magnetic moment of solid, powder and liquid samples with a differential sensitivity of 10^{-9} emu and can handle a maximum signal size of 0.5 emu.

A general view of the MPMS XL with its system components is shown in Fig. 3.15. SQUID magnetometers are used to characterize materials when the highest detection sensitivity over a broad temperature range and using applied magnetic fields up to several Tesla is needed. Nowadays, this instrument is widely used worldwide in research laboratories. The system is designed to measure the magnetic moment of a sample, from which the magnetization and magnetic susceptibility can be obtained. Therefore, SQUID magnetometers are versatile instruments that perform both, DC and AC magnetic moment measurement. MPMS MultiVu is the software application controlling the RSO system.



Fig. 3.15 MPMS XL SQUID Magnetometer.

The major components of a SQUID magnetometer are: The RSO sample rod consists of one long, graphite sample rod; one short, graphite sample rod; and two centering plugs, superconducting magnet, superconducting detection coil, a SQUID connected to the detection coil, superconducting magnetic shield. Superconducting magnets are solenoid made of superconducting wire which must be kept at liquid helium dewar. The uniform magnetic field is produced along the axial cylindrical bore of the coil. The superconducting pick-up coil system, which is configured as a second order gradiometer is placed in the uniform magnetic field region of the solenoidal superconducting magnet. The SQUID device is usually a thin film that functions as an extremely sensitive current to voltage converter.

RSO sample rods are specially designed to insert a drinking straw shown in Fig. 3.16, which holds a sample, into the sample chamber. The centering plugs help keep a loose sample inside the straw and protect the straw from rubbing against the inside wall of the sample chamber. RSO sample rods may be used for RSO, DC, or AC measurements. The RSO option provides an alternative way of using the MPMS to measure the magnetic moment of samples. The RSO option measures a sample by moving it rapidly and sinusoidally through the SQUID pickup coils. The option's use of a high-quality servo motor and a digital signal processor (DSP) allow rapid measurements. The servo motor, unlike the stepper motor performing DC measurements, does not stop sample movement for each data reading. During an RSO measurement, a shaft encoder on the servo motor tracks the position of the sample. The position is recorded synchronous to the acquisition of the SQUID signal. The data is analyzed by using a nonlinear, least-squares fitting routine to fit the data to an ideal dipole response. The magnetic moment calibration for the MPMS is determined by measuring a palladium standard over a range of magnetic fields and by then adjusting the system calibration factors to obtain the correct moment for the standard. The standard is a right circular cylinder approximately 3 mm in diameter \times 3 mm in height. Samples of this size or smaller effectively imitate a point dipole to an accuracy of approximately 0.1%.

Measurements are done in this equipment by moving the samples through the second order gradiometer. Hence, the magnetic moment of the sample induces an electric current in the pick-up coil system. Superconducting magnetic shield is used to shield the SQUID sensor from the fluctuations of the ambient magnetic field of the place where the magnetometer is located and from the large magnetic field produced by the superconducting magnet. It is an important feature of the instrument that one can change the magnetic field either by "oscillate mode" or "no overshoot mode". The oscillate mode is used to minimize the remanent field of the magnet, whenever an accurate value of magnetic field is needed, e.g. in case of zero field cooling. In the hysteresis measurement the no overshoot mode has been selected, in which the field is changed directly from one value to another, and the magnet is returned to its persistent mode.

The MPMS XL features the new reciprocating sample measurement system. Unlike DC measurements where the sample is moved through the coils in discrete steps the RSO measurements are performed using a servomotor, which rapidly oscillates the sample is shown in Fig. 3.17. The RSO transport moves up and down, oscillating the sample around the measurement position. If autoranging is disabled, the MPMS repeats each measurement until it locates the emu

range that accommodates the SQUID's sensitivity. While the sample moves through the coils, MPMS MultiVu measures the SQUID's response to the magnetic moment of the sample. After a fit to the raw SQUID voltage data is performed for the specified number of cycles, MPMS MultiVu measures new SQUID voltage data and obtains another fit. This process is repeated until the measurements-to-average number is reached. Then MPMS MultiVu calculates the average sample moment from all the fits and also calculates the standard deviation if more than one measurement is averaged. The data is saved to the active data files. MPMS MultiVu uses a nonlinear, least-squares fitting routine to fit the data to an ideal dipole response in order to determine the sample position. MPMS MultiVu uses a measurement algorithm to compute the magnetic moment of the sample.

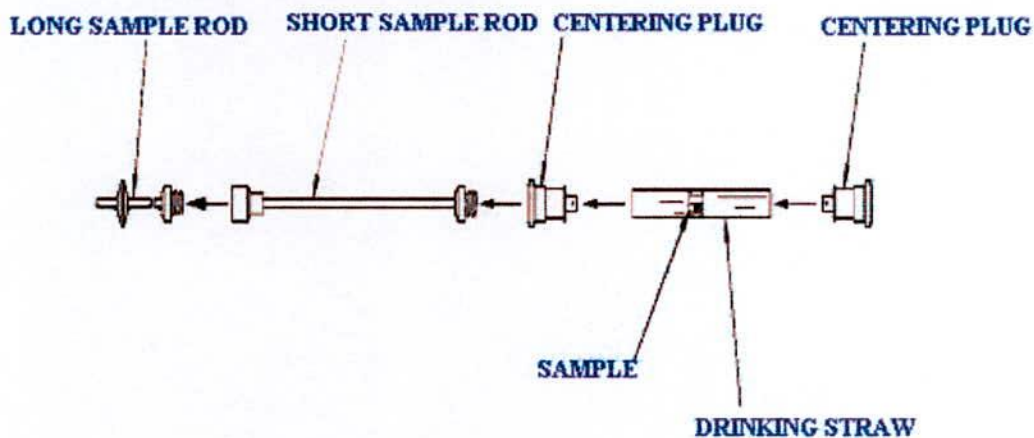


Fig. 3.16 Attaching the Sample to the Sample Rod.

The accuracy of an RSO sample measurement is determined by how well the sample is centered within the SQUID pickup coils. If the sample is not centered, the coils read only part of the magnetic moment of the sample. Properly centering the sample is particularly important if it will be measured at the maximum slope position. During maximum slope position measurements, MPMS MultiVu cannot use autotracking or the iterative regression algorithm, which both help keep the sample correctly positioned, even when temperature changes alter the geometry of the sample rod.

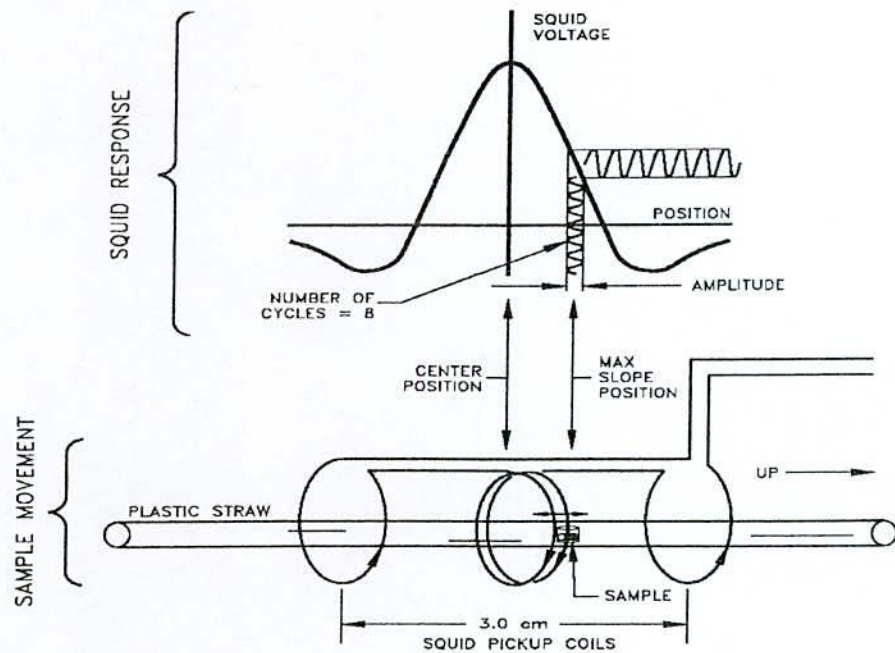


Fig. 3.17 Illustration of an RSO measurement with a very small amplitude. The large bold curve represents the ideal SQUID response to a dipole moving completely through the SQUID pickup coils.

The MPMSXL features significant improvements in the temperature control system. Utilizing a new design for the helium flow impedance, the MPMS XL has capability to operate continuously at temperatures below 4.2 K for indefinite periods of time- completely removing time limitations for making measurements in this temperature regime. The new MPMS XL eliminates the operations associated with filling and recycling the He reservoir. Thus, the system solves the traditional problems of temperature instability and hysteresis associated with rapid boil off of liquid helium when warming through 4.2 K. The results are smooth monotonic transitions across 4.2 K during both warming and cooling temperature sweeps. All these capabilities are fully automated for precise systems control and user-friendly operation. The addition to a redesigned impedance system, the MPMSXL uses a new thermometer design for improved temperature accuracy and precise thermal control. The new thermometry, designed and developed at Quantum Design, is installed in close proximity to the sample within the sensitive coil detection region. The improved design is combined with new temperature control capabilities to provide more accurate measurements of the sample chamber, even under extreme temperature changes.

The new temperature sweep mode of operation provides MPMSXL users with the ability to take magnetic measurements while sweeping the system temperature at a controlled rate, automatically with no manual intervention. This mode provides a controlled, monotonic change in temperature during a measurement sequence at rates up to 10 K/min. Measurements of temperature dependence over large temperature ranges, which previously required time consuming temperature stabilization, can now be made quickly and precisely using temperature sweep mode.

3.5.2 The Features of MPMS XL SQUID Magnetometer

The main components of a SQUID magnetometer are: (i) superconducting magnet (that must be acquired together is programmable bipolar power supply); (ii) superconducting detection coil which is coupled inductively to the sample (iii) a SQUID connected to the detection coil and (iv) superconducting magnetic shield.

High sensitivity is possible because this device responds to a fraction of the flux quantum. The SQUID device is usually a thin film that functions as a extremely sensitive current to voltage converter. A measurement is done in this equipment by moving the sample through the second order gradiometer. Hence the magnetic moment of the sample induces an electric current in the pick-up coil system. A change in the magnetic flux in these coils changes the persistent current in the detection circuit. So, the change in the current in the detection coils produce variation in the SQUID output voltage proportional to the magnetic moment of sample.

3.5.2.1 Improvement Sensitivity

The MPMS XL features the new reciprocating sample measurement system. Unlike DC measurements where the sample is moved through the coils in discrete steps the RSO measurements are performed using a servo motor which rapidly oscillates the sample as shown in Fig. 3.17. These measurements have a sensitivity of 5×10^{-9} emu.

A shaft encoder on the servo motor records the position of the sample synchronous with the SQUID signal. The data received is fitted to an ideal moment response. To ensure this assumption is applicable, samples need to be small; the calibration sample is a cylinder of 3mm diameter and 3mm height. Samples of these size or smaller match an ideal point dipole to an accuracy of

approximately 0.1%. RSO measurements can be made in one of two configurations: Centre or maximum slope. Center scans use large oscillations (2 to 3 cm) around the center point of the pickup coils. These scans take a long time but the sample always remains properly located and a large number of measurements are recorded. These give the most accurate reading.

The maximum slope method oscillates the sample over a small region (2mm) at the most linear part of the SQUID response as shown in Fig. 3.17. The smaller amplitude makes measurements quicker and prevents the sample being subjected to significant magnetic field variation however it also makes the measurement less accurate and susceptible to drift in the sample position.

3.5.2.2 Extended Low Temperature Capability

The MPMS XL features significant improvements in the temperature control system. Utilizing a new design for the helium flow impedance, the MPMS XL has the capability to operate continuously at temperatures below 4.2K for indefinite periods of time completely removing time limitations for making measurements in this temperature regime.

The new MPMS XL eliminates the operation associated with filling and recycling the He-reservoir. Thus, the system solves the traditional problem of temperature instability and hysteresis associated with rapid boil off of liquid helium when warming through 4.2K. The results are smooth monotonic transitions across 4.2 K during both warming and cooling temperature sweeps. All these capabilities are fully automated for precise systems control and user-friendly operation.

3.5.2.3 Reciprocating Sample Measurement System

Features:

- (i) New servo powered, shaft encoded transport allows precision oscillating sample motion,
- (ii) New sample rod with low thermal expansion and radial sample centering features,
- (iii) New high precision data acquisition electronics, including a digital signal processor,
- (iv) New MPMS software revision including a digital signal processor,
- (v) New MPMS software revision, including support for all Reciprocating sample features:

- SQUID signal analysis phase locked to sample motion
- Support of longitudinal and Transverse measurement axes
- Sample centering methods
- Support all measurements with new sample transport (AC, DC, Reciprocating samples),
- (vi) 16 measurement range from 10^{-5} emu to 5 emu,
- (vii) Frequency range: 0.5 - 4.0 Hz,
- (viii) Oscillating amplitude range: 0.5 to 50 mm P-P,
- (ix) Max. DC scan length: 87 mm,
- (x) Relative sensitivity: Max of $< 1 \times 10^{-8}$ emu or 0.1% (10 - 2500 Oe) and
- (xi) Upgrade available for all basic MPMS systems.

3.5.2.4 Continuous Low Temperature Control and Enhanced Thermometry

Features:

- (i) New dual impedance design allows continuous operation below 4.2K,
- (ii) New sample space thermometry improves temperature control,
- (iii) Transition through 4.2 K requires no ^4He reservoir refilling and recycling (no pot fill),
- (iv) New MPMS software revision for all continuous low Temperature features,
- (v) Temperature stability: $\pm 0.55\%$ (1.9- 4.2 K) and
- (vi) Upgrade available for all basic MPMS systems.

3.5.2.5 Configuration

The MPMS XL is offered in two high homogeneity magnet configurations – MPMS XL 5 (5 Tesla) and MPMS XL 7 (7 Tesla). Each system includes:

- (i) Reciprocating Sample Measurement System,
- (ii) Continuous low Temperature Control/ Temperature Sweep and
- (iii) MPMS MultiVu Software Interface.

3.5.2.6 Measurement Consideration

MPMS MultiVu measures the sample while the sample oscillates around one of two measurement positions: the center position or the maximum slope position.

(i) **Center of pickup coils:** The center position is the center of the SQUID pickup coils. When the sample oscillates around the center position, it remains properly located even when changing temperatures alter the geometry of the sample rod if enabled autotracking and selected the iterative regression algorithm. If the sample oscillates, with large amplitude, around the center position, the sample oscillates through most or all of the pickup coils while MPMS MultiVu takes a high number of voltage readings. Large amplitude, center position measurements can thus illustrate the entire SQUID response curve. If the sample is not centered, the coils read only part of the magnetic moment of the sample. Properly centering the sample is particularly important if it will be measured at the maximum slope position.

(ii) **Maximum slope position:** The maximum slope position is above the center of the SQUID pickup coils and is the steepest, most linear part of the SQUID voltage-versus-position curve. The distance between the center of the pickup coils and the maximum slope is defined by the position offset of the active SQUID axis. We can use the RSO diagnostic commands to set the longitudinal or transverse position offset. Maximum slope position measurements are thus ideal for hysteresis measurements and for very fast, precise measurements of magnetization

3.6 Transport Property

3.6.1 DC and AC Resistivity

Resistivity is an intrinsic property of a material. The technical importance of ferrites lies primarily in their high resistivity. The electrical resistivity measurements carried out by a two probe method on silver painted sample a Keithley Electrometer using pellet samples of diameter 8.3-8.8mm and of thickness 1.2 - 2.5 mm by applying silver electrodes on the surfaces. Samples were prepared by sintering the samples at 1050°C for Co-Cd ferrites and 1100°C for Co-Zn ferrites for 3hours. The samples were polished using metallurgical polishing machine with the help of silicon carbide papers with grit size 600. After that the samples were clean with acetone and then again polished with special velvet type polishing cloth named as α -gam, for finer

polishing using fine alumina powder of grain size 0.05 micron dispersed in a liquid. The powders were of various sizes starting with 1 micron to 0.05 micron. Samples are then cleaned in a ultrasonic cleaner and dried in surface at 150°C for several hours. Then the samples are again cleaned with acetone and silver paste was added to both the sides of the polished pellet samples together with two thin copper wires of 100 micron diameter for conduction. Again the samples are dried at 150°C to eliminate any absorbed moisture.

The DC and AC resistivity were measured as a function of frequency in the range 1 kHz-13MHz at room temperature by Electrometer Keithley model 6514 and impedance analyzer. Both the resistivity has been calculated using the formula:

$$\rho = \frac{RA}{l} = \frac{\pi r^2 R}{l} \quad (3.20)$$

where R is the resistance of the Pellet, r is the radius of the pellet and l is the thickness of the pellet .

Ferrites are semiconductors and their resistivity decreases with increasing temperature according to the relation

$$\rho = \rho_\alpha e^{\frac{E_p}{KT}} \quad (3.21)$$

where K the Boltzmann constant, T is the absolute temperature, E_p represents an activation energy which according to Verway and De Boer is the energy needed to release an electron from the ion to jump to the neighboring ion, thus giving rise to electrical conductivity. If we plot $\log \rho$ vs $\frac{1}{T}$ for various ferrites, a straight line is found in a wide temperature range with a slope corresponding to E_p according to the relation

$$E_p = 0.198 \times 10^{-3} \frac{d(\log \rho)}{d(1/T)} \quad (3.22)$$

3.6.2 Dielectric Constant

Dielectric measurement as a function of frequency in the range 100Hz-13MHz at room temperature were carried out by using Hewlett Packrat impedance analyzer in conjunction with a laboratory made furnace which maintain the desired temperature with the help of a temperature controller The real part of dielectric constant was calculated using the formula

$$\epsilon' = \frac{cd}{\epsilon_0 A}, \quad (3.23)$$

where c is the capacitance of the pellet in Farad, d the thickness of the pellet in meter , A the cross-sectional area of the flat surface of the pellet in m² and ϵ_0 the constant of permittivity for free space.

CHAPTER-IV
RESULTS AND DISCUSSION OF
 $\text{Co}_{1-x}\text{Cd}_x\text{Fe}_2\text{O}_4$ FERRITES

Results and Discussion of $\text{Co}_{1-x}\text{Cd}_x\text{Fe}_2\text{O}_4$ Ferrites

4.0 Introduction

Many ferrites have the spinel-type structure, which can be described in terms of a nearly cubic close-packed arrangement of anions with one-half of the octahedral interstices (B-sites) and one-eighth of the tetrahedral interstices (A-sites) filled with cations. CoFe_2O_4 is generally an almost inverse ferrite in which Co^{2+} ions mainly occupies B-sites and Fe^{3+} ions are distributed almost equally between A and B-sites. It has been demonstrated that the inversion is not complete in CoFe_2O_4 and the degree of inversion sensitively depends on the thermal treatment and method of preparation condition [4.1]. The partial replacement of divalent ions in such ferrites by Cd or Zn is expected to affect the magnetic properties such as magnetization, Curie temperature etc.

When magnetic dilution of the sublattices is introduced by substituting nonmagnetic ions in the lattice, frustration and/or disorder occurs leading to collapse of the collinearity of the ferromagnetic phase by local spin canting exhibiting a wide spectrum of magnetic ordering e.g. antiferromagnetic, ferrimagnetic, re-entrant spin-glass, spin-glass and cluster spin-glass [4.2, 4.3]. Small amount of site disorder i.e. cations redistribution between A and B sites is sufficient to change the super-exchange interactions which are strongly dependent on thermal history i.e. on sintering temperature, time and atmosphere as well as heating /cooling rates during materials preparation. CdFe_2O_4 and ZnFe_2O_4 are generally assumed to be normal spinel with all Fe^{3+} ions on B-sites and all Cd^{2+} and Zn^{2+} ions on A-sites [4.4, 4.5].

The magnetic properties of ferrites such as permeability, magnetization, coercive field, Curie temperature are affected by composition as well as by the type of substitution, cation distribution and method of preparation [4.6]. The partial replacement of nonmagnetic Cd ions in cobalt ferrite is expected to weaken the magnetic coupling resulting in decrease of Curie temperature. Magnetic behavior of mixed Co-Cd ferrites has been studied by Ghani *et. al.* [4.7], Wafik *et. al.* [4.8]. However, there is very few work found in literature on this system in extorted variation of composition. The variation of magnetization for Cu-Cd ferrite system with Cd concentration indicated the existence of a Yafet-Kittel type of magnetic ordering [4.9]. The aim of the present work is to investigate in detail the effects of substitution of Cd^{2+} ions in place of Co^{2+} ions covering a wide range of concentration ($x = 0.0 - 1.0$) on the structural magnetic and transport properties of Co-Cd ferrites which has not been studied in much detail by previous researcher.

4.1 X-ray Diffraction (XRD)

4.1.1 Phase Analysis

Structural characterization and identification of phases are prior for the study of ferrite properties. X-ray diffraction (XRD) studies of the samples were performed by using Philips X'PERT PRO X-ray Diffractometer using Cu-K α radiation in the range of $2\theta = 15^\circ$ to 65° in steps of 0.02° . The X-ray diffraction (XRD) patterns for the series of samples $\text{Co}_{1-x}\text{Cd}_x\text{Fe}_2\text{O}_4$ ($x = 0.0 - 1.0$ in steps of 0.1) sintered at 1050°C for 3 hours is shown in Fig. 4.1. All the samples show good crystallization with well defined diffraction lines. A phase analysis using X-ray diffraction technique was performed to confirm the formation of single-phase cubic spinel structure with no extra lines corresponding to any other crystallographic phase. The results obtained from XRD pattern for all the samples of $\text{Co}_{1-x}\text{Cd}_x\text{Fe}_2\text{O}_4$ with the (hkl) values corresponding to the diffraction peaks of different planes (111), (220), (311), (222), (400), (422), (511), and (440) which represent either odd or even indicating the samples are spinel cubic phase.

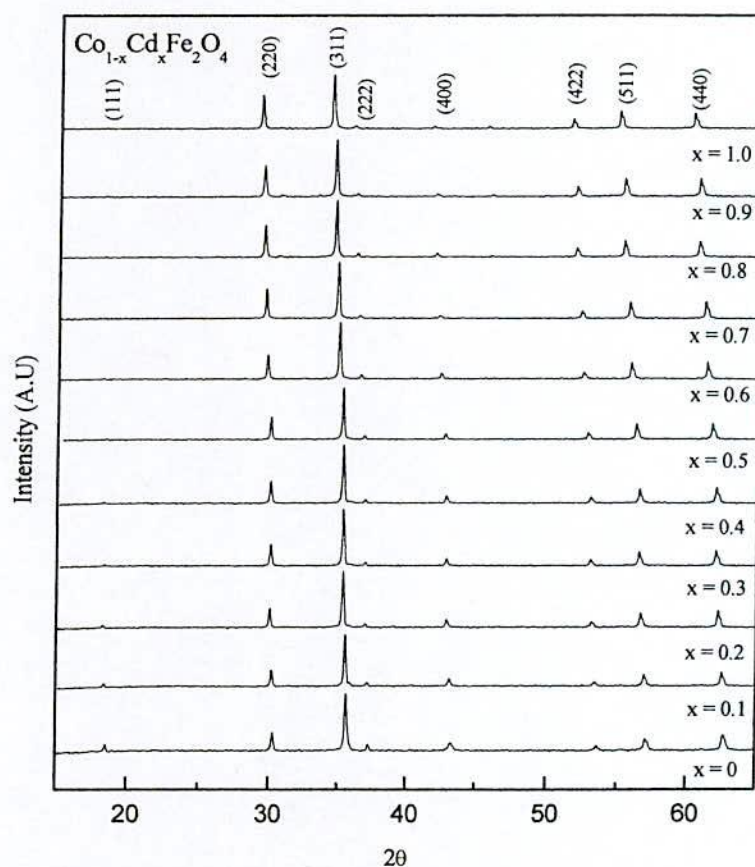


Fig. 4.1 XRD patterns in $\text{Co}_{1-x}\text{Cd}_x\text{Fe}_2\text{O}_4$ ferrites with different Cd content.

The peaks are found to shift slightly towards the lower d-spacing values which indicate that the lattice parameters are increasing with the increase of Cd content. The reflections also demonstrate the homogeneity of the studied samples. Therefore single phase spinel structure is confirmed for all the samples with increasing trend of the lattice parameter as the Cd content is increased. The diffraction pattern from the sample CoFe_2O_4 is shown separately in Fig. 4.2.

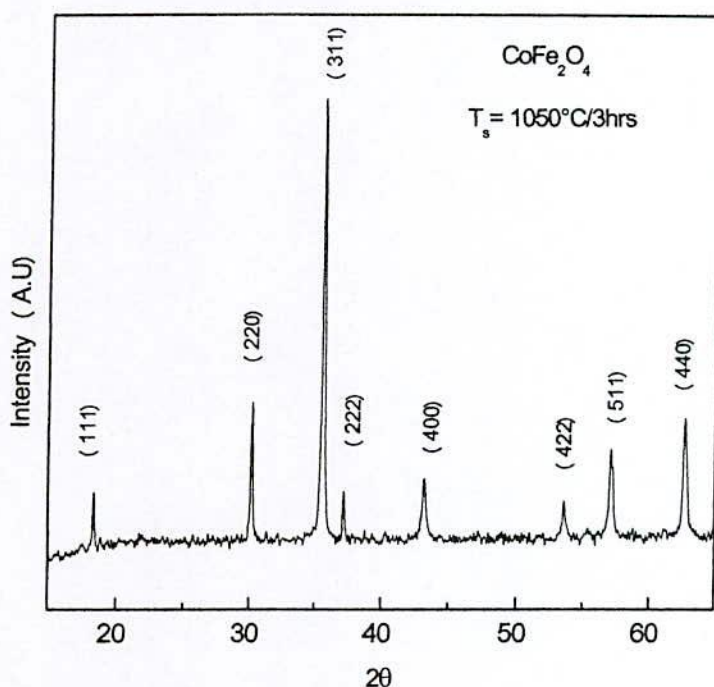


Fig. 4.2 XRD patterns CoFe_2O_4 ferrites.

4.1.2 Lattice Parameter

The accurate lattice parameter has been determined from the calculated lattice parameter 'a' corresponding to each plane of XRD pattern using Nelson-Riley function [4.10]

$$F(\theta) = \frac{1}{2} \left[\frac{\cos^2 \theta}{\sin \theta} + \frac{\cos^2 \theta}{\theta} \right],$$

where θ is the Bragg's angle, by extrapolating the lattice

parameter values to $F(\theta) = 0$ or $\theta = 90^\circ$. Variation of lattice parameter 'a' as a function of Cd content x is shown in Fig. 4.3 and also shown in Table - 4.1. From Fig. 4.3 it is observed that the lattice parameter increases linearly with increasing Cd content obeying Vegard's law [4.11]. This enhancement of lattice parameter is attributed to Cd^{2+} with larger ionic radius (0.97\AA) which replaces Co^{2+} having smaller ionic radius (0.72\AA) [4.12, 4.13]. It is well known that the distribution of cations on the octahedral B-sites and tetrahedral A-sites

determines to a great extent the physical, electrical and magnetic properties of ferrites. There exists a correlation between the ionic radius and the lattice constant, the increase of the lattice constant is proportional to the increase of the ionic radius [4.14]. Similar results for Co-Cd ferrite system have been reported by A. M. Abdeen *et.al* [4.15], A. R. Shitre *et.al* [4.12], O. M. Hemeda *et.al* [4.13], A. A. Ghani *et.al* [4.7]. It is also found that the values for CoFe_2O_4 and CdFe_2O_4 are 8.379 Å and 8.683 Å which is values in good agreement with the reported values [4.5].

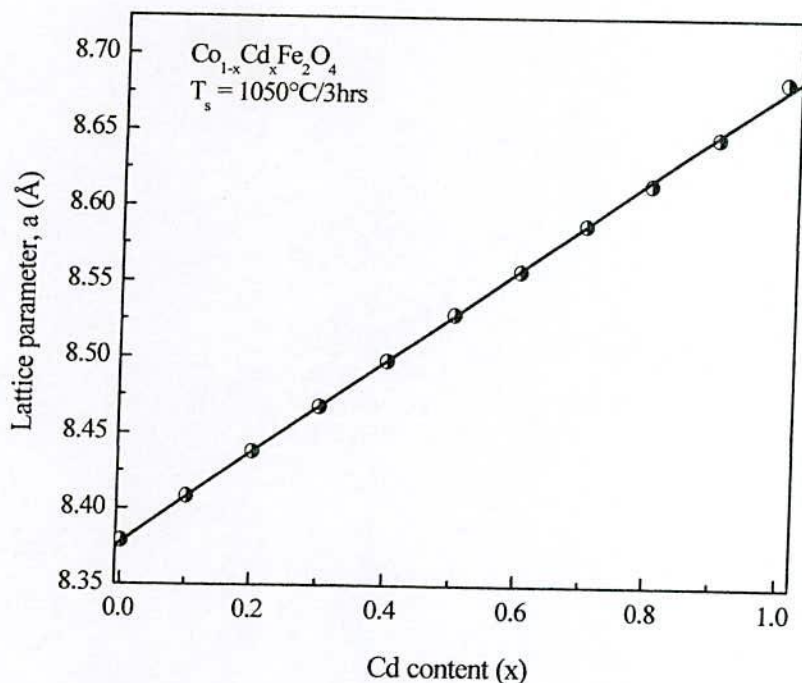


Fig. 4.3 Variation of lattice constant 'a' as a function of Cd content(x) of $\text{Co}_{1-x}\text{Cd}_x\text{Fe}_2\text{O}_4$ ferrites.

4.1.3 Density

Variation of density with Cd content is shown in Fig. 4.4. The bulk density, ρ_B , was measured by usual mass and dimensional consideration whereas X-ray density, ρ_X , was calculated from the molecular weight and the volume of the unit cell for each sample by using the equation (3.6) and (3.5). The calculated values of the bulk density and theoretical or X-ray density of the present ferrite system are listed in Table - 4.1. It is observed that the bulk density is lower than the X-ray density. This may be due to the existence of pores, which were formed and developed during the sample preparation or sintering process. The X-ray density increases linearly with increasing Cd concentration and bulk density increases faster at $x = 0.2$

and thereafter increases almost linearly. The result signifies that small amount of Cd has pronounced effect on the densification of the CoFe_2O_4 when it is substituted by Cd.

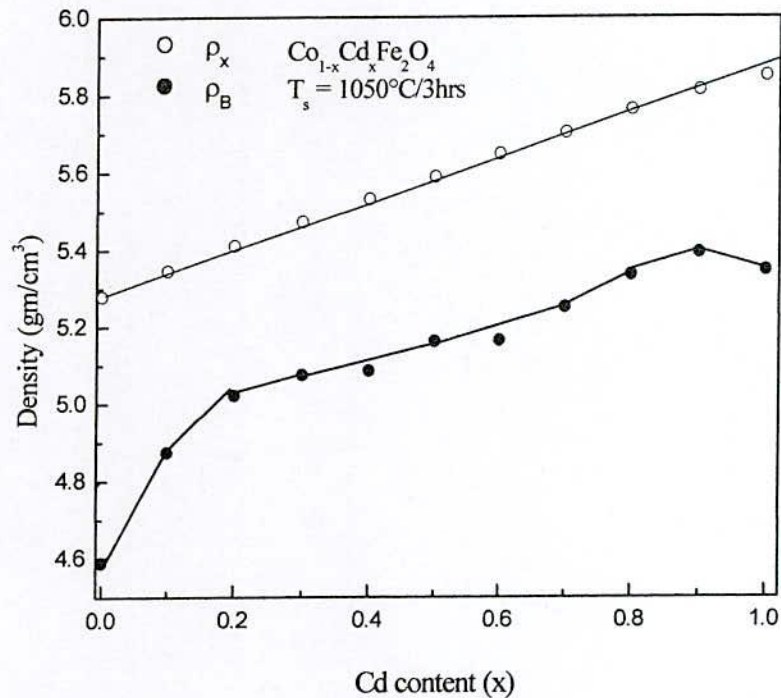


Fig. 4.4 Variation of density with Cd content (x) of $\text{Co}_{1-x}\text{Cd}_x\text{Fe}_2\text{O}_4$ ferrites.

The atomic weight and density of Co are 58.9 and 8.6 gm/cm^3 respectively while the corresponding values of Cd are 112 and 8.9 gm/cm^3 respectively [4.16]. Therefore an increase of density with increasing Cd^{2+} is obviously expected. Moreover, due to lower melting point of CdO, sintering mechanism is accelerated resulting in an enhancement of density of the prepared samples. It is worthwhile to mention that density play an important role on the magnetic properties especially on the structure sensitive extrinsic property such as permeability, porosity changes slightly with Cd content and is shown in Table - 4.1. This porosity which is intrinsic for any oxide materials plays an important role in deciding the magnetic and electrical properties.

Table - 4.1 Data of the lattice parameter (a), X-ray density (ρ_x), bulk density (ρ_B), porosity (P%), Curie temperature (T_c), permeability (μ') at frequency 100 kHz and DC resistivity (ρ_{dc}) of $Co_{1-x}Cd_xFe_2O_4$ samples sintered at 1050°C /3hrs.

Cd content (x)	a (Å)	ρ_x (g/cm ³)	ρ_B (g/cm ³)	P%	T_c (K)	$T_s = 1050^\circ\text{C}$ μ' (100KHz)	ρ_{dc} ($\Omega\text{-cm}$)
0	8.379	5.28	4.59	13.9	728	51	1.16×10^3
0.1	8.409	5.35	4.87	8.8	683	65	3.91×10^3
0.2	8.438	5.41	5.02	7.2	613	86	5.32×10^3
0.3	8.468	5.47	5.08	7.3	563	111	7.43×10^3
0.4	8.498	5.53	5.09	8.0	491	149	6.27×10^3
0.5	8.529	5.59	5.16	7.6	413	226	2.58×10^3
0.6	8.557	5.65	5.17	8.6	353	334	3.75×10^2
0.7	8.588	5.70	5.25	7.9	262	45	3.65×10^2
0.8	8.615	5.76	5.34	7.4	-	-	3.44×10^2
0.9	8.646	5.81	5.39	7.2	-	-	-
1	8.683	5.85	5.35	8.9	-	-	-

4.2 Magnetic Properties

4.2.1 Temperature Dependence of Initial Permeability

Fig. 4.5 shows the temperature dependence of initial permeability, μ' for the toroid shaped samples (where $x = 0.0 - 0.6$), which is measured at a constant frequency (100 kHz) of an AC signal by using Impedance Analyzer. It is observed that the initial permeability increases with the increase in Cd content while it falls abruptly close to the Curie point. This is because Cd in these compositions not only increases the magnetic moment and, but also lowers anisotropy, K_1 [4.17]. On the other hand, permeability increases with the decrease of

K_1 as the temperature increases according to the relation $\mu' \propto \frac{M_s^2 D}{\sqrt{K_1}}$ [4.18, 4.19]. It is

observed from Fig. 4.5 that the permeability falls density sharply when the magnetic state of the ferrite samples changes from ferromagnetic to paramagnetic. When the anisotropy constant reaches to zero just below the Curie temperature, μ' attains its maximum value and then drops off sharply to minimum value at the Curie point. The sharpness of the permeability drop at the Curie point can be used as a measure of the degree of compositional homogeneity [4.20] which has also been confirmed by X-ray diffraction that no impurity phases could be detected. Fig. 4.6 (a, b) represents the variation of complex permeability and temperature derivatives of

permeability as a function of temperature of the sample $x = 0.5$. It is observed that the imaginary part of permeability μ'' and temperature derivatives of permeability, $d\mu'/dT$ show peaks at temperature, T which excellently matches with the sharp fall of permeability at $T = T_c$.

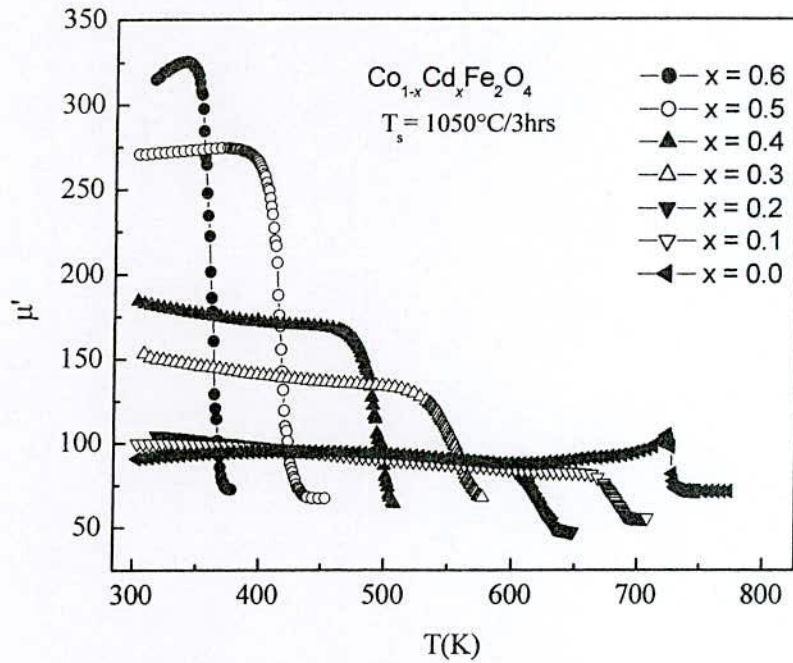


Fig. 4.5 Temperature dependence of permeability, μ' of $\text{Co}_{1-x}\text{Cd}_x\text{Fe}_2\text{O}_4$ ferrites.

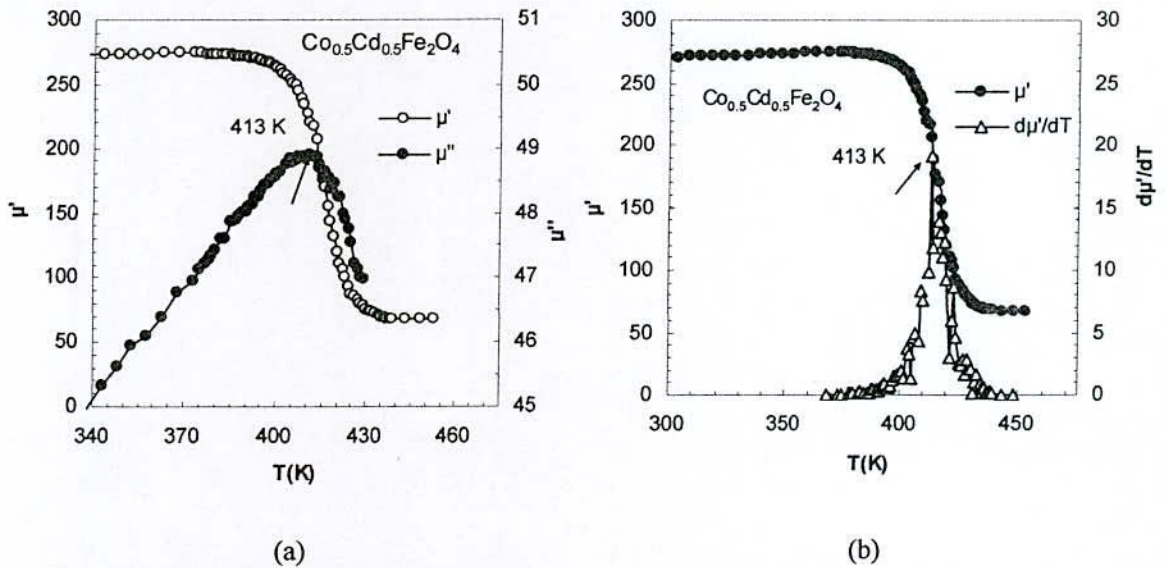


Fig. 4.6 (a, b) Determination of Curie temperature from the temperature dependence of μ' , μ'' and $d\mu'/dT$ as a function of temperature.

The μ' - T plot does not show any secondary maximum that occur due to excess formation of Fe^{2+} ions, there by indicating the single phase formation of the samples. This observation is supported by XRD patterns as well. Fig. 4.7 (a) and (b) shows temperature dependence of initial permeability, μ' for $x = 0.0$ and 0.5 samples of $\text{Co}_{1-x}\text{Cd}_x\text{Fe}_2\text{O}_4$ ferrites measured during heating and cooling cycles sintered at 1050°C for 3 hrs. The initial permeability is directly proportional to square of the magnetization and inversely proportional anisotropy constant of the sample. It is well known that anisotropy constant decreases considerably with temperature. In most cases, anisotropy decreases from a high value (at lower temperature) to zero near T_c [4.18]. It is observed that for the sample $x = 0.0$ the μ' increases with temperature to a maximum value just below the T_c which is the manifestation of Hopkinson effect. This occurs, because the crystal anisotropy becomes almost zero near T_c [4.13, 4.18]. Since anisotropy decreases faster than magnetization on heating, the initial permeability expectantly increasing with temperature tends to infinity just below the T_c and then abruptly falls to low value when the samples become paramagnetic.

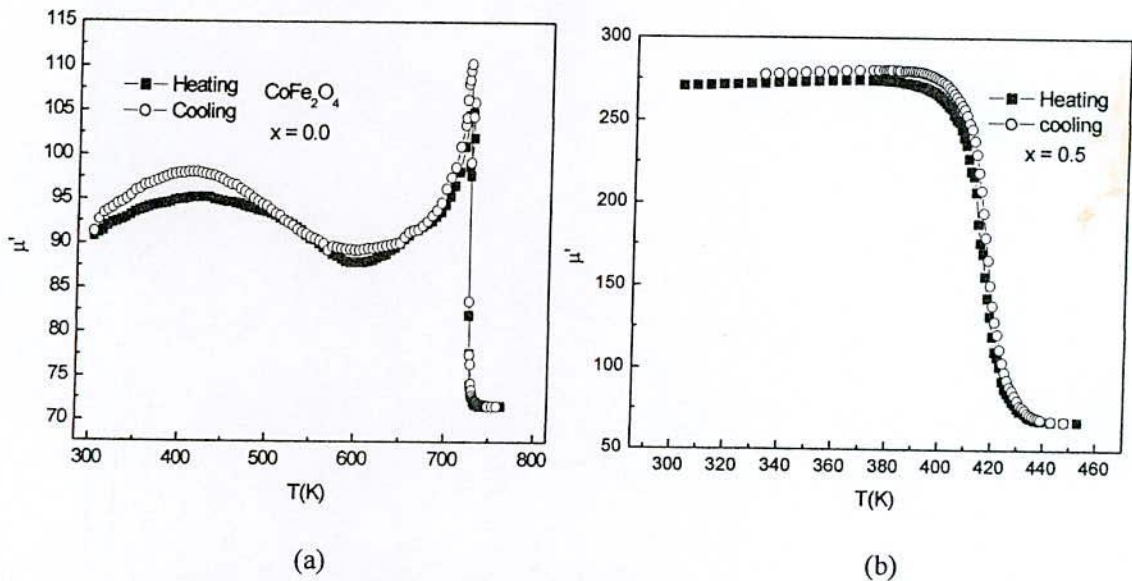


Fig. 4.7 Temperature dependence of initial permeability, μ' for (a) $x = 0.0$ and (b) $x = 0.5$ of $\text{Co}_{1-x}\text{Cd}_x\text{Fe}_2\text{O}_4$ ferrites samples sintered at 1050°C /3hrs.

It is also noticed that there is a hump (permeability maximum) in μ - T curve around 450K. This is probably due to the resultant anisotropy compensation by Co^{2+} ion having positive anisotropy constant with the host with negative contribution. But for sample $x = 0.5$ μ - T is smooth indicating that the temperature dependence of anisotropy is well compensated due to the substitution of Cd for Co resulting in decrease of anisotropy energy for the sample

$x = 0.5$. It is also reflected in the value of permeability that μ has attained a value as high as $\mu \approx 270$ compared with $\mu \approx 90$ for the pure CoFe_2O_4 ferrite. The slight thermal hysteresis in permeability is also due to anisotropy effect in these samples.

4.2.2 Compositional Dependence of Curie Temperature

Fig. 4.8 shows the variation of Curie temperature T_c with Cd content of $\text{Co}_{1-x}\text{Cd}_x\text{Fe}_2\text{O}_4$ ferrites. T_c of the studied sample was determined from μ' - T curve. The temperature corresponding to the peak value of $d\mu/dT$ has been taken as the Curie temperature of the sample. The T_c values are shown in Table - 4.1. T_c is the transition temperature above which the ferrite material loses its magnetic properties. The Curie temperature gives an idea of the amount of energy required to break up the long-range ordering in the ferromagnetic material. The Curie temperature mainly depends upon the strength of A-B exchange interaction.

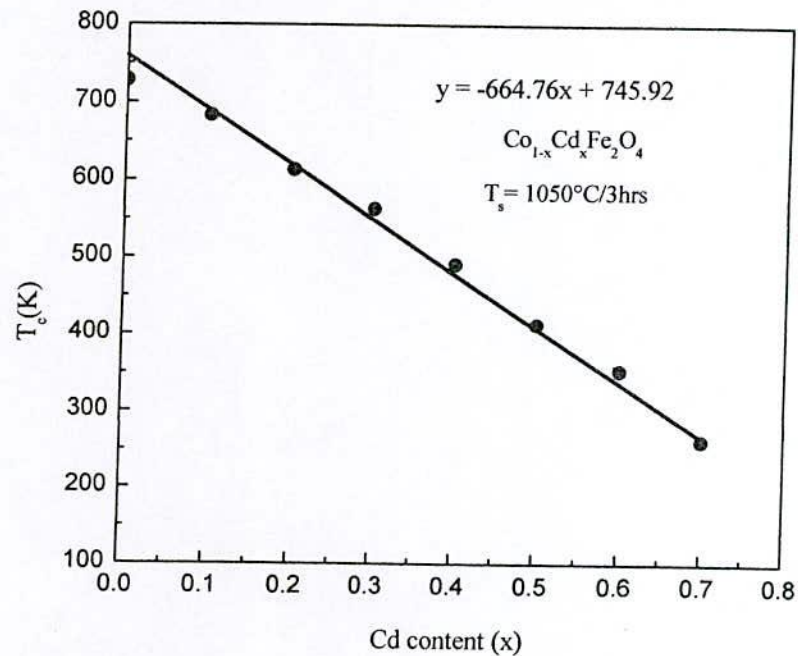


Fig. 4.8 Variation of Curie temperature, T_c with Cd content (x) of $\text{Co}_{1-x}\text{Cd}_x\text{Fe}_2\text{O}_4$ ferrites.

From Fig. 4.8 it is observed that Curie temperature linearly decreases with increasing Cd content. The non-magnetic Cd^{2+} ions replaced the magnetic Fe^{3+} ions on A-sites and thus the number of Fe^{3+} decreases on A-sites. This tends to decrease the strength of A-B exchange interactions. The decrease of T_c is due to the weakening of the A-B exchange interaction as well as due to increase of lattice parameter with Cd^{2+} content which increases the distance between the magnetic cations. A linear dependence of T_c with Cd content is observed upto

$x = 0.7$ beyond which well defined T_c could not be determined due to complex magnetic structures and competing magnetic interactions of highly diluted compositions. The linear decrease of T_c with x content is attributed to the progressive weakening of J_{AB} exchange interactions resulting from substitution of nonmagnetic Cd in the tetrahedral (A-site) occupancy. A linear fitting of the Curie temperature with x gives an empirical relation for the samples as, $T_c(x) = T_c(0) - 664.76x$, where $T_c(0)$ is the Curie temperature of the pure Co-ferrite and $T_c(x)$ corresponds to the Curie temperature of any composition having Cd concentration (x). From this empirical relation Curie temperature of pure Co-ferrite is found to be 746K. Our experimental value of the Co-ferrite is 728 K, the literature values are 735 K [4.5], 793 K [4.21] and 860 K [4.22, 4.23]. The difference in the determined T_c values by various authors are due to the deviation of the cation distributions as affected by thermal history of the samples as well as method of sample preparation.

4.2.3 Frequency Dependence of Initial Permeability

The optimization of the dynamic properties such as complex permeability in the high frequency range requires a precise knowledge of the magnetization mechanisms involved. The magnetization mechanisms contributing to the complex permeability, $\mu = \mu' - i\mu''$, where, μ' is the real permeability (in phase) and μ'' the imaginary permeability (90° out of phase). Complex permeability has been determined as a function of frequency, f upto 13 MHz at room temperature for all the samples of series $Co_{1-x}Cd_xFe_2O_4$ ferrites by using the conventional technique based on the determination of the complex impedance of a circuit loaded with toroid shaped sample. Fig. 4.9 represents the results of the real part of the permeability, μ' and imaginary part, μ'' as a function of frequency for the whole series of ferrite samples sintered at 1050°C , 1075°C and 1100°C for 3 hours.

From Fig. 4.9 it is noticed that the real component of permeability, μ' is fairly constant with frequency up to certain frequency range, and then falls rather rapidly to very low value at higher frequency. We can call this real part of the permeability, μ' as initial permeability. The permeability of compositions with $x = 0.0 - 0.3$ were stable up to 10 MHz and the cut-off frequencies of samples were above 13 MHz, the maximum frequency limit of the instrument. The permeability of the $x = 0.4 - 0.6$ composition was stable up to about 3 MHz and the permeability dispersion initiated above 3 MHz.



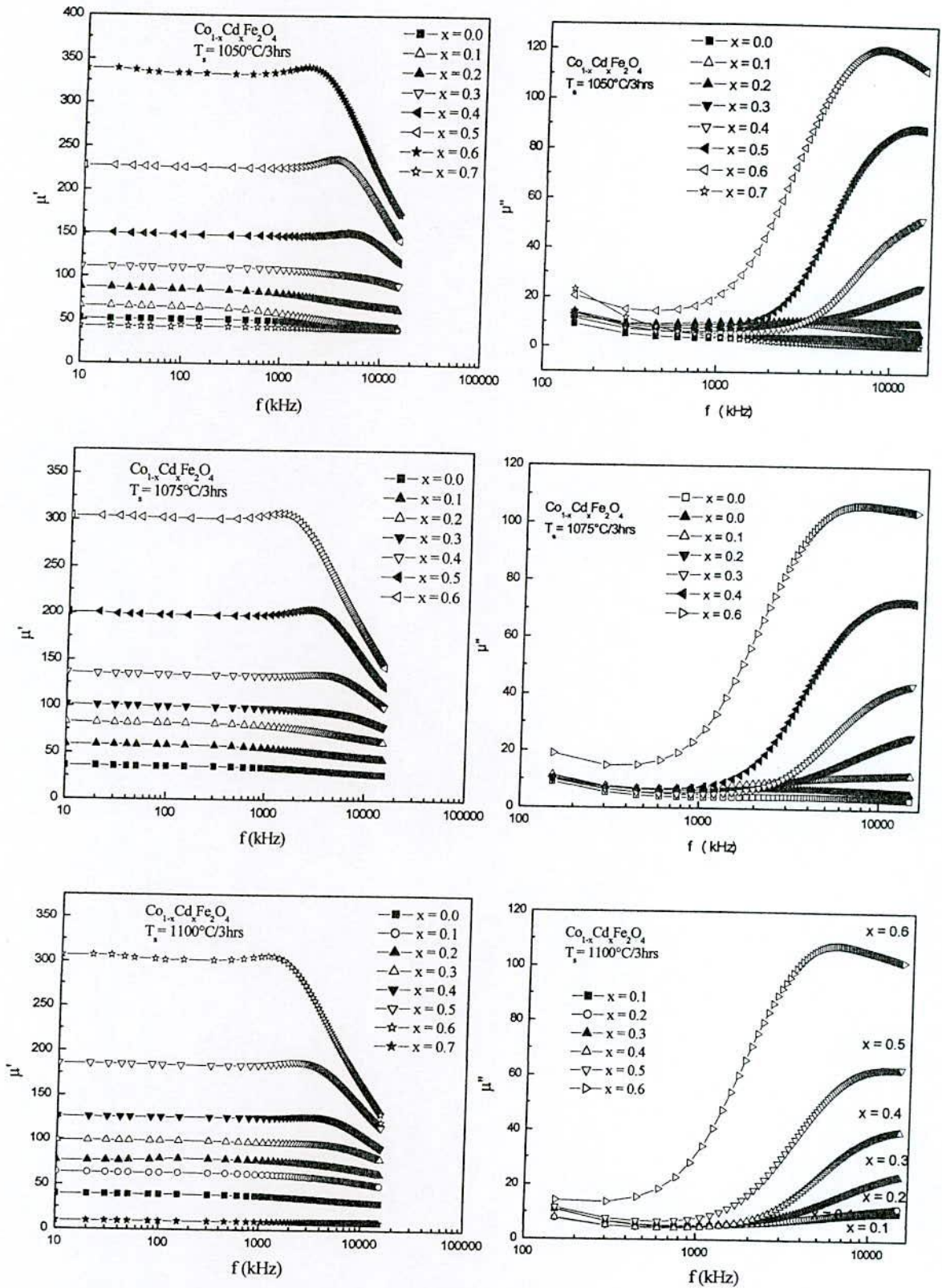


Fig. 4.9 Frequency dependence of the real part of the permeability, μ' and imaginary component, μ'' of $\text{Co}_{1-x}\text{Cd}_x\text{Fe}_2\text{O}_4$ ferrites sintered at 1050°C, 1075°C and 1100°C for 3hrs.

When ferrite specimens are subjected to an ac field, permeability shows several dispersions; as the field frequency increases, the various magnetization mechanisms become unable to follow the ac field. The dispersion frequency for each mechanism is different, since they have different time constant. The low frequency dispersions are associated with domain wall dynamics [4.24]. The lower frequency dispersion was due to the much higher permeability of the composition ($x = 0.6$) compared to others. The dispersion behavior could be explained by Snoek's law, which states that the cut-off frequency is inversely proportional to the magnetic permeability [4.25].

It is clearly evident from these figures that the initial permeability as a function of frequency in the range 1 kHz to 13 MHz increases with Cd content, x i.e the permeability μ' increases monotonically upto $x = 0.6$ and thereafter decreases. It is quite obvious science the sample above $x > 0.6$ is paramagnetic at room temperature. Therefore the permeability should be zero. The small finite value of permeability at $x = 0.7$ as shown in Fig. 4.9 is an experimental artifact arising from the small applied field (10^{-3} Oe) that influences the magnetic domains to give rise to small magnetization and hence small value of μ' is observed. For all sintering temperatures initial permeability increases with the increase of Cd content upto $x = 0.6$.

Fig. 4.10 shows that the variation of initial permeability at frequency 100 kHz with Cd content of $\text{Co}_{1-x}\text{Cd}_x\text{Fe}_2\text{O}_4$ ferrites sintered at 1050°C, 1075°C and 1100°C for 3hrs. It was observed that the permeability increases slowly at low Cd content and then increase sharply up to $x = 0.6$ for all the sintering temperature and there after decreases rapidly. For the sample with $x = 0.6$ the maximum initial permeability is observed at a sintering temperature of $T_s = 1050^\circ\text{C}$. As the T_s increases the permeability decreases. The decrease of permeability with increasing sintering temperature T_s may be explained on the basis of intragranular pores entrapped within the grains which create constraint on the domain wall mobility. As a result permeability decreases. Again the increase of permeability with Cd content is connected with increased magnetization, density, grain size and possible reduction of anisotropy energy with the addition of nonmagnetic Cd.

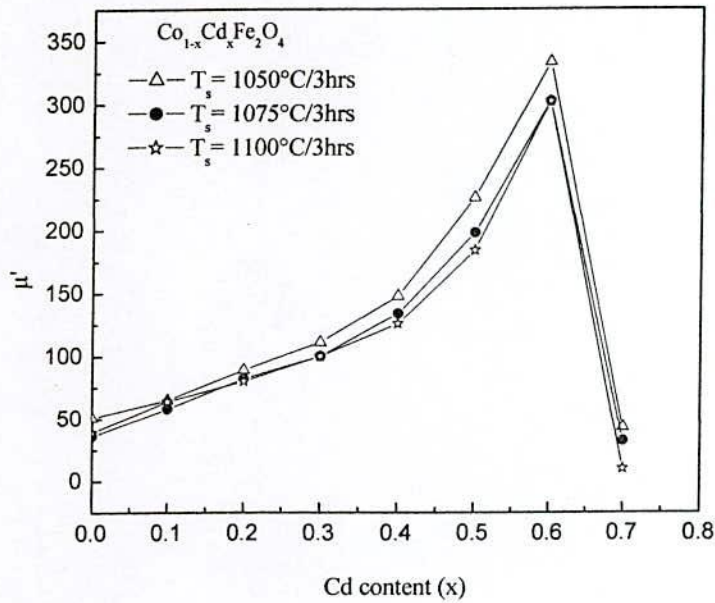


Fig. 4.10 Variation of initial permeability, μ' at frequency 100 kHz with Cd content of $\text{Co}_{1-x}\text{Cd}_x\text{Fe}_2\text{O}_4$ ferrites.

Moreover as the sintering temperature increases dispersion of μ' - f spectra also shifts to the lower frequency range as a result of increasing density and grain size, as proposed by Nakamura [4.26]. An increase in the density of ferrites not only results in the reduction of demagnetization field due to the presence of pores but also raise the spin rotational contribution, which in turn increases the permeability [4.27].

4.2.4 Low Field B-H loop at Room Temperature

Fig. 4.11 represents the B-H loops at room temperature were measured with B-H loop tracer at constant frequency ($f = 1\text{kHz}$) and applied field $H = 0 - 15\text{ Oe}$ for the whole series of $\text{Co}_{1-x}\text{Cd}_x\text{Fe}_2\text{O}_4$ ferrite samples sintered at 1050°C , 1075°C and 1100°C for 3 hours. From these loops the remanence induction (retentivity B_r), saturation induction B_s and the coercive force (coercivity H_c) were determined. Saturation induction (B_s) is found to increase with increase of Cd content upto $x = 0.5$ while the B_r/B_s ratio decreases gradually with Cd content. For all sintering temperatures coercivity (H_c) decreases almost linearly with increasing Cd content up to $x = 0.6$ and also the remanence induction (B_r) decreases with increase of Cd content. Fig 4.12 shows the coercivity, H_c and permeability, μ' versus composition x of $\text{Co}_{1-x}\text{Cd}_x\text{Fe}_2\text{O}_4$ ferrite with $x = 0 - 0.6$ sintered at $1050^\circ\text{C}/3\text{hrs}$ measured constant frequency $f = 1\text{ kHz}$.

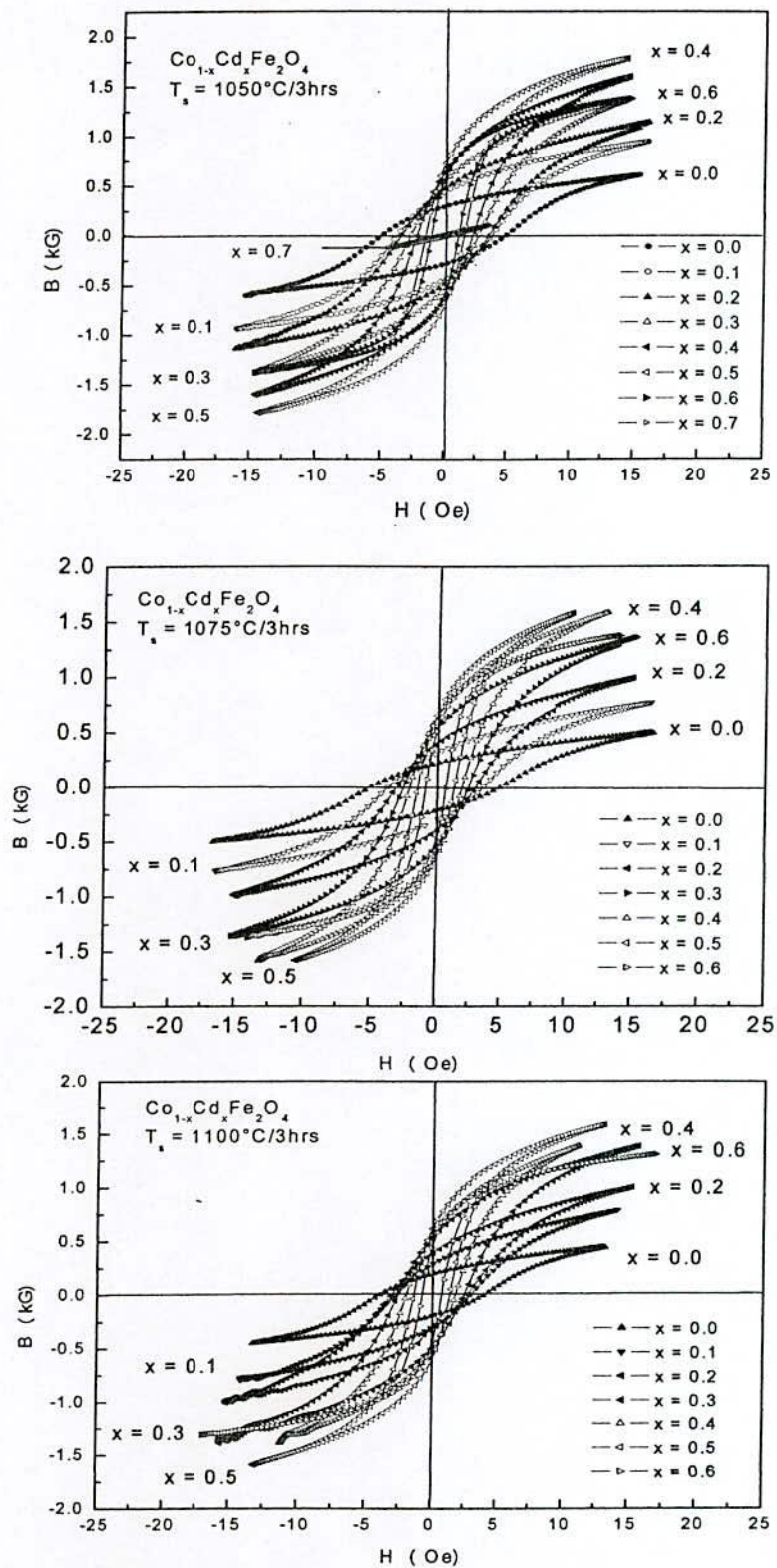


Fig. 4.11 Magnetic hysteresis graphs of $\text{Co}_{1-x}\text{Cd}_x\text{Fe}_2\text{O}_4$ ferrite sintered at 1050°C , 1075°C and 1100°C for 3 hours at constant frequency $f = 1\text{kHz}$.

The hysteresis behavior and initial permeability reveals the softer ferromagnetic nature of the studied materials with the increase of Cd content. This clearly indicates that Cd substitution for Co in $\text{Co}_{1-x}\text{Cd}_x\text{Fe}_2\text{O}_4$ system has profound effect of magnetic softening and may be interpreted as due to reduction of magnetic anisotropy energy and enhancement of magnetization of the studied samples [4.28]. The dependence of H_c and μ' is inversely proportional as found in Fig. 4.12 which concomitant with the theoretical prediction. Since H_c is the indicator of magnetic hardness while μ' is the indicator of magnetic softness. Sample with $x = 0.7$ has low H_c and also very low μ' due to its paramagnetic state at room temperature. The B-H loop of this sample is also very narrow and almost reversible.

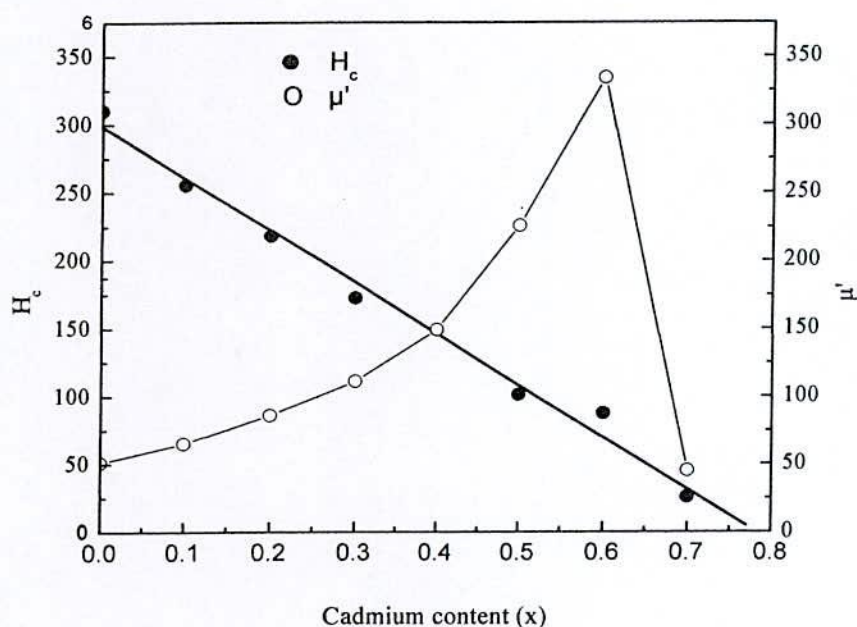


Fig.4.12. The coercivity, H_c and permeability, μ' versus composition x of $\text{Co}_{1-x}\text{Cd}_x\text{Fe}_2\text{O}_4$ ferrite with $x = 0.0 - 0.6$ rings sintered for $1050^\circ\text{C}/3\text{hr}$ at constant frequency $f = 1\text{k Hz}$

Table-4.2 Data of the coercivity (H_c), retentivity (B_r), saturation induction (B_s), B_r/B_s ratio and losses of $Co_{1-x}Cd_xFe_2O_4$ ferrite with $x = 0.0 - 0.7$ rings sintered for 1050°C, 1075°C and 1100°C for 3 hours at constant frequency $f = 1$ kHz.

Cd content (x)	T_s (°C) /3hrs	H_c (Oe)	B_r (kG)	B_s (kG)	B_r/B_s	Losses (W/kg)
0.0	1050	4.96	0.29	0.59	0.49	14.10
	1075	4.97	0.21	0.50	0.42	14.20
	1100	3.97	0.19	0.42	0.45	14.10
0.1	1050	4.09	0.43	0.92	0.47	18.15
	1075	3.74	0.31	0.77	0.40	18.92
	1100	3.01	0.26	0.79	0.33	16.27
0.2	1050	3.49	0.48	1.11	0.43	19.58
	1075	2.90	0.39	0.99	0.40	20.38
	1100	2.76	0.39	0.10	3.9	21.92
0.3	1050	2.76	0.53	1.35	0.39	17.38
	1075	2.42	0.53	1.35	0.39	22.28
	1100	2.36	0.54	1.34	0.40	24.86
0.4	1050	2.38	0.62	1.59	0.40	17.28
	1075	2.24	0.52	1.58	0.33	25.31
	1100	1.71	0.56	1.38	0.40	22.22
0.5	1050	1.62	0.71	1.79	0.40	13.10
	1075	1.52	0.65	1.58	0.41	18.42
	1100	1.46	0.62	1.60	0.39	15.36
0.6	1050	1.40	0.54	1.37	0.39	7.72
	1075	0.75	0.51	1.58	0.32	7.98
	1100	0.73	0.44	1.30	0.34	7.03
0.7	1050	0.41	0.01	0.10		

4.2.5 Magnetization Measurement

Magnetization as a function of applied magnetic field upto 50 kOe measured with a SQUID magnetometer at $T = 5$ K of $Co_{1-x}Cd_xFe_2O_4$ system for the samples with $0 < x \leq 1.0$ is shown in Fig. 4.13. It is observed that the magnetization increases sharply at very low field ($H < 1$ kOe) which corresponds to magnetic domain reorientation and thereafter increases slowly up to saturation. The samples with $x \geq 0.7$ do not saturate even at $H = 50$ kOe.

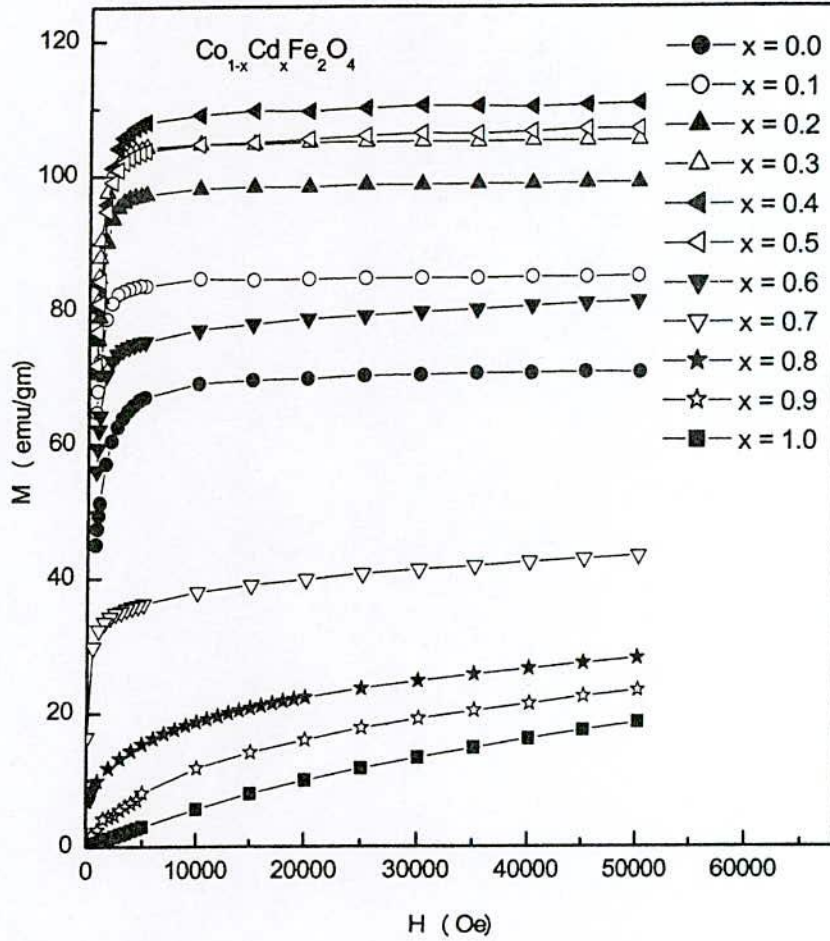


Fig. 4.13 Field dependence of magnetization for $x = 0.0 - 1.0$ of $\text{Co}_{1-x}\text{Cd}_x\text{Fe}_2\text{O}_4$ ferrites at temperature $T = 5\text{K}$.

The saturation magnetization (M_s) of the $\text{Co}_{1-x}\text{Cd}_x\text{Fe}_2\text{O}_4$ ferrites as a function of Cd content at $T = 5\text{K}$ upto $x = 0.8$ is shown in Fig. 4.14 and Table - 4.3. It is observed that saturation magnetization, increases with the increase of Cd content up to $x = 0.4$ and decrease thereafter. The observed variation in saturation magnetization can be explained on the basis of cation distribution and the exchange interactions between A and B sites, respectively. From these values of saturation magnetization, the magneton number i.e., saturation magnetization per formula unit in Bohr magneton, n_B at $T = 5\text{K}$ was calculated using the relation [4.29]

$$n_B = \frac{MM_s}{\mu_B N} \quad (4.1)$$

where M is the molecular weight of the ferrite sample, M_s is the saturation magnetization emu/gm, N the Avogadro's number and μ_B the Bohr magneton. The value of M_s , magneton numbers, n_B (experimental, theoretical) for each of the samples measured at $T = 5\text{K}$ is given

in Table - 4.2.2. The dependence of magnetization, n_B in Bohr magneton along with the theoretical magnetization as a function of Cd content is depicted in Fig. 4.15. It is observed that saturation magnetization, increases with the increase of Cd content up to $x = 0.4$ and decrease thereafter.

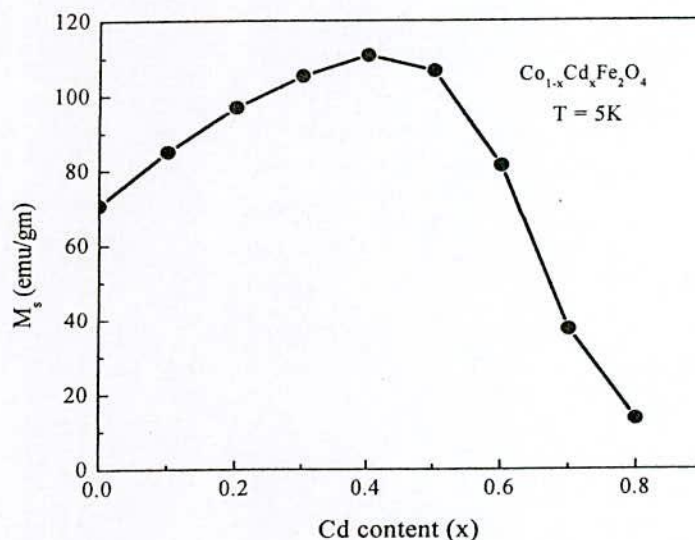


Fig. 4.14 Saturation magnetization (M_s) of $\text{Co}_{1-x}\text{Cd}_x\text{Fe}_2\text{O}_4$ as a function of Cd content (x) at temperature, $T = 5\text{K}$.

Initial increase of magnetization is attributed to the preferential occupation of A-sites by Cd^{2+} , thus displacing an equal amount of Fe^{3+} from A-sites to B-sites leading to the difference in magnetization between the B sublattice and the A sublattice, $M = M_B - M_A$ in the antiferromagnetic coupling. This enhancement of magnetization with increasing cadmium content is explained based on Neel's two sublattice model [4.30]. Magnetic moment of any composition depends on the distribution of Fe^{3+} ions between A and B sublattices since Cd^{2+} is nonmagnetic having zero net magnetic moment and that of Fe^{3+} is $5\mu_B$. The replacement of x amount of Cd^{2+} ions (Cd^{2+} occupies A-sites) for Co^{2+} can give rise to $(1-x)$ Fe^{3+} ions on A-sites and $(1+x)$ Fe^{3+} ions on B-sites and considering that all Co^{2+} occupies B-sites with magnetic moment of $3\mu_B$. The cation distribution then takes the following form; $(\text{Cd}_x\text{Fe}_{1-x})_A[\text{Co}_{1-x}\text{Fe}_{1+x}]_B$. The Cd^{2+} substitution leads to increased Fe^{3+} ions on B-sites and consequently magnetization of the B-sites increases while that of A-sites decreases resulting in an increase of net magnetization $M = M_B - M_A$. Samples with $x > 0.5$, magnetization is found to decrease gradually. This can be explained due to non-collinear spin structure in the B-sites, i.e spin canting effects in B sublattice known as Yafet-Kittel type of spin arrangement [4.31, 4.32]

according to the random canted model. Substitution of diamagnetic cations in one sublattice of ferrimagnet leads to spin canting in the other sublattice resulting in decrease in total magnetization per formula unit. The reason for the decrease in magnetization beyond $x = 0.4$ is that the magnetization of A-sublattice is so diluted that the A-B exchange interaction no longer remains stronger and thereby B-B sublattice interaction plays also an important role which in turn disturbs the parallel arrangement of spin magnetic moments on the B-site and hence canting of spin occurs.

Neel's two-sublattice collinear ferrimagnetism is observed for the system up to $x \leq 0.4$ and beyond this limit three-sublattice non-collinear spin canting model is predominant. The existence of canted spin gives rise to the Yafet-Kittel angle (α_{Y-K}), which compares the strength of A-B and B-B exchange interactions [4.31]. Y-K angles are calculated at 5K using the following formula

$$n_B = M_B(x)\cos \alpha_{Y-K} - M_A(x), \quad (4.2)$$

where α_{Y-K} is the canted angle. The condition for Y-K angles to occur in Zn containing Ni-Zn ferrites was investigated by Satya Murthy *et.al.* [4.33] in molecular field approximation using the non-collinear three-sublattice model. According to the similarities between Ni-Zn, Mg-Zn and Co-Cd ferrites, the existence of Y-K angles in the present Co-Cd system for $x > 0.4$ is assumed. The values of α_{Y-K} are presented in Table-4.3. It is observed that α_{Y-K} angles for the samples $x = 0.0 - 0.4$ are non-zero, i.e Y-K has a small value. This means that the cation distribution is not exactly as proposed by theory. Ignoring this small Y-K angle value we can consider that the calculated values of the Y-K angles for the present system are non-zero and reasonably high for $x > 0.4$ and the non-zero Y-K angles suggest that the magnetization behavior can not be explained by Neel's two-sublattice model due to the presence of spin canting on B-sites, which increases the B-B interaction and consequently decreases the A-B interaction. Increase in Y-K angles for the samples with Cd content ($x > 0.4$) is attributed to the increased favour of triangular spin arrangements on B-sites leading to the reduction in the A-B exchange interaction and subsequent decrease in magnetization [4.34, 4.35]. Almost all Zn^{2+} and Cd^{2+} substituted ferrites have shown a similar type of canting behavior above a certain limit of their content [4.35 - 4.37]. Hence in the present system of ferrites, frustration and randomness increases as Cd content increase in the Co-ferrites and shows significant departure from Neel's collinear model.

In Fig. 4.15 it is observed that the theoretical magnetization increases linearly with Cd content reaching a value of $n_B = 10\mu_B$ for CdFe_2O_4 . In the theoretical calculation, no frustration or spin canting has been taken into account.

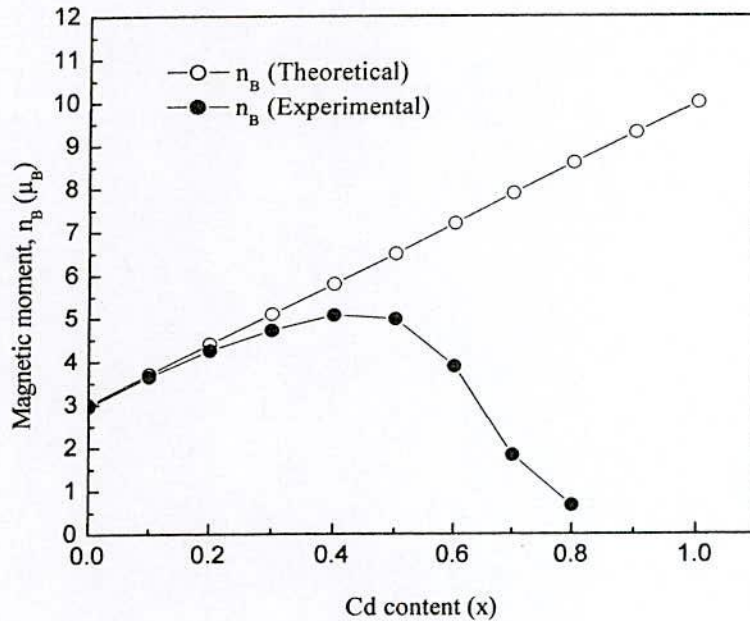


Fig. 4.15 Variation of magnetic moment as a function of Cd content (x) of $\text{Co}_{1-x}\text{Cd}_x\text{Fe}_2\text{O}_4$ ferrites.

Table- 4.3 Data of saturation magnetization (M_s), theoretical and experimental magnetic moment (n_B) and Yafet-Kittel angle (α_{Y-K})

Cd content (x)	Saturation Magnetization M_s (emu/gm)	Magnetic Moment n_B (μ_B)		Yafet-Kittel angle
		theoretical	experimental	α_{Y-K}
0	71	3	2.97	5
0.1	85	3.7	3.65	7
0.2	97	4.4	4.25	11
0.3	105	5.1	4.72	17
0.4	111	5.8	5.07	24
0.5	106	6.5	4.98	34
0.6	81	7.2	3.88	50
0.7	38	7.9	1.83	69
0.8	14	8.6	0.67	80

4.3 Electrical Transport Property

4.3.1 Compositional Dependence of DC Electrical Resistivity

DC resistivity is an important electrical property of ferrites in high frequency application. Fig. 4.16 gives the room temperature values of resistivity (ρ_{dc}) versus Cd content of the samples of series $\text{Co}_{1-x}\text{Cd}_x\text{Fe}_2\text{O}_4$ ferrites by using a Keithley Electrometer. For measurements, the pellet shaped samples were coated with silver paint on the both surfaces of each sample to obtain good ohmic contact. Table 4.1 gives the DC resistivity values for all the samples under study. The DC resistivity is found to increase with Cd content up to $x = 0.4$. Resistivity is found to decrease with further addition of Cd content. This decrease of resistivity may be attributed to the entrapped intragranular porosity, Sankpal *et.al.* and Shaikh *et.al.* measured resistivity as a function of composition in their work on Ni-Cu and Li-Cd ferrites [4.38, 4.39]. They obtained the similar trend of decreasing resistivity with the increase of Cu content. This trend could be attributed to the high activation energy, which is associated with high resistivity at room temperature. The decrease of resistivity has been related to the decrease of porosity since pores are non-conductive, which increase the resistivity of the materials [3.40].

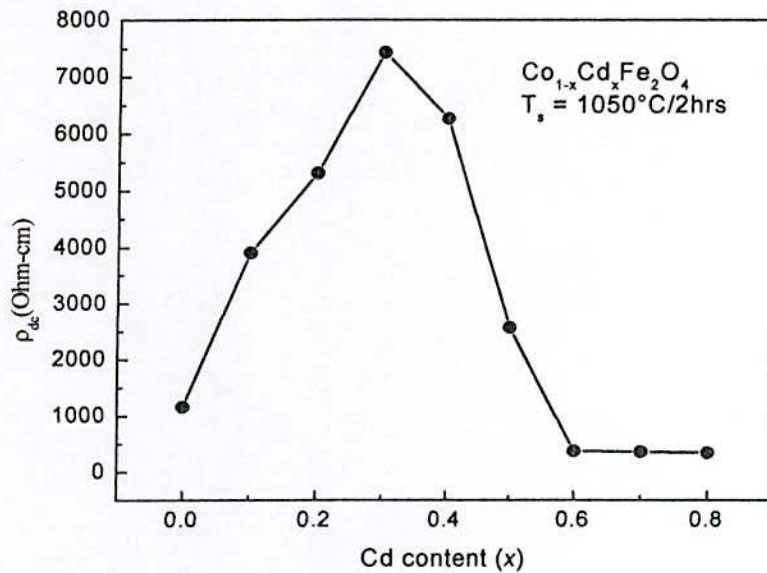


Fig. 4.16 Room temperature DC resistivity as a function of Cd content of $\text{Co}_{1-x}\text{Cd}_x\text{Fe}_2\text{O}_4$ ferrites.

4.3.2 Frequency Dependence of AC Resistivity

The electrical properties of ferrite materials depend upon the method of preparation, chemical composition, grain size and sintering temperature. The frequency dependence of AC electrical resistivity of ferrites is crucial because of its huge applications with frequency characteristics. The AC resistivity decreases as the frequency increases from 1 kHz to 13 MHz and is shown in Fig 4.17 at room temperature. All the samples show the significant dispersion with frequency which is the normal ferrimagnetic behavior. The resistivity of the ferrites is expected to decrease with an increase in the frequency; this may be due to the low dielectric constant and also depends on the porosity and composition [4.41]. Ferrite structurally forms cubic closed packed oxygen lattices with the cations at the octahedral (B) and the tetrahedral (A) sites. The distance between two metal ions at B site is smaller than the distance between a metal ion at B site and another metal ion at A-site. The electron hopping between A and B sites under normal conditions therefore has a very small probability compared with that for B-B hopping. Hopping between A and A sites does not exist for the reason that there are only Fe^{3+} ions at the A site and Fe^{2+} ions formed during processing preferentially occupy B sites only.

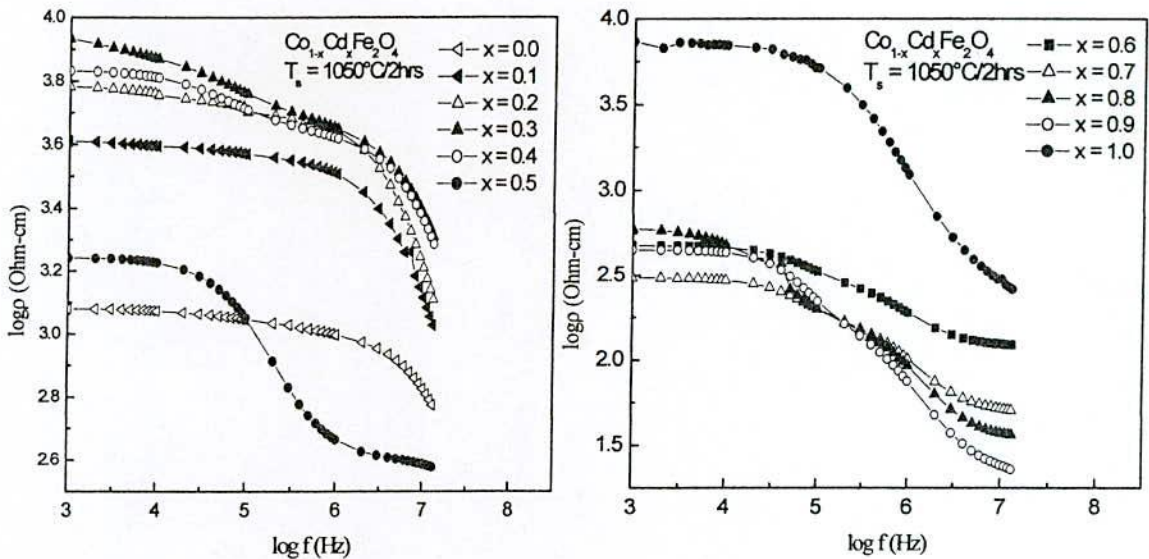


Fig. 4.17 Frequency dependence of AC resistivity of $\text{Co}_{1-x}\text{Cd}_x\text{Fe}_2\text{O}_4$ ferrites sintered at $1050^\circ\text{C}/2\text{hrs}$.

The conduction mechanism in ferrites is explained on the basis of hopping of charge carriers between the Fe^{2+} and Fe^{3+} ions on octahedral site. The increase in frequency enhances the hopping frequency of charge carriers resulting in an increase in the conduction process

thereby decreasing the resistivity. Ferrites are low mobility materials and the increase in conductivity does not mean that the number of charge carriers increases, but only the mobility of charge carriers increases. The minimum resistivity occurred when the frequency of the hopping charge carriers is equal to the applied field frequency termed as resonance frequency i.e. the jumping frequency of hopping charge carriers are almost equal to that of the applied AC electric field.

4.3.3 Frequency Dependence of Dielectric Constant

Fig. 4.17 shows the variation of dielectric constant, ϵ' with frequency for different composition of $\text{Co}_{1-x}\text{Cd}_x\text{Fe}_2\text{O}_4$ ferrites sintered at $1050^\circ\text{C}/2\text{hrs}$ from 100 Hz to 13 MHz at room temperature. It can be seen from the figure that the dielectric constant is found to decrease continuously with increasing frequency for all the specimens exhibiting a normal dielectric behavior of ferrites. The dielectric dispersion is rapid at lower frequency region and it remains almost independent at high frequency side. The incorporation of Cd into Co-Cd ferrites has no pronounced effect on the dielectric constant in high frequency, but significantly decreases the dielectric constant in the low frequency range.

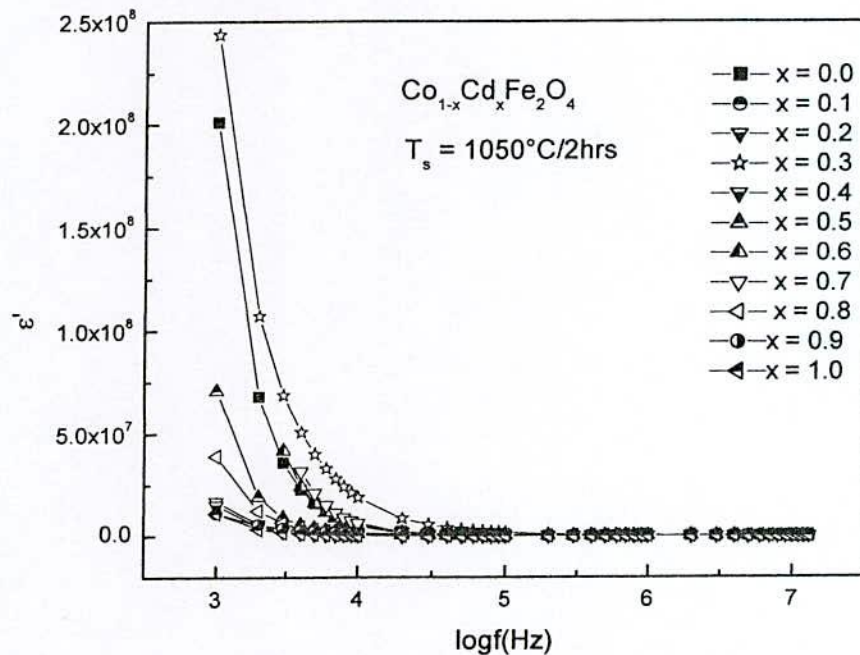


Fig. 4.18 Dielectric constant as a function of frequency of the ferrite system $\text{Co}_{1-x}\text{Cd}_x\text{Fe}_2\text{O}_4$ ferrite sintered at $1050^\circ\text{C}/2\text{hrs}$.

This type of behavior was observed in a number of ferrites such as Li-Co ferrites [4.42], Cu-Cd ferrites [4.43] Ni-Cu-Zn ferrites [4.44], Li-Mg-Ti ferrites [4.45], Mg-Cu-Zn ferrites [4.46, 4.47]. The dielectric behavior of ferrites may be explained on the basis of the mechanism of the dielectric polarization process and is similar to that of the conduction process. The electronic exchange $Fe^{2+} \leftrightarrow Fe^{3+}$ gives the local displacement of electrons in the direction of applied electric field, which induces the polarization in ferrites [4.43, 4.48].

The magnitude of exchange depends on the concentration of Fe^{2+}/Fe^{3+} ion pairs present on B site for the present ferrite. The sample $x = 0.0$ and 0.3 showed the maximum dispersion while that with $x = 1.0$ showed a least frequency dependence. The presence of Fe^{2+} ions in excess amount favors the polarization effects. Thus, the more dispersion observed in the sample with $x = 0.0$ and 0.3 can be attributed to the presence of Fe^{2+} ions in excess amount which could be formed at elevated sintering temperature. Similarly the weak dependence of dielectric constant on frequency can be due to lack of Fe^{2+}/Fe^{3+} ions concentration. All samples have high values of ϵ' in the order of 10^5 - 10^8 at low frequencies. This could be explained using Koop's phenomenological theory [4.49] which was based on the Maxwell-Wagner model [4.50, 4.51] for the inhomogeneous double layer dielectric structure. The dielectric structure was supposed to be composed of the fairly well conducting ferrite grains. These are separated by the second thin layer of grain boundaries which are poorly conducting substances. These grain boundaries could be formed during the sintering process due to the superficial reduction or oxidation of crystallites in the porous materials as a result of their direct contact with the firing atmosphere [4.52]. The grain boundaries of lower conductivity were found to be effective at lower frequencies while ferrite grains of high conductivity are effective at high frequencies [4.49, 4.53].

4.4 Summary

Powder X-ray diffractometry of the ferrite samples reveals the single-phase cubic spinel structure, as well as defined reflections are observed without any ambiguity. Variation of lattice parameter with Cd content obey's Vegard's law and the linear variation of X-ray densities with Cd content suggest that the substituted atom preferentially occupies tetrahedral (A) site. Bulk density is found to increase while porosity decreases with increasing Cd content. Curie temperature decreases linearly with the addition of Cd ions. This is due to the fact that the replacement of Fe^{3+} ions by Cd^{2+} ions in the A-sites results in the decrease of strength of A-B super exchange interactions. The initial permeability increases with Cd content and sintering temperature has little effect on permeability. The increase in the permeability can be attributed to the presence of Cd ions activating the sintering process in ferrites and leading to increase in density and grain size. Saturation magnetization increases with increasing copper Cd content at $x \geq 0.4$ and then it decreases. The hysteresis behavior and initial permeability reveals the softer ferromagnetic nature of the studied sample. DC electrical resistivity is found to increase with the increase of Cd content which is attributed to the fact that the incorporation of Cd in B site of ferrite may decrease the concentration of $\text{Fe}^{2+}/\text{Fe}^{3+}$ ion pairs.

CHAPTER-V
RESULTS AND DISCUSSION OF
 $\text{Co}_{1-x}\text{Zn}_x\text{Fe}_2\text{O}_4$ FERRITES

Results and Discussion of $\text{Co}_{1-x}\text{Zn}_x\text{Fe}_2\text{O}_4$ Ferrites

5.0 Introduction

Co-Zn ferrites are quite important materials in the field of microwave industry, which is a mixture of CoFe_2O_4 with long range ferromagnetic ordering and ZnFe_2O_4 with antiferromagnetic ordering [5.1]. Zinc plays a decisive role in determining the ferrite properties [5.2]. The magnetic properties of ferrites are dependent on the type of magnetic ions residing on the A and B sites and the relative strengths of the inter (J_{AB}) and the intra sublattice (J_{BB} , J_{AA}) interaction. ZnFe_2O_4 and CdFe_2O_4 are generally assumed to be normal spinel with all Fe^{3+} ions on B-sites and all Zn^{2+} and Cd^{2+} ions on A sites [5.3, 5.4]. The magnetization behavior and magnetic ordering of Zn substituted Co-Zn, Cu-Zn, Ni-Zn and Mg-Zn ferrites have been studied by many workers [5.1, 5.5 - 5.7] and extensive works have been performed on the solid solution of $\text{Co}_{1-x}\text{Zn}_x\text{Fe}_2\text{O}_4$, where x ranging from 0.0 - 1.0. But exact nature of magnetic ordering for all the compositions are not yet very clear. Magnetic properties of Co-Zn ferrites have been reported only for particular value of x or limiting values [5.8].

The magnetic properties of ferrites such as permeability, magnetization, coercive field, Curie temperature are affected by composition as well as by the type of substitution, cation distribution and method of preparation [5.9]. Globus *et. al.* [5.10] studied the size effect of nonmagnetic ions Zn and Cd on the magnetic properties of Ni-ferrites and concluded that the variation of magnetic properties results from the ion concentration as well as difference in ionic radius. Satyamurthy *et. al* [5.6] reported that in the Yafet-Kittel (Y-K) model the B-sublattice can be split in to two sublattices having magnetic moments equal in magnitude and each making an angle α_{Y-K} with the direction of the net magnetization at 0 K. Smit and Wijn [5.11] reported that in mixed Zn ferrites the A-B interaction is reduced with increasing Zn content and the Curie temperature decreases. Zn substituted spinel ferrites showed good magnetic properties which are characterized by a maximum in saturation magnetization in certain composition [5.12 - 5.14]. Most of the Zn substituted ferrites like Ni-Zn [5.15], Fe-Zn [5.16], Cu-Zn [5.5] and Mg-Zn [5.17, 5.18] show a canted spin arrangement on the octahedral or B-sites when the substitution of Zn exceeds a certain limit. The canting of the spins gives rise to Yafet-Kittel angles (Y-K), which suggests that A-B and B-B superexchange interactions are comparable in strength. Therefore, it would be interesting to investigate similar effects in the Zn substituted cobalt ferrite system. In order to study the influence of Zn ion on the structural and magnetic properties of $\text{Co}_{1-x}\text{Zn}_x\text{Fe}_2\text{O}_4$ with $x = 0.0 - 1.0$ have been prepared and reported in the present work.

5.1 X-ray Diffraction Analysis

5.1.1 Phase Analysis

Structural characterization and identification of phases is a prior for the study of ferrite properties. Optimum magnetic and transport properties of the ferrites necessitate having single phase cubic spinel structure. X-ray diffraction patterns for $\text{Co}_{1-x}\text{Zn}_x\text{Fe}_2\text{O}_4$ samples sintered at $1100^\circ\text{C}/2\text{hr}$ are shown in Fig. 5.1. The XRD patterns for all the samples were indexed for fcc spinel structure and the Bragg planes are shown in the patterns. All the samples show good crystallization with well defined diffraction lines. It is obvious that the characteristic peaks for spinel Co–Zn ferrites appear in the samples as the main crystalline phase with a slight shifting in the position of peaks towards the lower d-spacing values. The fundamental reflections from the planes of (111), (220), (311), (222), (400), (422), (511) and (440) characterizing the cubic spinel structures are observed.

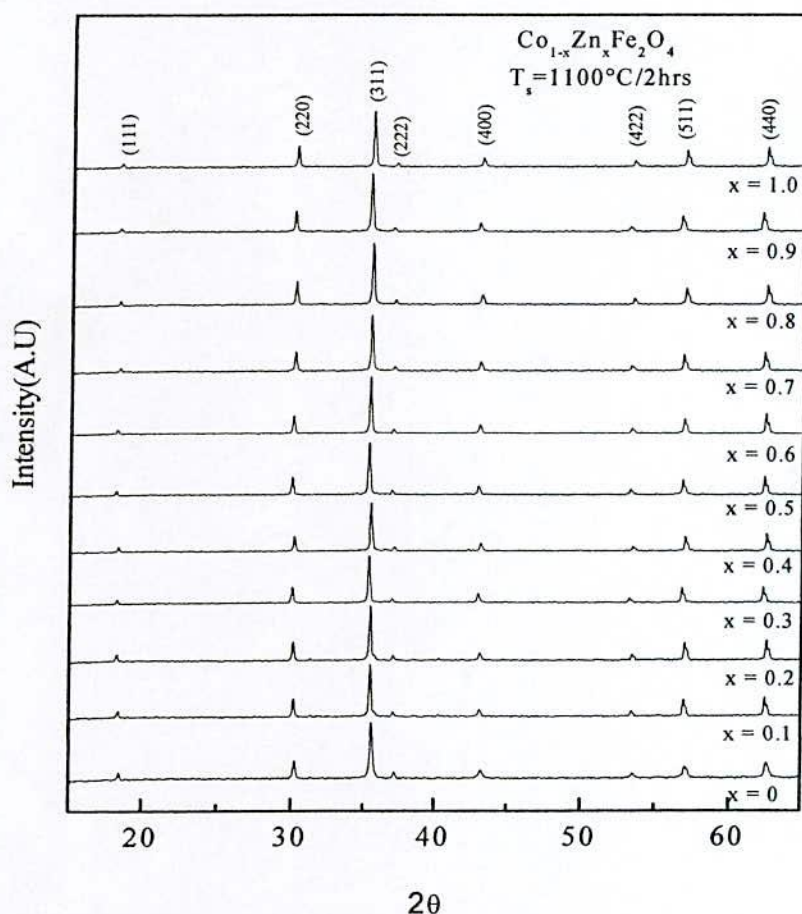


Fig. 5.1 XRD patterns of $\text{Co}_{1-x}\text{Zn}_x\text{Fe}_2\text{O}_4$ ferrite with different Zn content.

This indicates that the synthesized ferrite compositions are of single phase cubic spinel since no ambiguous reflections other than the spinel structures are evidenced. This also demonstrates the homogeneity of the prepared samples.

5.1.2 Lattice Parameter

The lattice constant of all the samples have been precisely determined considering the reflections with the Cu- k_α radiation using the extrapolated Nelson-Riley function $F(\theta) = 0$ at $\theta = 90^\circ$. The least square linear fitting gives the precise lattice constant as an intercept of the Y-axis. The lattice constant as a function of Zn content have been plotted in Fig. 5.2 and are tabulated in Table - 5.1. From Fig. 5.2 it is observed that the lattice constant increases linearly with increasing Zn content obeying Vegard's law [5.19]. The lattice constant increases with increasing x content, because the ionic radius of Co^{2+} (0.72\AA) [5.20] is smaller than that of Zn^{2+} (0.82\AA) [5.21]. Since the radius of the substituted ions is larger than that of the displaced ions it is expected that the lattice should expand increase the lattice constant.

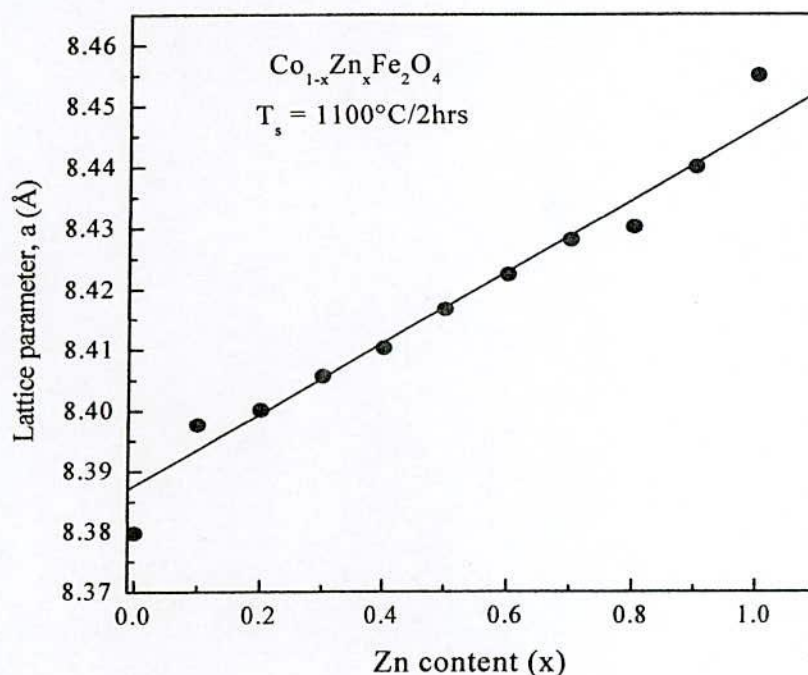


Fig. 5.2 Variation of lattice constant 'a' as a function of Zn content (x) of $\text{Co}_{1-x}\text{Zn}_x\text{Fe}_2\text{O}_4$ ferrites.

The increase in lattice constant with x is similar in nature to that has been reported in the Zn-Mg [5.22 - 5.24], Cu-Zn [5.25] and Co-Zn [5.26, 5.27] ferrite system. Lattice constant of ZnFe_2O_4 ferrite is 8.633\AA [5.28] and 8.471\AA [5.29]. Our value of lattice constant is 8.455\AA . The difference in the values of the lattice constant may be due to different sintering atmosphere, technique and the possibility of experimental error.

5.1.3 Density

The dependence of bulk density d_B and X-ray density ρ_x upon Zn content x is presented in Fig. 5.3. X-ray density ρ_x was calculated from the molecular weight and the volume of unit cell for each sample where as the bulk density ρ_B was measured usual mass and dimensional consideration. The bulk density increases significantly with increasing Zn content indicating improved densification by the substitution of Zn for Co in the ferrite. The increase of density with Zn content can be attributed to the atomic weight and density of Zn (65.37 and $7.14\text{gm}/\text{cm}^3$) which is higher than those of Co (58.9 and $8.6\text{ gm}/\text{cm}^3$) respectively .

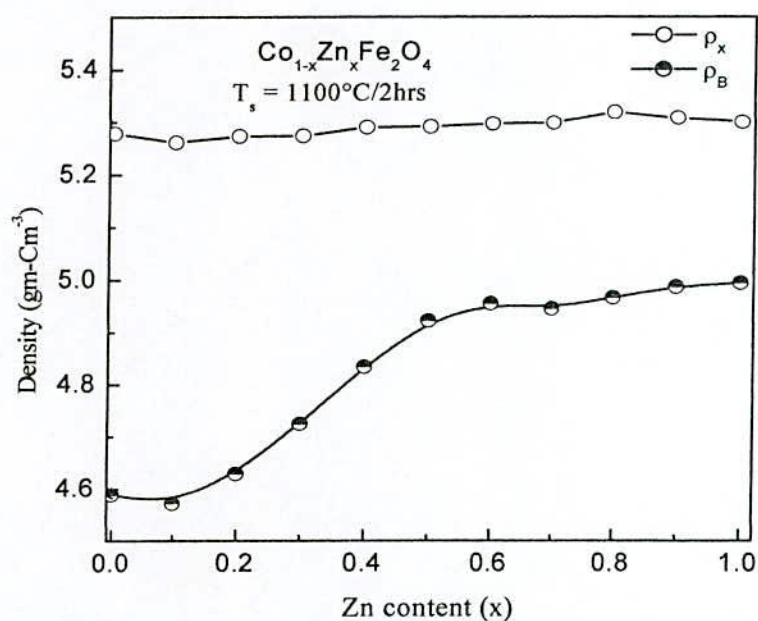


Fig. 5.3 Variation of density with Zn content(x) of $\text{Co}_{1-x}\text{Zn}_x\text{Fe}_2\text{O}_4$ ferrites.

The replacement of Co^{2+} by Zn^{2+} ions in the spinel leads to a variation in bonding and consequently interatomic distance and density. The oxygen ions which diffuse through the material during sintering also accelerate the densification of the material. The apparent density of the same composition reflects the same general behavior of the X-ray density ρ_x . The X-ray

density is higher than the apparent density value due to the existence of pores which depends on the sintering condition.

The percentage of porosity was also calculated using the equation (3.7). Porosity changes slightly with Zn content (x). It is understood from the data of Table - 5.1, porosity values are found to decrease significantly with increasing Zn concentration, thereby giving an impression that zinc might be helping in the densification of the materials. The composition $x = 0.8$ has the highest density and lowest porosity may be due to the increase of oxygen vacancies [5.30].

Table- 5.1 Lattice parameter (a), X-ray density (ρ_x), bulk density (ρ_B), porosity (P%) of $\text{Co}_{1-x}\text{Zn}_x\text{Fe}_2\text{O}_4$ ferrite with different Zn content sintered at 1100°C/2hrs.

Zn content (x)	a (Å)	ρ_x (gm/cm ³)	ρ_B (gm/cm ³)	P%
0	8.380	5.278	4.589	13.0
0.1	8.398	5.261	4.572	13.1
0.2	8.400	5.273	4.629	12.2
0.3	8.409	5.261	4.725	10.2
0.4	8.415	5.290	4.834	8.6
0.5	8.417	5.291	4.923	6.9
0.6	8.422	5.297	4.956	6.7
0.7	8.430	5.297	4.946	6.6
0.8	8.431	5.322	4.975	6.5
0.9	8.442	5.309	4.920	7.3
1.0	8.455	5.300	4.827	8.9

5.2 Electromagnetic Properties

5.2.1 Temperature Dependence of Initial Permeability

Curie temperature, T_c is a basic quantity in the study of magnetic materials. It corresponds to the temperature at which a magnetically ordered material becomes magnetically disordered. Fig. 5.4 shows the Curie temperature, T_c is obtained from the initial permeability, μ' versus temperature profiles of different composition at $x = 0.0 - 0.5$. It was found that the initial permeability increases with the increase of temperature, while it falls abruptly close to the Curie temperature. It is observed from the Fig. 5.4 that the initial permeability increases with increasing Zn content. The abrupt fall of permeability indicates the homogeneity and the single phase of the studied samples, which have also been confirmed by X-ray diffraction as evidenced from the XRD patterns for each sample. Curie temperature,

T_c of the sample with $x = 0.6$ and above has been determined from the temperature dependence of magnetization, M using SQUID magnetometer.

Fig. 5.5 represents the variation of the complex permeability, μ' , μ'' and temperature derivative of permeability, $d\mu'/dT$ as a function of temperature of $\text{Co}_{1-x}\text{Zn}_x\text{Fe}_2\text{O}_4$ with $x = 0.4$. At the Curie temperature, where complete spin disorder takes place, corresponds to maximum of imaginary part and the temperature derivative of the real permeability and sharp fall of the real part of permeability towards zero. From this figure it is observed that the imaginary part of permeability and temperature derivatives of permeability show peaks at value a temperature, T which excellently matches with the sharp fall of permeability at $T = T_c$.

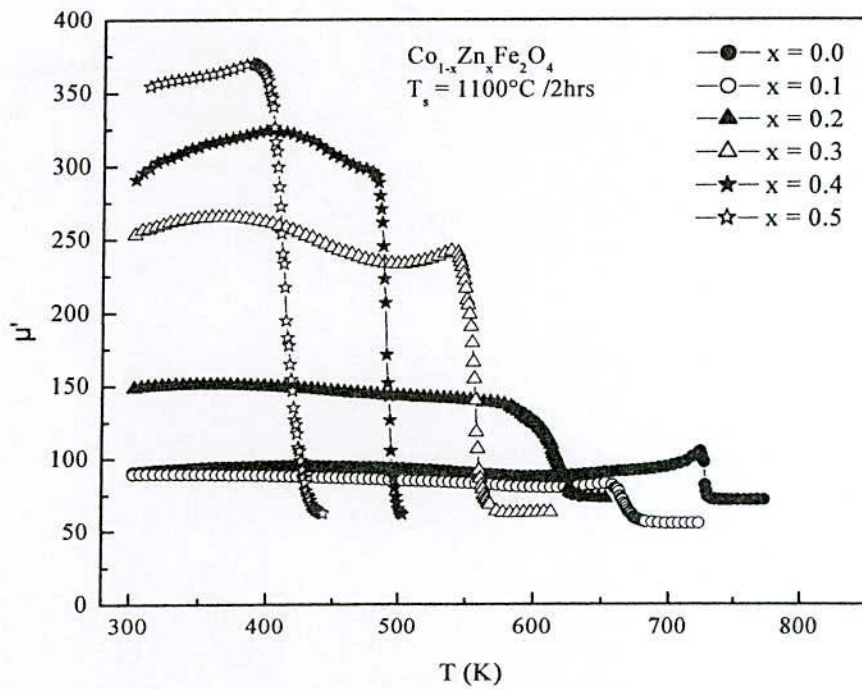


Fig. 5.4 Temperature dependence of permeability, μ' of $\text{Co}_{1-x}\text{Zn}_x\text{Fe}_2\text{O}_4$ ferrites with different Zn content.

In Fig. 5.6 the variation of Curie temperature T_c as a function of Zn content of $\text{Co}_{1-x}\text{Zn}_x\text{Fe}_2\text{O}_4$ system. It is observed that T_c decreases continuously with the increase of Zn^{2+} content. The linear decrease of T_c with increasing Zn content may be explained by modification of the A-B exchange interaction strength due to the change of the iron distribution between A and B sites when nonmagnetic Zn is substituted for Co. The basic magnetic properties of CoFe_2O_4 system originate from Co^{2+} ions only in the octahedral B-sites since Fe^{3+} ions are distributed A-sites replacing an equal amount of Fe^{3+} to the octahedral B-sites. In such a situation J_{AA} becomes weaker. Therefore decrease of T_c is due to the weakening of A-B exchange

interaction and this weakening becomes more pronounced when more Zn replaces more tetrahedral Fe^{3+} to octahedral B-sites. The similar trend in the variation of T_c has been observed by many researches in Zn substituted Mg-Zn and Ni-Zn [5.7, 5.31] and other ferrite systems.

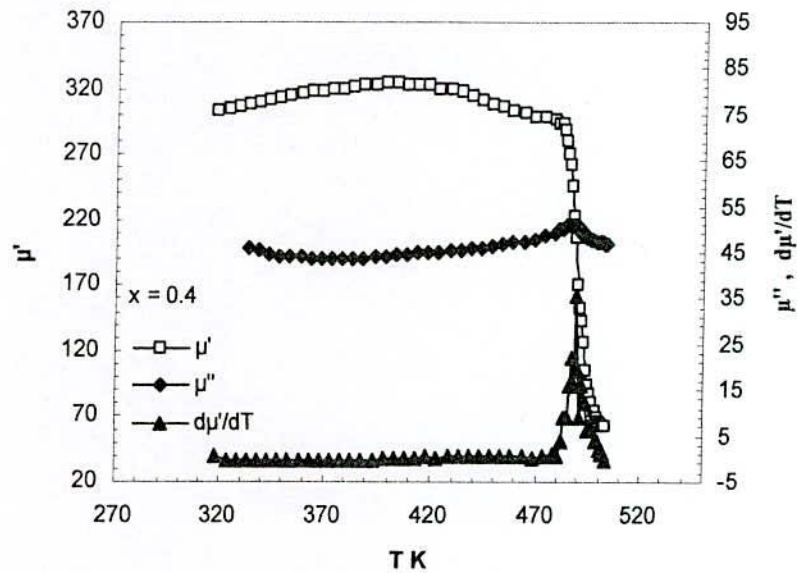


Fig. 5.5 Determination of Curie temperature from the temperature dependence of μ' , μ'' and $d\mu'/dT$ as a function of temperature of $\text{Co}_{1-x}\text{Zn}_x\text{Fe}_2\text{O}_4$ ferrites with $x = 0.4$.

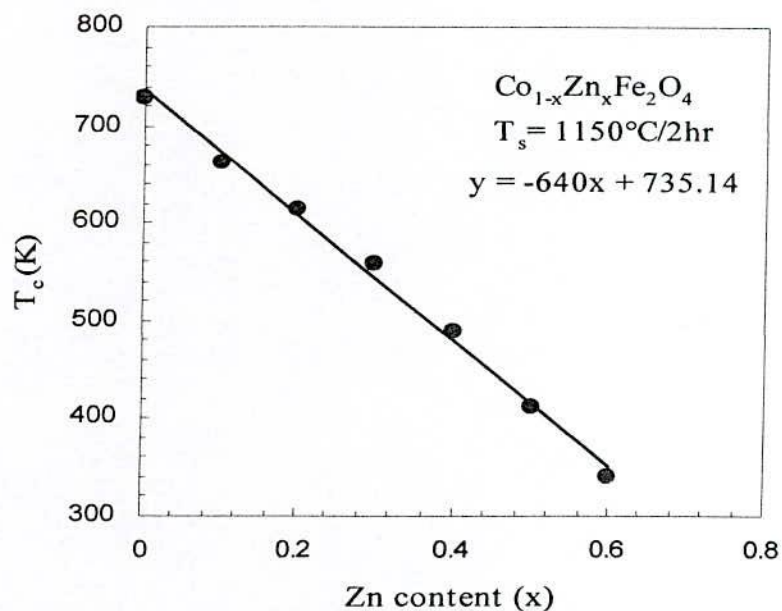


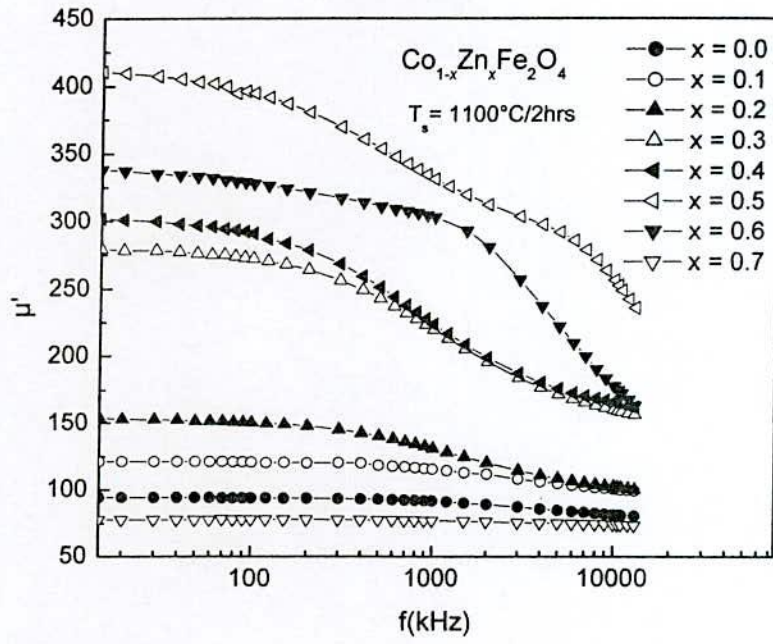
Fig. 5.6 Variation of Curie temperature, T_c with Zn content (x) of $\text{Co}_{1-x}\text{Zn}_x\text{Fe}_2\text{O}_4$ ferrites.

A linear dependence of T_c with Zn content is observed with $x \leq 0.7$ beyond which well defined T_c could not be determined due to complex magnetic structures and competing interactions of highly diluted composition. A linear least square fitting of the Curie temperature with x , gives an empirical relation for the whole $\text{Co}_{1-x}\text{Zn}_x\text{Fe}_2\text{O}_4$ system as follows, $T_c(x) = T_c(0) - 640x$, where $T_c(0)$ is the Curie temperature of the pure Co-ferrite and $T_c(x)$ corresponds to the Curie temperature of any composition having Zn concentration x . From this empirical relation, Curie temperature of Co-ferrite is found to be 735K. Our experimental result is 728K listed in Table - 5.2.

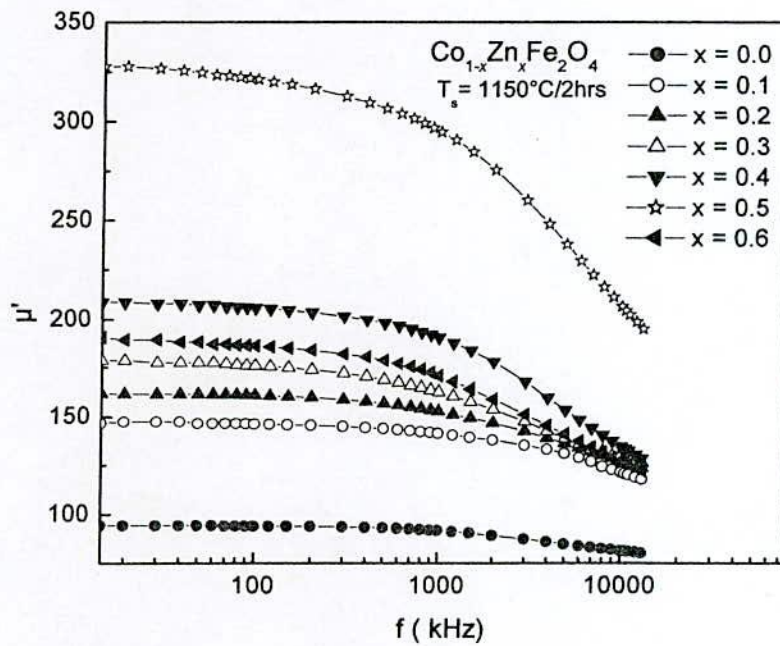
5.2.2 Frequency Dependence of Initial Permeability

Fig. 5.7 (a) and (b) shows the variation of the real part of permeability with frequency of the system $\text{Co}_{1-x}\text{Zn}_x\text{Fe}_2\text{O}_4$ for different values of x at different temperature 1100°C and 1150°C for 2 hours. For all the samples sintered at 1100°C and 1150°C, the values of initial permeability increases with increasing Zn content upto $x = 0.5$, because the sintered density increases and porosity decreases with increase of Zn content. Initial permeability would be resolved into two types of mechanisms such as contribution from spin rotation and contribution from domain wall motion. But the contribution from spin rotation was found to be smaller than domain wall motion and it is mainly due to reversible motion of domain walls in the presence of a weak magnetic field [5.32, 5.33].

Permeability is related to the saturation magnetization and anisotropy by the relation $\mu' \propto \frac{M_s^2 D}{\sqrt{K_1}}$ [5.34, 5.35], where M_s is the saturation magnetization, K_1 is the anisotropy constant and D is the grain size of the sample. According to the relation increase in μ' with Zn content is attributed to the increase in M_s with increasing Zn content and may also be due to decrease in K_1 . An increase in the density of ferrites not only resulted in the reduction of demagnetizing field due to decreased porosity but also raised the contribution due to rotation of spin, which in turn increased the permeability [5.36]. Fig. 5.8 shows the variation of initial permeability, μ' at frequency 100 kHz with Zn content of $\text{Co}_{1-x}\text{Zn}_x\text{Fe}_2\text{O}_4$ ferrites with sintering temperature 1100°C and 1150°C. It was observed that the permeability increases slowly at low Zn content and then increase sharply upto $x = 0.5$ and thereafter decreases. It also observed permeability decreases with increase of sintering temperature. The decrease of permeability with increasing T_s may be explained on the basis of intragranular pores entrapped within the grains which create constraint on the domain wall mobility. As a result initial permeability decreases.



(a)



(b)

Fig. 5.7 Frequency dependence of real part of permeability of $\text{Co}_{1-x}\text{Zn}_x\text{Fe}_2\text{O}_4$ ferrites sintered at (a) 1100°C and (b) 1150°C for 2 hours.

At high sintering temperature pores cannot move so first as compared with the grain growth. Therefore the pores cannot move to the grain boundary rather they are trapped within the grains. The results of μ' at 100 kHz for all the samples sintered at 1100°C and 1150°C tabulated in Table - 5.2.

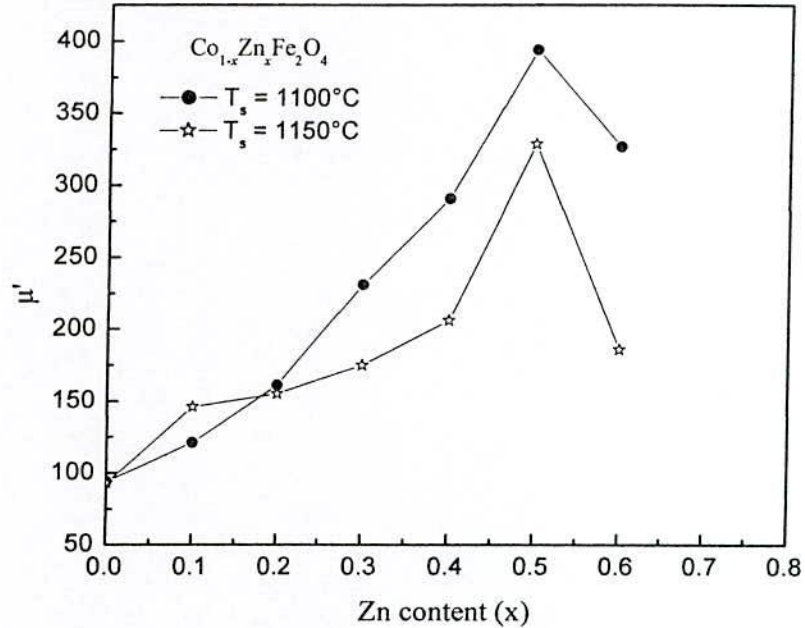


Fig. 5.8 Variation of initial permeability, μ' at frequency 100 kHz with Zn content (x) of $\text{Co}_{1-x}\text{Zn}_x\text{Fe}_2\text{O}_4$ ferrites sintered at temperature 1100° and 1150° for 2 hours.

Table-5.2 Data of the Curie temperature (T_c), permeability (μ') at frequency 100 KHz sintered at 1100°C and 1150°C for 2hrs and dc resistivity (ρ_{dc}) at room temperature, of $\text{Co}_{1-x}\text{Zn}_x\text{Fe}_2\text{O}_4$ samples

Zn content (x)	T_c (K)	$T_s = 1100^\circ\text{C}$ μ' (100KHz)	$T_s = 1150^\circ\text{C}$ μ' (100KHz)	dc resistivity (ρ_{dc}) $\Omega\text{-cm}$
0	728	94	93	1.16×10^3
0.1	663	121	146	1.62×10^3
0.2	613	161	155	3.47×10^3
0.3	558	231	175	32.33×10^3
0.4	488	291	206	42.56×10^3
0.5	413	394	329	91.27×10^3
0.6	339	327	186	27.9×10^4
0.7	242	77		196.9×10^4

5.2.3 Low Field B-H loop at Room Temperature

The B-H loops at room temperature of the investigated compositions $\text{Co}_{1-x}\text{Zn}_x\text{Fe}_2\text{O}_4$ sintered at 1100°C and 1150°C were measured at constant frequency ($f = 1 \text{ kHz}$) shown in Fig. 5.9 (a) and (b).

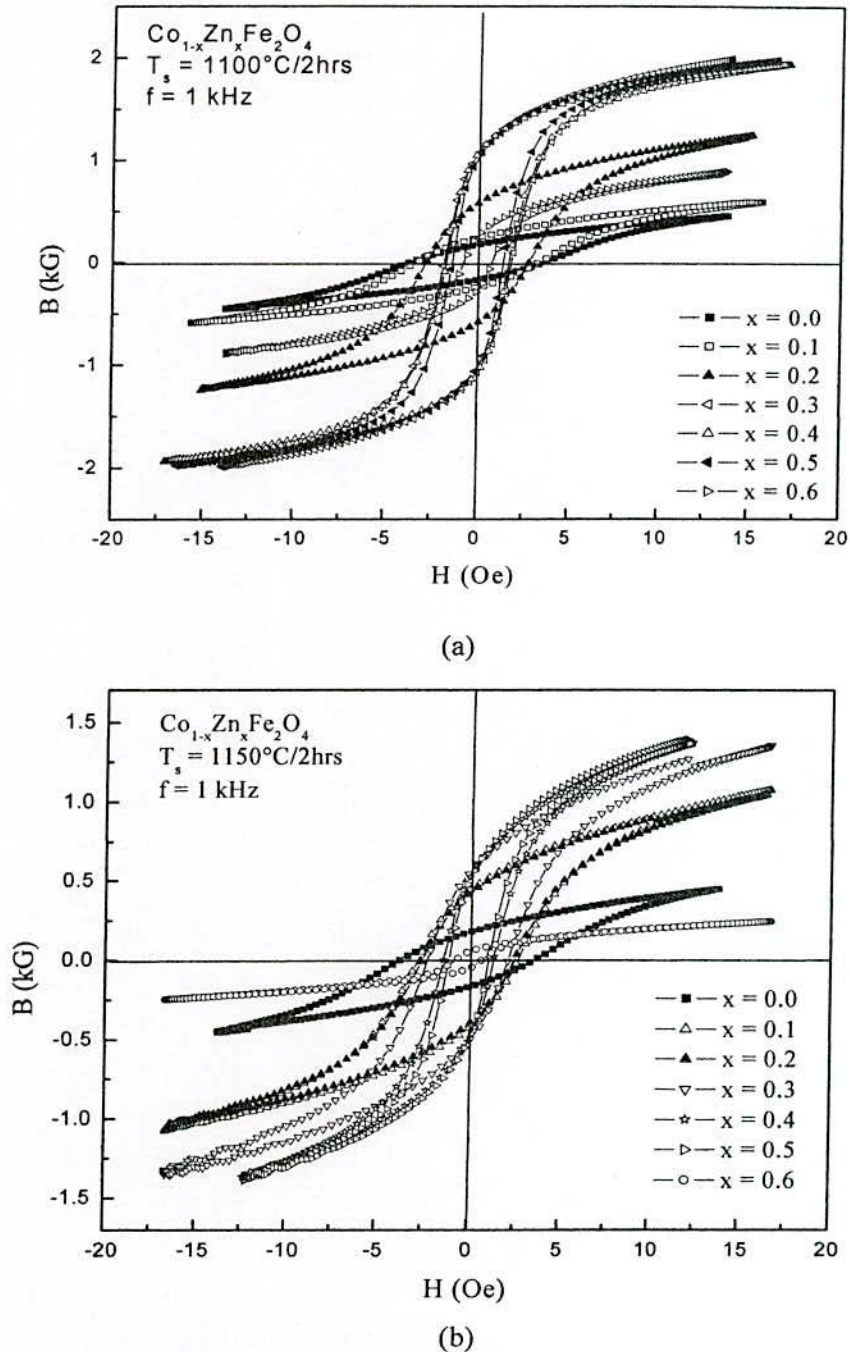


Fig. 5.9 Magnetic hysteresis graphs of $\text{Co}_{1-x}\text{Zn}_x\text{Fe}_2\text{O}_4$ ferrite with x sintered at (a) 1100°C and (b) 1150°C for 2 hours at constant frequency $f = 1 \text{ kHz}$.

From the B-H loops, the remanence induction B_r , saturation induction B_s and coercive force H_c were determined and studied with x and sintering temperature. From this loops the heigh coersitivity, H_c is observed at $x = 0.0$ and it decreases almost linearly with increasing Zn content up to $x = 0.6$ both the sintering temperature listed in Table - 5.3. The low coercive force and higher permeability, confirms that the development of soft magnetic characteristic properties of cobalt ferrite, which is well known as hard magnet with the substitution of Zn for cobalt. It is also observed that the decrease of coercivity with increase in sintering temperature. The difference in the H_c values is understandable because of the substantial increase in grain size in response to the increase in sintering temperature which facilitating the movement of the magnetic domain. Saturation induction (B_s), is found to increase with increasing Zn content. The different values of retentivity, and B_r/B_s ratio observed are interpreted in a quantitative way by means of domain theory.

Table-5.3 The calculated values of coercive force (H_c), remanence induction (B_r), saturation induction (B_s), B_r/B_s ratio and losses of $Co_{1-x}Zn_xFe_2O_4$ samples at room temperature with constant frequency ($f = 1\text{kHz}$) at different temperature

Zn content (x)	$T_s(^{\circ}C)$ /3hrs	H_c (Oe)	B_r (kG)	B_s (kG)	B_r/B_s	Losses (W/kg)
0.0	1100	3.70	0.18	0.45	0.40	6.23
	1150	3.66	0.18	0.45	0.40	6.21
0.1	1100	3.20	0.25	0.59	0.42	10.09
	1150	2.58	0.44	1.06	0.42	19.51
0.2	1100	2.79	0.58	1.24	0.47	18.41
	1150	2.60	0.42	1.03	0.41	20.06
0.3	1100	2.03	1.08	1.98	0.55	20.42
	1150	2.10	0.54	1.33	0.41	24.06
0.4	1100	1.86	1.16	1.93	0.60	18.79
	1150	1.39	0.53	1.39	0.38	13.24
0.5	1100	1.50	1.08	1.97	0.55	14.82
	1150	1.12	0.48	1.39	0.35	11.76
0.6	1100	1.07	0.29	0.89	0.33	3.59
	1150	0.66	0.35	0.44	0.79	0.67

5.2.4 Magnetization Measurement

Field dependence of magnetization measured at $T = 5\text{K}$ with an applied field 20 kOe for the ferrite sample $Co_{1-x}Zn_xFe_2O_4$ at $0 < x \leq 1.0$ to reach saturation values and the results are plotted in Fig. 5.10. It is observed that the magnetization increases sharply at very low field ($H < 1\text{kOe}$) which corresponds to magnetic domain reorientation and thereafter increases slowly

up to saturation corresponding to spin rotation. The samples with $x \leq 0.7$ seems to saturate easily while samples with $x > 0.7$ do not show any sign of saturation even with an applied field $H = 50$ kOe indicating high anisotropic nature of sample due to disorder frustration and competing interactions. Bhowmik and Ranganathan [5.8] showed that the magnetization $\text{Co}_{0.2}\text{Zn}_{0.8}\text{Fe}_2\text{O}_4$ samples is not saturated even in the presence of 12 T applied magnetic field.

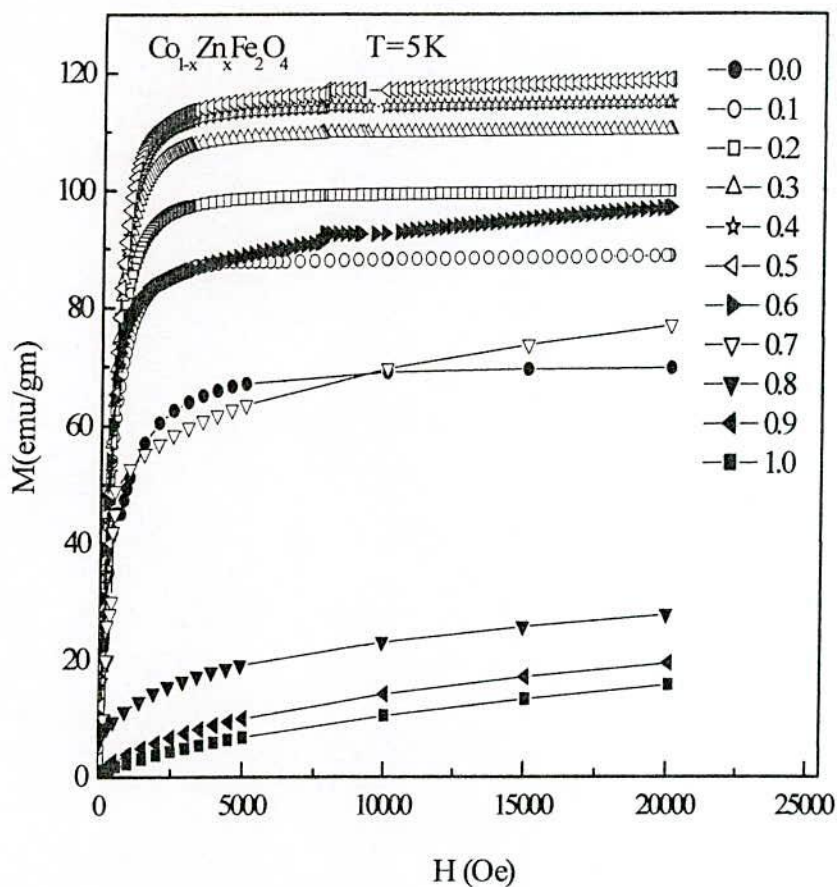


Fig. 5.10 Field dependence of magnetization for $x = 0.0 - 1.0$ of $\text{Co}_{1-x}\text{Zn}_x\text{Fe}_2\text{O}_4$ ferrites at temperature $T = 5\text{K}$.

Fig. 5.11 shows the variation saturation magnetization, M_s of the $\text{Co}_{1-x}\text{Zn}_x\text{Fe}_2\text{O}_4$ ferrites as a function of zinc content. It is observed from the Fig. 5.11 and Table - 5.4 that M_s increases upto $x = 0.5$ and then it decreases with increasing zinc content. The variation of n_B with Zn^{2+} content is shown in Fig. 5.12. It is observed that the saturation magnetization M_s and n_B increases with the increase of Zn content up to $x = 0.5$ and decreases thereafter. Magnetic moment of any composition depends on the distribution of Fe^{3+} ions between A and B sublattice. The Zn^{2+} substitution leads to increase Fe^{3+} ions on B-sites. Zn is nonmagnetic having zero net magnetic moment and Fe^{3+} is $5\mu_B$. So the magnetization of the B-sites

increases while that of A-sites decreases resulting in increases of net magnetization i.e $M = M_B - M_A$. The initial increase of magnetic moment with increase of Zn content is due to the increase in resultant sublattice magnetic moment on the basis of Neel's two sublattice model [5.37].

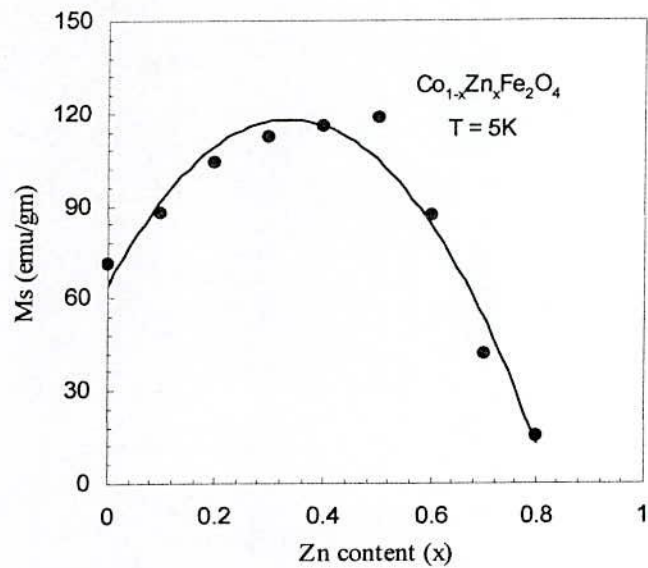


Fig. 5.11 Saturation magnetization, M_s versus Zn content in $Co_{1-x}Zn_xFe_2O_4$ ferrites.

Table-5.4 Data of saturation magnetization (M_s), theoretical and experimental magnetic moment (n_B) and Yafet-Kittel angle (α_{Y-K}) of $Co_{1-x}Zn_xFe_2O_4$ ferrites at temperature $T = 5K$.

Zn content (x)	M_s (emu/gm)	n_B (μ_B)		α_{Y-K}
		theoretical	experimental	
0.0	71	3	2.97	3
0.1	88	3.7	3.69	3
0.2	104	4.4	4.38	4
0.3	112	5.1	4.75	16
0.4	116	5.8	4.92	26
0.5	119	6.5	5.05	33
0.6	87	7.2	3.71	52
0.7	42	7.9	1.78	70
0.8	15	8.6	0.65	80

Samples at $x \geq 0.6$ magnetization is found to decrease gradually. The reason for the decrease of magnetization is that A-sublattice is so much diluted that the A-B exchange interaction no longer remains stronger and thereby B-B sublattice interaction becomes comparable to A-B exchange interaction which in turn disturbs the parallel arrangement of spin magnetic moments on the B-site and hence canting of spin occurs. This can be explained due to non-collinear spin structure in the B-sites. Spin canting effects in B sublattice is known as Yafet-Kittle type of spin arrangement [5.37, 5.38].

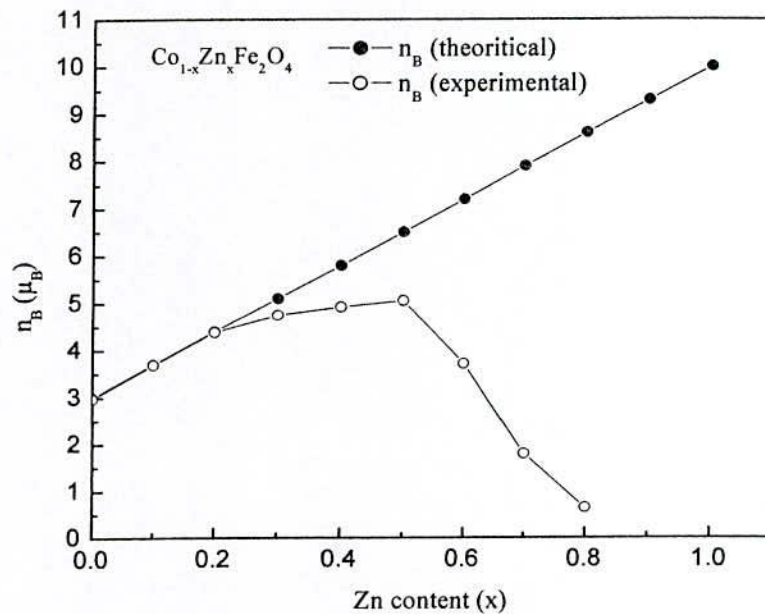


Fig. 5.12 Variation of magnetic moment, n_B as a function of Zn content (x) of $\text{Co}_{1-x}\text{Zn}_x\text{Fe}_2\text{O}_4$ ferrites.

Hence this discrepancy in the Neel's theory was resolved by Yafet and Kittel and they formulated non-collinear model of ferrimagnetism. This the increase in Y-K angles for the samples with Zn content ($x > 0.5$) is attributed to the increased favor of triangular spin arrangements on B-sites leading to the reduction in the A-B exchange interaction and subsequent decrease in average magnetization [5.38].

5.2.5 DC Electrical Resistivity

DC resistivity (ρ_{dc}) versus $\text{Co}_{1-x}\text{Zn}_x\text{Fe}_2\text{O}_4$ ferrites measured at room temperature is presented as a function of Zn content in Fig. 5.12 and corresponding values are listed in Table-5.2. It was found that resistivity increases markedly with the addition of Zn^{2+} up to $x = 0.7$ and thereafter decreases.

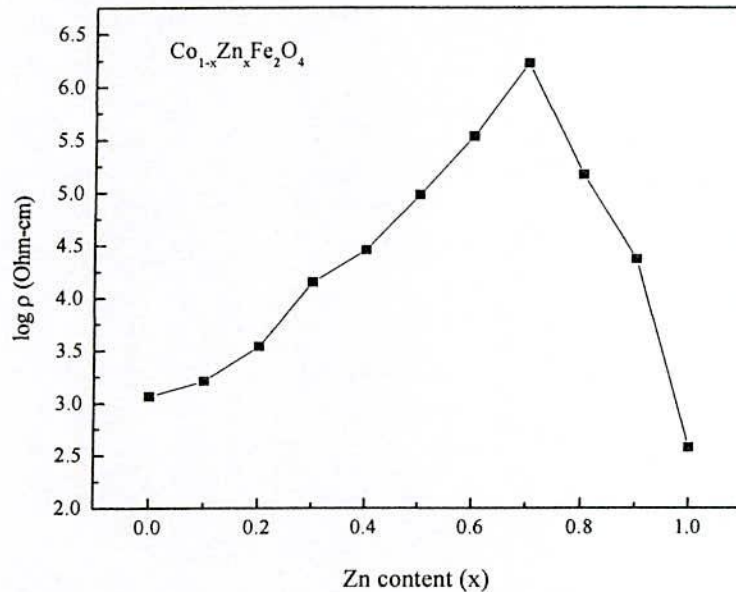


Fig. 5.12 Room temperature DC resistivity as a function of Zn content (x) $\text{Co}_{1-x}\text{Zn}_x\text{Fe}_2\text{O}_4$ ferrites.

The conduction mechanism in ferrite is considered as the electron hopping between Fe^{2+} and Fe^{3+} ions in B-sites [5.39]. DC resistivity is an important parameter of ferrites in high frequency applications. Fe^{2+} ion concentration is a characteristic property of a ferrite material and depends upon several factors such as sintering temperature/time and atmosphere including the grain structure. It is well known that resistivity of ferrites depends on their chemical composition [5.11] and heat treatment. Fe^{2+} ions in the lattice are created due to zinc loss during the sintering process.

5.4 Summary

The XRD pattern confirmed the single-phase cubic spinel structure of the samples. The lattice parameter increases linearly with increasing Zn content. Bulk density is found to increase while porosity decreases with increasing Zn content. Curie temperatures show a decreasing trend with the successive addition of Zn^{2+} ions. With increasing Zn content, the initial permeability increases with Zn content upto $x = 0.5$. But the permeability decreases with increasing sintering temperature. From the low field B-H loop the coercivity decreases with increasing Zn content it reveals the softer ferromagnetic nature of the studied sample. Saturation magnetization and magnetic moment is found to increase with Zn content up to $x \leq 0.5$, and thereafter it decreases. DC resistivity increases substantially with Zn content upto $x = 0.7$.

CHAPTER-VI
RESULTS AND DISCUSSION OF
DILUTE FERRITES

Results and Discussion of Dilute Ferrites

6.0 Introduction

Magnetic moment of spinel ferrites has successfully been explained in terms of Neel's two sublattice collinear model of ferrimagnetism [6.1]. Soon after that it was observed that substitution of more than few tenths of non-magnetic substituent atoms per formula unit showed significant departures from the Neel's collinear model [6.2, 6.3]. It has been observed that magnetic moment in spinel ferrites $A_{1-x}M_xB_2O_4$, where A is divalent metal ions, M is the non-magnetic metal ions and B is trivalent Fe^{3+} ions increases gradually with the increase of non-magnetic ion, M in the A-sublattice until $x = 0.4 - 0.5$ depending on type of ferrites, beyond which a decrease of magnetic moment has been reported [6.4]. When A-sublattice dilution of magnetic moment occurs with non-magnetic substitution greater than 0.5, intrasublattice interaction, J_{BB} become comparable and/or more predominant than inter-sublattice interaction, J_{AB} . In such a situation disorder and frustration takes place in the spin subsystem leading to the manifestation of various magnetic structures: ferrimagnetic order, local spin canting (LSC), antiferrimagnetic order, re-entrant spin-glass and spin-glass etc [6.5].

Yafet and Kittel [6.6] were the first to give proper interpretation that non-magnetic substitutions in one sublattice could lead to a non-collinear or canted spin arrangement on the other sublattice. They developed a split-sublattice molecular field model to calculate a uniform canting angle α_{Y-K} . They argued on a uniform canting approach in which one sublattice is divided into two halves, each oppositely canted at some uniform angle relative to the average magnetization. A localized canting model it is assumed that the individual moments on one sublattice are canted at different angles, depending on the specifics of the local magnetic environment [6.7, 6.8]. A re-entrant spin-glass is a highly frustrated and disordered magnetic system in which there is a competition between spin-glass order and long range ferromagnetic order.

In other words a system where there exists a majority of ferromagnetic couplings between the individual spins but a sufficiently large number of antiferromagnetic couplings to create substantial frustration leading to a competition between spin-glass order and long range ferromagnetic order when the temperature is lowered. In such a material it exhibits a transition from a paramagnetic (PM) to a ferromagnetic (FM) state and on further lowering the temperature typical spin-glass like behavior generally known as re-entrant spin-glass (RSG) appears [6.9, 6.10]. Highly diluted ferrites with high degree of randomness and frustration

belong to a class of disordered magnetic system known as spin-glass. An important class of random systems is the bond disordered system in which the magnetic interactions are taken randomly from a distribution of both positive (ferromagnetic) and negative (antiferromagnetic) interactions. If all the interactions are ferromagnetic (FM) the low temperature ordered phase is the ferromagnetic phase. If a few interactions, taken at random, are changed to be antiferromagnetic (AF), the low temperature phase will have long range ferromagnetic order but some magnetic moments will be frustrated. On increasing the concentration of random AF interactions, frustration increases and above some concentration, long range ferromagnetic order is no longer favorable. In such a bond disordered system the low temperature phase is the spin-glass phase [6.9, 6.10].

Spin-glass (SG) states have been found in a wide variety of systems including the magnetic insulators or amorphous alloys with the following common features (1) frozen in magnetic moments below some freezing temperature T_f , (2) lack of periodic long range magnetic order and (3) remanence and magnetic relaxation over macroscopic time scales below T_f when there are changes of magnetic field. From the macroscopic point of view, these properties have been characterized by the temperature dependence of dc magnetization, ac susceptibility in the field-cooled (FC) and zero-field-cooled (ZFC) conditions, hysteresis effects and magnetic relaxation experiments. However, it is important that the macroscopic properties of many systems (e.g. canted, RSG systems) undergoing multiple magnetic phase transitions may show common features, although the microscopic natures and underlying physics could be quite different. To differentiate between these systems, a careful low field dc magnetization in FC and ZFC condition as well as ac susceptibility study with frequency and field dependence in the FC and ZFC condition is necessary. In the spinel ferrite in the magnetically diluted condition, a modified version of SG system generally called "cluster glass" (CG) is also manifested. A cluster glass can be considered to be a set of clusters which are formed due to short range ordering around the Curie temperature, T_c . The cluster glass system is expected to show spin glass like behavior with increased magnetic spin density at low temperature due to freezing of the magnetic spin.

6.1 Field cooled (M_{FC}) and Zero field cooled (M_{ZFC}) Magnetization

Fig. 6.1 (a) and (b) shows the temperature dependence of low field FC and ZFC dc magnetization with $H = 50$ Oe for the sample $Co_{1-x}Cd_xFe_2O_4$ and $Co_{1-x}Zn_xFe_2O_4$ at $x = 0.7$ system. It is observed from these curves that magnetization rises sharply on lowering the temperature from paramagnetic state to a high value indicating a PM-FM phase transition and display a plateau until sufficiently low temperature followed by a rapid fall at much lower temperature designated as T_f where the divergence between M_{ZFC} and M_{FC} is observed. This low temperature drop of magnetization at T_f corresponds to spin freezing temperature and referred to as re-entrant spin-glass (RSG) behavior. Therefore RSG follows transitions in the sequence of phases, PM-FM- RSG when temperature is lowered. Para-ferromagnetic transition temperatures, T_c determined from dM/dT of the $M(T)$ data have been found to be 262K for $Co_{0.3}Cd_{0.7}Fe_2O_4$ and 242K for the $Co_{0.3}Zn_{0.7}Fe_2O_4$ respectively with corresponding spin freezing temperature $T_f = 46K$ and $48K$.

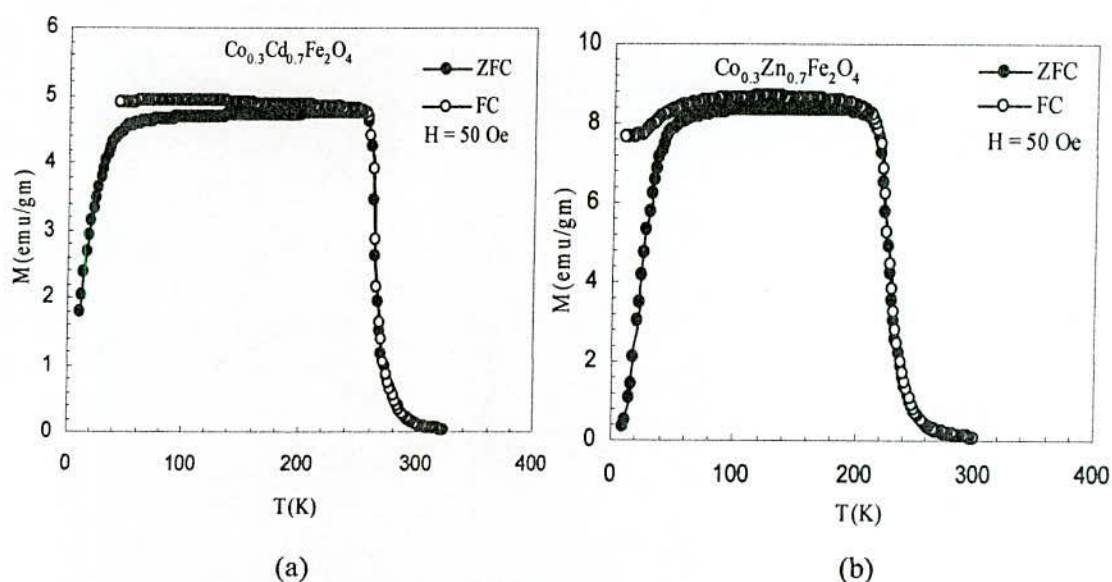


Fig. 6.1 M_{ZFC} and M_{FC} curves of the sample (a) $Co_{0.3}Cd_{0.7}Fe_2O_4$ (b) $Co_{0.3}Zn_{0.7}Fe_2O_4$ with field $H = 50$ Oe

The temperature dependence of zero-field cooled DC magnetization $M_{ZFC}(T)$ and M_{FC} of sample $Co_{0.2}Cd_{0.8}Fe_2O_4$ with various applied field ($H = 50 - 200$ Oe) is shown in Fig. 6.2(a). Fig. 6.2(b) for clarity with $M_{ZFC}(T)$ with $H = 50$ Oe the derivative dM/dT as a function of temperature to determine the possible phase transition temperature. It is observed from the Fig.6.2 (a) that magnetization increases with decreasing temperature attaining a maximum value and decreases thereafter sharply to a value with further decrease of temperature

indicating the randomly freezing of magnetic spins below the spin freezing temperature, T_f . It is also observed from $M_{ZFC}(T)$ curves that the temperature corresponding to maximum magnetization M_{max} does not show any significant shift with increasing applied magnetic field. From this temperature dependence it is difficult to determine any para-ferromagnet magnetic phase transition.

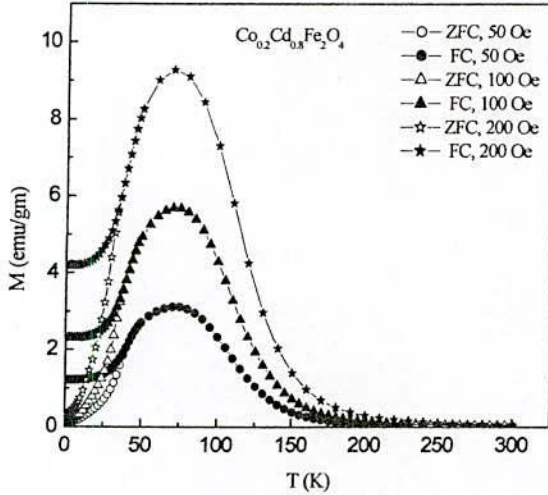


Fig. 6.2 (a) M_{ZFC} and M_{FC} Curves of the sample $Co_{0.2}Cd_{0.8}Fe_2O_4$ with applied field $H = 50 - 200$ Oe.

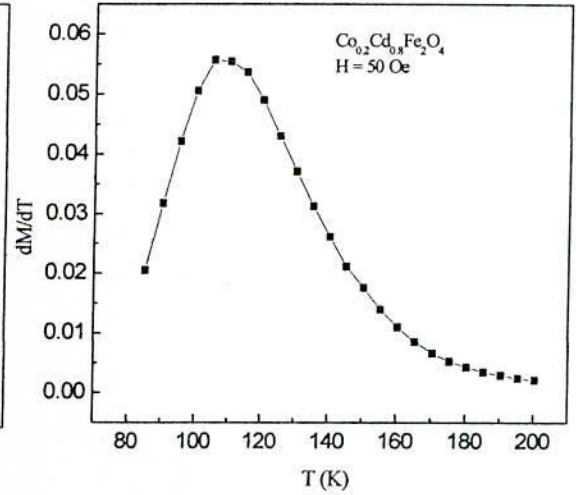


Fig. 6.2 (b) Derivative of dM/dT as a function of temperature of the sample $Co_{0.2}Cd_{0.8}Fe_2O_4$ with applied field $H = 50$ Oe.

From the dM/dT it appears that $T = 100$ K may be the T_c of this composition show Fig. 6.2(b) i.e the sample is ferrimagnetic below T_c which has also been verified with the appearance of spontaneous magnetization from the Arrott plots drawn from the high field $M(H)$ data at $T = 5 - 100$ K as shown in Fig. 6.2(c). It is observed that linear extrapolation of Arrott plot (M^2 vs H/M) at $T = 100$ K almost passes through the origin signifying that the sample has a Curie temperature close to this temperature as confirmed by dM/dT of the sample. The decrease of magnetization above freezing temperature is very sluggish and smeared which indicates that the clustering effect is very prominent until high temperature as high as $T = 150$ K. The temperature dependence of the inverse mass susceptibility of the sample is shown in Fig. 6.2(d) which can be fitted to a Curie-Weiss law, $\chi = \frac{C}{T - \theta_p}$ in the temperature range 250 - 300 K with paramagnetic Curie temperature $\theta_p = 200$ K compared with ferromagnetic $T_c = 100$ K. Large difference between T_c and θ_p implies the existence of large amount of short-range ordering above T_c . It seems that strong short range ferrimagnetic ordering and frustration coexists within the antiferromagnetic spinel matrix.

This gives rise to distribution of ferromagnetic phase transition temperatures that makes difficult for precise determination of T_c for this diluted alloy.

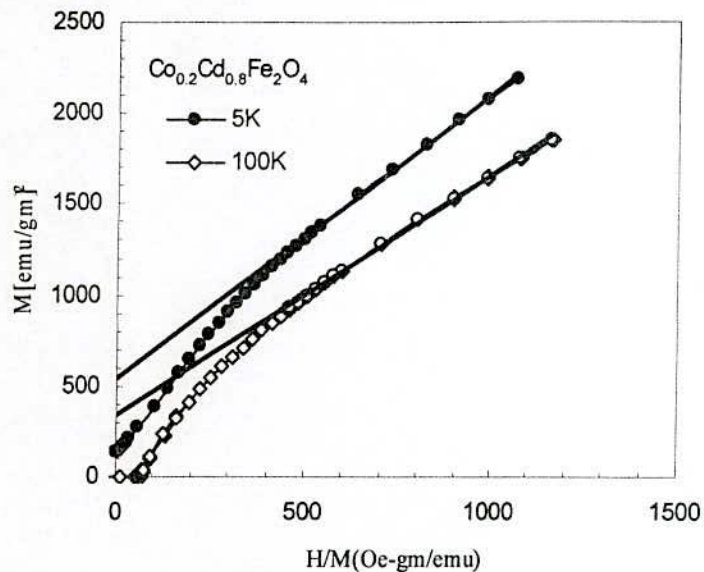


Fig. 6.2(c) ABK from $T = 5 - 100\text{K}$ with field $H = 50 \text{ kOe}$ of $\text{Co}_{0.2}\text{Cd}_{0.8}\text{Fe}_2\text{O}_4$ ferrites.

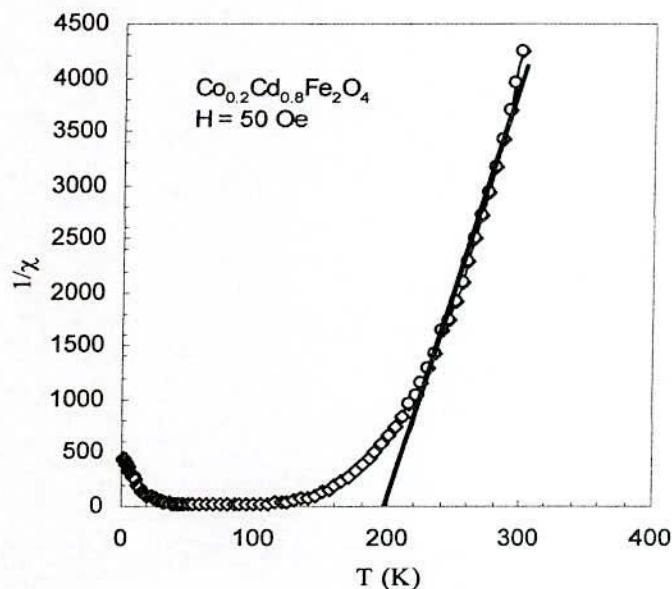


Fig. 6.2(d) Inverse of susceptibility vs temperature curve of the sample $\text{Co}_{0.2}\text{Cd}_{0.8}\text{Fe}_2\text{O}_4$ with applied field $H = 50 \text{ Oe}$.

Temperature dependence of $M(T)$ for the sample $\text{Co}_{0.2}\text{Zn}_{0.8}\text{Fe}_2\text{O}_4$ in the M_{ZFC} measured with $H = 50$ Oe is displayed in Fig. 6.3 (a). From this measurement a cusp corresponding to spin freezing is observed at $T_f = 41.35\text{K}$ and no well defined magnetic phase transition temperature is noticed until high temperature. The $M(T)$ curve looks sluggish having peculiar temperature dependence from above T_f to until 150 K. In order to find any magnetic phase transition temperature, Arrott plots were drawn from $M(H)$ curve measured at 5K and 100K is shown in Fig. 6.3 (b). From the Arrott plots it has been found that spontaneous magnetization almost close to zero at $\frac{H}{M} \rightarrow 0$ at $T = 100\text{K}$ signifying that this sample has a T_c close to $T = 100\text{K}$. But $M(T)$ curve does not clearly show any sign of ferromagnetic order above 41K. This means that strong competitive exchange interaction between ferromagnetic and antiferromagnetic ordering occurs in this sample.

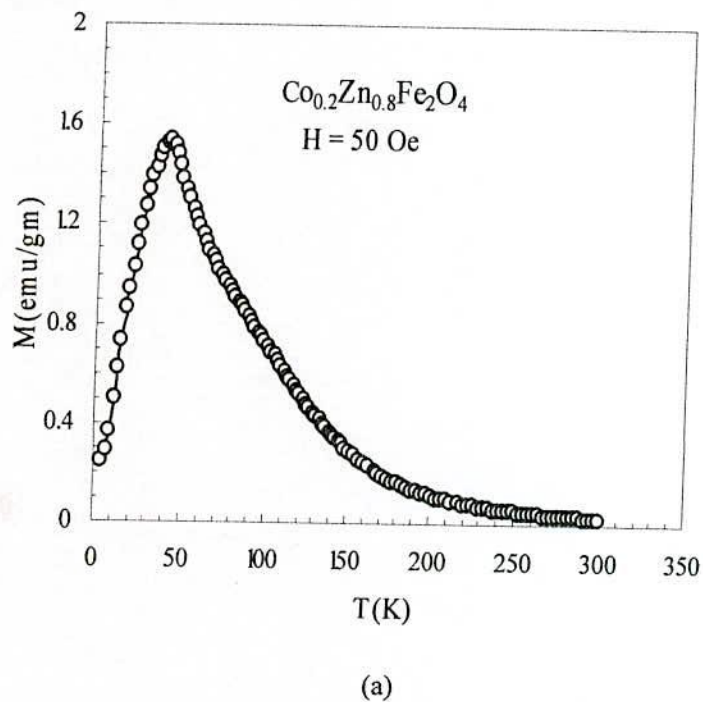
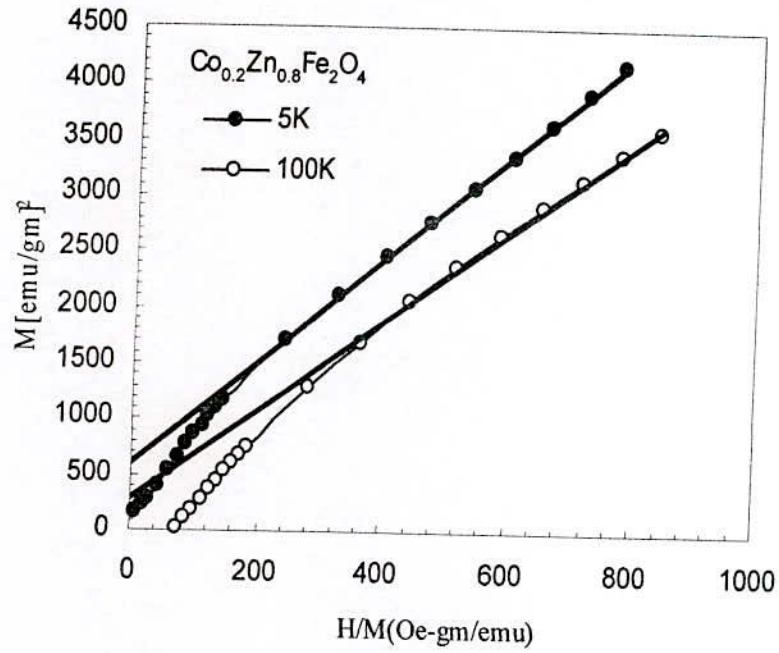


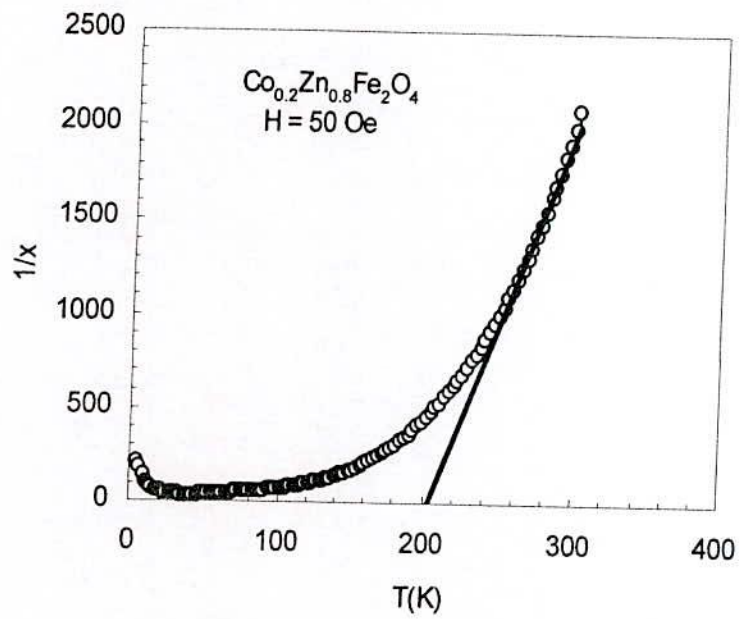
Fig. 6.3 (a) M_{ZFC} Curves of the sample $\text{Co}_{0.2}\text{Zn}_{0.8}\text{Fe}_2\text{O}_4$ with applied field $H = 50$ Oe.

Temperature dependence of inverse of mass susceptibility has been measured from 5K-300K with an applied field $H = 50$ Oe and displayed in Fig. 6.3 (c). The inverse susceptibility is well described by Curie-Weiss law above 240 K with a paramagnetic Curie temperature $\theta_p = 200\text{K}$ in good coincidence with similar composition $\text{Co}_{0.2}\text{Cd}_{0.8}\text{Fe}_2\text{O}_4$ and the large difference between T_c and θ_p clearly indicates a strong short range ordering.



(b)

Fig. 6.3 (b) ABK plot from $T = 5 - 100\text{K}$ with field $H = 50\text{ kOe}$ of $\text{Co}_{0.2}\text{Zn}_{0.8}\text{Fe}_2\text{O}_4$ ferrites.



(c)

Fig. 6.3 (c) Inverse of susceptibility vs temperature curve of the sample $\text{Co}_{0.2}\text{Zn}_{0.8}\text{Fe}_2\text{O}_4$ with applied field $H = 50\text{ Oe}$.

Spin-glass like behavior with the manifestation of a sharp cusp at low temperature from the temperature dependence of low field dc magnetization with $H = 50$ Oe is shown in Fig. 6.4 (a, b) and Fig. 6.5 (a, b) for $\text{Co}_{1-x}\text{Cd}_x\text{Fe}_2\text{O}_4$ and $\text{Co}_{1-x}\text{Zn}_x\text{Fe}_2\text{O}_4$ sample with $x = 0.9$ and $x = 1.0$ respectively.

Low field dc $M_{\text{FC}}(T)$ and $M_{\text{ZFC}}(T)$ magnetization are frequently used to elucidate spin glass or spin glass like behavior of diluted magnetic system. The nature of $M(T)$ curve does not resemble with any ferromagnetic material. It is observed that magnetization, M_{FC} and M_{ZFC} both increase with as the temperature is lowered with the manifestation of divergence after passing through a maximum. A sharp well defined cusp in the $M_{\text{ZFC}}(T)$ at $T = 29.74\text{K}$ and 20.47K for $\text{Co}_{1-x}\text{Cd}_x\text{Fe}_2\text{O}_4$ with $x = 0.9$ and 1.0 and $T = 22.29\text{K}$ and 14.50K for $\text{Co}_{1-x}\text{Zn}_x\text{Fe}_2\text{O}_4$ with $x = 0.9$ and 1.0 is observed. The temperature corresponding to this cusp is considered as spin freezing temperature, T_f below which magnetization in the ZFC condition drastically reduced to a very low value. There is a divergence between the FC and ZFC magnetization from much higher temperature of $150 - 200\text{K}$ for $\text{Co}_{1-x}\text{Zn}_x\text{Fe}_2\text{O}_4$ samples while no such divergence is noticed for the $\text{Co}_{1-x}\text{Cd}_x\text{Fe}_2\text{O}_4$ samples. This divergence is assumed to be due to ferromagnetic clusters embedded in a paramagnetic matrix. The spin freezing temperature, T_f is lower for Co-Zn samples. The divergence between the ZFC and FC magnetization at sufficiently low temperature has been observed in other spin-glass like materials [6.11]. The spin freezing temperature, T_f is lower for Co-Zn samples. The divergence between the ZFC and FC magnetization at sufficiently low temperature has been observed in other spin-glass like materials [6.11 - 6.13].

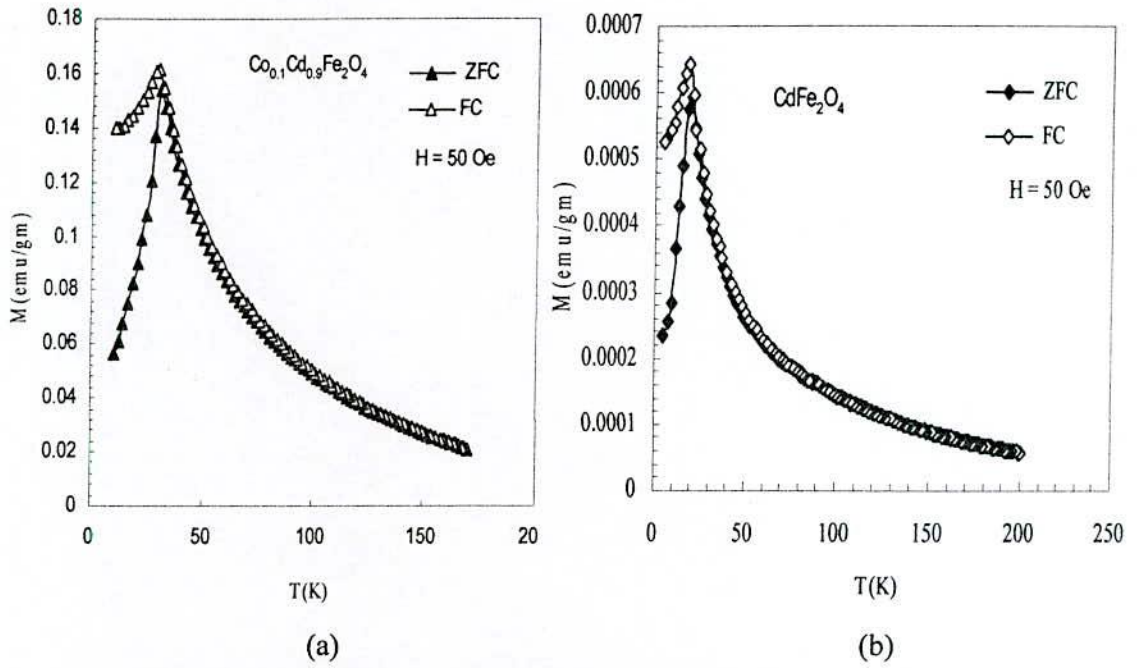


Fig. 6.4 M_{ZFC} and M_{FC} curves of the sample (a) $Co_{0.1}Cd_{0.9}Fe_2O_4$ (b) $CdFe_2O_4$ with applied field $H = 50$ Oe.

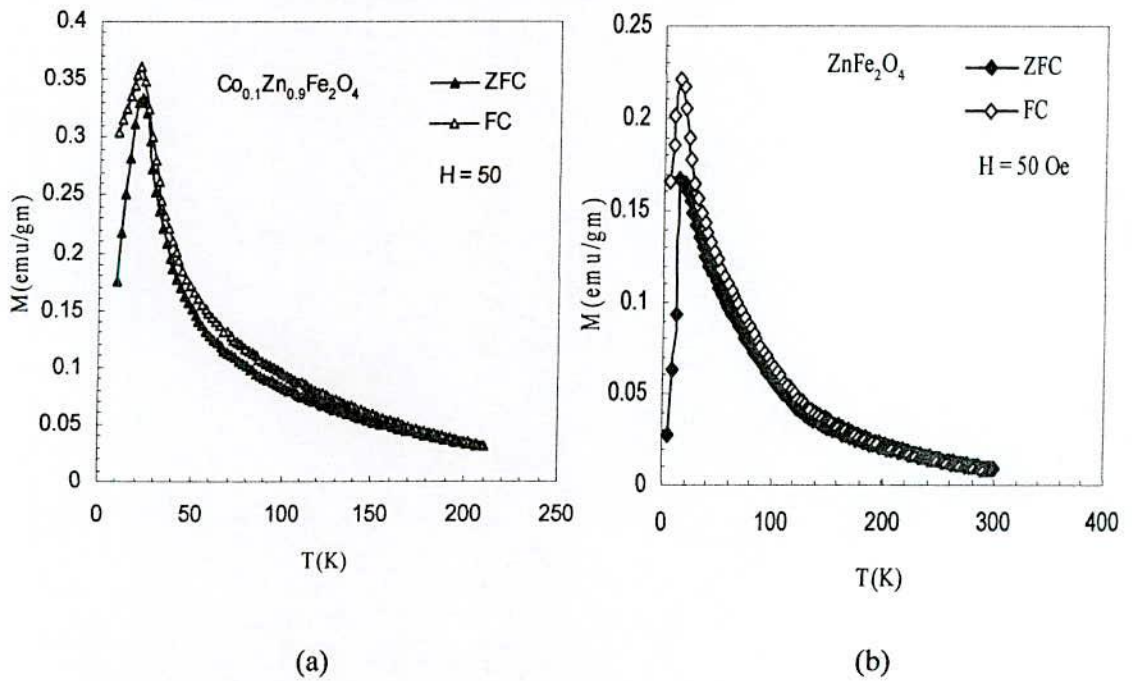


Fig. 6.5 M_{ZFC} and M_{FC} curves of the sample (a) $Co_{0.1}Zn_{0.9}Fe_2O_4$ (b) $ZnFe_2O_4$ with applied field $H = 50$ Oe

The samples with $x = 0.9$ and 1.0 does not show any spontaneous magnetization at $T = 5\text{K}$ from Arrot plots as shown in Fig. 6.6 (a, b) and Fig. 6.7 (a, b).

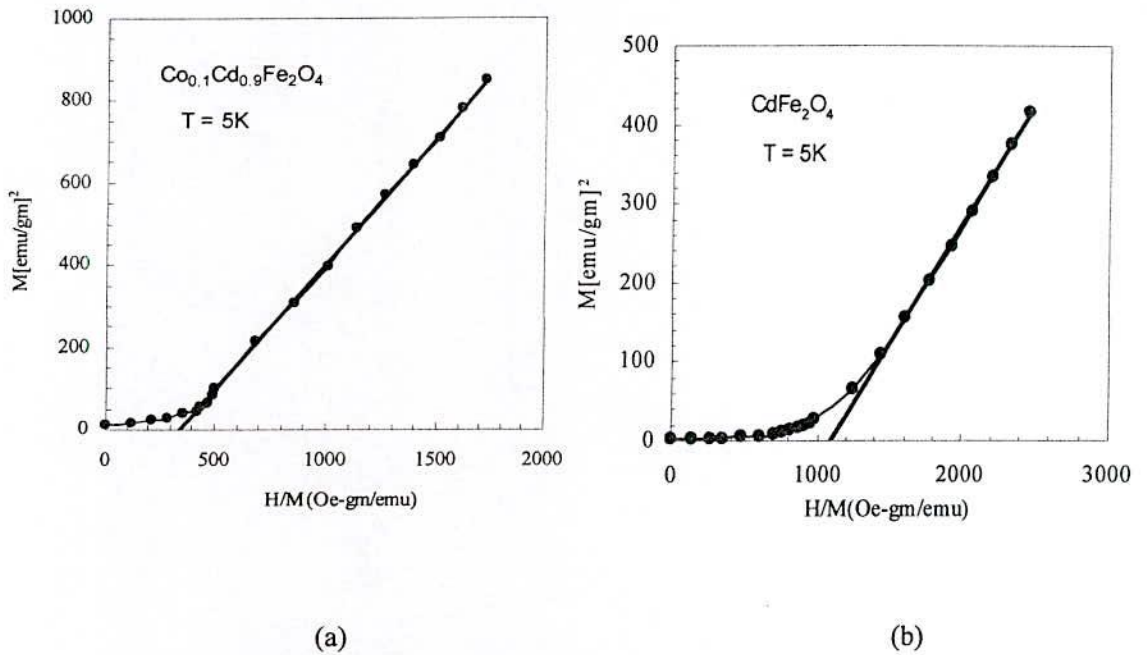


Fig. 6.6. ABK plot from $T = 5\text{K}$ with field $H = 50\text{ kOe}$ of (a) $\text{Co}_{0.1}\text{Cd}_{0.9}\text{Fe}_2\text{O}_4$ (b) CdFe_2O_4 ferrites.

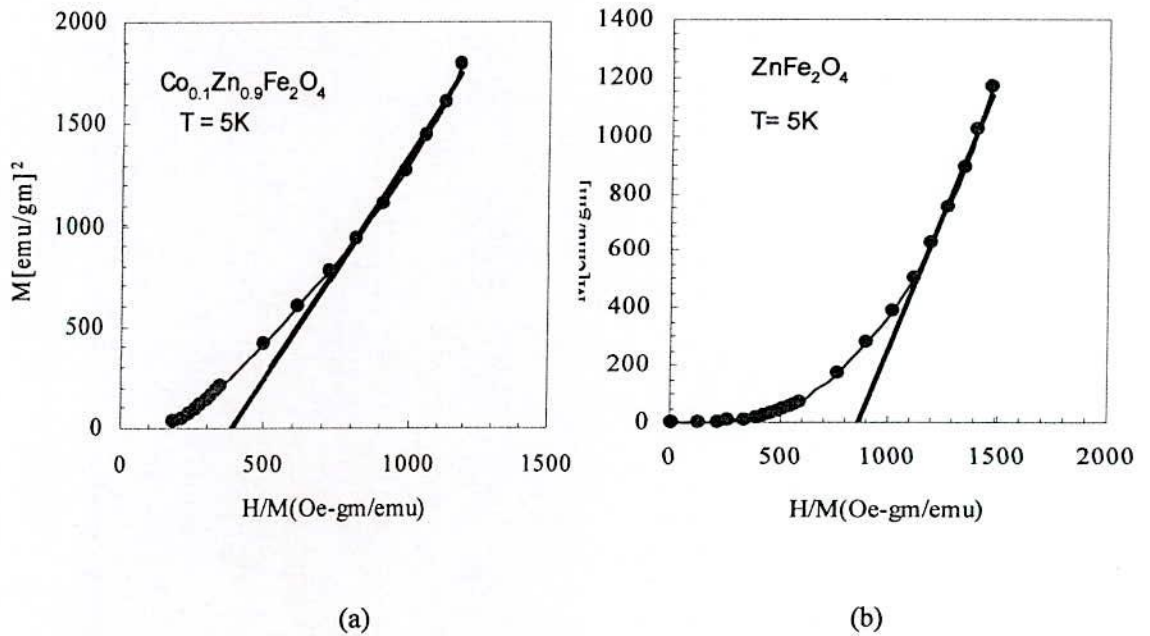


Fig. 6.7 ABK plot from $T = 5\text{K}$ with field $H = 50\text{ kOe}$ of (a) $\text{Co}_{0.1}\text{Zn}_{0.9}\text{Fe}_2\text{O}_4$ (b) ZnFe_2O_4 ferrites.

Pure CdFe_2O_4 and ZnFe_2O_4 ferrites are long been considered as typical antiferromagnet with normal spinel with Neel temperature of $T_N = 10\text{K}$ and $T_N = 9\text{K}$ respectively [6.14, 6.15]. It has been claimed that zinc ferrite with ideal normal spinel structure is a three dimensional spin frustrated magnet.

Dilute alloys with $x \geq 0.7$ display RSG and SG behavior as shown in Fig. 6.8 of magnetic phase diagram of $\text{Co}_{1-x}\text{Cd}_x\text{Fe}_2\text{O}_4$ ferrite system.

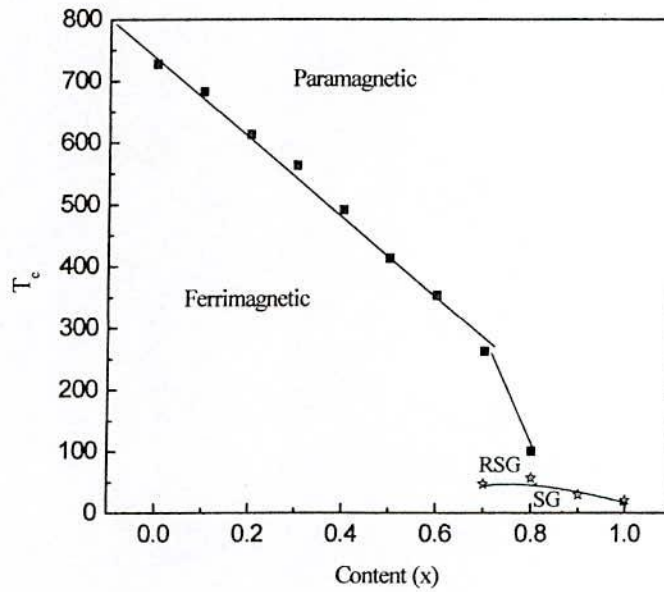


Fig. 6.8 Magnetic phase diagram.

6.2 High field Hysteresis behavior

Fig. 6.9 (a, b) shows the hysteresis behavior at $T = 5$ and 100K of the sample $x = 0.7$ for both the system where a substantial hysteresis with $H_c = 502$ Oe at $T = 5\text{K}$ for both the samples has been observed (see inset Fig. (6.9. a, b)) with no noticeable hysteresis detected at $T = 100\text{K}$ for both the samples. It is seen from the $M(H)$ curves that the magnetization is not saturated even with an applied magnetic field of $H = 50$ kOe indicating a strong spin canting effect due to strong J_{BB} interaction having $\alpha_{\text{Y-K}}$ angle of $\approx 70^\circ$ for both the samples. This is to note that the magnetization value at $H = 50$ kOe is larger for Zn ($x = 0.7$) substituted sample at $T = 5$ and 100K with 90.5 emu/gm at $T = 5\text{K}$ compared with Cd ($x = 0.7$) substituted samples having 74.6 emu/gm at $T = 5\text{K}$.

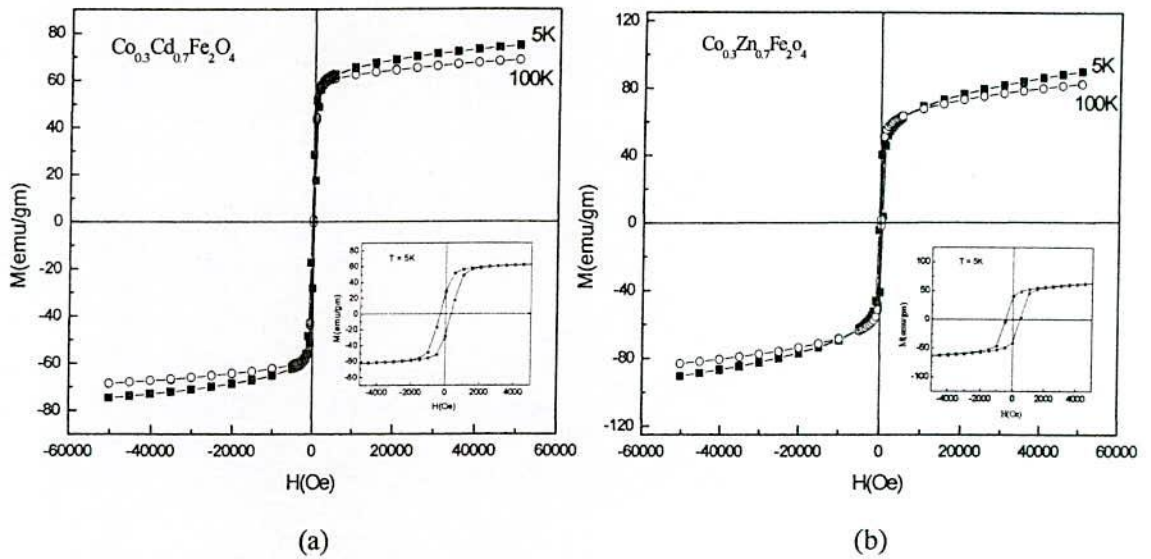


Fig. 6.9 Magnetization hysteresis loops at $T = 5\text{K}$ and 100K with field $H = 50\text{ kOe}$ of the sample (a) $\text{Co}_{0.3}\text{Cd}_{0.7}\text{Fe}_2\text{O}_4$ (b) $\text{Co}_{0.3}\text{Zn}_{0.7}\text{Fe}_2\text{O}_4$. Inset at $T = 5\text{K}$.

A large hysteresis with a coercivity of $H_c = 1966\text{ Oe}$ for Co-Cd ($x = 0.8$) against $H_c = 620\text{ Oe}$ for Co-Zn ($x = 0.8$) is observed at $T = 5\text{K}$ with no hysteresis at $T = 100\text{K}$. $M(H)$ curves of the sample $x = 0.8$ for both the system show that magnetization increases continuously with H with no sign of saturation indicating high anisotropy of the sample with higher Yaffet-Kittel (α_{Y-K}) angle of $\approx 80^\circ$. Fig. 6.10 (a, b) shows the hysteresis loop measured at different temperatures $T = 5 - 300\text{K}$ with $H = \pm 50\text{ kOe}$. It is observed that the nature of $M-H$ curves up to $T = 100\text{K}$ is looks like ferromagnetic, while $M-H$ at $T = 300\text{K}$ looks typically paramagnetic. Inset of Fig. 6.10 (a, b), an extended view of hysteresis loops at $T = 5\text{ K}$ for both the samples are depicted where hysteresis effect is clearly noticed with the appearance of large hysteresis as mentioned above having higher value of H_c for Cd system than that of Zn. Hysteresis loops measured at $T = 5\text{K}$ and 50K are displayed in Fig. 6.11 (a, b) for Co-Cd and Fig. 6.12 (a, b) for Co-Zn at $x = 0.9$ and $x = 1.0$. Large hysteresis with $H_c = 2509\text{ Oe}$ for $x = 0.9$, $H_c = 1300\text{ Oe}$ for $x = 1.0$ for $\text{Co}_{1-x}\text{Cd}_x\text{Fe}_2\text{O}_4$ system is observed while that of for $x = 0.9$ and $x = 1.0$ are $H_c = 501\text{ Oe}$ and $H_c = 590\text{ Oe}$ for $\text{Co}_{1-x}\text{Zn}_x\text{Fe}_2\text{O}_4$ system respectively.

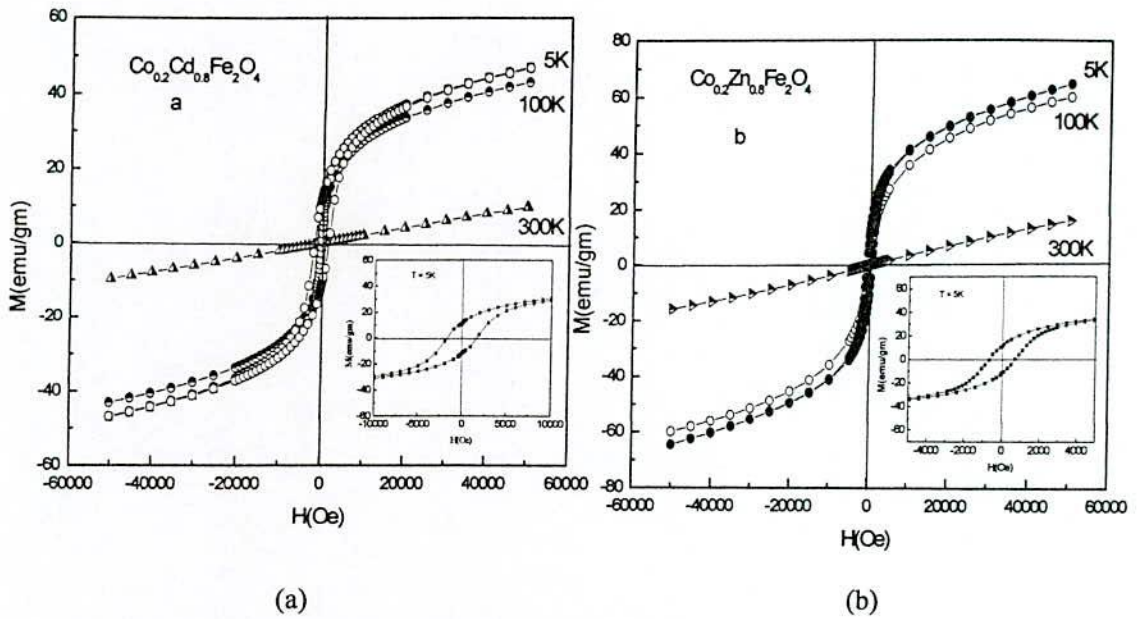


Fig. 6.10 Magnetization hysteresis loops at different temperatures between $T = 5\text{K} - 300\text{K}$ with field 50 kOe of the sample (a) $\text{Co}_{0.2}\text{Cd}_{0.8}\text{Fe}_2\text{O}_4$ (b) $\text{Co}_{0.2}\text{Zn}_{0.8}\text{Fe}_2\text{O}_4$. Inset at $T = 5\text{K}$.

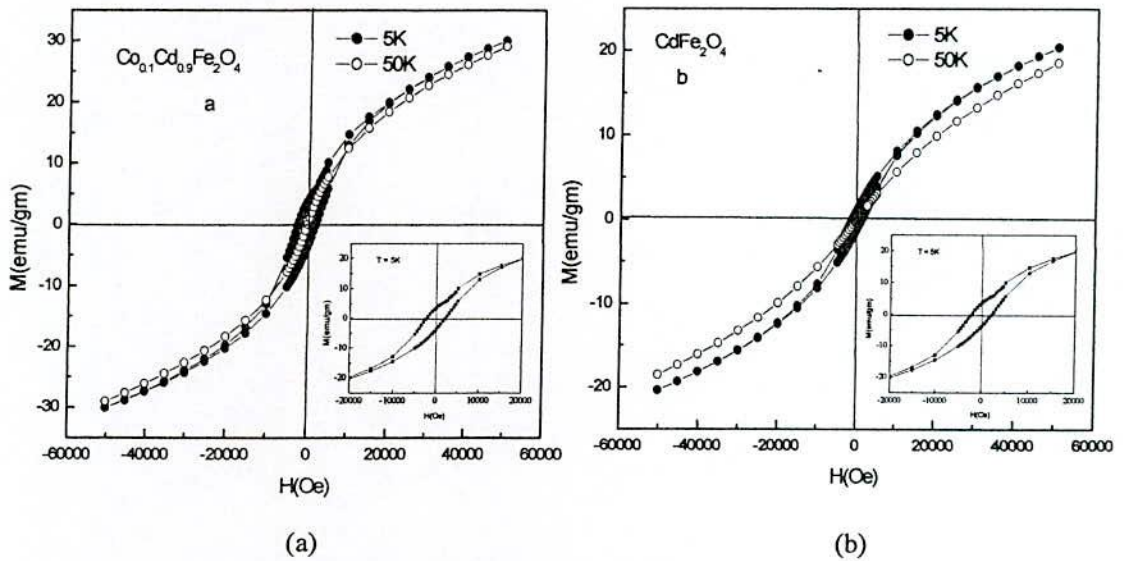


Fig. 6.11. Magnetization hysteresis loops at different temperatures between $T = 5\text{K}$ and 50K with field 50kOe of the sample (a) $\text{Co}_{0.1}\text{Cd}_{0.9}\text{Fe}_2\text{O}_4$ (b) CdFe_2O_4 . Inset at $T = 5\text{K}$.

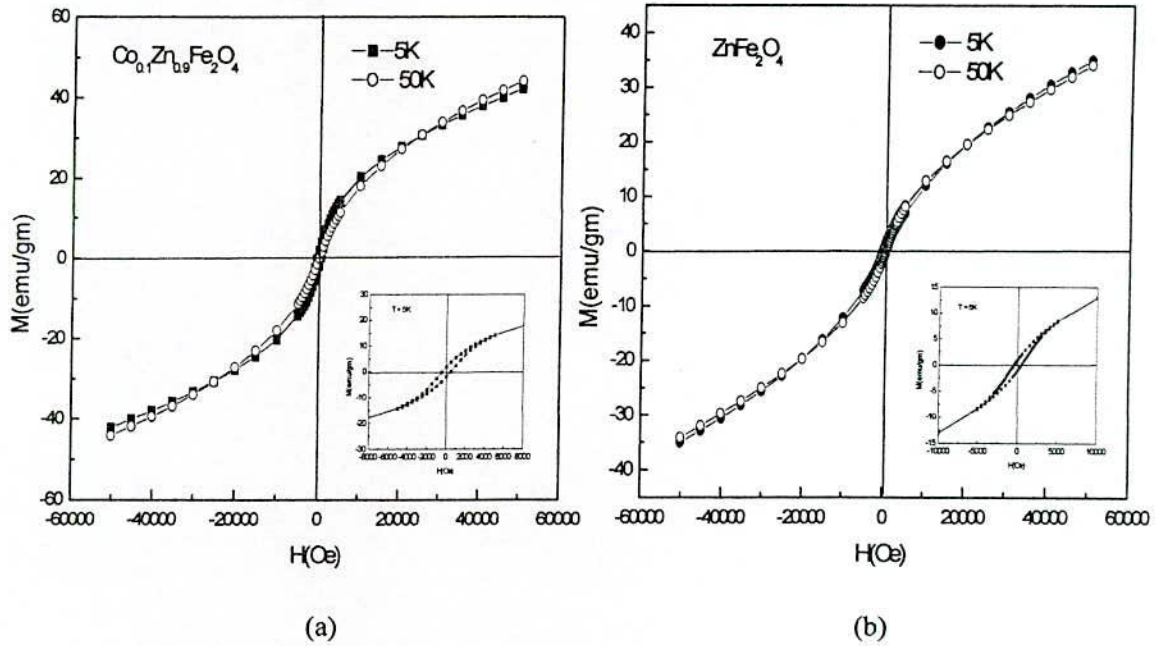


Fig. 6.12 Magnetization hysteresis loops at different temperatures between $T = 5\text{ K} - 50\text{ K}$ with field 50 kOe of the sample (a) $\text{Co}_{0.1}\text{Zn}_{0.9}\text{Fe}_2\text{O}_4$ (b) ZnFe_2O_4 (Inset: $T = 5\text{ K}$).

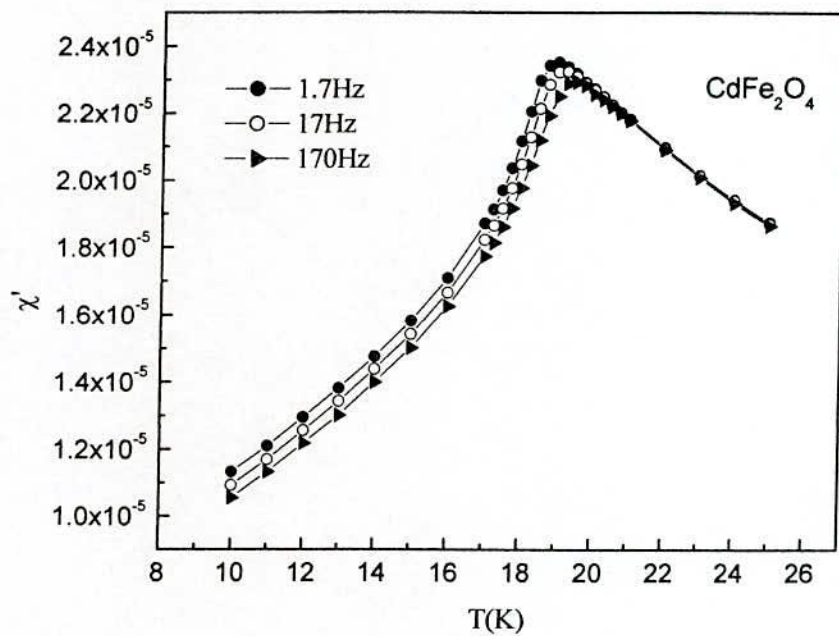
Table-6.1 Data of the spin freezing temperature (T_f), coercive force (H_c) at $T = 5\text{ K}$ of $\text{Co}_{1-x}\text{Cd}_x\text{Fe}_2\text{O}_4$ and $\text{Co}_{1-x}\text{Zn}_x\text{Fe}_2\text{O}_4$ ferrites (with $x = 0.7 - 1.0$)

Content (x)	$\text{Co}_{1-x}\text{Cd}_x\text{Fe}_2\text{O}_4$		$\text{Co}_{1-x}\text{Zn}_x\text{Fe}_2\text{O}_4$	
	T_f (K)	H_c (Oe) ($T = 5\text{ K}$)	T_f (K)	H_c (Oe) ($T = 5\text{ K}$)
0.7	47	502	48	502
0.8	57	1966	41.35	620
0.9	29.74	2509	22.29	501
1.0	20.47	1300	14.50	590

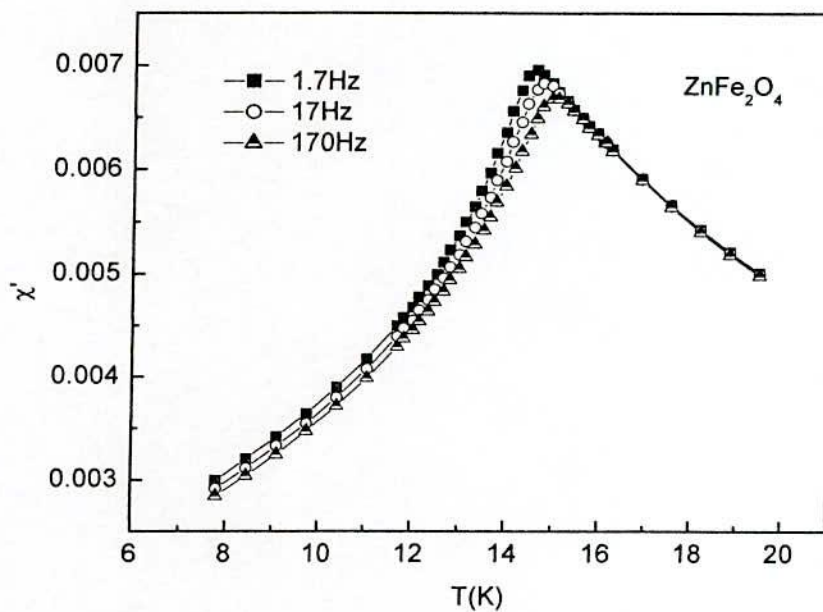
6.3 Temperature and Frequency Dependence of Complex AC Susceptibility

AC susceptibility measurements are useful to understand the dynamics of freezing of the spin-glass systems in which the temperature associated with the maxima of χ' , corresponding to spin freezing temperature which varies slowly with the measuring frequency [6.16]. Fig. 6.13(a, b) illustrates the temperature dependence of the in-phase component of the AC susceptibility (χ') at three different frequencies. Spin-glass behavior is usually characterized by the ac susceptibility, and the spin freezing temperature T_f , dependent on frequency f , can be accurately determined by the position of the cusp of the real part of AC susceptibility, χ' . In other words, the maximum relaxation time of the system τ is equal to $1/f$ at T_f . It is observed in Fig. 6.13(a, b) that the peak of AC susceptibility shifts to lower temperatures with decreasing measuring frequency. Below the freezing temperature T_f , the amplitude of χ' highly depends on the measuring frequency $\frac{\omega}{2\pi}$, while it becomes almost frequency independent at temperature above T_f . This behavior is typical of a conventional spin glass. Such a frequency shift is not expected for the usual antiferromagnetic or ferromagnetic long-range-ordered system [6.17]. This result implies that a transition takes place from paramagnetic phase to spin glass phase (PM-SG) in the present CdFe_2O_4 and ZnFe_2O_4 ferrites.

Fig. 6.14(a, b) shows the out of phase component of the AC susceptibility (χ'') at three different frequencies for CdFe_2O_4 and ZnFe_2O_4 ferrites. $\chi''(T)$ is non-zero below T_f and sharply falls toward zero just above T_f , passing through a sharp maximum which is frequency dependent as in the case of χ' . A freezing temperature $T_f(\omega)$ corresponding to the cusp in the in-phase or the inflexion point in the out-of-phase component of the AC susceptibility may be ascribed to each frequency. The spin-glass characteristic is in fact the sharp and frequency dependent onset of a finite out of phase component at a temperature corresponding to T_f (in fact, the inflexion point of the sharp up rise closely coincides with the maximum in χ').

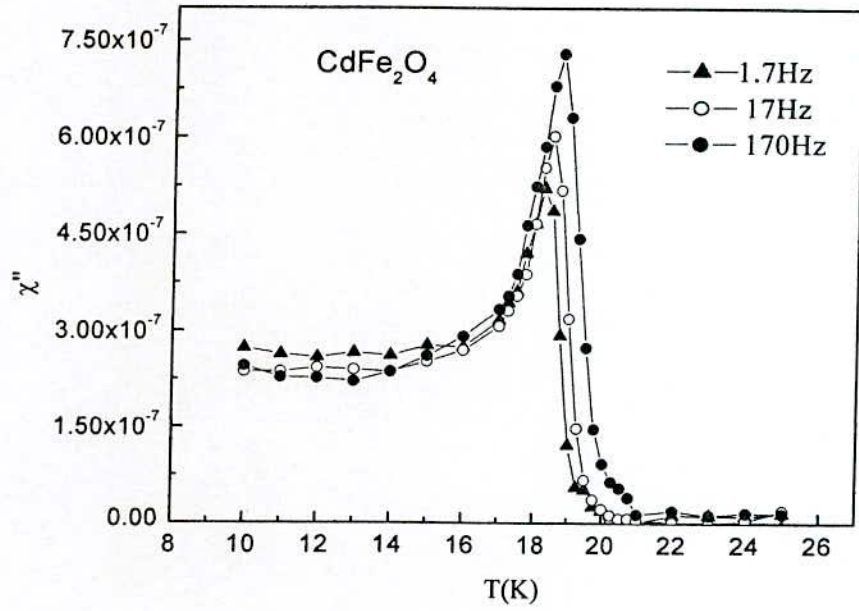


(a)

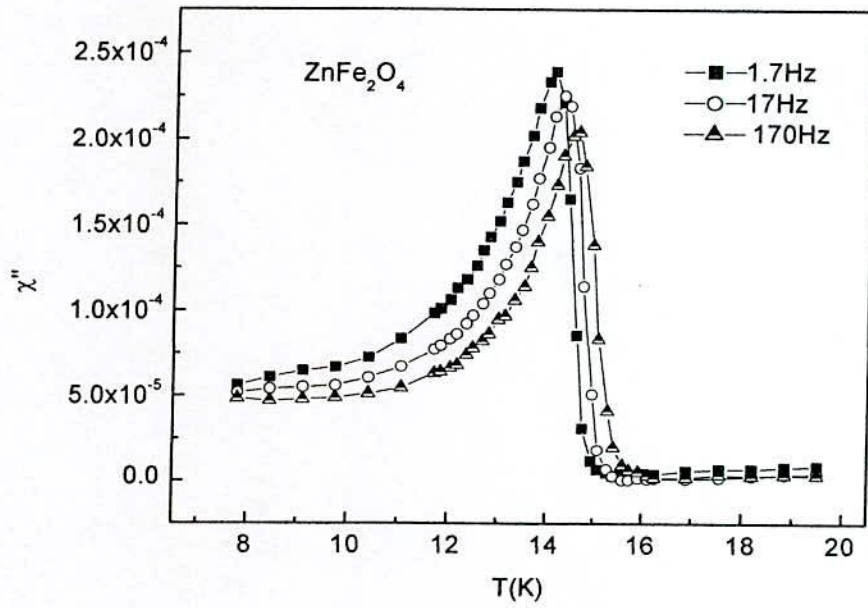


(b)

Fig. 6.13 The temperature dependence of the real part of AC susceptibility, χ' measured at $\omega/2\pi = 1.7, 17$ and 170 Hz, respectively for (a) CdFe_2O_4 and (b) ZnFe_2O_4 ferrites.



(a)



(b)

Fig. 6.14 Variation of imaginary part of AC susceptibility, χ'' with temperature for different frequencies of (a) CdFe₂O₄ and (b) ZnFe₂O₄.

6.4 Ageing, Rejuvenation and Memory Effects

To elucidate a real spin glass behavior nonequilibrium dynamics of the spin glass phase is required to study. Aging, rejuvenation and memory effects are intriguing characteristic of the non-equilibrium dynamics in spin-glasses proposed by Mathieu *et. al* [6.18]. A simple DC magnetization measurement is typically used to disclose nonequilibrium spin glass characteristics such as aging, memory and rejuvenation when specific single stop cooling protocols are utilized. In such experiments, the sample was first cooled rapidly in zero magnetic field from a temperature $T > T_f$ down to the stop temperature $T_s < T_f$ and the cooling is temporarily stopped at the temperature below the spin freezing temperature. In the present case, the sample was cooled from a temperature well above T_f to a stopping temperature T_s ($T_s/T_f = 0.8$) and was kept at T_s for $t_w = 3$ h. After a waiting time $t_w = 3$ h, the cooling was then subsequently resumed down to the lowest measurement temperature, where a small dc magnetic field $H = 10$ Oe was applied and the magnetization (M_{ZFC}) recorded on reheating. This measurement is superimposed on the M_{ZFC} and the M_{FC} measured using the same protocol but without any intermittent stop. The results thus obtained are shown in Fig. 6.15(a, b).

The M_{ZFC} curves involving a stop coincide with the reference M_{ZFC} curve in a temperature range well below T_s . The M_{ZFC} curve corresponding to an isothermal holding of 3 hrs is found to lie significantly below the M_{ZFC} reference curve (without holding time) in a limited temperature range centered at T_s . As the temperature increases in a range above T_s , the M_{ZFC} curves gradually tend to merge with the M_{ZFC} reference curves and eventually coincide with the reference curve at little higher temperature above T_s . During the isothermal holding, the magnetization relaxes to a lower value due to a rearrangement of its spin configuration towards the equilibrium state. The equilibrium of the spin configuration at the holding temperature corresponds to aging. When reheated, the SG remembers its former magnetization state with reference to its previous temperature during aging and follows a path which lies below the reference M_{ZFC} curve retrieves its former state and resumes its former evolution. The system thus remembers its age, and the observed phenomenon is known as a memory effect. A spin-glass system has been shown to be able to memorize information from several isothermal holdings if they are sufficiently separated [6.19]. The merging of the M_{ZFC} curve having isothermal holding with the reference curve implies that the system is rejuvenated.

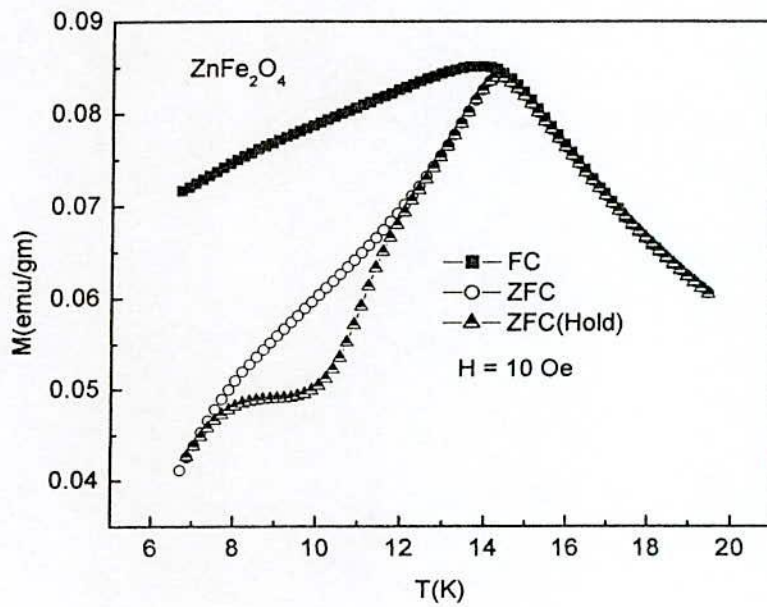
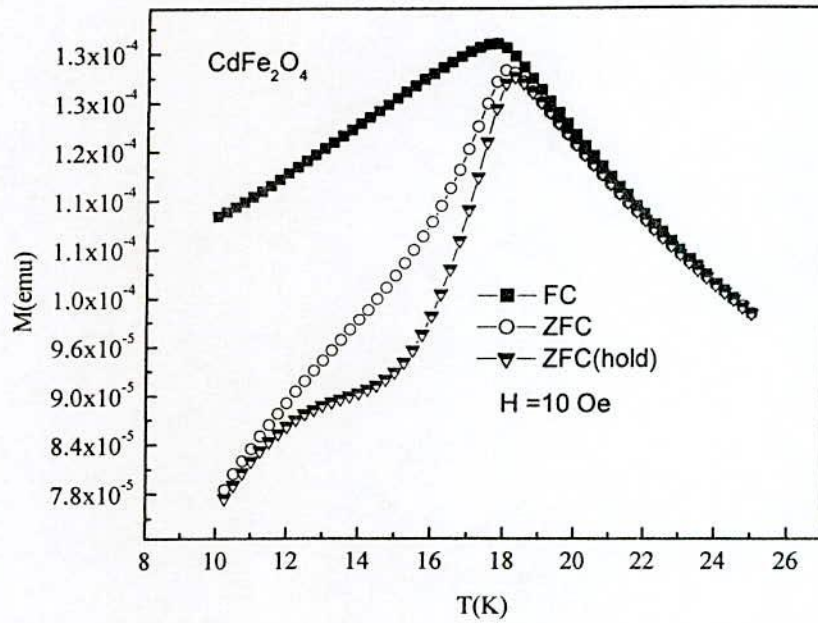


Fig. 6.15 FC and ZFC magnetizations superimposing ZFC curves with isothermal holding time at $T_s/T_f = 0.8$ for 3h of (a) CdFe_2O_4 and (b) ZnFe_2O_4 ferrites.

6.5 Summary

M_{FC} and M_{ZFC} of the samples $Co_{1-x}Cd_xFe_2O_4$ and $Co_{1-x}Zn_xFe_2O_4$ at $x = 0.7, 0.8$ are observed that magnetization sharply rises to a high value indicating a PM-FM transition ($T_c = 262$ K and 242 K at $x = 0.7$) and develops a plateau followed by sharp fall of M_{ZFC} at much lower temperature, T_f where a divergence between M_{ZFC} and M_{FC} is observed. It follows transitions in the sequence of phases, PM-FM-RSG transition with a plateau characteristic of ferromagnetic ordering followed by a drop in ZFC magnetization at the lower temperature T_f indicating spin freezing. Similar behavior was also observed in the case of Co-Cd and Co-Zn at $x = 0.8$ sample. The M_{ZFC} and M_{FC} curves $Co_{1-x}Cd_xFe_2O_4$ and $Co_{1-x}Zn_xFe_2O_4$ at $x = 0.9, 1.0$ samples diverge below spin freezing temperature, T_f exhibiting M_{ZFC} cusps at $T = 29.74$ K and 20.47K for $Co_{1-x}Cd_xFe_2O_4$ with $x = 0.9$ and 1.0 and $T = 22.29$ K and 14.50K for $Co_{1-x}Zn_xFe_2O_4$ with $x = 0.9$ and 1.0 is observed. This is an indication of spin glass behavior (PM-SG). Large magnetic hysteresis effect has been observed at low temperature for the diluted ferrite composition. Frequency dependent complex AC susceptibility and DC magnetization measurement reveal that the sample exhibit spin-glass behavior. The samples show typical spin glass behavior (PM-SG) with the manifestation of nonequilibrium dynamics of the spin glass such aging, rejuvenation and memory effects.

CHAPTER-VII
RESULTS AND DISCUSSION OF
SUBSTITUTION IN DILUTED $\text{Co}_{0.2}\text{M}_{0.8}\text{Fe}_2\text{O}_4$
(M = Zn, Cd) FERRITES

Results and Discussion of Rare-earth Substitution in Diluted $\text{Co}_{0.2}\text{M}_{0.8}\text{Fe}_2\text{O}_4$ (M = Zn, Cd) Ferrites

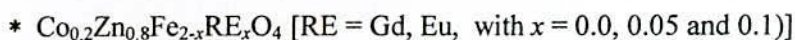
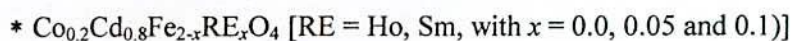
7.0 Introduction

Small amount of additive/substitutions in the spinel ferrites are found to display interesting properties such as physical, electrical and magnetic properties. They also act as microstructure refinement agent. It is well known that the magnetic properties of spinel ferrites are strongly dependent on microstructure. The rare-earth oxides are recently becoming the promising and potential additives for the improvement of the properties of ferrites. Rare-earth element has large magnetic moments, large magnetocrystalline anisotropy and very large magnetostriction at low temperatures due to their localized nature of 4f electrons being totally screened by 5s and 5p orbital. But the solubility of rare-earth in the spinel lattice is limited. It has been demonstrated that even a low content of rare-earth substitution in the spinel ferrite show phase segregation and diffusion of rare-earth species to the grain boundaries as extra crystalline phases like orthoferrites (REFeO_3) [7.1, 7.2].

In spite of phase segregation, some unique and controversial magnetic results have been reported [7.3 - 7.6]. It has been accepted that the rare-earth ions commonly reside at octahedral sites [7.7] and have limited solubility in the spinel lattice due to their large ionic radii. But the exact value of their solubility in the spinel lattice is not known. Most of the research work performed earlier by RE substitution have been done with basic ferrite compositions that are strongly ferromagnetic having long-range ferromagnetic ordering with high T_c . Dilute $\text{Co-MFe}_2\text{O}_4$ with nonmagnetic M (Zn, Cd) content higher than percolation limit where frustration and competing interaction start to play dominant role has hitherto not been studied in much detail except a detail study carried out by Bhowmik et.al on $\text{Co}_{0.2}\text{Zn}_{0.8}\text{Fe}_2\text{O}_4$ with the substitution of Rh^{3+} , Ho^{3+} , Ga^{3+} , Dy^{3+} and Er^{3+} [7.8 - 7.11].

The composition $\text{Co}_{0.2}\text{M}_{0.8}\text{Fe}_2\text{O}_4$ (M = Zn, Cd) is chosen because this diluted composition is expected to show complex magnetic structures that consists of long-range ferromagnetic ordering, antiferromagnetic ordering and clustering effects. Since this composition contain only 0.2 (Fe^{3+}) magnetic ion in A-site according to the cation distribution scheme $(\text{M}^{2+}_{0.8}\text{Fe}^{3+}_{0.2})_A[\text{Co}^{2+}_{0.2}\text{Fe}^{3+}_{1.8}]_B$ which is below the percolation limit for long-range ferromagnetic order. Substitution of RE for Fe^{3+} in the octahedral site may show some interesting electromagnetic properties.

The system studied in detail for magnetization behavior with RE substitution as follows:



7.1 X-ray Diffraction (XRD)

XRD patterns are demonstrated in Fig. 7.1 (a, b, c, d) for undoped and RE doped samples of $\text{Co}_{0.2}\text{M}_{0.8}\text{Fe}_{2-x}\text{RE}_x\text{O}_4$ [M = Cd and Zn, RE = Ho, Sm, Gd and Eu with $x = 0.0, 0.05, 0.10$]. It is clearly noticed that undoped samples show formation of cubic spinel single phase structure with no extra peak as shown in fig 7.1 while all RE doped samples show additional peaks other than spinel and probably corresponding to a second phase of REFeO_3 (orthoferrites) shown in Fig. 7.1 (a, b, c, d). Determination of exact phase could not be possible, since the number of extra peaks other than spinel is not sufficient for accurate analysis. It has already been stated earlier that RE doped ferrites show extra crystalline phases due to their low solubility [7.12]. The formation of a secondary phase may be the result of diffusion of some Ho^{3+} ions having larger ionic radius than that of Fe^{3+} during the sintering process into the grain boundaries while the rare earth ions having smaller size can enter in to the spinel lattice forming single phase. The lattice parameters slightly increases for Ho^{3+} doped samples compared with undoped sample while it decreases for doping with other RE cations such as Sm, Gd, Eu. Melargiriyappa *et al* [7.13], Mansour Al-Haj [7.2] and Viswanathan *et.al* [7.14] have observed a decrease of lattice parameter on Sm substitution in spinel ferrites. Similar effect has been found for Gd in Ni-Zn ferrites [7.15].

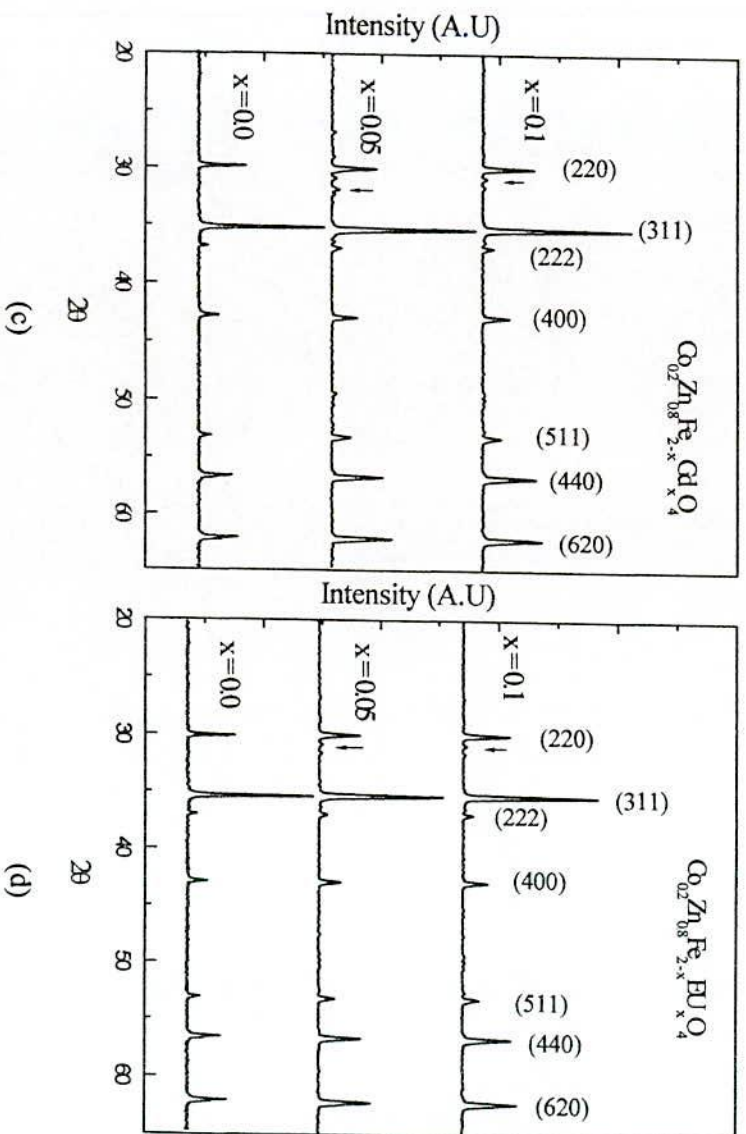
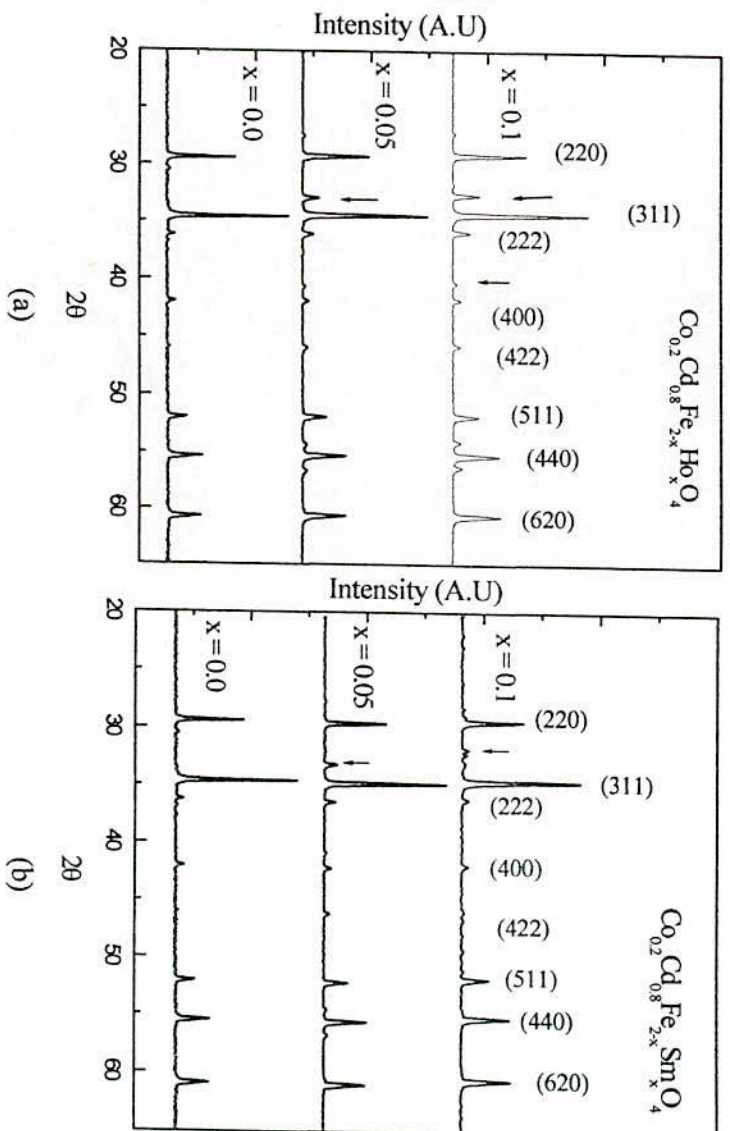


Fig. 7.1 XRD patterns of sample $\text{Co}_{0.2}\text{Cd}_{0.8}\text{Fe}_{2-x}\text{RE}_x\text{O}_4$ with (a) RE = Ho, (b) RE = Sm and sample $\text{Co}_{0.2}\text{Zn}_{0.8}\text{Fe}_{2-x}\text{RE}_x\text{O}_4$ with (c) RE = Gd, (d) RE = Eu for ($x = 0.0, 0.05, \text{ and } 0.1$).

7.2 Temperature Dependence of Magnetization (M_{ZFC} and M_{FC})

The temperature dependence of zero-field-cooled DC magnetization $M_{ZFC}(T)$ of sample $\text{Co}_{0.2}\text{Cd}_{0.8}\text{Fe}_{2-x}\text{RE}_x\text{O}_4$ ($x=0.0$), with various applied field ($H = 10 - 5000$ Oe) is shown in Fig. 7.2. It is observed from the curves that magnetization increases with decreasing temperature attaining a maximum value and decreases thereafter sharply to a low value with further decrease of temperature indicating the randomly freezing of magnetic spins below the spin freezing temperature, $T_f = 57$ K. It is also observed from the graph of Fig. 7.2 that the temperature corresponding to maximum magnetization does not shift noticeably as the applied magnetic field increases. From this temperature dependence it is difficult to determine any magnetic phase transition. From the dM/dT it appears that $T = 100$ K may be the T_c of this composition i.e the sample is ferrimagnetic below T_c which has also been verified with the appearance of spontaneous magnetization from the Arrott plots drawn from the high field (M-H) data at $T = 5 - 100$ K (Fig. 6.2.c)

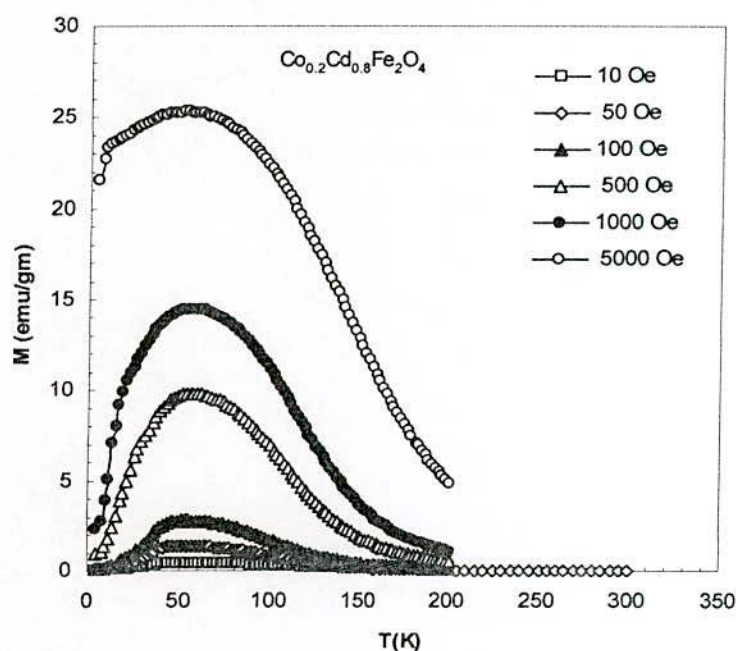


Fig. 7.2 M_{ZFC} Curves of the sample $\text{Co}_{0.2}\text{Cd}_{0.8}\text{Fe}_2\text{O}_4$ with applied field $H = 10 - 5000$ Oe curves.

The decrease of magnetization above freezing temperature is very sluggish and smeared which indicates that the clustering effect is prominent until high temperature as high as $T = 150$ K. The temperature dependence of the inverse mass susceptibility which can be fitted to a

Curie-Weiss law, $\chi = \frac{C}{T - \theta_p}$ in the temperature range 250 - 300K with paramagnetic Curie temperature $\theta_p = 200$ K (Fig. 6.2. d) compared with ferromagnetic $T_c = 100$ K. Large difference between T_c and θ_p implying the existence of large amount of short-range ordering above T_c . It seems that strong short range ferrimagnetic ordering and frustration coexists within the antiferromagnetic matrix. This gives rise to distribution of ferromagnetic phase transition temperatures that makes difficult for precise determination of T_c for this diluted alloy shown in Fig. 7.3. The numerical derivative of $M(T)$ data were carried out from M_{FC} and M_{ZFC} magnetization and found nicely to superimposed on each other. T_c was approximately taken as that temperature where $\frac{dM}{dT}$ attains its maximum value (See inset of Fig. 7.3) and found to be 100 K.

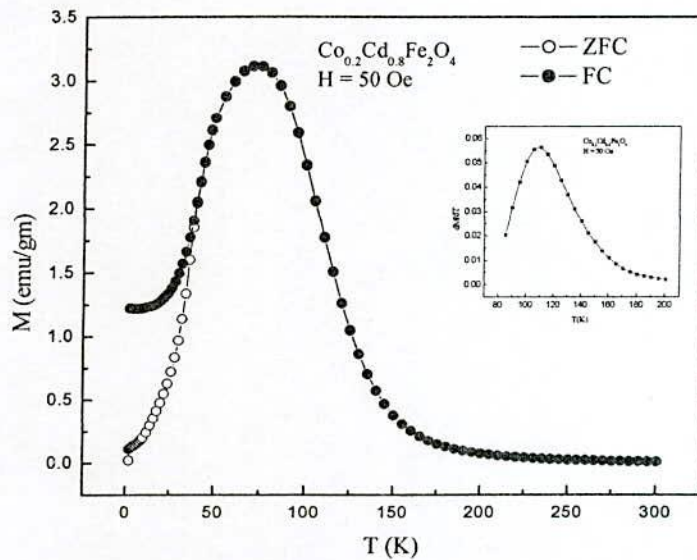


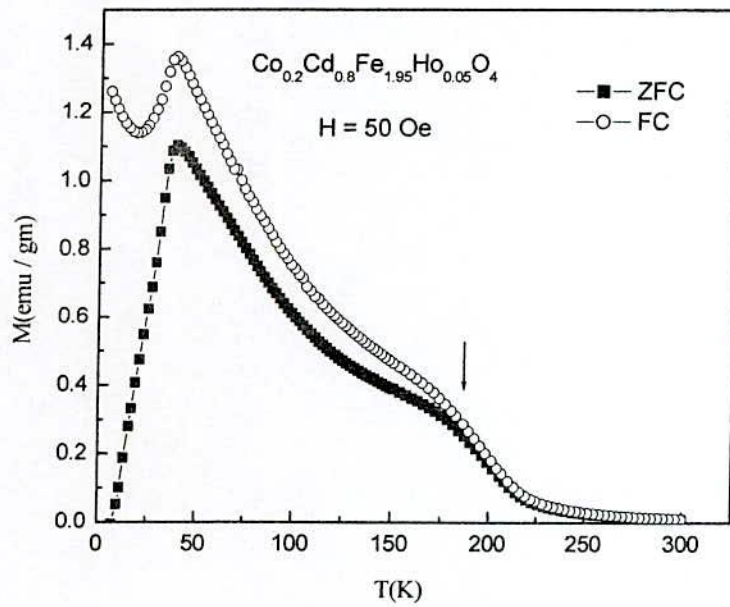
Fig. 7.3 M_{ZFC} and M_{FC} Curves of the sample $\text{Co}_{0.2}\text{Cd}_{0.8}\text{Fe}_2\text{O}_4$ with applied field $H = 50$ Oe.

Inset: $\frac{dM}{dT}$ dM/dT curve

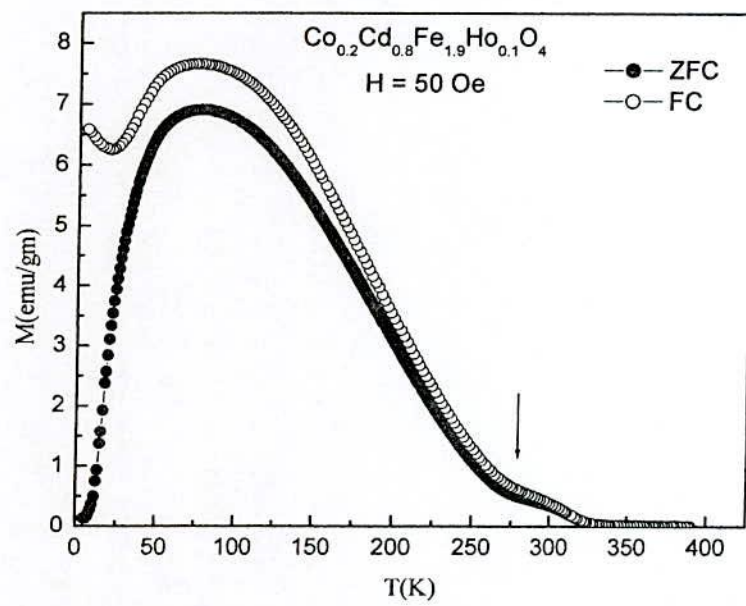
Temperature dependence of field-cooled $M_{FC}(T)$ and zero-field-cooled $M_{ZFC}(T)$ magnetization of Ho^{3+} doped samples with holmium content $x = 0.05$ and 0.10 are displayed in Fig. 7.4 (a, b) measured with an applied field of $H = 50$ Oe. Some salient features of these curves are: (1) the spin freezing temperature, T_f shifts to lower value, i.e., $T_f = 39$ K for $x = 0.05$ while it shifts to higher value of $T_f = 77$ K for $x = 0.1$ compared with $T_f = 57$ K for the undoped sample as well as M_{max} has been broadened and extended to lower temperature. The shift of spin freezing temperature is FC and ZFC magnetization with higher content of Ho^{3+} doping may be related to the changes in the microscopic magnetic interaction A shift of T_g

with increasing Mn content has also been observed in the canonical Cu(Mn) spin-glass [7.16]. (2) The value of M_{\max} for $x = 0.1$ content has increased substantially. The increase of magnetization at low temperature of the Ho^{3+} doped sample may be explained as due to higher magnetic moment of holmium free ions of $10\mu_B$, when some Ho^{3+} ions enter into the spinel lattice. Magnetization may increase due to stronger, Ho-Ho interaction than Fe-Fe and accordingly the T_c is expected to increase and decrease of coercivity of Ho^{3+} doped sample is due to reduction of intergranular pores in line with the previous reports [7.17, 7.18]. (3) T_f shifts to lower temperature with increasing magnetic field. (4) There is a second peak visible at around $T = 180\text{K}$ and 300K for $x = 0.05$ and 0.1 respectively which may be ascribed as due to some ferromagnetic clusters having well defined T_c and found to be 196K and 311K respectively for $x = 0.05$ and 0.1 determined from the numerical derivative $\frac{dM}{dT}$ of magnetization, $M(T)$ data. (5) It is noticed that low temperature magnetization in the M_{FC} condition below the spin freezing temperature takes an upturn to higher value after decreasing magnetization below T_f .

The magnetization minimum at $T \approx 14\text{K}$ may be connected with the spin reorientation effect of Ho^{3+} free ion. Similar effect has been observed by Bhowmik *et al* [7.9] in Zn substituted cobalt ferrite and other researchers [7.19, 7.20]. It is worthwhile to note that the second peak corresponding to a phase transition of $x = 0.05$ and 0.1 Ho^{3+} containing sample has been eliminated when magnetization M_{ZFC} and M_{FC} have been measured with higher magnetic field of $H = 5000$ Oe for $x = 0.05$ and $x = 0.1$ with field $H = 500$ Oe respectively as shown in Fig.7.5 (a, b). This behavior is related to the strong magnetocrystalline anisotropy due to anisotropy field of Ho^{3+} moments and that the local anisotropy field due to Ho^{3+} ion is dominant at low field. As the field is increased the global ferromagnetic ordering suppresses this effect and as a result for higher magnetic field this effect is not seen.



(a)



(b)

Fig. 7.4 M_{ZFC} and M_{FC} curves of sample $Co_{0.2}Cd_{0.8}Fe_{2-x}Ho_xO_4$ (a) $x = 0.05$ (b) $x = 0.1$ with field $H = 50$ Oe.

Fig. 7.6 (a, b) for $x = 0.05$ and Fig. 7.7 (a, b) for $x = 0.1$ shows the temperature dependence of real, χ' (T) and imaginary χ'' (T) part of ac susceptibility and compared with superimposed dc field $H_{dc} = 100$ Oe for the Ho^{3+} doped samples.

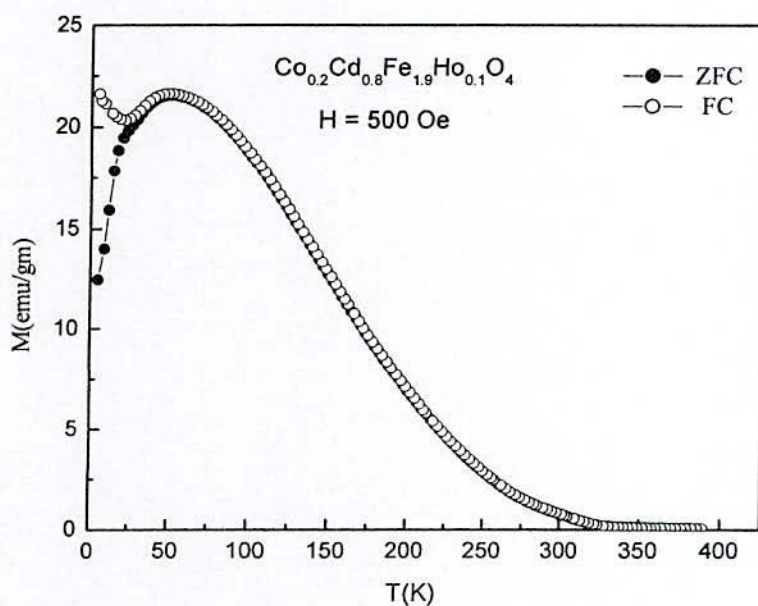
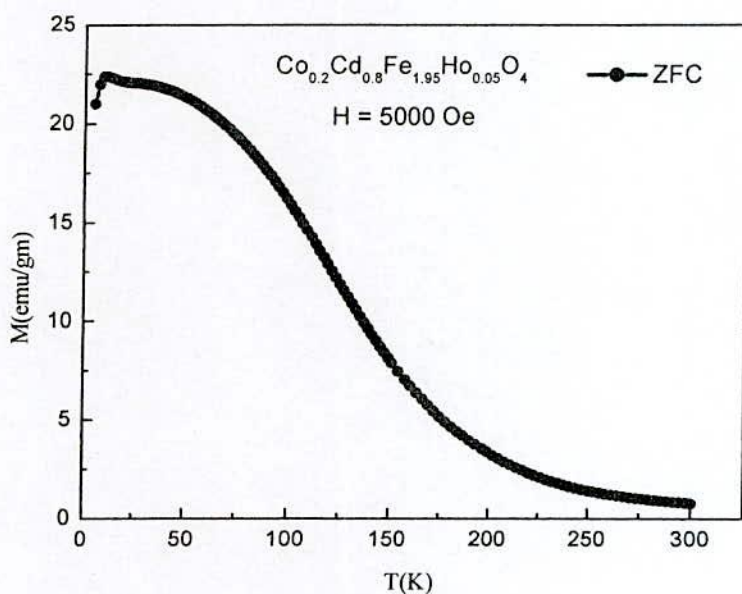


Fig. 7.5 M_{ZFC} and M_{FC} curves of sample $\text{Co}_{0.2}\text{Cd}_{0.8}\text{Fe}_{2-x}\text{Ho}_x\text{O}_4$ (a) $x = 0.05$ with field $H = 5000$ Oe (b) $x = 0.1$ with field $H = 500$ Oe.

It is observed that the cusp in χ' at T_f is frequency independent for $x = 0.05$ while a broad maxima is observed in χ' for $x = 0.10$ which also does not show any significant effect of frequency change, but a phase transition is observed above 100K and 200K in case of $x = 0.05$, while for $x = 0.1$ similar two phase transitions are observed around $T \approx 250$ K and 320K. The phase transitions have been well reflected in the measurement of imaginary part, χ'' of ac susceptibility, the data of which are two order of magnitude sensitive that χ' .

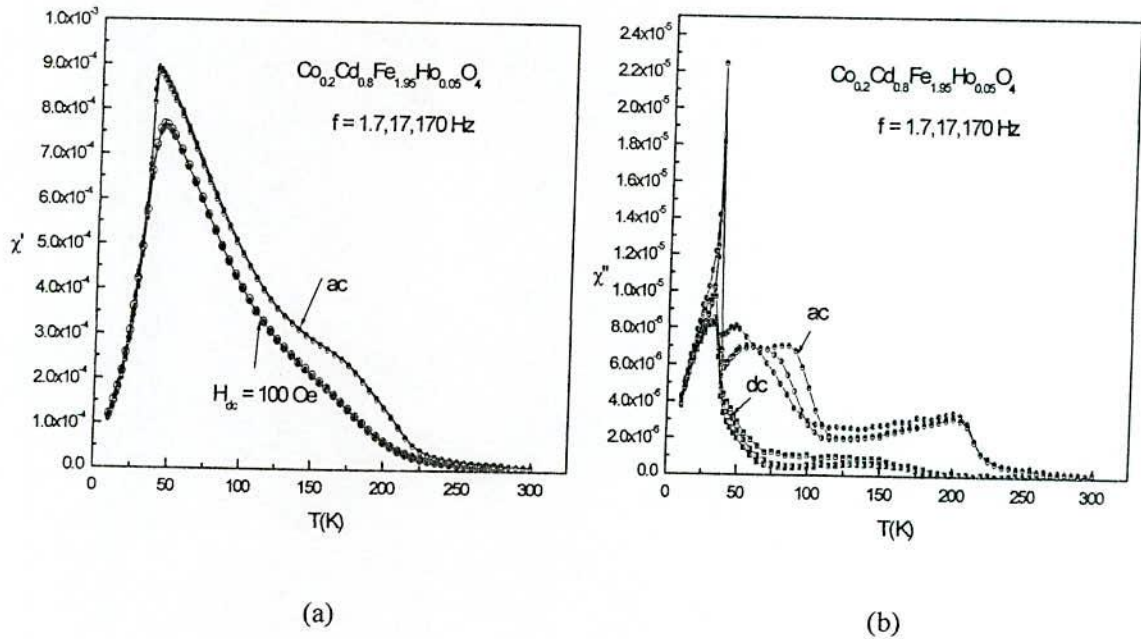


Fig. 7.6 The temperature dependence of AC susceptibility measured at $\frac{\omega}{2\pi} = 1.7, 17$ and 170 Hz respectively for (a) the real $\chi'(T)$ part and (b) imaginary $\chi''(T)$ part of $\text{Co}_{0.2}\text{Cd}_{0.8}\text{Fe}_{1.95}\text{Ho}_{0.05}\text{O}_4$ ferrites.

AC susceptibility measurement has been performed with a superimposed DC field of $H = 100$ Oe and shown in Fig. 7.5 and Fig. 7.6 where a suppression of susceptibility is observed that indicates the cluster glass effect. It is understood that the suppression of χ' upon application of dc field has saturated the cluster magnetization resulting in a decrease of susceptibility compared with ac susceptibility with no dc applied field. It is clearly observed that temperature corresponding to χ'' does not shift with frequency and that the χ'' maximum occurs at the inflection point of χ' below and above T_f . These feature of ac susceptibility clearly indicate the system as cluster spin glass below T_f and does not belong to spin glass behavior while the second maxima of χ'' at $T = 224$ K corresponding to blocking of

superparamagnetic cluster in line with the experimental evidence of Bhowmik *et. al.* [7.9] for Ho^{3+} doped Co-Zn ferrite. This has also been demonstrated in the divergence between $M_{\text{ZFC}}(T)$ and $M_{\text{FC}}(T)$ for the Ho^{3+} doped samples with $x = 0.05$ and 0.1 as shown in Fig. 7.4 (a,b). Thus we can conclude that Ho^{3+} doped samples show ferromagnetic cluster effect as claimed by previous researchers [7.9, 7.21].

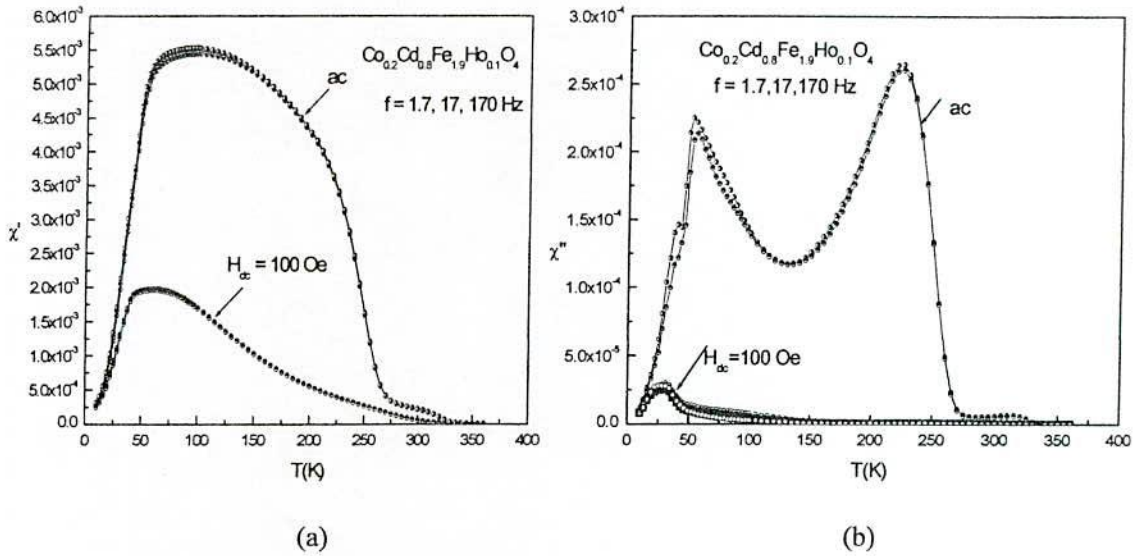
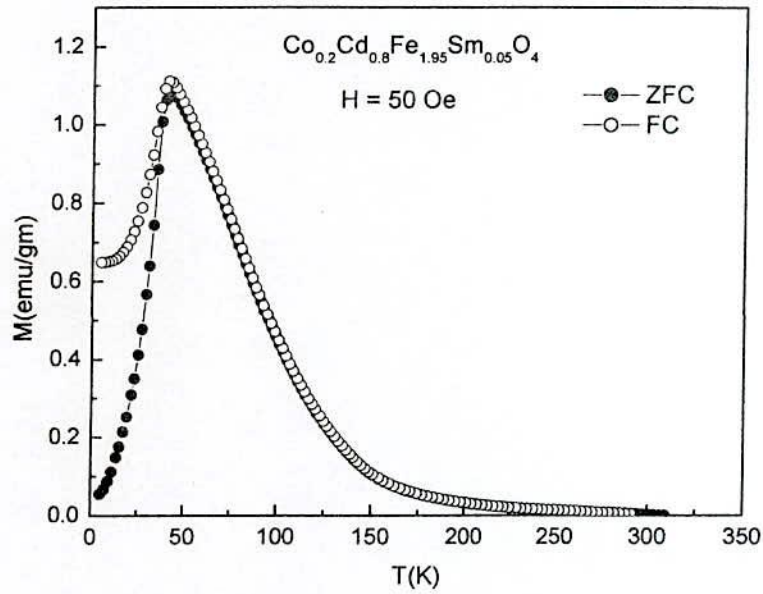


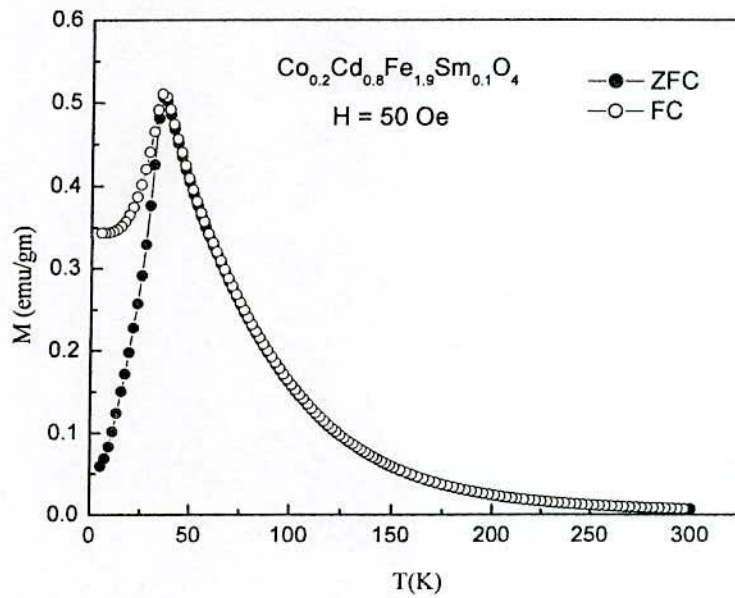
Fig. 7.7 The temperature dependence of AC susceptibility measured at $\frac{\omega}{2\pi} = 1.7, 17$ and 170 Hz respectively for (a) the real χ' (T) part and (b) imaginary χ'' (T) part of $\text{Co}_{0.2}\text{Cd}_{0.8}\text{Fe}_{1.9}\text{Ho}_{0.1}\text{O}_4$ ferrites.

Temperature dependence of M_{ZFC} and M_{FC} curves for Sm doped $\text{Co}_{0.2}\text{Cd}_{0.8}\text{Fe}_{2-x}\text{Sm}_x\text{O}_4$ ferrites are shown in Fig. 7.8 (a, b) for $x = 0.05$ and 0.1 with field $H = 50$ Oe and Fig. 7.9 (a,b) for $x = 0.05$ with field $H = 5000$ Oe and $x = 0.1$ with field $H = 500$ Oe respectively. Unlike Ho^{3+} doped samples, Sm^{3+} doped samples do not show any significant behavior in $M(T)$ measurement. Only a shift of T_f to lower temperature i.e. 41K and 35K for $x = 0.05$ and 0.1 respectively is observed compared with $T_f = 57\text{K}$ for undoped one. Also no divergence between M_{ZFC} and M_{FC} as well as no extra phase transition has been observed. No ferromagnetic phase transition above the spin freezing temperature as in the case of undoped samples with $T_c = 100\text{K}$ have been observed. Similar situation has also been observed for high field $M(T)$ measurement, only difference being higher magnetization value for high field and the broad maxima at the freezing temperature. From $M(H)$ measurement it has been observed that magnetization M substantially decrease for Sm doped samples having a value of 37 emu/gm compared with 46.7 emu/gm for the un doped samples. The decrease of magnetization with Sm^{3+} substitution for Fe^{3+} may be explained as due

to lower free ion magnetic moment of Sm^{3+} i.e. $1.58\mu_B$ [7.22] compared with $5\mu_B$ for Fe^{3+} ion. A similar result for Sm^{3+} substitution in Mg-Zn ferrite has been observed by Monsour [7.2].

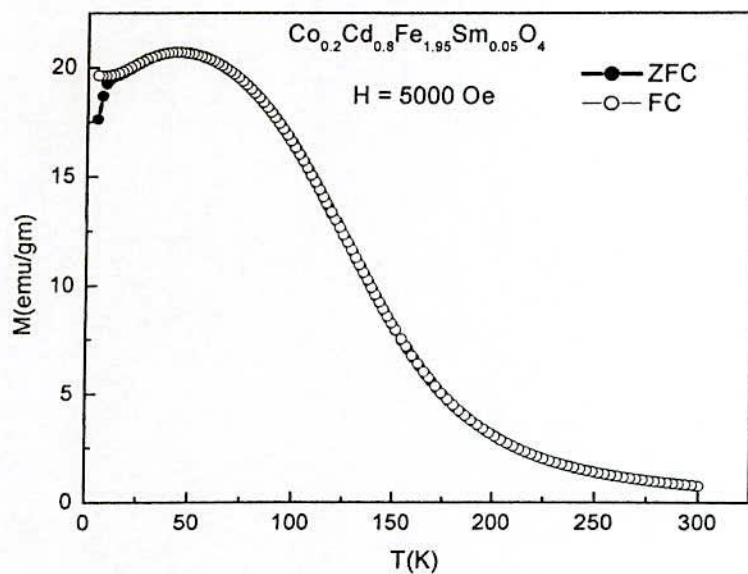


(a)

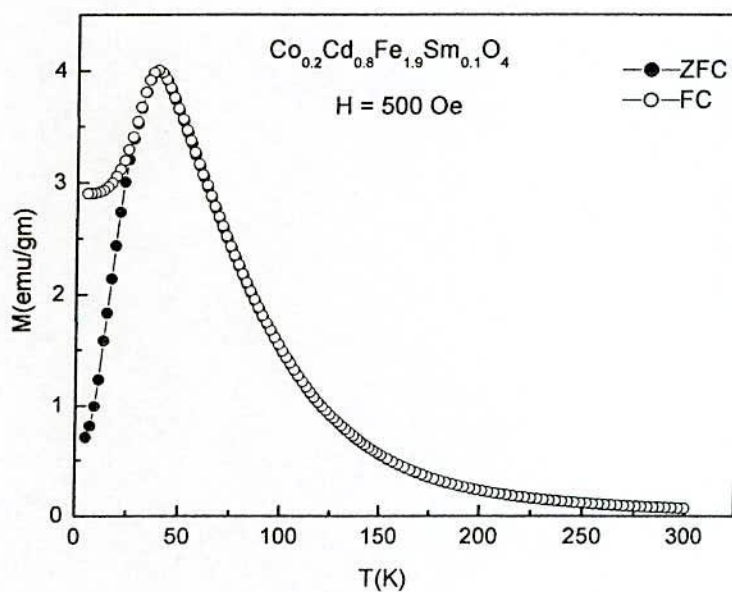


(b)

Fig. 7.8 M_{ZFC} and M_{FC} curves of sample $\text{Co}_{0.2}\text{Cd}_{0.8}\text{Fe}_{2-x}\text{RE}_x\text{O}_4$; RE = Sm
(a) $x = 0.05$ (b) $x = 0.1$ with field $H = 50$ Oe.



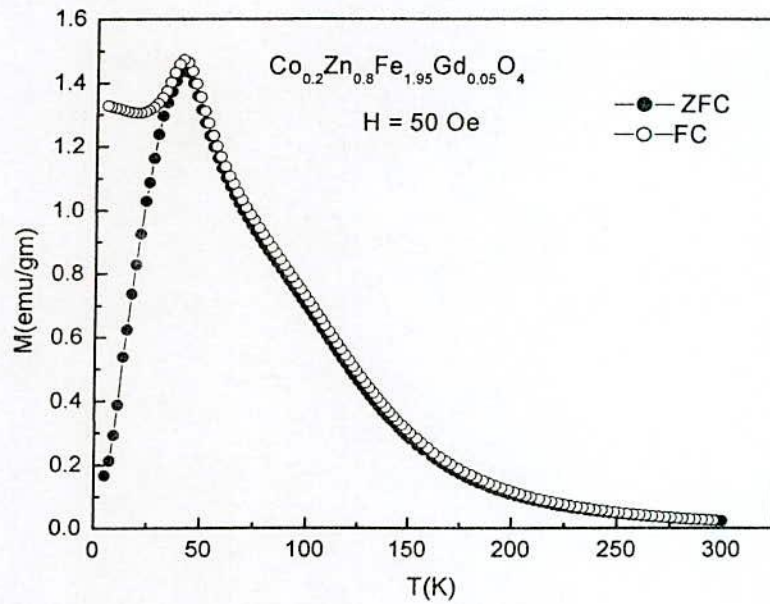
(a)



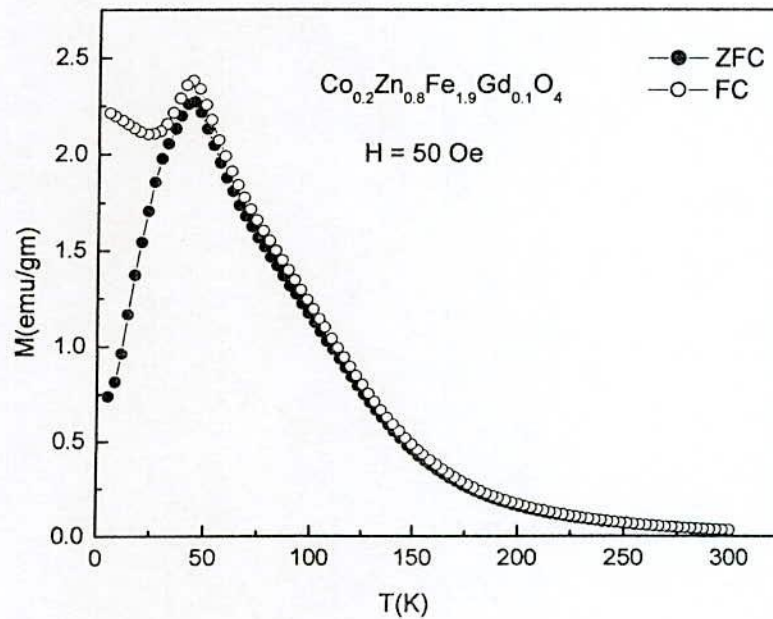
(b)

Fig. 7.9 M_{ZFC} and M_{FC} curves of sample $\text{Co}_{0.2}\text{Cd}_{0.8}\text{Fe}_{2-x}\text{Sm}_x\text{O}_4$ (a) $x = 0.05$ with field $H = 5000$ Oe (b) $x = 0.1$ with field $H = 500$ Oe

Fig. 7.10 (a, b) shows the temperature dependence of magnetization M_{ZFC} and M_{FC} of Gd doped $\text{Co}_{0.2}\text{Zn}_{0.8}\text{Fe}_{2-x}\text{Gd}_x\text{O}_4$ with $x = 0.05$ and 0.1 with applied magnetic field of $H = 50$ Oe and Fig. 7.11 (a, b) for $H = 500$ Oe respectively.



(a)

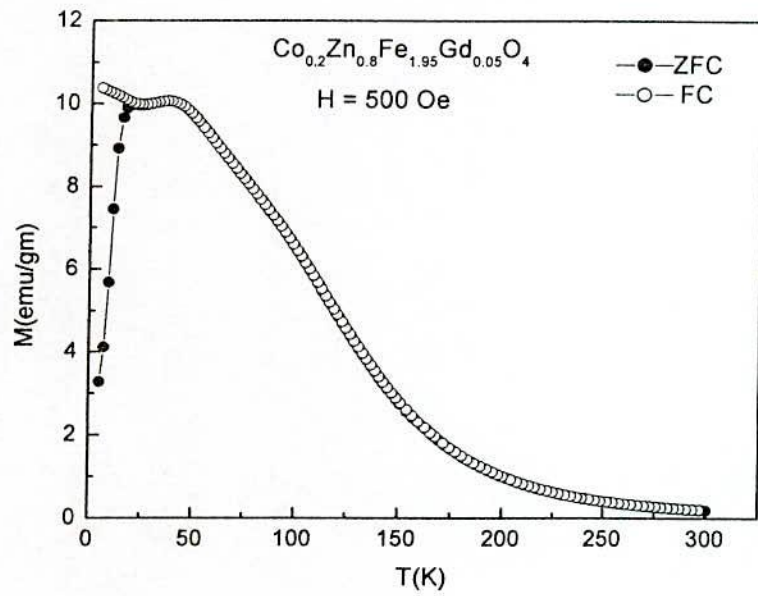


(b)

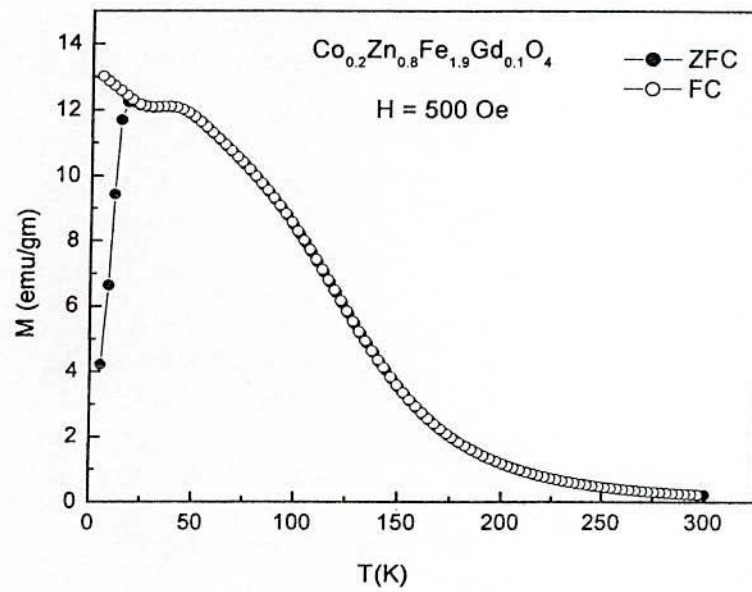
Fig. 7.10 M_{ZFC} and M_{FC} curves of sample $\text{Co}_{0.2}\text{Zn}_{0.8}\text{Fe}_{2-x}\text{Gd}_x\text{O}_4$
 x = 0.05 (b) x = 0.10 with field H = 50 Oe.

It is observed that like undoped samples $M(T)$ measurement does not show any clear magnetic phase transition, but the nature of $M(T)$ is very similar with undoped samples (Fig.6.3. a). This is a magnetization minima around 20K after spin freezing temperature T_f beyond which magnetization slightly increases to higher value probably due to spin

reorientation of Gd^{3+} ion at low temperature. When $M(T)$ measurement is carried out with an applied field of $H = 50$ Oe, the M_{FC} and M_{ZFC} merges until 5K having no divergence even at temperature as low as 5K, while in case of $H = 50$ Oe and 500 Oe the divergence between M_{FC}/M_{ZFC} is clearly manifested.



(a)



(b)

Fig. 7.11 M_{ZFC} and M_{FC} curves of sample $Co_{0.2}Zn_{0.8}Fe_{2-x}Gd_xO_4$
(a) $x = 0.05$ (b) $x = 0.1$ with field $H = 500$ Oe.



There is one specificity of intermediate high field ($H = 500$ Oe) $M(T)$, that below T_f there is a plateau of $M(T)$ curve after which magnetization rises to higher value. This peculiarity may also have some connection with the spin reorientation temperature of Gd^{3+} ion at low temperature.

7.3 High field Magnetic Hysteresis

In order to elucidate detail magnetic parameters, complete hysteresis loops have been measured with $H = \pm 50$ k Oe. Fig. 7.12 (a,b) and 7.13 (a,b) shows the hysteresis loops of $Co_{0.2}Cd_{0.8}Fe_{2-x}Ho_xO_4$ ($x = 0.05, 0.1$) and $Co_{0.2}Cd_{0.8}Fe_{2-x}Sm_xO_4$ ($x = 0.05, 0.1$) respectively. It is observed that all the samples show large hysteresis with manifestation of large coercive field, H_c especially at low temperature, $T = 5$ K with $H_c = 891$ and 603 Oe is found for $Ho = 0.05$ and 0.1 respectively compared to that of $H_c = 1695$ and 1809 Oe for $Sm = 0.05$ and 0.1 respectively while $H_c = 1966$ Oe for undoped sample. It is interesting to note that the hysteresis loops are constricted for the Ho doped samples in the low field region close to the origin having slightly higher value for the lower Ho content. This may be attributed to the larger constriction of Ho ($x = 0.1$) hysteresis loops at $T = 5$ K compared with the sample $x = 0.05$. Also no coercive field has been found at higher temperature.

The constricted hysteresis loops for the Ho doped samples are due to spin reorientation temperature of Ho^{3+} ion at low temperature. From the hysteresis loops maximum magnetization at $H = 50$ kOe have been determined. An enhancement of magnetization with Ho^{3+} doping level of $Ho^{3+} = 0.1$ with $M_{(H=50\text{ kOe})} = 57$ emu/gm have been achieved compared with $M = 46.8$ emu/gm for the undoped samples with almost no change of magnetization for $Ho = 0.05$ with $M = 51.7$ emu/gm. But a decrease of magnetization with $H = 50$ kOe for the Sm doped samples are clearly observed having higher value for Sm content. This means that Sm^{3+} ions do not contribute to the overall magnetization of the $Co_{0.2}Cd_{0.8}Fe_2O_4$ sample. The hysteresis parameters such as M at $H = 50$ kOe and H_c are shown in Table-7.1. It is noticed that the magnetization is not saturated with field, H as high as 50 kOe implying a highly disordered and frustrated system along with a high anisotropy.

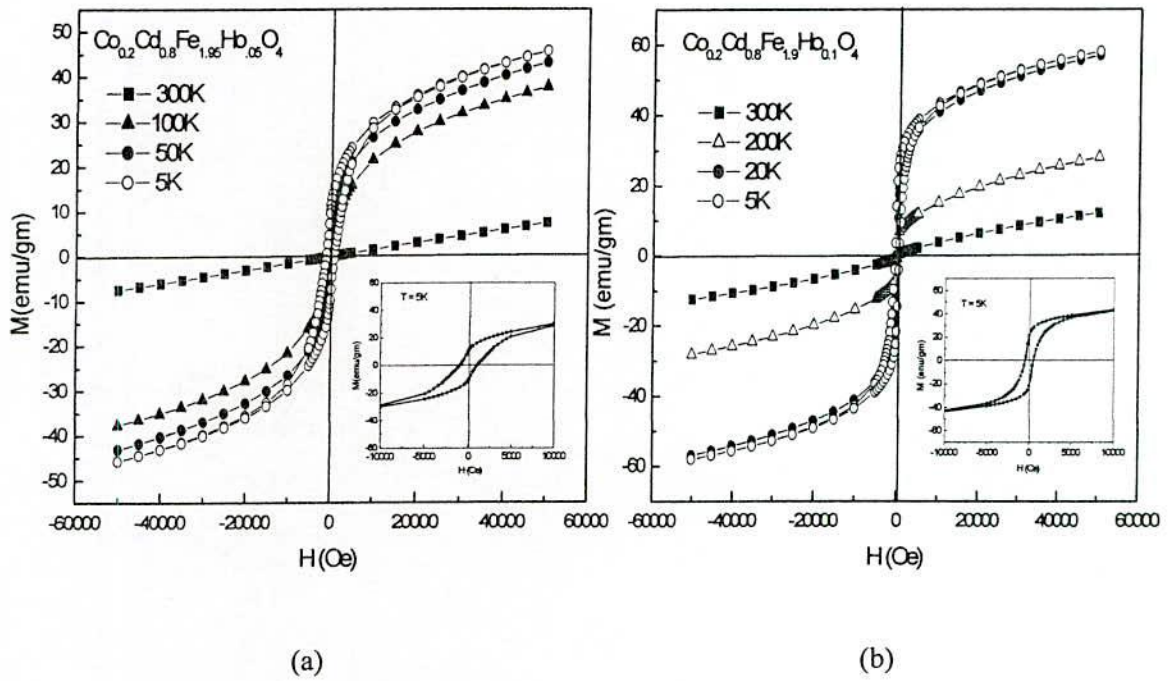


Fig. 7.12 Magnetization hysteresis loops of sample $\text{Co}_{0.2}\text{Cd}_{0.8}\text{Fe}_{2-x}\text{Ho}_x\text{O}_4$ (a) $x = 0.05$, (b) $x = 0.1$ at different temperatures 5K - 300K with field $H = 50$ kOe .

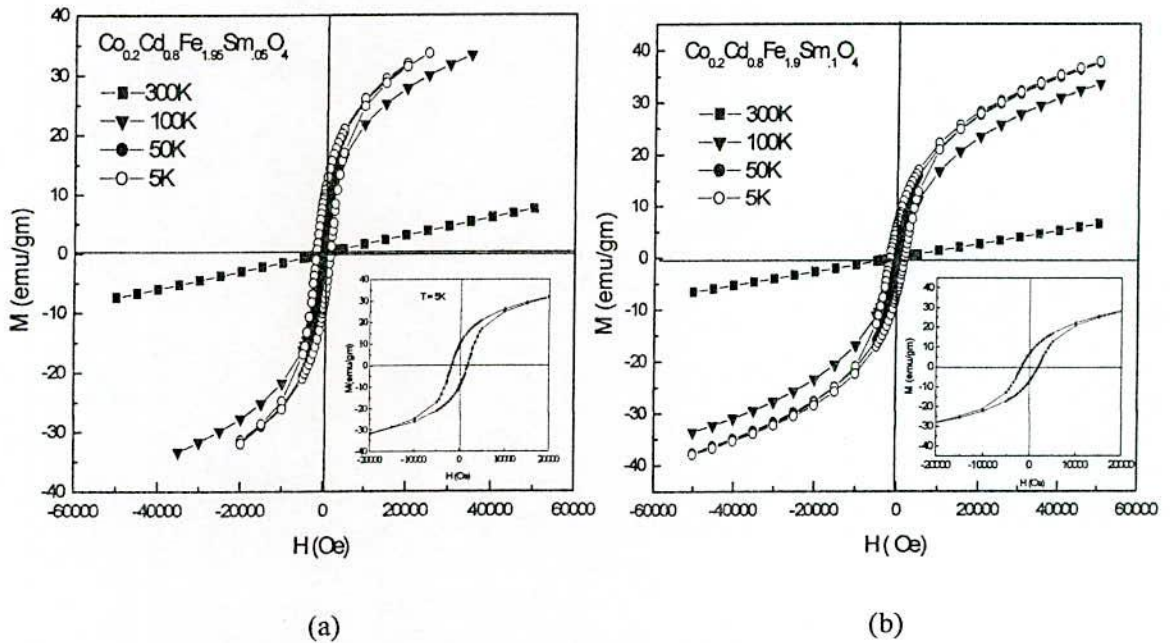


Fig. 7.13 Magnetization hysteresis loops of sample $\text{Co}_{0.2}\text{Cd}_{0.8}\text{Fe}_{2-x}\text{Sm}_x\text{O}_4$ (a) $x = 0.05$ and (b) $x = 0.1$ at different temperatures 5 K - 300 K with Field $H = 50$ kOe.

Fig. 7.14 (a, b) and Fig. 7.15 (a, b) shows the hysteresis loops of $\text{Co}_{0.2}\text{Zn}_{0.8}\text{Fe}_{2-x}\text{Gd}_x\text{O}_4$ ($x = 0.05, 0.1$) and $\text{Co}_{0.2}\text{Zn}_{0.8}\text{Fe}_{2-x}\text{Eu}_x\text{O}_4$ (0.05, 0.1) with $H = \pm 50$ kOe. It is observed that magnetization like Co-Cd system does not saturate with high field up to $H = 50$ kOe.

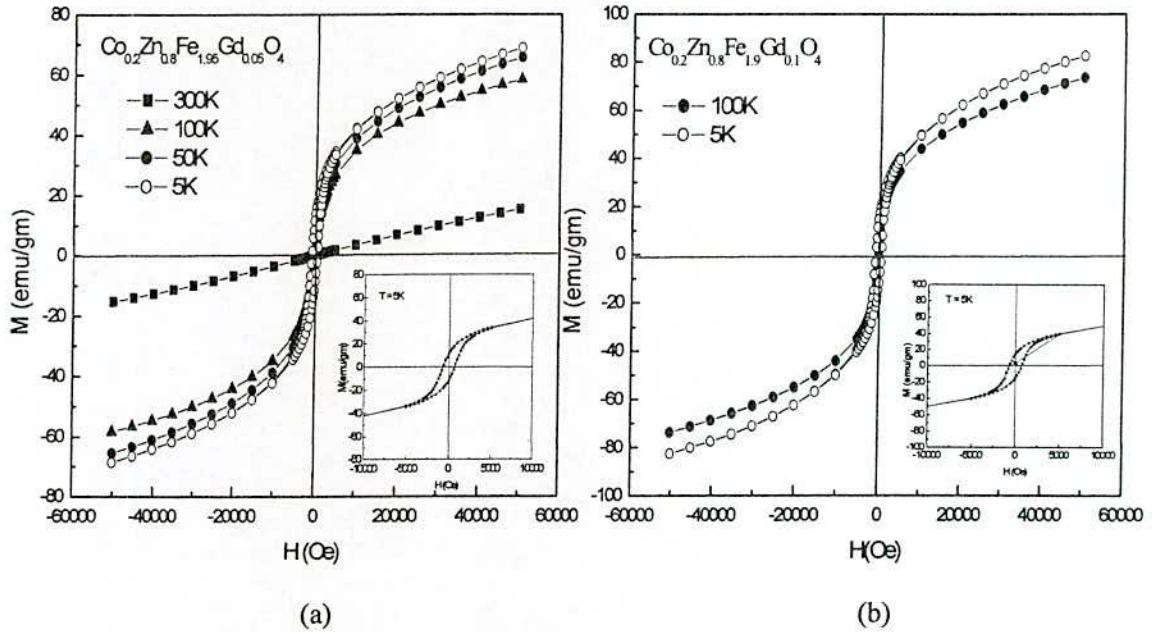


Fig. 7.14 Magnetization hysteresis loops of sample $\text{Co}_{0.2}\text{Zn}_{0.8}\text{Fe}_{2-x}\text{Gd}_x\text{O}_4$ (a) $x = 0.05$ and (b) $x = 0.1$ at different temperatures 5 K- 300 K with field $H = 50$ kOe.

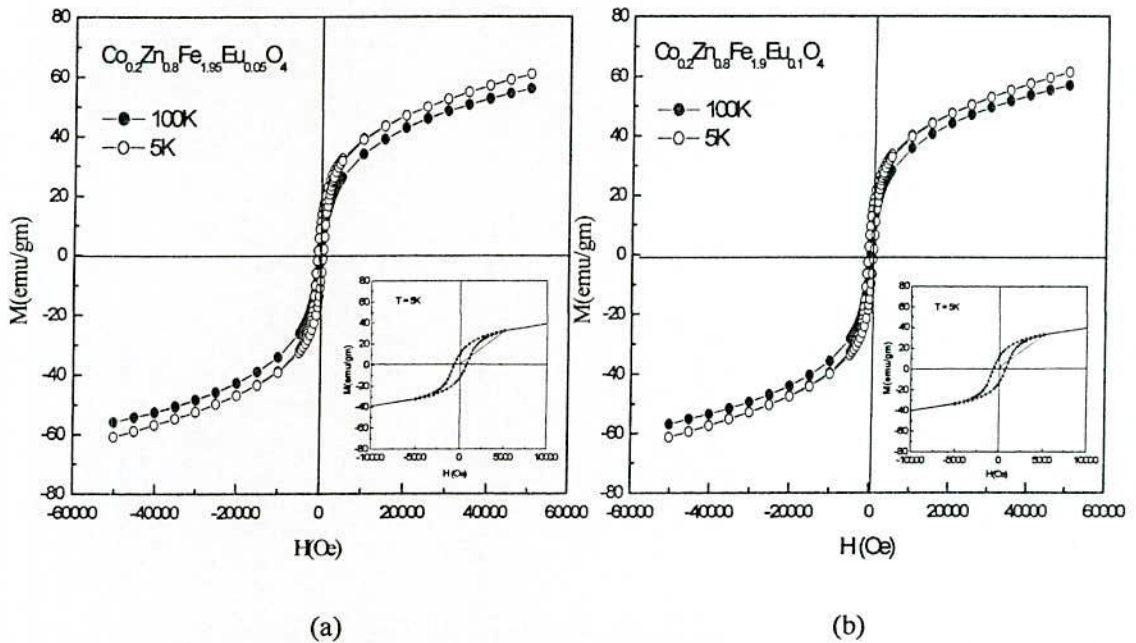


Fig. 7.15 Magnetization hysteresis loops of sample $\text{Co}_{0.2}\text{Zn}_{0.8}\text{Fe}_{2-x}\text{Eu}_x\text{O}_4$ (a) $x = 0.05$ (b) $x = 0.1$ at different temperatures 5 K - 300 K with field $H = 50$ kOe.

Coercive field $H_c = 690$ Oe for undoped $\text{Co}_{0.2}\text{Zn}_{0.8}\text{Fe}_2\text{O}_4$ sample at $T = 5\text{K}$ which increases significantly for the Gd doped samples and slightly for Eu doped samples. This is worthwhile to mention that magnetization has substantially increased for the Gd^{3+} doped samples while it slightly decreased for Eu doped samples. The enhancement of magnetization at $T = 5\text{K}$ for Gd^{3+} doping sample is probably due to high magnetic moment of Gd^{3+} free ion of $7.8\mu_B$ and that higher Gd^{3+} doping has higher magnetization of 82.58 emu/gm compared with 64.51 emu/gm for the undoped samples. The decrease of magnetization for Eu doping is due to nonmagnetic nature of Eu which has no magnetic moment of the free Eu^{3+} ion even at low temperature. All the magnetization data are listed in Table-7.1

Table -7.1 The hysteresis parameters such as magnetization (M) at $H = 50$ kOe, and Coercive field H_c at different temperature $T = 5 - 300$ K.

Composition	M(emu/gm) at $H = 50$ kOe					
	T = 5K	T =50K	T =100K	T =200K	T =300K	H_c (Oe)
$\text{Co}_{0.2}\text{Cd}_{0.8}\text{Fe}_2\text{O}_4$	46.87	46.97	43.07		9.66	1966
$\text{Co}_{0.2}\text{Cd}_{0.8}\text{Fe}_{1.95}\text{Ho}_{0.05}\text{O}_4$	51.71	49.15	47.7		12.4	891
$\text{Co}_{0.2}\text{Cd}_{0.8}\text{Fe}_{1.9}\text{Ho}_{0.1}\text{O}_4$	56.95			28.08	12.12	603
$\text{Co}_{0.2}\text{Cd}_{0.8}\text{Fe}_{1.95}\text{Sm}_{0.05}\text{O}_4$	33.62* ($H=2.5\text{T}$)	31.61	33.31		7.39	1695
$\text{Co}_{0.2}\text{Cd}_{0.8}\text{Fe}_{1.9}\text{Sm}_{0.1}\text{O}_4$	37.61	37.61	33.64		6.57	1809
$\text{Co}_{0.2}\text{Zn}_{0.8}\text{Fe}_2\text{O}_4$	64.51	66.9	59.59		15.66	690
$\text{Co}_{0.2}\text{Zn}_{0.8}\text{Fe}_{1.95}\text{Gd}_{0.05}\text{O}_4$	68.75	65.65	58.38		15.31	802
$\text{Co}_{0.2}\text{Zn}_{0.8}\text{Fe}_{1.9}\text{Gd}_{0.1}\text{O}_4$	82.58	71.29	64.62			798
$\text{Co}_{0.2}\text{Zn}_{0.8}\text{Fe}_{1.95}\text{Eu}_{0.05}\text{O}_4$	60.63	62.64	55.99			603
$\text{Co}_{0.2}\text{Zn}_{0.8}\text{Fe}_{1.9}\text{Eu}_{0.1}\text{O}_4$	61.36	63.42	56.93			802

7.4 Summary

Rare-earth (RE) doping of Ho^{3+} and Sm^{3+} in $\text{Co}_{0.2}\text{Cd}_{0.8}\text{Fe}_{2-x}\text{RE}_x\text{O}_4$ ferrite is that Ho^{3+} shows some interesting property with the appearance of a second phase having higher T_c than the undoped sample which again increases with Ho^{3+} content. An extra second phase has also been detected from XRD pattern which might be some orthoferrite (REFeO_3) phase. Magnetization is found to increase slightly with Ho^{3+} having higher value for higher Ho^{3+} content. The lattice constant is found to increase with Ho^{3+} content indicating that some Ho^{3+} entered into the spinel lattice. The effect of Sm^{3+} is insignificant. It reduces the saturation magnetization and decreases lattice constant. Doping of Gd^{3+} and Eu^{3+} in $\text{Co}_{0.2}\text{Zn}_{0.8}\text{Fe}_{2-x}\text{RE}_x\text{O}_4$, it is observed that substantial increase of magnetization occurs with Gd^{3+} which attains higher value with higher content of Gd^{3+} while it decreases with Eu^{3+} doping. It may be attributed to the higher magnetic moment of Gd^{3+} of $7.8\mu_B$ per free ion and zero magnetic moment of Eu^{3+} free ion. The lattice parameter slightly decreases in both types of dopant.

CHAPTER-VIII

Conclusion

Conclusion

The synthesis, characterization and detail study of electromagnetic properties have been carried out on $\text{Co}_{1-x}\text{Cd}_x\text{Fe}_2\text{O}_4$ and $\text{Co}_{1-x}\text{Zn}_x\text{Fe}_2\text{O}_4$ ferrite samples ($0 \leq x \leq 1$) using standard double sintering ceramic method, sintered at 1050°C - 1150°C for 2-3 hours. The X-ray diffraction pattern confirmed the single phase cubic spinel structure of both Cd and Zn-substituted ferrites. The lattice parameter increases with increasing Cd and Zn content obeying Vegard's law. The bulk density is lower than the X-ray density. Bulk density increases monotonically with increasing Cd and Zn content signifying that the non magnetic ion has a pronounced effect on the densification of the ferrites. Curie temperature is found to decrease linearly with the successive addition of non-magnetic Cd and Zn ions. This decrease is attributed to the addition of the non-magnetic ions that replaced the magnetic Fe^{3+} ions at the A-sites. Thus, the number of Fe^{3+} ions decreases at the A-sites which tend to decrease the strength of A-B exchange interactions of the type $\text{Fe}_A^{3+} - \text{O}^{2-} - \text{Fe}_B^{3+}$. These decrease the linkages between the magnetic ions that determine the magnitude of the Curie temperature.

Initial permeability increases with the increase of Cd and Zn content upto $x = 0.5 - 0.6$. From permeability spectra it is noticed that for $x = 0.1 - 0.3$ samples, the permeability is almost frequency independent upto 13 MHz while for $x = 0.4 - 0.6$, it is almost stable upto 6 MHz - 10MHz beyond which it decreases sharply. From low field B-H loops the high coercivity, H_c is observed at $x = 0.0$ and it decreases almost linearly with increasing both Cd and Zn content up to $x = 0.6$. The low coercive force and higher permeability confirm the softer magnetic characteristic properties of cobalt ferrite with the substitution of non magnetic ions for cobalt which is well known as hard magnet.

Saturation magnetization and magnetic moment are found to increase with Cd upto $x \leq 0.4$, and Zn content upto $x \leq 0.5$ and thereafter decreases. Zn and Cd substitution in the Co-ferrites leads to increase of Fe^{3+} ions on the B-sites and consequently decreases Fe^{3+} ions on A-sites. So, the net magnetization increases accordingly upto $x = 0.4 - 0.5$ based on Neel's two sublattice collinear model. The decrease in the magnetic moment after $x > 0.4$ indicates the possibility of a non-collinear spin canting effect in the system. The existence of canted spin gives rise to Yafet-Kittel angle ($\alpha_{Y,K}$) which compares the strength of A-B and B-B exchange interaction. The increase in Y-K angles for the samples with Cd content ($x > 0.4$) and Zn content ($x > 0.5$) is attributed to the increased preference of triangular spin arrangements on B-sites due to frustration of B-B exchange interaction. An increase in initial permeability has also been found with increasing zinc content.

The complex magnetic behavior of diluted Cd and Zn-substituted $\text{Co}_{1-x}\text{Cd}_x\text{Fe}_2\text{O}_4$ and $\text{Co}_{1-x}\text{Zn}_x\text{Fe}_2\text{O}_4$ ($x = 0.7, 0.8, 0.9$ and 1.0) ferrites have been studied by field-cooled (M_{FC}) and zero-field-cooled (M_{ZFC}) magnetization and complex AC susceptibility measurements. M_{ZFC} of the sample $x = 0.7$ is characterized by a gradual rise of magnetization at $T_c = 262$ K for Cd and $T_c =$

242 K for Zn substitution signifying a PM-FM transition with a plateau characteristic of ferromagnetic ordering followed by a drop in magnetization at the lower temperature, T_f indicating spin freezing temperature and commonly called re-entrant spin glass. Sample with $x = 0.8$, a paramagnetic Curie temperature $\theta_p = 200\text{K}$ compared with ferromagnetic $T_c = 100\text{K}$ has been found for both Cd and Zn substitution. It seems that strong short range ferrimagnetic ordering and frustration coexists within the antiferromagnetic spinel matrix. While the samples with $x = 0.9$ and 1.0 it is observed that magnetization, M_{FC} and M_{ZFC} both increase as the temperature is lowered with the manifestation of divergence after passing through a maximum. A sharp well defined cusp in the M_{ZFC} (T) at $T = 29.74\text{K}$ and 20.47K for $\text{Co}_{1-x}\text{Cd}_x\text{Fe}_2\text{O}_4$ with $x = 0.9$ and 1.0 respectively and $T = 22.29\text{K}$ and 14.50K for $\text{Co}_{1-x}\text{Zn}_x\text{Fe}_2\text{O}_4$ with $x = 0.9$ and 1.0 is observed which again shifts as a function of frequency. The samples show typical spin-glass behavior (PM-SG) with the manifestation of nonequilibrium dynamics of the spin-glass such as aging, rejuvenation and memory effects for CdFe_2O_4 and ZnFe_2O_4 .

DC electrical resistivity increases with the increase of Zn-content which is attributed to the fact that the incorporation of Zn in B-site of ferrite may decrease the concentration of $\text{Fe}^{2+}/\text{Fe}^{3+}$ ion pairs. Both ρ_{ac} and ϵ' decrease as the frequency of applied AC electric field increases. This was explained on the basis of the double layer dielectric structure. Dielectric constant, ϵ' decreases with increasing frequency exhibiting normal dielectric behaviour of ferrites. The dielectric behavior of ferrites may be explained on the basis of the mechanism of the dielectric polarization process and is similar to that of the conduction process.

The substitution of rare-earth for Fe in the diluted $\text{Co}_{0.2}\text{M}_{0.8}\text{Fe}_2\text{O}_4$ ($M = \text{Zn}, \text{Cd}$) ferrite produced secondary phase detected from XRD pattern which might be some orthoferrite (REFeO_3) phase. Ho^{3+} show some interesting property with the appearance of a second phase having higher T_c . Magnetization is found to increase slightly with Ho^{3+} having higher value for higher Ho^{3+} content. The effect of Sm^{3+} is insignificant. It reduces the saturation magnetization and slightly decreases lattice constant. In the case of doping with Gd^{3+} and Eu^{3+} it is observed that substantial increase of magnetization occurs with Gd^{3+} which attains higher value with higher content of Gd^{3+} while it decreases with Eu^{3+} doping. The lattice parameter slightly decreases in both types of dopants. Large magnetic hysteresis effect has been observed at low temperature for the diluted ferrite composition due to frustration and spin canting with the appearance of spin-glass type of behavior.

Finally the outcome of the present research work may be concluded that cadmium and zinc substitution $\text{Co}_{1-x}\text{Cd}_x\text{Fe}_2\text{O}_4$ and $\text{Co}_{1-x}\text{Zn}_x\text{Fe}_2\text{O}_4$ ferrites has profound effect on the magnetic softening of cobalt ferrite together with the appearance of re-entrant spin glass and spin glass behavior in the extreme magnetic diluted compositions of the studied system which has hitherto not been done before. Noteworthy that magnetization is found to increase with RE doping such as Ho^{3+} and Gd^{3+} at low temperature.

References

References

CHAPTER-I

- 1.1. S. Hilpert, Ber. Deutseh. Chem. Ges. BD2, 42 (1909) 2248.
- 1.2. J. L. Snoek,, New developments in Ferrimagnetism, 139pp.
- 1.3. T. Takai, J. Electr. Chems. Japan, 5 (1937) 411.
- 1.4. L. Neel, "Properties Magnetique des ferrites; Ferrimagnetism et Antiferromagnetism" Annales de Physique, 3 (1948)137.
- 1.5. J. Smit, and H. P. J. Wijn, Ferrites, Wiley, New York (1959) 369pp.
- 1.6. K. J. Standley, Oxide Magnetic Materials, (1962)204pp.
- 1.7. J. S. Smart, "The Neel Theory of Ferromagnetism", Amer. J. Physics, 23 (1955) 356.
- 1.8. W. P. Wolf, "Ferrimagnetism," Reports on Prog. in Phys., 24 (1961)212.
- 1.9. E. W. Gorter, "Some properties of ferrites in connection with their chemistry", Proc I.R.E., 43 (1955) 1945.
- 1.10. E. C. Snelling, Soft Ferrites: Properties and Applications, 2nd edition, Butterworths, London, 1988, p-1.
- 1.11. Toshiyuki Suzuki, Terimitsu Tanaka, Kaoru Ikemizu, "High density recording capability for advanced particulate media", J. Magn. Magn. Mater. 235 (2001)159.
- 1.12. T. Giannakopoulou, L. Kompotiatis, A. Kontogeorgakos, G. Kordas, "Microwave behavior of ferrites prepared via sol-gel method", J. Magn. Magn. Mater. 246 (2002) 360.
- 1.13. E. Olsen, J. Thonstad, "Nickel ferrites as inert anodes in aluminium electrodes: Part I Material fabrication and preliminary testing", J. Appl. Electrochem. 29 (1999) 293.
- 1.14. C. O. Augustin, D. Prabhakaran. L.K. Srinivasan, "Fabrication and characterization of NiCr₂O₄ spinel", J. Mater. Sci. Lett. 12 (1993) 383.
- 1.15. P. C. Rajath, R. S. Mannab, D. Baneree, M. R. Varma, K. G. Suresh, A. K. Nigame, J. Alloys Comp. 453 (2008) 298.
- 1.16. J. G. Lee, J. Y. Park, Y. J. Oh, C. S. Kim, J. Appl. Phys. 84 (1998) 2801.
- 1.17. R. K. Sharma, O. Suwalka, N. Lakshmi, K. Venugopalan, A. Banerjee, P. A. Joy, J. Alloys Comp. 419 (2006) 155.
- 1.18. A. Balayachi, J. L. Dormann, and M. Nogues, "Critical analysis of magnetically semi-disordered systems: critical exponents at various transitions", J. Phys. Condens Matter 10 (1998) 1599.
- 1.19. M. A. Hakim, M. Manjurul Haque, M. Huq, Sk. Manjura Hoque and P. Nordblad, "Re-entrant Spin Glass and Spin Glass Behavior of Diluted Mg-Zn Ferrites", CP 1003, Magnetic Materials, International Conference on Magnetic Materials (ICMM-2007) AIP. P-295.
- 1.20. H. Martinho, N. O. Moreno, J. A.Sanjurjo, C. Rettori, D. L. Huber, S. B. O Seroff, W. Ratcliff, S. W. Cheong, Phys. Rev. B 64 (2001) 024408
- 1.21. P. N. Vasambekar, C. B. Kolekar, A.S. Vaingankar, "Magnetic behavior of Cd²⁺ and Cr³⁺ substituted cobalt ferrites", J. Mater. Chem. Phys, 60 (1999)282.
- 1.22. N. Chand Pramanik, T. Fujii, M. Nakanishi and J. Takada, Materials Letters 59 (2005) 88.
- 1.23. K. P. Chae, J. G. Lee, H. S. Kweon and Y. B. Lee, J. Magn. Magn. Mater., 283 (2004) 103.
- 1.24. K. Haneda and A.H. Morrish, J. Appl. Phys. 63 (8) (1988).

- 1.25. Kurikka V. P. M. Shafi and Aharon Gedanken "Sonochemical Preparation and Size-Dependent Properties of Nanostructured CoFe_2O_4 Particles" *Chem Mater* 10 (1998) 3445.
- 1.26. M. Rajendran, R. C. Pullac, A. K. Bhattacharya, D. Das, S. N. Chintalapudi and C. K. Majumdar, *J. Magn. Magn. Mater.*, 232 (2001) 71.
- 1.27. V. A. M. Brabers-Progress in Spinel Ferrite Research in Handbook of Magnetic Materials, Edited by K. H. J. Buchow, North Holland Publishing Inc. 8 (1995)189.
- 1.28. A. Goldman, Modern Ferrite Technology, Van Nostrand.Reinhold, New York, 1990.
- 1.29. A. M. Samy, H.M.E. L Sayed, A. A.Sattar, *Phy. stat. Sol.(a)*.200(2)(2003)401.
- 1.30. A. Globus, H. Pascard and V. Cagan, "Distance between magnetic ions fundamental properties in ferrites", *J. Physique (call)* 38 (1977) C1-163.
- 1.31. R. G. Kulkarni and V. G. Panicker, "Study of canted spin structure in Cu-Cd ferrites", *J. Mater. Sci.* 19 (1984) 890.
- 1.32. I. Nowik, *J.Appl. Phy.* 40 (1969) 872.
- 1.33. M. M. Girigis, Awad A. Mel. *Mater. Chem. Phys.*, 36 (1993) 48.
- 1.34. M. Guillot, J. Ostorero, A. Marchand, "High magnetic field magnetization study in cadmium-cobalt ferrite single crystal", *Z. Phys. B-Condensed Matter* 71(1988) 193.
- 1.35. A. H. Wafik, A. A. Sattar, "Depending of the Irreversible Magnetization $\text{Co}_{1-x}\text{Cd}_x\text{Fe}_2\text{O}_4$ on the Magnetization field" *Physica. Status. Solidi (a)* 117 (1990) K61.
- 1.36. M. A .Gabal, S. S. Ata-Allah, "Effect of diamagnetic substitution on the structureal, electrical ang magnetic properties of CoFe_2O_4 " *Materials Chemistry and Physics* 85(2004) 104.
- 1.37. A.M. Abdeen, O.M. Hemedda, E.E. Assem and M.M. El-Sehly, " Structural, electrical and Transport phenomena of Co- ferrite substituted by Cd,*J.Magn.Magn. Mater.*, 238(2002) 75.
- 1.38. J. Smit, H. P. J. Wijn, *Ferrites*, Philips Technical Library, Eindhoven, The Netherlands, 1959, p.151.
- 1.39. J. L. Dormann, M. Nogues, "Magnetic structures of substituted ferrites", *J. Phys.: Condens. Matter* 2 (1990) 1223.
- 1.40. J. Dormann, "Ordered and disordered states in magnetically diluted insulating system", *Hyperfine Interactions* 68 (1991) 47.
- 1.41. A. Balayachi, J. L. Dormann, and M. Nogues, "Critical analysis of magnetically semi-disordered systems: critical exponents at various transitions", *J. Phys.: Condens. Matter* 10 (1998) 1599.
- 1.42. S. C. Bhargav and N. Zeeman, "Mössbauer study of $\text{Ni}_{0.25}\text{Zn}_{0.75}\text{Fe}_2\text{O}_4$. II. Noncollinear spin structure", *Phys. Rev. B* 21 (1980) 1726.
- 1.43. Y. Yafet and C. Kittel, "Antiferromagnetic arrangements in ferrites", *Phys. Rev.* 87 (1952) 290.
- 1.44. K. H. J. Buchow, *Handbook of Magnetic Materials*, Vol. 8, Elsv. Sci, 1995, 189.
- 1.45. G. Toulouse, *Commun. Phys.* 2 (1977) 115.
- 1.46. V. Cannella and J. A. Mydosh, "Magnetic ordering in gold-iron alloys", *Phys. Rev. B* 6 (1972) 4220.
- 1.47. M. A. Ahmed and M. H. Wasfy, "Effect of charge transfer behavior on the dielectric and ac conductivity of Co-Zn ferrite doped with rare earth element" *Indian J. Pure. Appl. Phys.* 41(2003)713.
- 1.48. T. M. Meaz, S. M. Attia and A. M. Abo El Ata, "Effect of tetravalent ions substitution on the dielectric properties of Co-Zn ferrites" *J. Magn. Magn. Mater.*, 257 (2003)296.
- 1.49. P. N. Vasambekar, C. B. Kolckar and A.S. Vaingankar, "Cation distribution and susceptibility study of Cd-Co and Cr^{3+} substituted Cd-Co ferrites" *J. Magn. Magn. Mater.*, 186 (1998)333.

- 1.50. O. M. Hemeda and M. M. Barakat, "Effect of hopping rate and jump length of hopping electrons on the conductivity and dielectric properties of Co-Cd ferrite" *J. Magn. Magn. Mater.*, 223 (2001)127.
- 1.51. Kwang Pyo Chae, Young bae Lee, Jae Gwang Lee and Sung Ho Lee, "Crystallographic and magnetic properties of $\text{CoCr}_x\text{Fe}_{2-x}\text{O}_4$ ferrite powders" *J. Magn. Magn. Mater.*, 220(2000)59
- 1.52. Seung Wha Lee, Sung Yong An and Chul Sung Kim, "Atomic migration in $\text{CoIn}_{0.1}\text{Fe}_{1.9}\text{O}_4$ ", *J. Magn. Magn. Mater.* 226-230(2001)1403.
- 1.53. C. B. Kolekar, P. N. Kamble, A. S. Vaingankar, *Ind. J. Phys.* A68 (6) (1994) 529.
- 1.54. J. C. G. Btinzli, G. R. Choppin, Lanthanide probes in life, Chemical and Earth Sciences. Theory and practice, Elsevier, Amsterdam, 1989.
- 1.55. N. Rezlescu, E Rezlescu, C Pasnicu and M L Craus, "Effect of the rare-earth ions on some properties of a nickel-zinc ferrite" *J. Phy. Condens. Matter* 6 (1994) 5707.
- 1.56. Mansour Al-Hal, "Structural characterization and magnetization of $\text{Mg}_{0.7}\text{Zn}_{0.3}\text{Sm}_x\text{Fe}_{2-x}\text{O}_4$ ferrites" *J. Magn. Magn. Mater.* 299 (2006) 435.
- 1.57. A. M. M. Farea, Shatendra Kumar, Khalid Mujasam Batoo, Ali Yousef, Alimuddin. "Influence of frequency, temperature and composition on electrical properties of polycrystalline $\text{Co}_{0.5}\text{Cd}_x\text{Fe}_{2.5-x}\text{O}_4$ ferrites", *Physica B*, 403 (2008) 684.
- 1.58. A. A. Ghani, A. A. Sattar and J. Pierre, "Composition dependence of Magnetization in $\text{Co}_{1-x}\text{Cd}_x\text{Fe}_2\text{O}_4$ ferrites", *J. Magn. Magn. Mater.* 97 (1991)141.
- 1.59. M. Bhagavantha Reddy and P. Venugopal Reddy, "Low-frequency dielectric behavior of mixed Li-Ti ferrites", *J. Phys. D : Applied Phys.* 24 (1991)975.
- 1.60. H. Mohan, I.A. Shaikh, R.G. Kulkarni, "Magnetic properties of the mixed spinel $\text{CoFe}_{2-x}\text{Cr}_x\text{O}_4$ " *Physica B* 217 (1996)292.
- 1.61. A. R. Shitre, V. B. Kawade, G. K. Bichile, K.M. Jadhav", "X-ray diffraction and dielectric study of $\text{Co}_{1-x}\text{Cd}_x\text{Fe}_{2-x}\text{Cr}_x\text{O}_4$ ferrite system", *Materials Letters* 56 (2002) 188.
- 1.62. M. A. Ahmed, "Electrical properties of Co-Zn ferrites", *phys. stat. sol.(a)* 111 (1989)567.
- 1.63. P. B. Pandya, H.H. Joshi, R. G. Kulkarni, "Bulk magnetic properties of Co-Zn ferrites prepared by the Co-precipitation method" *J. materials Science* 26 (1991) 5509.
- 1.64. M. Manjurul Haque, M. Huq, M. A. Hakim, "Effect of Zn^{2+} substitution on the magnetic properties of $\text{Mg}_{1-x}\text{Zn}_x\text{Fe}_2\text{O}_4$ ferrites" *Phycica B*, 404 (2009) 3915.
- 1.65. O. M. Hemeda "Structural and magnetic properties of $\text{Co}_{0.6}\text{Zn}_{0.4}\text{Mn}_x\text{Fe}_{2-x}\text{O}_4$ " *Turk J Phys.*, 28 (2004)121.
- 1.66. A. K. M. Akther Hossain, S. T. Mahmud, M. Seki, T. Kawai and H. Tabata, "Structural, electrical transport and magnetic properties of $\text{Ni}_{1-x}\text{Zn}_x\text{Fe}_2\text{O}_4$ ", *J. Magn. Magn. Mater.* 312 (2007) 210.
- 1.67. R. N. Bhowmik, R. Ranganathan, "Cluster glass behavior in $\text{Co}_{0.2}\text{Zn}_{0.8}\text{Fe}_{2-x}\text{Rh}_x\text{O}_4$ ($x = 0.0-1.0$)", *J.Magn. Magn Mater.* 237 (2001)27.
- 1.68. Jingjing sun, Jianbao Li, Geliang Sun, "Effects of La_2O_3 and Gd_2O_3 on some properties of Ni-Zn ferrite," *J.Magn. Magn. Mater.* 250 (2002) 20.
- 1.69. A. A. Sattar, "Temperature dependence of the electrical resistivity and thermoelectric power of rare earth substituted Cu-Cd ferrite", *Egypt. J. Sol.* 26(2) (2003)113.
- 1.70. S. S. Bellad, S. C. Watawe, B. K. Chougule, "Microstructure and permeability studies of mixed Li-Cd ferrites", *J. Magn. Magn. Mater.* 195(1999) 57.

- 1.71. M. Manjurul Haque, M. Huq and M. A. Hakim, "Thermal Hysteresis of permeability and Transport Properties of Mn-substituted Mg-Cu-Zn Ferrites", *Journal of Physics D: Applied Physics* 41(2008) 055007.
- 1.72. R. V. Upadhyay, S. N. Rao and R. G. Kulkarni, "Yafet-Kittel type of magnetic ordering in Mg-Cd ferrites", *Mater. Lett.* 3(7,8) (1985) 273.
- 1.73. N. S. Satya Murthy, M. G. Natera, S. I. Youssef, R. J. Begum and C. M. Srivastava, "Yafet-Kittel angles in zinc-nickel ferrites", *Phys. Rev.* 181 (1969) 969.
- 1.74. Mazen, S. F. Mansour and H. M. Zaki, "Some physical and magnetic properties of Mg- Zn ferrites", *Cryst. Res. Technol.* 38(6) (2003) 471.
- 1.75. Mazhar U. Rana, Misbah-Ul-Islam, Ishtiaq Ahmad and Tahir Abbas, "Determination of magnetic properties and Y-K angles in Cu-Zn-Fe-O system", *J. Magn. Magn. Matter.* 187 (1998) 242.
- 1.76. D. Ravinder, A. V. Ramana Reddy and G. Ranga Mohan, "Abnormal dielectric behavior in polycrystalline zinc-substituted manganese ferrites at high frequencies", *Mater. Lett.* 52 (2002) 299.
- 1.77. A. K. M. Zakaria, M. A. Hakim, M. A. Asgar, "Effect of substitution of Al for Fe on the magnetic phase transition and initial permeability of Zn- Co ferrites" *J. Bangladesh Academy of Sci.* 32(2008)1
- 1.78. B. R. Karche, B.V. Khasbardar and A.S Vaingankar, "X-ray, SEM and magnetic propertie of Mg-Cd ferrites" *J. Magn. Magn. Matter* 168 (1997) 292.
- 1.79. L. Zhao, Y. Cui, H. Yang, L. Yu, W. Jin, S. Feng, *Mat. Lett.* 60 (2006) 104.

CHAPTER-II

- 2.1. B. Jeyadevan, C. N. Chinnasamy, K. Shinoda, K. Tohji, "Mn-Zn ferrite with higher magnetization for temperature sensitive magnetic fluid", *J Appl. Phys.*, vol. 93(2003) pp. 8450.
- 2.2. Fowler, Michael, "Historical Beginnings of Theories of Electricity and Magnetism". Retrieved 2008.
- 2.3. Vowles, P. Hugh "Early Evolution of Power Engineering". *Isis (University of Chicago Press)* 17 (2): (1932) 412.
- 2.4. Kip Thorne, *Spacetime Warps and the Quantum: A Glimpse of the Future*, ITP & CalTech, 1999.
- 2.5. N. Spaldin *Magnetic materials: Fundamentals and device applications* Cambridge: Cambridge University press, 2003.
- 2.6. William D. Callister, *The University of Utah; Materials Science and Engineering* 6th ed., Wiley 2003.
- 2.7. D. Hadfield, *Lliffe Books, LTD, London, John Wiley and Sons, "Permanent magnets and Magnetism", Inc., New York, 1961.*
- 2.8. Rollin j. parker and Robertj. Studders, *john Wiley and Sons, "Permanent magnets and Their Applications", Inc., New York, 1962.*
- 2.9. Rollinj. Parker, *John Wiley and sons, "Advances in permanent Magnetism", Inc., New York, 1990.*
- 2.10. Malcolm McCaig, *John Wiley and Sons, "Permanent magnets in Theory and Practice", Inc., Toronto, 1977.*
- 2.11. D. S. Parasnis, *Harper and Brothers, "Magnetism: From Lodestone to polar Wandering", New York, 1961.*
- 2.12. J. Smit, *H. P. J. Wijn. Ferrites, John Wiley and Sons, New York, (1959).*

- 2.13. J. D. Livingston, *Driving Forces. The Natural Magic of Magnets*: Harvard University Press: Cambridge, (1996).
- 2.14. E. H. Frei. S. Shtrikman, D. Treves. *Phys. Rev.*, 106(1957)446.
- 2.15. B. D. Cullity, *Introduction to Magnetic Materials*, Addison-Wesley Publishing Com., 1972.
- 2.16. Alex Goldman, "Modern Ferrite Technology" Van nostrand Reinhold New York, 1990.
- 2.17. C. W. Chen, *Magnetism and Metallurgy of Soft Magnetic Materials*, New York (1977).
- 2.18. D. J. Craik, 1957, *Magnetic Oxide*, part I, John Wiley and Sons, Ltd, Bristol England.
- 2.19. E. J. W. Verway and E. L. Heilmann, *J. Chem. Phys.* 15(4), (1947), 174.
- 2.20. F. C. Romeign, *Philips Res. Rep.* 8, NR-5 (1953), 304.
- 2.21. J. Smit and W. J. P. Wijn, *Ferrites*, Philips Technical Library (Wiley, New York, (1959).
- 2.22. B. Viswanathan, VRK Murthy, "Ferrite Materials Science and Technology", Spring Verlag, Noarsa Publishing House, New Delhi, (1990).
- 2.23. S. Krupicka and P. Novak. *Oxide spinels*. In E. P. Wohlfarth, editor, *Ferromagnetic Materials*, volume 3, chapter 4, pages 189-304. North-Holland, The Netherlands, 1982.
- 2.24. Y. Yafet and C. Kittel, "Antiferromagnetic arrangements in ferrites", *Phys. Rev.* 87 (1952) 290.
- 2.25. M. Gabay and G. Toulouse, "Coexistence of spin-glass and ferromagnetic orderings", *Phys. Rev. Lett.* 47 (1981) 201.
- 2.26. M. A. Moore and A. J. Brag, "Critical behaviour at the spin glass transition in a magnetic field", *J. Phys. C* 15 (1982) L301.
- 2.27. Johan Mattsson, "Dynamics of random magnets", Ph.D. thesis, Uppsala University, Sweden, 1994.
- 2.28. M. Mezard, G. Parisi, and M. A. Virasoro, *Spin Glass Theory and Beyond* (World Scientific, Singapore, (1987).
- 2.29. J. A. Mydosh, *Spin Glasses-An Experimental Introduction*, Taylor and Francis (London) 1993.
- 2.30. L. W. Bernardi, H. Yoshino, K. Hukushima, H. Takayama, A. Tobo, and A. Ito, "Aging of the zero-field-cooled magnetization in Ising spin glasses: experiment and numerical simulation.", *Phys., Rev. Lett.* 86 (2001) 720.
- 2.31. H. Yoshino, A. Lemaître, and J.-P. Bouchaud, "Multiple domain growth and memory in the droplet model for spin-glasses.", *Eur. Phys. J. B* 20 (2001) 367.
- 2.32. C. Djurberg, K. Jonason, and P. Nordblad, "Magnetic relaxation phenomena in a CuMn spin glass", *Eur. Phys. J. B.* 10 (1999) 15.
- 2.33. T. Jonsson, K. Jonason, P. Jönsson, and P. Nordblad, "Nonequilibrium dynamics in a three-dimensional spin glass", *Phys. Rev. B* 59 (1999) 8770.
- 2.34. K. Jonason, P. Nordblad, E. Vincent, J. Hammann, and J.-P. Bouchaud, "Memory interference effects in spin glasses", *Eur. Phys. J. B.* 13 (2000) 99.
- 2.35. V. Dupuis, E. Vincent, J.-P. Bouchaud, J. Hammann, A. Ito, and H. Aruga Katori, "Aging, rejuvenation, and memory effects in Ising and Heisenberg spin glasses", *Phys. Rev. B* 64 (2001) 174204.
- 2.36. P. Nordblad, "Spin glasses: model systems for non-equilibrium dynamics", *J. Phys.: Condens Matter* 16 (2004) S715.
- 2.37. A. A. Samokhvalov and A. G. Rustamov, *Sov. Phys. Solid State*, 6 (1964) 749.
- 2.38. A. J. Bossmann and C. Crevecoeur, "Mechanism of the electrical conduction in Li-doped NiO", *Phys. Rev.* 144 (1966) 763.
- 2.39. G. H. Jonker, J. H. Van Santen, "Magnetic compounds with perovskite structure III. ferromagnetic compounds of cobalt", *Physica* 19 (1953) 120.

CHAPTER-III

- 3.1. L. B. Kong, Z. W. Li, G. Q. Lin and Y. B. Gan, "Magneto-dielectric properties of Mg-Cu-Co ferrite ceramics: II. Electrical, dielectric and magnetic properties", *J. Am. Ceram. Soc.* 90(7) (2007) 2104.
- 3.2. S. K. Sharma, Ravi Kumar, Shalendra Kumar, M. Knobel, C. T. Meneses, V. V. Siva Kumar, V. R. Reddy, M. Singh and C. G. Lee, "Role of interparticle interactions on the magnetic behaviour of $Mg_{0.95}Mn_{0.05}Fe_2O_4$ ferrite nanoparticles", *J. Phys.: Condens. Matter* 20 (2008) 235214.
- 3.3. Soilah Zahi, Mansor Hashim and A. R. Daud, "Synthesis, magnetic and microstructure of Ni-Zn ferrite by sol-gel technique", *J. Magn. Magn. Mater.* 308 (2007) 177.
- 3.4. M. A. Hakim, D. K. Saha and A. K. M. Fazle Kibria, "Synthesis and temperature dependent structural study of nanocrystalline Mg-ferrite materials", *Bang. J. Phys.* 3 (2007) 57.
- 3.5. A. Bhaskar, B. Rajini Kanth and S. R. Murthy, "Electrical properties of Mn added Mg-Cu-Zn ferrites prepared by microwave sintering method", *J. Magn. Magn. Mater.* 283 (2004) 109.
- 3.6. Zhenxing Yue, Ji Zhou, Longtu Li, and Zhilun Gui, "Effects of MnO_2 on the electromagnetic properties of Ni-Cu-Zn ferrites prepared by sol-gel auto-combustion", *J. Magn. Magn. Mater.* 233 (2001) 224.
- 3.7. P. Reijnen, 5th Int. Symp. React. In Solids (Elsevier, Amsterdam) (1965) p-562.
- 3.8. C. W. Chen, *Magnetism and Metallurgy, Soft Mag. Mat.*, North-Holland Pub.Com. (1977).
- 3.9. C. Kittel, *Introduction to Solid State Physics*, 7th edition, John Wiley and sons, Inc., Singapore (1996).
- 3.10. J. B. Nelson, D. P. Riley, "An experimental investigation of extrapolation methods in the derivation of accurate unit-cell dimensions of crystals", *Proc. Phys. Soc. London* 57 (1945) 160.
- 3.11. Tahir Abbas, M.U Islam, and M.Ashraf Ch., *Mod. Phy.Letts.B*, 9(22), (1995), 1419.
- 3.12. J. Smit and H. P. J Wijn, *Ferrites*, Wiley, New York, (1959)250.

CHAPTER-IV

- 4.1. V. A. M. Brabers-Progress in Spinel Ferrite Research in Handbook of Magnetic Materials, Edited by K. H. J. Buchow, North Holland Publishing Inc. 8 (1995)189.
- 4.2. J. L. Dormann, M. Nogues, "Magnetic structures of substituted ferrites", *J. Phys.: Condens. Matter* 2 (1990) 1223.
- 4.3. A. Belayachi, J. L. Dormann and M. Nogues, "Crystal analysis of magnetically semi-disordered systems: critical exponents at various transitions", *J. Phys.: Condens. Matter* 10 (1998) 1599.
- 4.4. A. Goldman, "Modern Ferrite Technology", Van Nostrand.Reinhold, New York,1990.
- 4.5. P. N. Vasambekar, C. B. Kolekar, A. S.Vaingankar, "Magnetic behaviour of Cd^{2+} and Cr^{3+} substituted cobalt ferrites", *J. Mater. Chem. Phys.*, 60 (1999)282.
- 4.6. A. M. Samy, H. M. E. LSayed, A. A.Sattar, *Phy.stat.Sol.(a)*.200(2) (2003) 401.
- 4.7. A. A. Ghani, A. A. Sattar and J. Pierre, "Composition dependence of magnetization in $Co_{1-x}Cd_xFe_2O_4$ ferrites", *J. Magn. Magn. Mater.*, 97 (1991)141.
- 4.8. A. H. Wafik, A. A. Sattar, "Depending of the Irreversible Magnetization $Co_{1-a}Cd_aFe_2O_4$ on the Magnetization field" *Physica. Status. Solidi (a)* 117 (1990) K61.

- 4.9. R. G. Kulkarni and V. G. Panicker, "Study of canted spin structure in Cu-Cd ferrites", *J. Mater. Sci.* 19 (1984) 890.
- 4.10. J. B. Nelson, D. P. Riley, "An experimental investigation of extrapolation methods in the derivation of accurate unit-cell dimensions of crystals", *Proc. Phys. Soc. London* 57 (1945) 160.
- 4.11. L. Vegard, "Die konstitution der mischkristalle und die raumfullung der atome", *Z. Phys.* 5 (1921)17.
- 4.12. O. M. Hemida, M. M. Barakat, "Effect of hopping rate and jump length of hopping electrons on the conductivity and dielectric properties of Co-Cd ferrite" *J. Magn. Magn. Mater.*, 223 (2001)127.
- 4.13. A. R. Shitre, V. B. Kawade, G. K. Bichile, K. M. Jadhav, " X-ray diffraction and dielectric study of $\text{Co}_{1-x}\text{Cd}_x\text{Fe}_{2-x}\text{Cr}_x\text{O}_4$ ferrite system", *Materials Letters* 56 (2002)188.
- 4.14. A. Globus, H. Pascard and V. Cagan, "Distance between magnetic ions and fundamental properties in ferrites", *J. Phys.*, 38 (1977)C1-163.
- 4.15. A. M. Abdeen, O. M. Hemeda, E. E. Assem, M. M. El-Sehly, "Structural, electrical and transport phenomena of Co ferrite substituted by Cd", *J. Magn. Magn. Mater.* 238 (2002) 75.
- 4.16. S. A. Patil, V. C. Mahajan, A. K. Ghatage, S. D. Lotke, "Structure and magnetic properties of Cd and Ti/Si substituted cobalt ferrites", *Materials Chemistry and Physics* 57 (1998) 86.
- 4.17. A. Goldman, "Hand book of Modern Ferromagnetic Materials", Kulwer Academic Publishers, Boston,USA, 1999.
- 4.18. G. C. Jain, B . K. Das, R. S. Khanduja and S. C. Gupta, "Effect of intragranular porosity of initial permeability and coercive force in a manganese zinc ferrite", *J. Mater. Sci, II* (1976) 1335
- 4.19. S. Chikazumi, "Physics of Magnetism", John wiley andv sons, Inc, New York, 1966.
- 4.20. M. Srivastava, S. N. Shringi, R. G. Srivastava and N. G. Nandikar, "Magnetic ordering and domain-wall relaxation in zinc-ferrous ferrite", *Phys. Rev B* 14 (1976) 2032.
- 4.21. M. Rajendran, R. C. Pullar, A. K. Bhattacharya, D. Das, S. N. Chintalapudi and C.K. Majumdar, "Magnetic properties of nanocrystalline CoFe_2O_4 powders prepared at room temperature: variation with crystallite size". *J. Magn. Magn. Mater.*, 232 (2001) 71.
- 4.22. J. Smit, H. P. J. Wijn, *Ferrites*, Wiley, New York, 1959, P.157.
- 4.23. Wang Li and Li Fa-Shen "Structural and magnetic properties of $\text{Co}_{1-x}\text{Zn}_x\text{Fe}_2\text{O}_4$ nanoparticles" *Chinese Phys. B*, 17(5) (2008)1858.
- 4.24. F. G. Brockman, P.H. Dowling and W.G. Steneck, "Dimensional effects resulting from a high dielectric constant Found in a ferromagnetic ferrite", *Phys. Rev.* 77 (1950) 85.
- 4.25. Y. Bai, J. Shou, Z. Gui, Z. Yue, L. Li, *J. Magn. Magn. Mater.* 264 (2003) 44.
- 4.26. T.Nakamura, "Low temperature sintering of Ni-Zn-Cu ferrite and its permeability spectra", *J. Magn. Magn. Mater.*, 168(1997) 285.
- 4.27. J. J. Shrotri, S. D. Kulkarni, C. E. Deshpande, S. K. Date, *Mater. Chem. Phys.* 59(1999)1.
- 4.28. Ana Maria Rangel de Figueiredo Teixeira, Tsuneharu Ogasawara, Maria Cecilia de Souza Nobrega," Investigation of Sintered Cobalt-Zinc Ferrite Synthesized by Coprecipitation at Different Temperatures: A Relation between Microstructure and Hysteresis Curves" *Materials Research*, Vol. 9(3) (2006)257.
- 4.29. J. Smit, *Magnetic properties of Materials*, Mcgraw Hill Book Co. (1971) p89.
- 4.30. L. Neel, *Aun, De Phys*, 3(1948)137.
- 4.31. Y. Yafet and C. Kittel, "Antiferromagnetic arrangement in ferrites", *Phys. Rev.* 87(1952)290.
- 4.32. C. E. Patton, Y. Liu, "Localized canting models for substituted magnetic oxides", *J. Phys. C : Solid State Phys.* 16(1983)5995.

4. 33. N. S. Satya Murthy, M. G. Natera, S. Youssef, R. J. Begum, C. M. Srivastava, "Yafet-Kittle angles in Zinc-nicle ferrites", *Phys., Rev.* 181(1969) 4412.
4. 34. S. Geller, "Comments on "Molecular-Field Theory for Randomly Substituted Ferrimagnetic Garnet Systems" by I. Nowik", *Phys. Rev.* 181(1969)980.
4. 35. S. S. Bellad, and B. K. Chougule, "Structural and magnetic properties of some mixed Li-Cd ferrites", *Mater. Chem.phys.* 52(1998)166.
4. 36. S. S. Bellad, S. C. Watawe, and B. K. Chougule, "Microstructure and permeability studies of mixed Li-Cd ferrites", *J.Magn. Magn. Mater.*, 195 (1999)57.
4. 37. S. S. Bellad, and B. K. Chougule, "Microstructure-dependent magnetic properties of Li-Cd ferrites" *Mater. Res. Bull.* 33(8) (1998)1165.
4. 38. A. M. Sankpal, S. R. Sawant, A.S. Vaingankar, I. J. Pure, *Appl. Phys.* 26(1988) 459.
4. 39. A. M. Shaikh, S.S.Bellad, B. K. Chougule, *J. Magn. Magn. Mater.* 195(1999)384.
4. 40. M. A. E. Hiti, A. I. E. Shora, S. M. Hammad, *Mter. Sci. Tech.* 13(1997) 625.
4. 41. A, Globus, P. Duplex, "Effective Anisotropy in Polycrystalline Materials. Separation of Components", *J. Appl. Phys.* 39 (1968) 727.
4. 42. Nutan Gupta, S. C. Kashyap and D. C. Dube, "Dielectric and magnetic properties of citrate-route-processed Li-Co spinel ferrites", *Phys. Stat. Solidi (a)* 204(7) (2007) 2441.
4. 43. C. B. Kolekar, P. N. Kamble, S. G. Kulkarni and A. S. Vaingankar, "Effect of Gd^{3+} substitution on dielectric behaviour of copper-cadmium ferrites", *J. Mater. Sci.* 30 (1995) 5784.
4. 44. Zhenxing Yue, Zhou Ji, Zhilun Gui, and Longtu Li, "Magnetic and electrical properties of low-temperature sintered Mn-doped NiCuZn ferrites", *J. Magn. Magn Mater.* 264 (2003) 258.
4. 45. S. S. Bellad, and B. K. Chougule, "Composition and frequency dependent dielectric properties of Li-Mg-Ti ferrites", *Mater.s Chem.Phys.* 66 (2000) 58.
4. 46. A. Bhaskar, B. Rajini Kanth, S. R. Murthy, "Electrical properties of Mn added MgCuZn ferrites prepared by microwave sintering method", *J. Magn. Magn. Mater.* 283 (2004) 109.
4. 47. Zhenxing Yue, Zhou Ji, Longtu Li, Xiaolui Wang and Zhilun Gui, "Effect of copper on the electromagnetic properties of Mg-Zn-Cu ferrites prepared by sol-gel auto-combustion method", *Mater. Sci EngB* 86 (2001) 64.
4. 48. K. Iwauchi, "Dielectric Properties of Fine Particles of Fe_3O_4 and Some Ferrites", *Jpn. J. Appl. Phys.* 10 (1971)1520.
4. 49. C. G. Koops, "On the Dispersion of Resistivity and Dielectric Constant of Some Semiconductors at Audiofrequencies", *Phys. Rev.* 83 (1951) 121.
4. 50. Maxwell J 1873 *Electricity and Magnetism*, Vol.1, Oxford University Press, London.
4. 51. Wangner K 1913 *Ann. Phys.* 40 817.
4. 52. P. Venugopal Reddy, T. Seshagiri Rao, "Dielectric behaviour of mixed Li-Ni ferrites at low frequencies", *J. Less Common Met.* 86 (1982) 255.
4. 53. B. Kumar Kunar, G. Srivastava, "Dispersion observed in electrical properties of titanium-substituted lithium ferrites", *J. Appl. Phys.* 75 (1994) 6115

CHAPTER-V

- 5.1. G. A. Pettit, D. W. Forester, "Mossbauer Study of Cobalt-Zinc Ferrites" *Phys. Rev.* B4(1971)3912.
- 5.2. R.G. Kulkarni, V. U. Patil, "Magnetic ordering in Cu-Zn ferrite" *J. Mater. Sci.* 17 (1982) 843.
- 5.3. V. A. M. Brabers, in. K. H. Buschow (edition), "Handbook of magnetic materials", 8(1995)189.
- 5.4. A. Goldman, *Modern Ferrite Technology*, Van Nostrand.Reinhold, New York,1990.

- 5.5. R. G. Kulkarni, V. U. Patil, "Magnetic ordering in Cu-Zn ferrite", *J. Mater. Sci.* 17 (1982) 843.
- 5.6. N. S. Satya Murthy, M.G. Natera, S. I. Youssef, R. J. Begum, C. M. Srivastava, "Yafet-Kittel angles in zinc-nickel ferrites", *Phys. Rev.* 181(2) (1969)969.
- 5.7. M. Manjurul Haque, M. Huq, M. A. Hakim, "Effect of Zn²⁺ substitution on the magnetic properties of Mg^{1-x}Zn_xFe₂O₄ ferrites" *Physica B*, 404 (2009) 3915.
- 5.8. R. N. Bhowmik, R. Ranganathan, "Anomaly in cluster glass behavior of Co_{0.2}Zn_{0.8}Fe₂O₄ spinel oxide" *J. Magn. Magn. Mater* 248(2002)101.
- 5.9. A. M. samy, H. M. E. LSayed, A. A. Sattar, *Phy. stat. Sol.(a)*.200(2)(2003)401.
- 5.10. A. Globus, H. Pascard and V. Cagan, *J. de. Phys*38 (1977)C1-163.
- 5.11. J. Smit, H.P.J. Wijn, *Ferrites*, Wiley, New York, 1959, P.157.
- 5.12. M.M. Girigis, Awad A. Mel. *Mater. Chem. Phys.* 36(1993)48.
- 5.13. M. Gulliot, J. Ostoreso, A. Merch and Z. Phy, *B. Condensed Matter* 71(1988)193.
- 5.14. A. H. Wafik, A. A.Satter, *Phy. Stat. solidi A*117 (1990) K61.
- 5.15. J. M. Daniels and A. Rosencwaig, "Mossbauer study of the Ni-Zn ferrite system", *Can. J. Phys.* 48 (1970) 381.
- 5.16. C. M. Srivastava, S. N. Shringi, R. G. Srivastava and N. G. Nandikar, "Magnetic ordering and domain-wall relaxation in zinc-ferrous ferrite", *Phys. Rev B* 14 (1976) 2032.
- 5.17. H. H. Joshi, R .G. Kulkurni, *J. Mater. Sci.* 21(1986)2138.
- 5.18. R. B. Pujar, S. S. Bellad, S. C. Watawe and B. K. Chougule, "Magnetic properties and microstructure of Zr⁴⁺ substituted Mg-Zn ferrites", *J.Mater. Chem. and Phys.* 57 (1999) 264.
- 5.19. B. D. Cullity, "Elements of X-ray diffraction" 2nd edition, Addison Wesley publishing Co., USA, (1978).
- 5.20. A, K. Nikumbh, A.V. Nagawade, V. B. Tadke, P.P.Bakare, *J. Mater. Sci.* 36 (2001)653.
- 5.21. S. T. Alone and K. M. Jadhav, "Structural and magnetic properties of Zinc and aluminum-substituted cobalt ferrite prepared by Co-precipitation method", *Indian Academy of Sciences* 70(2008)173.
- 5.22. S. A. Mazen, S. F. Mansour and H. M. Zaki, "Some physical and magnetic properties of Mg-Zn ferrite", *Cryst. Res. Technol.* 38 (6) (2003) 471.
- 5.23. H. H. Joshi, R. G. Kulkarni, R. V. Upadhyay, *Ind. J. Phys. A* 65(4) (1991) 310.
- 5.24. B. P. Ladgaonkar, P. N. Vasambekar, A. S. Vaingankar, " Effect of Zn²⁺ and Nd³⁺ substitution on magnetisation and AC susceptibility of Mg ferrite", *J. Magn. Magn Mater* 210 (2000) 289.
- 5.25. R.G. Kulkarni and V. U. Patil, "Magnetic ordering in Cu-Zn ferrite" *J. Mater. Sci.* 17(1982)843.
- 5.26. Wafaa Bayoumi, "Structural and electrical properties of zinc- substituted cobalt ferrite" *J. Mater. Sci.* 42(2007)8254.
- 5.27. M.A Ahmed, "Electrical properties of Co-Zn ferrites" *phys. stat. sol.(a)* 111, 567(1989).
- 5.28. G. Chandrasekaran and P. Nimy Sebastian, "Magnetic study of Zn_xMg_{1-x}Fe₂O₄ mixed ferrites", *Materials Letters* 37 (1998) 17.
- 5.29. A.K.M. Akther Hossain, H. Tabata, T. Kawai, "Magnetoresistive properties of Zn_{1-x}Co_xFe₂O₄ ferrites", *J. Magn. Magn Mater* 320 (2008) 1157.
- 5.30. Misbah-ul-Islam, M. Ashraf Chaudhry, T. Abbas, M. Umar, "Temperature dependent electrical resistivity of Co-Zn-Fe-O system", *J.Mater. Chem. and Phys.* 48 (1997) 227.
- 5.31. Anjali Verma, Ratnamala Chatterjee " Effect of Zinc concentration on the structural, electrical and magnetic properties of mixed Mn-Zn and Ni- Zn ferrites synthesized by the citrate precursor technique" *J. Magn. Magn Mater* 306 (2006) 313.
- 5.32. E. C. Snelling, "Soft ferrites: Properties and Applications", Iliffe Books Ltd., London., 1969.

- 5.33. A. M. Abdeen, "Electric conduction in Ni-Zn ferrites", *J. Magn. Magn. Mater.*, 185(1998) 199.
- 5.34. A. Globus, P. Duplex, "Effective Anisotropy in Polycrystalline Materials Separation of Components", *J. Appl. Phys.* 39 (1968) 727.
- 5.35. A. R. Shitre, V.B.Kawade, G.K.Bichile, K.M. Jadhav *Materials Letters* 56 (2002) 188.
- 5.36. J. J. Shrotri, S. D. Kulkarni, C. E. Deshpande, A. Mitra, S. R. Sainkar, P. S. Anil Kumar, S. K. Date, *Mat. Chem. Phys.* 59 (1999)1.
- 5.37. L. Neel, *J. Phys. Radium* 12(1959)258.
- 5.38. Y. Yafet and C. Kittel, *Phys. Rev. B* 4 (1971) 3912.
- 5.39. M. A. El Hiti, "DC conductivity for $Zn_xMg_{0.8-x}Ni_{0.2}Fe_2O_4$ ferrites", *J. Magn. Magn. Mater.* 136 (1994) 138.

CHAPTER-VI

- 6.1. Gorter E W C. R. Acad. Sci., Paris 230 (1950) 192.
- 6.2. Guillaud C and Creveaux H 1950 C. R. Acad. Sci., Paris 230(1950)1458.
- 6.3. Neel L *Phys. Rad.* 9 (1948) 184.
- 6.4. C. E Patton and Y. Liu, "Localised canting models for substituted magnetic oxides", *J. Phys. C: Solid state Phys.* 16 (1983) 5995.
- 6.5. J. L. Dormann and M. Nogues, "Magnetic structures in substituted ferrites", *J. Phys. Condens. Matter* 2 (1990) 1223.
- 6.6. Y. Yafet and C. Kittel, "Antiferromagnetic arrangements in ferrites", *Phys. Rev* 87(1952) 290.
- 6.7. Gelles, *Phys. Rev.* 181(1969) 980.
- 6.8. Gellers, Williams H. J. Sherwood RC and Espinosa GP 1962 *J. Appl. Phys* 33s1195.
- 6.9. K. H. Fisher and J. A. Hertz, *Spin Glasses*, Cambridge University Press, Cambridge, 1991.
- 6.10. B. H. Verbeek, G. J. Nievwenhuys, H. Stocker, and J. A. Mydosh, *Phys. Rev. Lett.* 40, 586 (1978).
- 6.11. C. Y. Haung, "Some experimental aspects of spin glasses" A review., *J. Magn. Magn. Mater* 51 (1985)1.
- 6.12. J. L. Soubeyroux, D. Fiorani and E. Agostinelli, "Spin-glass behavior in cobalt oxyspinel $CoGa_2O_4$ ", *J. Magn. Magn. Mater* 54-57(1986)83.
- 6.13. M. A. Hakim, M. Manjurul Haque, Sk. Manjura Hoque, M. Huq and P. Nordblad "Re-entrant spin glass and spin glass behavior of diluted Mg-Zn ferrites". *AIP conf. Proc* (2008) 295, ICMM 2007.
- 6.14. K. Kamazawa, Y. Tsunoda, H. Kadowaki and K. Kohn, "Magnetic neutron scattering measurements on a single crystal of frustrated $ZnFe_2O_4$ ", *Phys. Rev. B* 68 (2003) 024412.
- 6.15. T. Usa, K. Kamazawa, H. Sekiya, S. Nakamura, Y. Tsunoda, K. Kohn and M. Tanaka, "Magnetic Properties of $ZnFe_2O_4$ as a 3-D Geometrical Spin Frustration System", *J. Phys. Soc. Jpn.* 73 (2004) 2834.
- 6.16. A. Ray, R. N. Bhowmik, R. Rangnathan, A. Roy, J. Ghose and S. Caudhury, "Magnetic ordering in $Fe_{2-x}Zn_xMoO_4$ ($x = 0.1-1$) spinel", *J. Magn. Magn. Mater.* 223 (2007) 39.
- 6.17. J. A. Mydosh, "Disordered magnetism and spin glasses", *J. Magn. Magn. Mater* 157-158 (1996) 606.
- 6.18. R. Mathieu, P. Jonsson, D. N. H. Nam and P. Nordblad, "Memory and superposition in a spin glass", *Phys. Rev. B* 63(9) (2001) 092401.
- 6.19. P. E. Jönsson, R. Mathieu, P. Nordblad, H. Yoshino, H. Aruga Kattri and A. Ito, "Nonequilibrium dynamics of spin glasses: Examination of the ghost domain scenario", *Phys. Rev. B* 70 (2004) 174402.

CHAPTER- VII

- 7.1. L. Ben Tahar, M. Artus, S. Ammar, L. S. Smiri, F. Herbst, M.-J. Vaulay, V. Richard, J.-M. Greneche, F. Villain, F. Fievert "Magnetic properties of $\text{CoFe}_{1.9}\text{RE}_{0.1}\text{O}_4$ nanoparticles (RE = La, Ce, Nd, Sm, Eu, Gd, Tb, Ho) prepared in polyol". *J. Magn. Magn. Mater.* 320 (2008) 3242.
- 7.2. Mansour Al-Haj, "Structural characterization and magnetization of $\text{Mg}_{0.7}\text{Zn}_{0.3}\text{Sm}_x\text{Fe}_{2-x}\text{O}_4$ ferrite", *J. Magn. Magn. Mater.* 299 (2006) 435.
- 7.3. J. Sun, J. Li and G. Sun, *J. Magn. Mater.* 250 (2002), pp. 20-24.
- 7.4. E. Rezlescu, N. Rezlescu and P. D. Popa, *J. Magn. Magn. Mater.* 290/291 (2005), pp. 1001.
- 7.5. A. A. Sattar et al., *Phys. Stat. Sol.* 171 (1999), P.563.
- 7.6. M. H. Mahmoud and A. A. Satter, "Mössbauer study of Cu-Zn ferrite substituted with rare earth ions", *J. Magn. Magn. Mater.*, 277 (2004) 101.
- 7.7. A. A. Satter and K. M. El-Shokrofy, *J. Phys.* IV C1 (1997), P. 245.
- 7.8. R. N. Bhowmik, R. Ranganathan, "Cluster glass behavior in $\text{Co}_{0.2}\text{Zn}_{0.8}\text{Fe}_{2-x}\text{Rh}_x\text{O}_4$ ($x = 0-1.0$)", *J. Magn. Magn. Mater.* 237 (2001)27.
- 7.9. R. N. Bhowmik, R. Ranganathan, R. Nagarajan "Coexistence of spin glass and superpara magnetism with ferrimagnetic order in polycrystalline spinel $\text{Co}_{0.2}\text{Zn}_{0.8}\text{Fe}_{2-x}\text{Ho}_x\text{O}_4$ ", *J. Magn. Magn. Mater.* 299 (2006) 327.
- 7.10. R. N. Bhowmik, R. Ranganathan "Magnetic study on $\text{Co}_{0.2}\text{Zn}_{0.8}\text{Fe}_{2-x}\text{Ga}_x\text{O}_4$ ($x = 0 - 1$) spinel oxide". *J. Magn. Magn. Mater.* 257 (2003) 220.
- 7.11. R. N. Bhowmik, R. Ranganathan "Magnetic properties in rare-earth substituted spinel $\text{Co}_{0.2}\text{Zn}_{0.8}\text{Fe}_{2-x}\text{RE}_x\text{O}_4$ (RE = Dy, Ho and Er, $x = 0.05$), *J. Alloys and compounds*, 326 (2001)128.
- 7.12. M. A. Ahmed, E. Ateia, S. I. El-Dek, "Rare earth doping effect on the structural and electrical properties of Mg-Ti ferrite", *Materials Letters*, 57 (2003) 4256.
- 7.13. E. Melagiriappa, H. S. Jayanna, "Structural and magnetic susceptibility studies of samarium substituted magnesium-zinc ferrites", *J. Alloys and compounds* 482 (2009) 147.
- 7.14. B. Viswanathan, V. R. K. Murthy, *Ferritmaterials*, Narosa Publishing House, New Delhi, 1990, p.5.
- 7.15. N. Rezlescu, E. Rezlescu, C. Pasnicu and M. L. Craus, "Effects of the rare-earth ions on some properties of a nickel- zinc ferrite", *J. Phys. Condens. Matter* 6 (1994) 5707.
- 7.16. P. Gibbs, T. M. Harden, and J. H. Smith, *J. Phys. F: Met. Phys.* 15 (1985) 213.
- 7.17. K. Kirota, Y. Fujimoto, K. Watanabe and M. Sugimura, Private Communication (1986), Central Research Laboratory, Matsushiba Electric & Industrial Co., Ltd., Kadoma, Osaka, Japan.
- 7.18. M. Paulus, *Phys. Stat. Sol.* 2(1962)1325.
- 7.19. J. Dho, W.S. Kim, N. H. Hur, "Re entrant spin glass behavior in Cr- doped perovskite Manganite" *Phys. Rev. Lett.* 89(2002)027202.
- 7.20. J. Gal, I. Year, E. Arbaboff, H. Etedgi, F. J. Litterst, K. Aggarwal, J. A. Pereda, G. M. Kalvius, G. Will, W. Schafer "HoFe₄Al₈: An Unusual spin glass" *Phys. Rev. B* 40 (1989)745.
- 7.21. R. N. Bhowmik, R. Ranganathan, "Super-ferromagnetic" clusters in spinel oxide", *J. Magn. Magn. Mater.* 247(2002)83.
- 7.22. B. N. Figgis, in : G. Wilkinson, Gillard, J. A. MC Cleverty (Eds.), *Comprehensive coordination Chemistry*, I. Pergamon, New york, 1987. p.261.

Publication list

a) International/National Reviewed Journals

1. **Saroaut Noor**¹, S. S. Sikder, M. A. Hakim, "Structural and physical properties of Zn substituted cobalt ferrites", Journal of Engineering Science 02 (2010) 47-52.
2. **Saroaut Noor**¹, M. A. Hakim², S. S. Sikder¹, R. Mathieu³, Per Nordblad³ and S. Manjura Hoque², "Magnetic ordering in $\text{Co}_{0.2}\text{Cd}_{0.8}\text{Ho}_x\text{Fe}_{2-x}\text{O}_4$ ($x = 0.0, 0.05, 0.10$) spinel ferrite" International Conference on Magnetic Materials (ICMM) 2010, Oct 25-29, 2010, Saha Institute of Nuclear Physics, Kolkata, India, Proceedings AIP – 85
3. S. S. Sikder¹, **Saroaut Noor**¹, M. A. Hakim², Per Nordblad³ and Saiduzzaman⁴, "Magnetization behavior and spin canting in diluted $\text{Co}_{1-x}\text{Cd}_x\text{Fe}_2\text{O}_4$ ferrites" International Conference on Magnetic Materials (ICMM) 2010, Oct 25 - 29, 2010, Saha Institute of Nuclear Physics, Kolkata, India. Proceedings AIP - 98.

b) Paper Presented in International and National Conferences /Seminars

1. **Saroaut Noor**, M. A. Hakim, S. S. Sikder, D. K. Saha, A .K .m .Fazle Kibria "Nanometer– sized magnetic spinel oxides : synthesis, characterization and properties" International Physics Conference (BPS) held on May 15 - 17, 2009, BUET, Dhaka, Bangladesh.
2. **Saroaut Noor**, S. S. Sikder ,M. A. Hakim, , D. K. Saha " Structural and physical properties of Zinc substituted Cobalt ferrite" National Conference ,Department of physics ,Chittagong University of Engineering & Technology(CUET), 8 November,2009.
3. **Saroaut Noor**, S. S. Sikder, M. A. Hakim, , D. K. Saha, "Structural, magnetic and electrical properties of Cd substituted Co-ferrite" National Conference ,Department of physics, Chittagong University of Engineering & Technology(CUET), 8 November, 2009.
4. **Saroaut Noor**, M. A. Hakim, S. S. Sikder, Shireen Akhter, Per Nordblad, "Magnetization behavior and magnetic ordering in $\text{Co}_{1-x}\text{Cd}_x\text{Fe}_2\text{O}_4$ ferrites" The third international conference on structure, processing and properties of materials SPPM 2010, 24-26 February 2010, Dhaka, Bangladesh, SPPM-2010.
5. **Saroaut Noor**, S. S. Sikder, M. A. Hakim, Shireen Akhter, R. Mathieu, Saiduzzaman "Effect of Zn on the Magnetic ordering and Y-K angles of $\text{Co}_{1-x}\text{Zn}_x\text{Fe}_2\text{O}_4$ ferrites", international conference on magnetism and advanced materials (ICMAM-2010) March 3-7, 2010.
6. **Saroaut Noor**, M. A. Hakim, S. S. Sikder, Per Nordblad, S. Manjura Hoque, Robiul Islam, "Magnetic ordering and magnetization study of $\text{Co}_{0.2}\text{Cd}_{0.8}\text{Ho}_x\text{Fe}_{2-x}\text{O}_4$ ferrites" international conference on magnetism and advanced materials (ICMAM-2010) March 3-7, 2010 .
7. **Saroaut Noor**, M. A. Hakim, S. S. Sikder, S. Manjura Hoque and Saiduzzaman "Structural and electrical transport properties of $\text{Co}_{1-x}\text{Cd}_x\text{Fe}_2\text{O}_4$ ferrites", international conference on recent advance in physics-2010, Department of Physics, University of Dhaka, March 27-29,2010.
8. **Saroaut Noor**, S. S. Sikder, M. A. Hakim, Shireen Akhter, S. Manjura Hoque, "Composition dependence if some physical and magnetic properties in $\text{Co}_{1-x}\text{Cd}_x\text{Fe}_2\text{O}_4$ ferrites", processing Bangladesh Electronics Society Conference 2010, 2-3 June 2010, P 241-245.

9. Saroat Noor¹, M. A. Hakim², S. S. Sikder¹, R. Mathieu³, Per Nordblad³ and S. Manjura Hoque² "Magnetic ordering in $\text{Co}_{0.2}\text{Cd}_{0.8}\text{Ho}_x\text{Fe}_{2-x}\text{O}_4$ ($x = 0.0, 0.05, 0.10$) spinel ferrite" International Conference on Magnetic Materials (ICMM) 2010, Oct 25-29, 2010, Saha Institute of Nuclear Physics, Kolkata, India.
10. S. S. Sikder¹, Saroat Noor¹, M. A. Hakim², Per Nordblad³ and Saiduzzaman⁴, "Magnetization behavior and spin canting in diluted $\text{Co}_{1-x}\text{Cd}_x\text{Fe}_2\text{O}_4$ ferrites" International Conference on Magnetic Materials (ICMM) 2010, Oct 25 - 29, 2010, Saha Institute of Nuclear Physics, Kolkata, India.